Very energetic gamma rays from binary x-ray sources and other astronomical objects

Dowthwaite, J. C.

VERY ENERGETIC GAMMA RAYS FROM BINARY X-RAY SOURCES AND OTHER ASTRONOMICAL OBJECTS

By

J.C. DOWTHWAITE B.Sc.

A thesis submitted to the University of Durham
in accordance with the regulations for
admittance to the degree of
Doctor of Philosophy

Department of Physics,
University of Durham

June 1987

Acknowledgements.

I would like to thank Professor A.W. Wolfendale and Professor B.H. Bransden for the provision of the facilities of the Physics department of the University of Durham over the course of this work. I would also like to thank the Commander and staff of the U.S. Army base at the Dugway Proving Grounds in Utah.

I am indebted to my supervisor, Dr. K.J. Orford for his valuable advice. I would like to express my gratitude to my colleagues at the University of Durham, Paula Chadwick, Tim Currell, Andrew Harrison, Susan Hilton, Ian Kirkman, Allan Lotts, Hamish Macrae, Ken Tindale, Ted Turver and Mark Walmsley for their help, support and their company.

I would also like to thank Bill Hogg and the staff of the Physics department workshop for their help, and the Science and Engineering Research Council for my Research Studentship.

Keith Taylor of IBM United Kingdom Laboratories Ltd. is thanked for the loan of the BBC microcomputer used to prepare and edit this thesis, and I would also like to thank Wendy for her help.

Finally, I would like to thank my parents and Tanya for their support, their encouragement and their patience. This thesis is for them.

Abstract.

This thesis describes the observation of a number of astronomical objects using the University of Durham Atmospheric Cerenkov light detectors. The array of telescopes was used to study the Very High Energy (V.H.E.) gamma-radiation from these objects from June 1981 until November 1984.

The general features of Gamma-ray astronomy are briefly discussed, and a review of the main results of previous gamma-ray observations is given. The basic theory and general characteristics of Atmospheric Cerenkov Effect experiments are reviewed. Details of the design, operation and performance of the University of Durham facility are presented in addition to details of the improvements achieved in the development of a new telescope. In particular, the new optical system is described.

The main analysis procedures are explained. The adaptation of statistical techniques used to analyse the intensity of the Cerenkov light flash is described in some detail. A discussion of the problems involved in conducting an extensive search for periodicity in the data collected from Cygnus X-3 is given. A procedure for testing for transient pulsed gamma-ray emission from the Crab Pulsar is also described.

The results of the observations from several objects are presented., the binary X-ray sources, Cygnus X-3, Hercules X-1 and 4U0115+63, the Crab pulsar and the Galactic Plane. In addition, the preliminary results from observations of seven radio pulsars and seven other objects are given.

A review of the main production mechanisms of V.H.E. gamma-radiation is given with particular emphasis on the models proposed for the high energy processes in Cygnus X-3, other binary X-ray sources and pulsars.

Preface.

This work presents the details of the observation and analysis of data from the following objects; Cygnus X-3, Hercules X-1, 4U0115+ 63, the Crab pulsar and the Galactic plane. In addition, seven radio pulsars and seven miscellaneous objects have been observed.

The author was involved in the operation of the University of Durham Atmospheric Cerenkov light detector array on four occasions between October 1982 and November 1984. The author was responsible for the development and testing of a mirror system for an improved detector used in this experiment. He was also involved in the design of a mirror system for a completely new telescope.

The author was part of a team that performed the routine analysis of the data collected with the array. In addition he adapted and developed new analysis techniques in the following areas;

The investigation of the pulse amplitude distributions.

The search for transient pulsed emission from the Crab pulsar.

The search for millisecond, second, and long term periodicity in the V.H.E. gamma-ray flux from Cygnus X-3.

A preliminary analysis of the data from seven radio pulsars and seven miscellaneous objects.

The description of these analyses is presented in chapters 5 and 6 of this work and represents the major contribution of the author. The other results represent the work of other members of the group as indicated in the text.

The author has summarised the theoretical basis for V.H.E. gamma-ray emission in chapter 7. The source mechanisms are reviewed and compared with the results in the very high and ultra high energy regions.

Contents.

Page

Chapter 4: - Observation techniques

Chapter 5: - Data analysis techniques

Page

Chapter 6: The results of the gamma-ray observations

Chapter 1: Gamma-ray Astronomy.

1.1: Introduction.

Over the last few decades many advances have been made in observational astronomy, advances which have opened new areas of the electromagnetic spectrum to investigation. Some of the most striking results have come from experiments using rocket, balloon and satellite technology in the study of low energy cosmic gamma-rays. More recently, with the development of ground based arrays of specialised detectors, signals at even higher energies have been measured. Observations in the gamma-ray region show that many astronomical objects are dominated by violent processes releasing huge amounts of energy. These objects provide important new testing grounds for the laws of physics.

In addition to the gamma-ray emission, huge numbers of high energy particles are also expected to be released into the Galaxy by such objects. Unfortunately, a study of these high energy particles cannot reveal as much information about the source since even a weak general magnetic field of 10^{-6} G throughout the Galaxy scrambles particle directions for all but the most energetic. Gamma-rays are not deflected, and along with any neutrino emission will represent the only direct flux between energies 10^{6} eV and 10^{15} eV, from these exotic objects.

Gamma-ray astronomy was first investigated in 1958 by Morrison (Morrison, 1958). He showed that there should be a significant gamma-ray flux from celestial objects. Unfortunately, many of the initial hopes for high fluxes of gamma-rays have not been fulfilled, and serious underestimates were made of the problems caused by the

background radiation. Despite the relatively low fluxes at high energies, recent advances in both satellite and ground based techniques have established a number of astronomical objects as strong gamma-ray emitters. This thesis describes some of the interesting results obtained at Very High Energies (V.H.E.) i.e. energies between 10^{11} eV and 10^{13} eV using a number of telescopes specially designed and operated by a team from Durham University.

1.2. Observation Methods

The full electromagnetic spectrum is shown in fig 1.1 with the gamma-ray region extending from ~ 0.5 MeV to the highest photon energies - easily the widest single region. At the lowest energies there is an overlap with hard X-rays, the boundary is conveniently defined to correspond to the e^+,e^- annhilation line. Such a wide span in energy necessitates the use of very different methods of detection and these are briefly reviewed.

1.2.1: 0.5 MeV - 10 GeV

Gamma-rays interact with the atmosphere and so experiments in this energy range must be conducted at high altitude and are therefore flown on balloons or satellites. At the lowest energies (0.5 - 5 MeV) the interaction of gamma-rays via the 'Inverse Compton Effect' dominates, and scintillation counters, for instance, those containing sodium or caesium iodide crystals are used. The scintillations are then detected using sensitive photomultiplier systems. A number of such counters can be used in an array to give information on the arrival direction and the energy of the incident photon. For work where energy resolution is considered important, solid state detectors consisting of lithium drifted silicon or germanium devices are

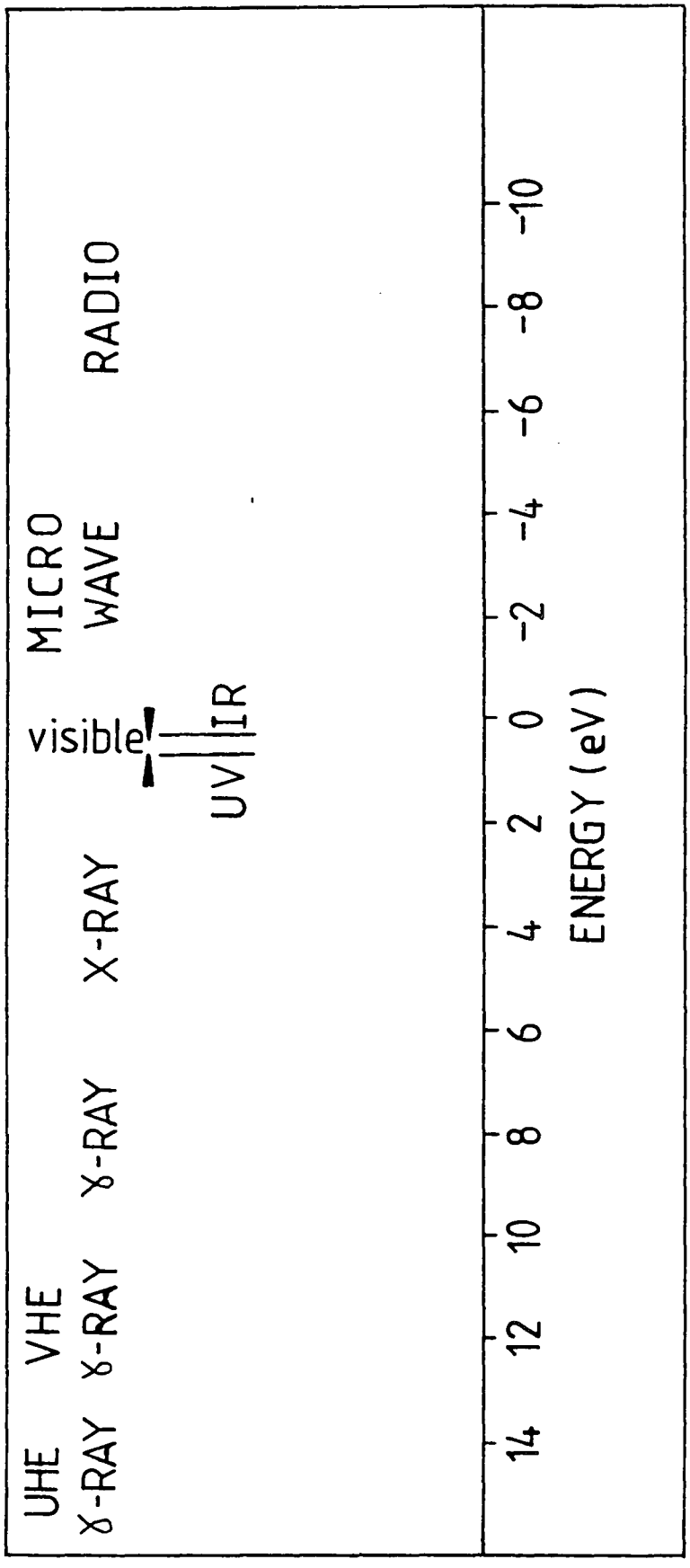

Figure 1.1: The electromagnetic spectrum.

employed.

At higher energies, pair production within the detector becomes more probable and experiments consisting of an array of spark chambers are used to delineate the gamma-ray trajectory.

Much of the information above 30 MeV has come from the two gamma-ray satellites, SAS II, operational from 1972-3; and COS-B from 1975-82. The SAS II satellite was subjected to a much lower cosmic ray induced background than the COS-B experiment, but was switched off after only six months of observations due to a technical fault. The European COS-B experiment operated for much longer than its design life, and produced a large amount of data. Together these two probes have made many of the important discoveries which developed this new field. Additional improvements are expected from another satellite - the Gamma-Ray Observatory (G.R.O.) which is designed to investigate the spectrum > 10 GeV, and is scheduled to begin observations at the end of the 1980's.

The details of the observations in this energy range relevant to this work are given in section 1.5.

1.2.2: 100 GeV - 20,000 GeV

The small collecting areas of gamma-ray satellites prevent work using these techniques above ~ 10 GeV. This is because the flux from astronomical objects falls off rapidly - see fig 2.1. Above 10^{11} eV a V.H.E. gamma-ray incident at the top of the atmosphere causes a cascade of particles by a process described in section 2.3. The particle cascade does not survive to ground level, but the Cerenkov radiation emitted as it descends through the atmosphere can be detected using the 'Ground based Cerenkov technique'. Collecting areas can be large, typically $10^4 m^2$, and measurable fluxes from astronomical objects are expected. Since 1960, ~ 30 experiments have

been performed using this method. All results presented in this thesis use this technique.

1.2.3: 10^{13} eV - 10^{16}eV

At these Ultra High Energies (U.H.E.) gamma-rays cause an 'extensive air shower' with the secondary particles in the cascade surviving to mountain altitudes for primary energies > 10^{13} eV. At even higher energies, lower altitude arrays of particle detectors search for showers with the unusually low muon content expected from gamma-ray initiated showers. Interest in Gamma-ray astronomy in this region has increased since the detection of a U.H.E. gamma-ray signal from the region around Cygnus X-3 by a group from the University of Kiel (Samorski and Stamm, 1983). As a result, many similar arrays have turned their attention to a search for more signals from this and other objects.

It is interesting to compare the angular resolution claimed for these techniques; satellites such as COS-B can resolve regions typically 1 degree across, as can both Cerenkov techniques (limited by the size of the Cerenkov flash) and extensive air shower arrays.

1.3: Gamma-ray production mechanisms.

Gamma-rays may be produced in the decay of radioactive particles and by a bremsstrahlung process in the gas clouds of interstellar space (Heitler, 1954). Although these processes may be important at the lowest energies, others are likely to dominate in the energy region that Cerenkov techniques are designed to investigate. The most important mechanisms in this region involve the interaction of cosmic-ray particles with the interstellar matter or radiation fields.

V.H.E. gamma-rays are therefore expected to be produced by the

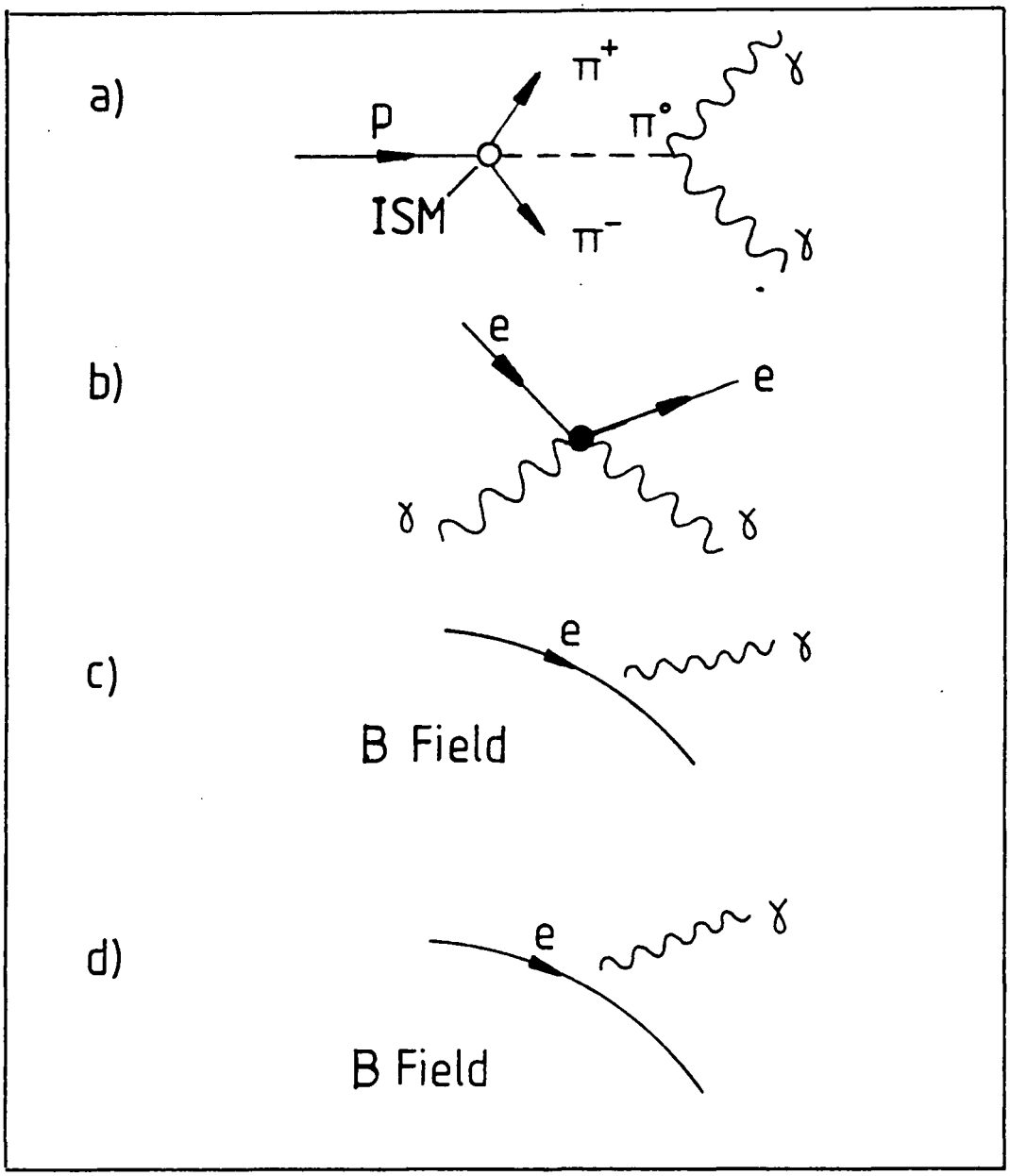

Figure 1.2: Emission processes for Gamma-rays.

following processes.

1.3.1: Meson decay.

The collisions between relativistic protons and other protons or nucleonic matter can give rise to the production of π and K mesons, with the subsequent decay of the meson to gamma-rays;

$$p + p = p + p + (\pi^0 = h\nu + h\nu)$$

If the spectrum of the injected protons is given by a power law of index p then the resulting spectrum of gamma-rays from π^0 decay is of the form,

$$I(E) \sim C.\ E^{-4/3(p-1/2)} \qquad - 1.1$$

where C is a constant.

The production of heavier mesons is also possible and may contribute to the gamma-ray flux at higher energies.

Pions are also produced in the annhiliation of a nucleon with an antinucleon, and although this is not important in the Galaxy where the ratio of antinucleon/nucleon is small, it may be significant in the production of cosmological gamma-rays.

If the cosmic ray flux detected at the top of the atmosphere is typical of that in the inner Galaxy, and if it permeates the clouds in the inter-stellar medium (ISM), then the diffuse gamma radiation at energies > 100 MeV can be explained by meson decay. However, there are indications (Fomin et al, 1977), (Dowthwaite et al, 1985) that the V.H.E. gamma-ray flux from the Galaxy does not map the hydrogen column density, which indicates that meson decay is not likely to be the main production mechanism.

Meson decay gives a characteristic signature to the spectrum, peaked at 70 MeV (i.e. 1/2 the rest mass of the pion), and may be enhanced in the vicinity of certain sources.

1.3.2: The Inverse Compton effect

This process occurs in regions with a flux of energetic cosmic ray electrons, for example around pulsars, and can be described as,

$$e^- + h\nu = e^- + h\nu'$$

- a high energy electron scattering off a low energy photon resulting in the transfer of energy and momentum to the photon. In the simple case of a low energy black body photon spectrum and a power law distribution of electron energies of index p_I, the resultant gamma-ray spectrum is given by,

$$I(E) = C_I . E^{-1/2(p_I+1)} . A^{1/2(p_I-3)} \qquad - 1.2$$

where A is the average initial photon energy, and C_I contains some energy dependent terms.

This process is particularly important in sources known to have high magnetic fields, inferred by the synchrotron signature to the radio and optical flux. In these cases, the required relativistic electrons and low energy synchrotron photons exist. In addition the 2.7 K background photons may also be transformed to gamma-ray energies by this process.

1.3.3: Synchrotron radiation

Much of the optical and radio emission from highly magnetised systems results from the interaction of a relativistic electron with a transverse magnetic field B_T - the synchrotron process. The spectrum will be peaked at an energy,

$$E_M = C . B_T . E^2 \qquad - 1.3$$

with C a constant.

This peak will normally occur at a much lower energy than the primary electron energy and so for normal systems this process is a source of low energy photons. However, models are proposed to accelerate electrons to energies $> 10^{17}$eV (-see chapter 7). Here, the synchrotron process may produce V.H.E. gamma-rays. For a power law distribution of electron energies of index p, the resulting photon spectrum will be of the form,

$$I(E) = C_A.B_T^{1/2(p+1)}.E^{-1/2(p+1)} \quad - 1.4$$

where C_A contains some energy dependent terms.

The lifetime of electrons against synchrotron radiation is short in many astronomical situations; for instance, a high energy electron travelling near to the light cylinder of a pulsar the lifetime is $< 10^{-4}$ s (Manchester and Taylor, 1977), and so a continuous source of high energy electrons is needed to supply objects radiating with the synchrotron signature. Probably the best example of such an object is the Crab Nebula, where electrons are accelerated by the rapidly spinning magnetised neutron star.

1.3.4: Curvature radiation

With the discovery of pulsars, another possible source of gamma-rays became apparent. Various methods have been proposed (Sturrock, 1971) for particles to suffer acceleration in the strong magnetic field associated with pulsars ($\sim 10^{12}$ G). In the particular case of a particle travelling along a curved flux line, photons are emitted in a fashion analogous to the bremsstrahlung process for particle deceleration in a electrostatic field. The spectrum is peaked at an energy,

$$E = C.10^{-7.8}.E_p^3.R \quad - 1.5$$

where R is the radius of curvature in cm.

This mechanism is most important close to the surface of a neutron star where the gamma-ray energies are comparable to those of the electrons.

The low energy gamma-ray spectrum from the pulsar PSR0833-45 can be explained by this process (Salvati and Massaro, 1978).

The gamma-rays produced in such processes are likely to be strongly attenuated by pair production.

The schematic descriptions of these emission processes are given in fig 1.2.

1.4: Gamma-ray absorption mechanisms

There are three main absorption processes thought to attenuate the gamma-ray flux significantly;

1.4.1: Absorption by matter

The absorption by pair production in the Coulomb field of hydrogen atoms and also by Compton scattering may be important in certain situations. Above 1 MeV pair production dominates the Compton scattering in the hydrogen gas and can be described as,

$$h\nu_1 + CF = e^+ + e^- + CF$$

where CF represents the Coulomb field. Above 200 MeV the cross section tends to a constant of $1.8 \cdot 10^{-26}$ cm^2, but the process is not considered important outside regions of high hydrogen atom density.

1.4.2: Absorption in magnetic fields.

A magnetic field (MF) may absorb momentum in an analogous fashion to the Coulomb field absorption described above. A gamma-ray can pair produce if the magnetic field is sufficiently intense,

$$T = E / m_e c^2 \ . \ B / B_q \qquad - 1.6$$

where $B_q = 2.m_e^2 \ .c^2/ \ e.h = 4.4 \ . \ 10^{13}$ G , and represents the measure of the field strength in natural quantum mechanical units.

Pair production is possible for $E > 2m_e c^2$ but the effective threshold is closer to a value,

$$T >\sim 0.1$$

above which the intense magnetic fields provide extremely efficient pair production. In many pulsars conditions of plasma magnetised to $\sim 10^{12}$ G exist and gamma radiation is strongly attenuated.

1.4.3: Absorption by photons.

Absorption of gamma-rays by starlight photons is negligible for all but the most extreme distances and is not thought to modify the V.H.E. flux significantly outside regions of high optical photon density. However, the interaction of U.H.E. gamma-rays with the 2.7 K Big Bang remnant is important. If an energetic photon collides with a 2.7K photon (of energy $\sim 2. \ 10^{-4}$eV) then the following process can occur,

$$\gamma_1 + \gamma_2 = e^- + e^+$$

The absorption comes into play at gamma-ray energies $>\sim 10^{14}$ eV, and the cross section is sufficiently large to impose a cut-off for gamma-rays of extragalactic origin (Gould and Schreder, 1966).
It is interesting to note that V.H.E. gamma-rays i.e. $E_\gamma < 10^{14}$ eV are not absorbed in this process and will represent the highest energy radiation detectable from extragalactic objects.

1.5: A review of gamma-ray sources.

The number of V.H.E. gamma-ray sources has increased in recent years, with the results from the Durham experiment making an important contribution. This thesis presents the detail of the observations of some of these objects, in particular, the binary X-ray pulsars, 4U0115+63 and Hercules X-1, the Crab pulsar and the unusual X-ray source, Cygnus X-3. In this section the extensive record obtained by other V.H.E. gamma-ray groups is reviewed along with important features of the emission at other energies.

1.5.1: Cygnus X-3.

Cygnus X-3 was discovered as an X-ray source (Giacconi et al, 1967), its most notable feature being the prominent low energy cut-off in the X-ray spectrum. The first indication that this object was unusual came in 1972 when a large radio burst was detected (Gregory, 1972). The radio flux rose to levels sufficient to make Cygnus X-3 the 2nd brightest radio source in the sky.

Since the 1972 radio outburst, Cygnus X-3 has been extensively observed from radio up to ultra-high energies. The detection of X-rays from the object stimulated gamma-ray interest in the source.

Observations were made by a Russian group from 1972 to 1976 using balloon based telescopes (Gal'per et al, 1976). They detected a 4.8 hour intensity modulation (previously seen at X-ray and Infra-red energies) at E > 40MeV. The gamma-ray flux from Cygnus X-3 dropped from $2.10^{-4}cm^{-2}s^{-1}$ shortly after the radio outburst, to an average value of, $(6.5+/-2.5).10^{-5}cm^{-2}s^{-1}$ in later observations. Other balloon measurements (Mckechnie et al, 1976), made during flights in 1972 and 1973 reported upper-limits to the Gamma-ray flux at E > 70MeV

well below that suggested by the Russian group.

Gamma-rays were detected by the SAS II telescope, again the high energy flux was modulated with the 4.8 hour period (Lamb et al, 1977). The reported time averaged flux was, however, lower than that detected by the Russian observers, viz.

$(10.9+/-3.1).10^{-6}cm^{-2}s^{-1}$ E > 35MeV

$(4.4 +/-1.1).10^{-6}cm^{-2}s^{-1}$ E > 100MeV

It is important to note that this reported flux was not confirmed in measurements made by the COS-B satellite (Strong, 1982) even though the COS-B X-ray detector did observe a 4.8 hour modulated signal (Van der Klis and Bonnet-Bidaud, 1981).

To summarise, observations in the 40-100 MeV energy region seem to indicate a reduction in the flux at these energies since 1972, though it should also be noted that the most extensive observations by the COS-B satellite which have received considerable new analysis (Hermsen, 1983) gave a firm null result.

At higher energies (E > 500 GeV), the atmospheric Cerenkov technique has been used by several groups. A team working at the Crimean Astrophysical Observatory monitored the source from 1972 to 1980 (e.g. Neshpor et al, 1979). They detected emission modulated by the 4.8 hour periodicity, with peaks in the emission occurring at phases 0.2 and 0.75, relative to the X-ray minimum in the 'light curve'. In addition, a random component to the gamma-ray flux was reported. A summary of the Russian results is given by Turver and Weekes (Turver and Weekes, 1981).

These results were confirmed in observations taken with telescopes at Tien Shan (Mukanov et al, 1980), and by more recent measurements at Mount Hopkins (Danaher et al, 1981), at the JPL (Lamb et al, 1982) and by the Durham group (Dowthwaite et al, 1983).

In particular, the June 1980 Mount Hopkins observations were

contemporary with satellite measurements, and showed a correlation between the 10^{12} eV emission and the increase in the X-ray flux seen by the COS-B X-ray detector (Weekes et al, 1981).

The later observations give strong indications that the relative strengths of the two peaks of periodic emission, have changed, with that at phase 0.63-0.75 in the 4.8 hour 'light curve' now predominating.

Early X-ray observations gave indications of a longer term variability to the high-energy flux. A period of 17 days has been suggested (Holt et al, 1976), 34.1 days (Molteni et al, 1980), and ~ 20 days (Bonnet-Bidaud and Van der Klis, 1981). This latter period is explained as apsidal motion in the binary system.

Recently, Cygnus X-3 has been detected by the University of Kiel Extensive Air Shower (E.A.S.) array, at energies in the range 10^{15} to 10^{16} eV (Samorski and Stamm, 1983), with confirmation by other arrays, Haverah Park, (Lloyd-Evans et al, 1983) and Akeno, (Kifune et al, 1986). The U.H.E. flux shows the familiar 4.8 hour modulation, with a peak in the emission detected by the Kiel group at phase 0.4 (defined using a different ephemeris to that generally used at lower energies (Van der Klis and Bonnet-Bidaud, 1981).

Recent very interesting results have come from experiments deep underground designed to detect proton decays (Marshak et al, 1985). An analysis of these data shows a modulation over the day peaked as Cygnus X-3 culminates. These results would seem to indicate a strong neutrino or particle flux from the object and infer that Cygnus X-3 may be a very unusual source.

Over the last decade an extensive database of observations has indicated that Cygnus X-3 is a very strange and challenging object, especially as the implied distance of > 10 kpc makes it one of the most energetic objects in the Galaxy.

1.5.2: Hercules X-1.

The first X-ray source in the constellation of Hercules was discovered in 1972 (Tannanbaum et al, 1972) and exhibits variations in the X-ray flux on three timescales;

A 1.24 s X-ray pulsation

A 1.7 day orbital period

A 35 day modulation

The latter comprises a period of high activity lasting 12 days and a low state of 23 days, containing an intermediate high state.

The object is believed to be a neutron star accreting matter from a low mass companion star identified as HZ-Herculis in 1972 (Forman et al, 1972).

The X-ray spectrum shows a strong peak at 58 keV, (Trumper et al, 1978) which has been interpreted as a cyclotron line, i.e. a transition of electrons from the first excited Landau level to the ground state. This observation implies a high magnetic field strength of $\sim$ 5.0 10^{12} G . This result is important as it indicates that Hercules X-1 is capable of accelerating particles to high energies, and may be a source of gamma-rays due to the mechanisms described in section 1.3. No detections of high energy radiation had been made until an outburst was detected by the Dugway array in April 1983 (Dowthwaite et al, 1984a). A subsequent low level flux was also observed. In July 1983 the 'Flys Eye' cosmic ray experiment also detected a burst at energies $> 10^{14}$ eV (Baltrusaitis et al, 1985). Details of the Durham observations are presented in section 6.4.

1.5.3: 4U0115 + 63

This binary X-ray pulsar has been reported as a transient X-ray source (Forman et al, 1976) and (Rappaport et al, 1978). The accreting

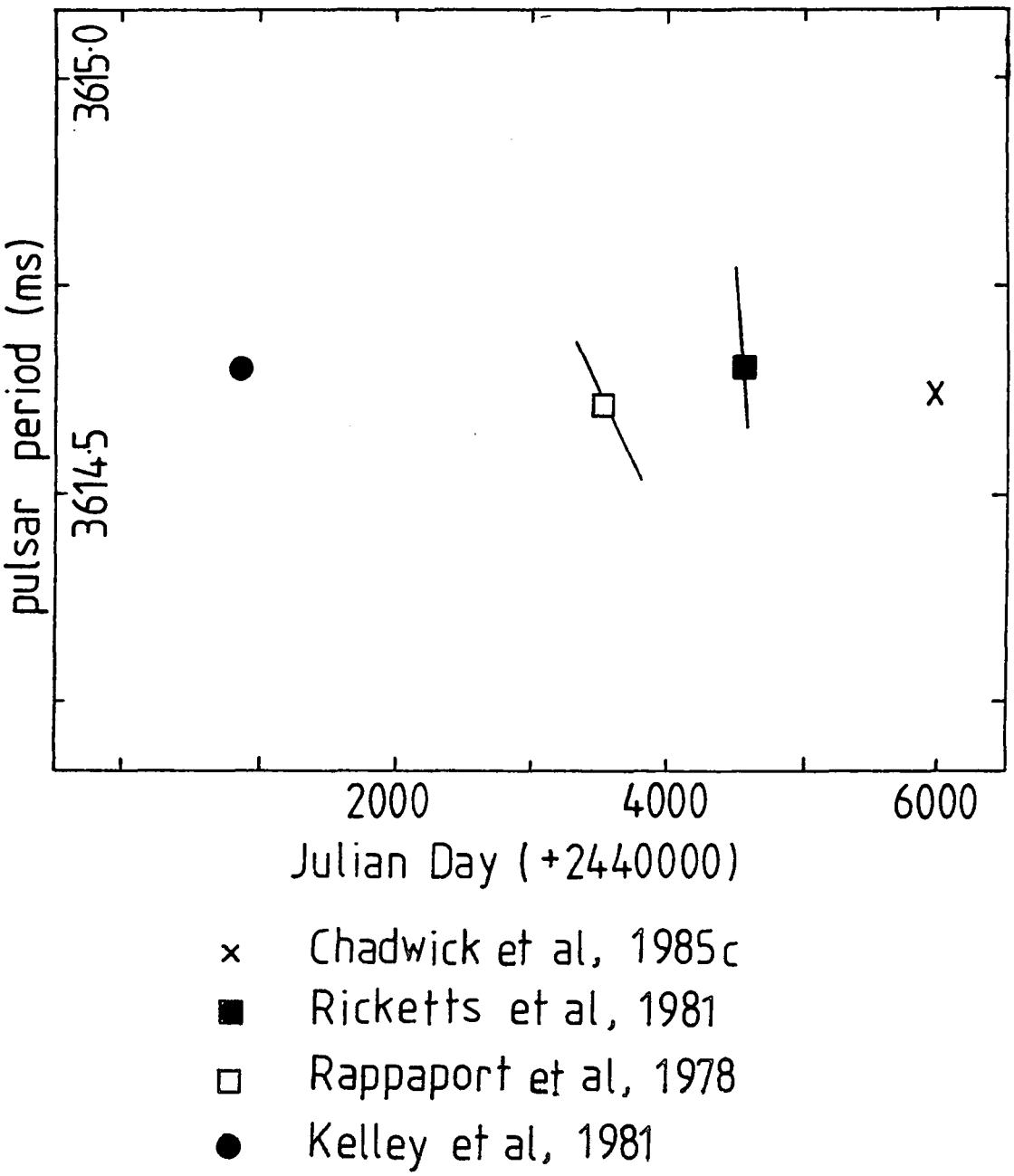

Figure 1.3: The variation of the period of the pulsar in the 4U0115 + 63 system.

collapsed object is contained in an eccentric orbit of period ~ 24.3 days, and shows X-ray pulsation with a period of ~ 3.61 s. The accuracy of the parameters defining this system were improved in observations conducted by the Ariel 6 satellite (Rickets et al, 1981). Interest in this object at V.H.E. stems from similarities in the X-ray flux from Hercules X-1 in particular the evidence for a cyclotron line at 20 keV (Wheaton et al, 1979).

The X-ray pulsations from this object are unusual. The period has hardly changed over the time of the X-ray observations - see fig 1.3, but the period derivative has been large and varied. This indicates that the system may undergo intermittent, enhanced accretion, with the consequent transient X-ray emission.

1.5.4: The Crab Pulsar.

The existence of two radio pulsars close to the centre of the Crab Nebula was shown using the Arecibo radio dish (Staelin and Reifenstein, 1968). A 33 ms period was discovered in the radio emission from one of them, PSR0531+21. Later, this same object was shown to pulsate at optical wavelengths (Cocke et al, 1969), and the optical star was then identified as the remnant of the Supernova.

Observations at X-ray energies (Fritz et al, 1969) and low energy gamma-rays (Albats et al, 1972) extended the detected pulsed spectrum. Over the last decade the two gamma-ray satellites SAS II and COS-B have detected high energy gamma-ray pulsations and given indications of variations in the emission with both time and energy (Wills et al, 1982).

The situation at V.H.E. has been somewhat confusing but there is now firm evidence from the Durham group for a continuous low level flux at energies $> 10^{12}$ eV (Dowthwaite et al, 1984b). In addition very strong bursts of periodic V.H.E. gamma-rays were detected in 1981, (Gibson et al, 1982a). Some details of these results are presented in

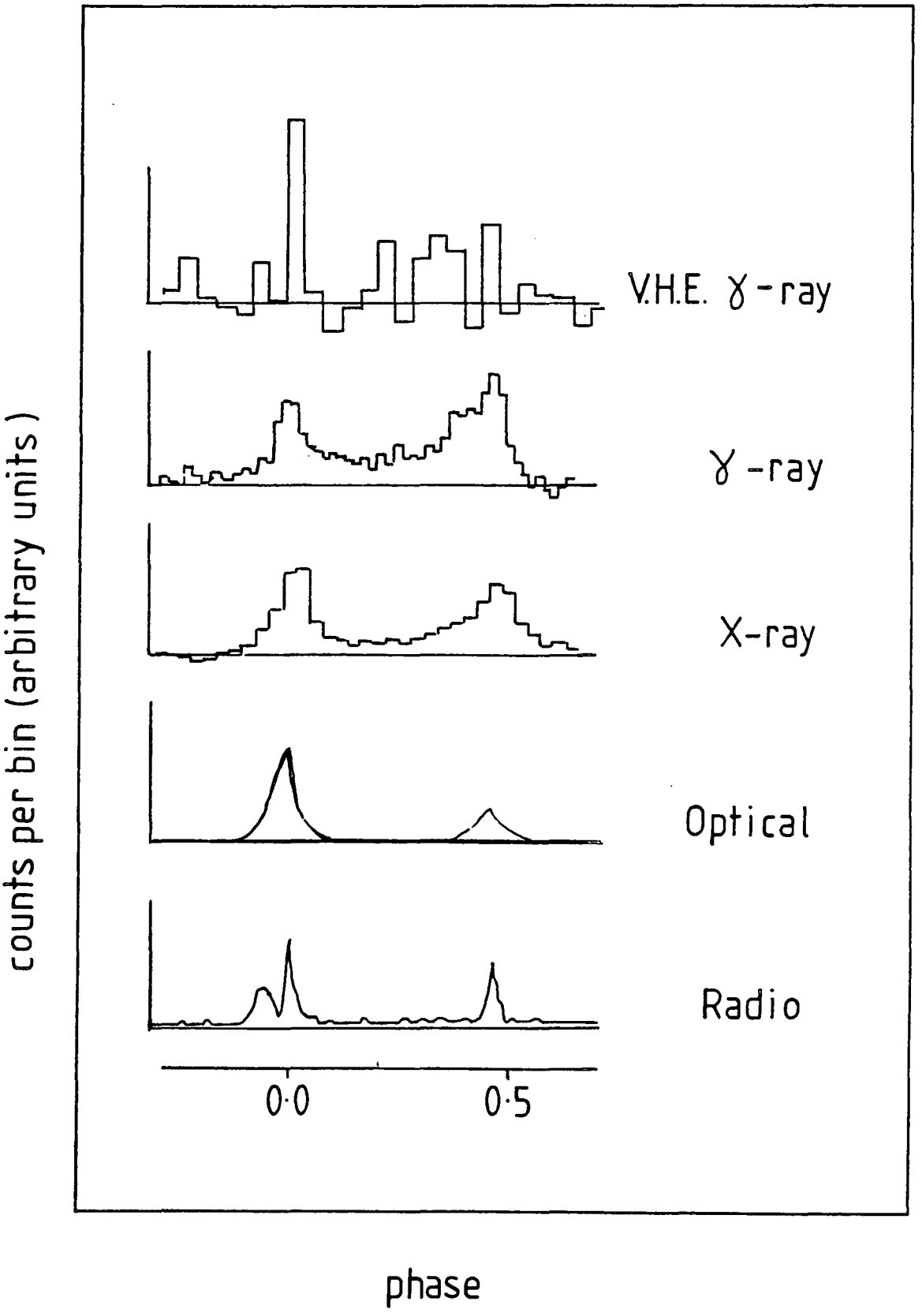

Figure 1.4: The variation of the width of the mainpulse emission from the Crab Pulsar from radio to V.H.E gamma-ray energies.

this thesis, with more extensive work described elsewhere (Kirkman, 1985).

In summary, the Crab Pulsar emits pulsed radiation from radio to 10^{12} eV energies with the peak luminosity corresponding to an energy of several MeV. The light curves over this wide range of energies are given in fig. 1.4 showing the coincidence in the position of the mainpulse over the whole range.

1.5.5: The Vela Pulsar

This is the only other radio pulsar detected at high significance at V.H.E ,(Bhat et al, 1980) and is also a very fast pulsar (89 ms period). Unlike the Crab pulsar there is no strong correlation between the light curves at different energies, and the luminosity is probably peaked at higher energies (> 1 GeV). A Southern hemisphere V.H.E. experiment presently being developed by the University of Durham will monitor this object as a priority, especially as there are similarities in the characteristics of the V.H.E. emission with that from the Crab pulsar.

1.5.6: Other radio pulsars.

There have been predictions for gamma-ray emission from radio pulsars (Buccheri et al, 1978). The extensive COS-B database was analysed in a search for those pulsars with parameters sufficiently well determined to allow folding of the gamma-ray data with the period. There are indications of pulsation from two pulsars PSR0740-30 and PSR1822-09 (Mayer-Hasselwander et al, 1980) though no firm detection has been claimed. The SAS II satellite reported the detection of PSR1818-04 and PSR1747-46 (Ogelman et al, 1976) though there is no confirmation in the COS-B data.

At higher energies a detection of the nearby pulsar PSR0950+08 has

been claimed by an Indian group, (Gupta et al, 1978) though more recent observations by the same group have failed to repeat the result.

To summarise, there is some tentative evidence for gamma-rays from radio pulsars, and with this in mind the Dugway array observed a selection of pulsars, including the two binary pulsars PSR1913+29 and PSR0655+64. The preliminary results are discussed in section 6.7, and a more detailed analysis is described elsewhere (Chadwick, Phd thesis in preparation).

1.5.7: 2CG065 + 00

A systematic search for fast radio pulsars in the error boxes defined by the unidentified COS-B sources has resulted in the association of the gamma-ray object 2CG065+00 with the 6 ms binary radio pulsar PSR1953+29 (Boriakoff et al, 1983). The only direct evidence for this association has come from the V.H.E. observations conducted with the Dugway array, (Chadwick et al, 1985a). Confirmation of this result is necessary and has not been made at the time of writing of this thesis.

1.5.8: Unidentified COS-B sources

Of the 25 objects detected by the COS-B satellite only 5 have been identified at other wavelengths. There have been various attempts to interpret the remaining sources as unresolved pulsars c.f. the Crab and Vela pulsars, as molecular clouds c.f. the ρ - Oph cloud and as young Supernova remnants, (Lamb , 1978).

No conclusive statement can be made, but in view of the wide range of gamma-ray sources identified it is possible that many different

types of object will be included in the COS-B catalogue of unidentified sources and will contribute to the diffuse gamma-ray background.

Two of the strongest 100 MeV sources 2CG195+04 (Geminga) and 2CG135+01 have received considerable attention, for instance, observations of both objects have been made by the Ariel 5 X-ray satellite (Coe et al, 1978). The unusual source, Geminga was discovered by the SAS II satellite and may have a 59s periodicity, however a detailed analysis of the COS-B observations does not give any clear indication of this period.

The V.H.E. gamma-ray measurements of both of these sources have led to upper limits (Porter and Weekes, 1978). An extensive series of observations of 2CG195+04 have been conducted using the Dugway array and the detailed analysis is continuing and will be reported elsewhere (Chadwick, PhD thesis in preparation).

1.5.9: Gamma-ray emission from Galaxies.

The gamma-ray continuum from the Galaxy was first reported, at energies > 50 MeV in 1968 (Clark et al, 1968). Subsequent surveys conducted by the satellites, SAS II and COS-B confirmed that there is clear enhancement of the gamma-ray flux in the region +/- 10 degrees of latitude about the Galactic plane, with a peak in the direction of the Galactic centre.

Observations conducted at V.H.E. have also shown a broad emission at the Galactic Plane in the region of longitude 40-80 degrees, with a 'dip' in the emission at the equator (Fomin et al, 1977) and (Weekes et al, 1979). Confirmation of this signature to the V.H.E. emission came from a similar observation conducted under very stable conditions using the Dugway array of telescopes, (Dowthwaite et al, 1985). These

results are discussed elsewhere (Walmsley, PhD thesis in preparation). In addition to the study of our own galaxy several groups have searched for V.H.E. gamma-rays from extragalactic objects. Upper limits from the nearest large galaxy, M31, a known X-ray source have been obtained (Porter and Weekes, 1978). Further work by the Durham group has shown that this galaxy may also emit V.H.E. gamma-rays with a luminosity of $\sim 10^{40}$ ergs^{-1} (Dowthwaite et al, 1984c) in good agreement with the suggested luminosity of our own galaxy at these energies.

Other observations have concentrated on the more unusual extragalactic objects such as the radio galaxy Centaurus A. Gamma-rays have been reported at energies $> 10^{12}$ eV from observations at Narrabri made in 1975 (Grindlay et al, 1975).

This object will be extensively monitored by the new Southern hemisphere observatory.

1.5.10: Other objects

Although the following objects are not considered to be very likely V.H.E. gamma-ray sources the Dugway detectors did make limited observations of them to confirm previous upper limit values. The details of the observations are summarised in table 4.2.

Perseus X-1 - a cluster of galaxies and an X-ray source.

Cas A - a supernova remnant, again seen at X-ray energies

SS433 - a complex binary X-ray source thought to be powered by particle acceleration in an accretion disc.

Cygnus X-1 - a black hole candidate interpreted as an accreting X-ray source.

NGC4151 - a Type I Seyfert Galaxy, seen as a strong X-ray source but not by the COS-B satellite (Perotti et al, 1979).

3C273 - a quasar, and a strong COS-B source.

2CG135+04 - an unidentified COS-B source.

Upper limits for V.H.E. emission from these objects have been derived from a number of Cerenkov experiments (Porter and Weekes, 1978).

The results obtained from these gamma-ray objects have served to firmly establish this field many years after the paper published by Morrison. The next generation of telescopes is expected to make many more interesting discoveries. Gamma-ray astronomy is developing into a complex subject, providing a very useful set of observations against which theories may be tested. In particular, the V.H.E. work has developed in its own right, in some cases it has provided results ahead of the satellite collaborations and has demonstrated the importance of the Atmospheric Cerenkov light technique.

Chapter 2: The Atmospheric Cerenkov technique.

2.1: Introduction

As only very small collecting areas are possible with gamma-ray satellites, their use is restricted to energies < 10 GeV. Work at higher energies requires different techniques. The effective collecting area of an array of ground-based Cerenkov light detectors is very large, of the order of 10^4 m^2 . This is due to the nature of the emission of Cerenkov light from a very high energy (V.H.E.) gamma-ray initiated cascade of relativistic particles. With such a large area a substantial number of gamma-rays should be detected despite the much lower incident flux at these very high energies. In fact, at present, this technique represents the only effective method for studying the intermediate energy range 10^{11} eV - 10^{13} eV.

There are serious limitations associated with experiments of this type, and these are apparent from fig. 2.1, a representation of the cosmic-ray spectrum at these energies compared to the spectrum of a typical strong V.H.E. gamma-ray source, Cygnus X-3. The cosmic ray flux is much higher than than that from the source, and produces a similar Cerenkov light signal in V.H.E. experiments; i.e. there is a large, and indistinguishable background. However, with the optimization of experimental design and the application of various statistical methods, gamma-ray signals have been extracted. The statistics applicable to this work are described in detail in Chapter 5. This chapter will review the basic features of the Cerenkov light from particle showers in the atmosphere and will describe some of the experiments designed to investigate the V.H.E. gamma-ray flux.

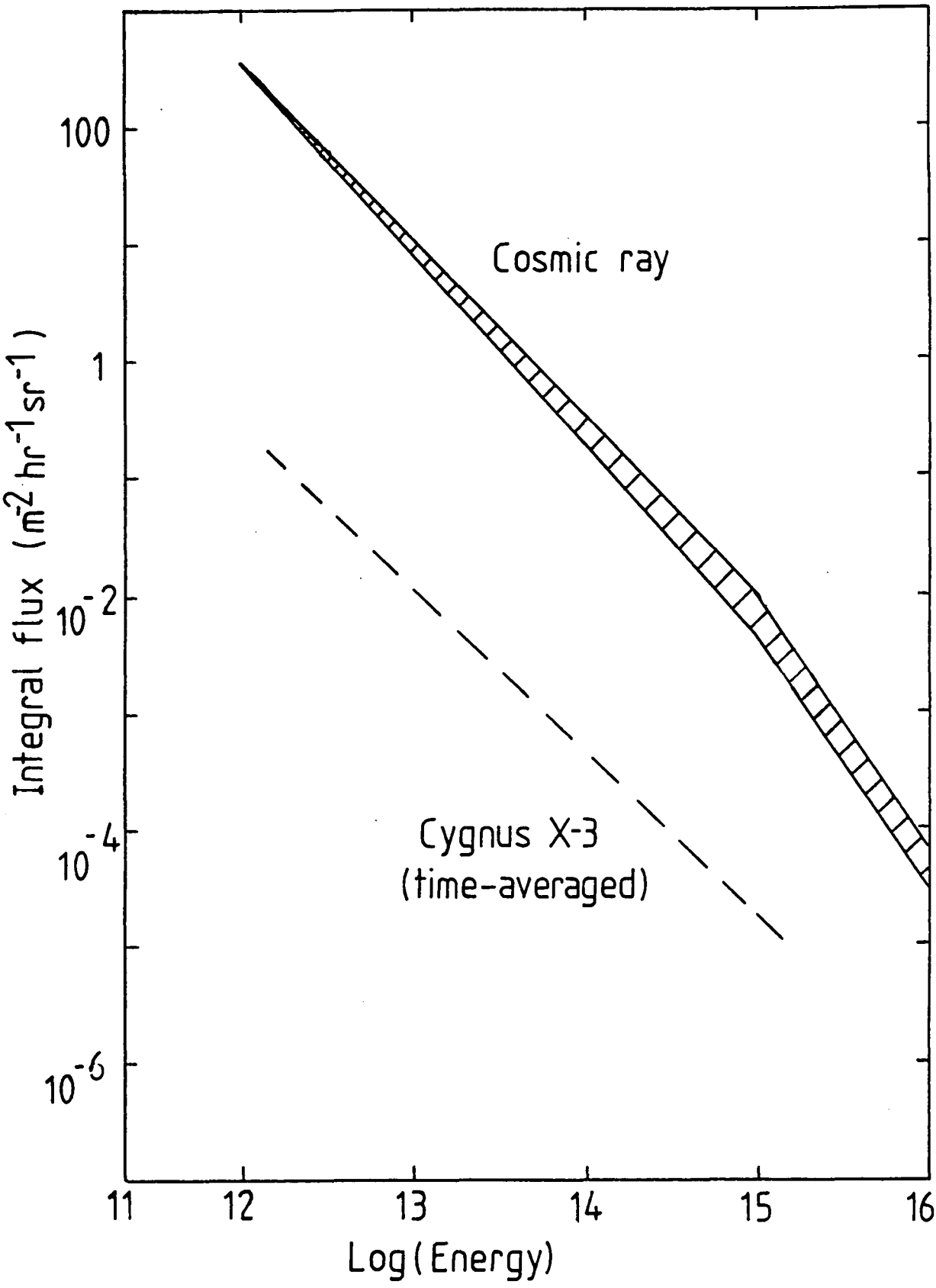

Figure 2.1: The cosmic ray background spectrum compared with the V.H.E. gamma-ray spectrum from Cygnus X-3.

2.2: The Nature of Cerenkov Radiation.

If a charged particle moves through a dielectric medium with a velocity greater than the phase velocity of light in that medium, the medium itself will emit radiation in a continuous spectrum and at an angle to the particle trajectory. This effect was discovered independently by Mallet (Mallet, 1926) and Cerenkov (Cerenkov, 1934), and is called Cerenkov radiation. The classical physics of the emission is described in detail elsewhere (Jelley, 1968) and will be outlined below.

As the fast charged particle moves through the dielectic medium it causes a local polarisation. The polarisation of atoms in the medium at some point, S close to a small element of the particle trajectory is shown in fig. 2.2a - the direction of net polarisation resolved into the radial and axial components is given in fig. 2.2b. Only the axial component will be detectable at some distance from the axis - cylinderical symmetry cancels the radial component. The single element of the particle trajectory then acts essentially as an elementary dipole. Generally, wavelets emitted from all such small elements will destructively interfere and there will be no coherent radiation. However, at velocities, v, greater than the phase velocity, V_{ph}, constructive interference can occur between wavelets emitted from many such small elements. The Huygens construction shown in fig. 2.3 represents this effect.

For coherent emission to be produced the particle must travel the distance XY in the same time, t, that the light travels from X to Z. If the refractive index of the medium is, n, then the coherent

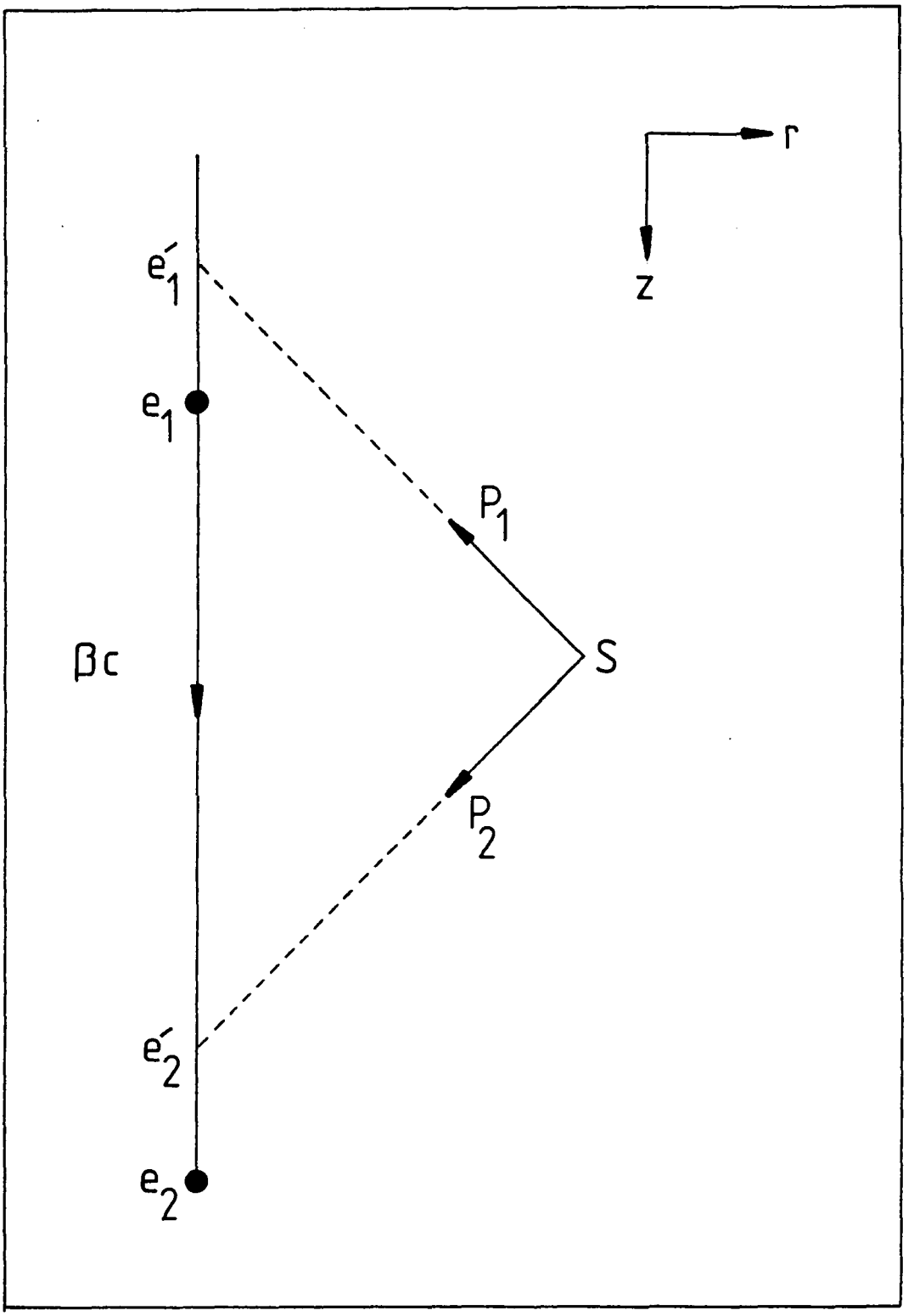

Figure 2.2a: The polarisation of atoms in the 'Cerenkov Effect'.

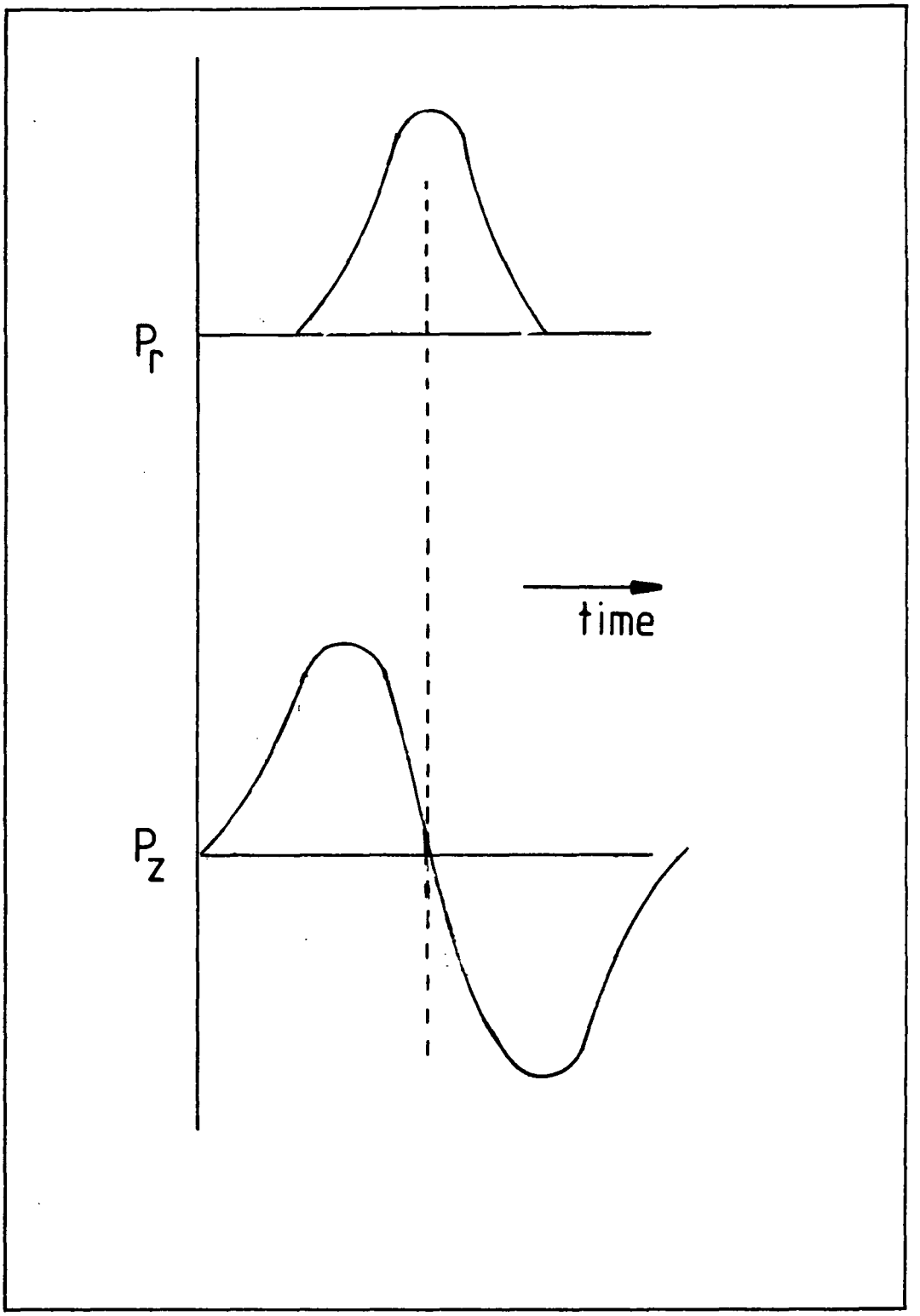

Figure 2.2b: The net polarisation of atoms in the 'Cerenkov Effect' resolved into radial, r and axial, z components.

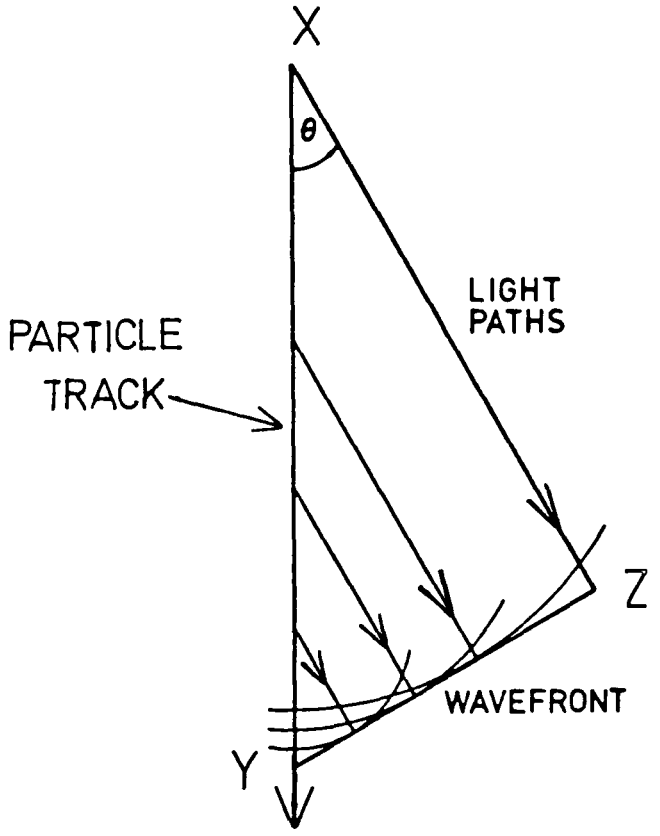

Figure 2.3: A Huygens Construction of the constructive interference between wavlets emitted by adjacent atoms.

radiation is emitted at an angle A to the particle trajectory given by, (see fig. 2·3)

$$\cos A = \frac{XZ}{XY}$$

$$= \frac{V_{ph}}{v.n}$$

$$= \frac{1}{B.n} \qquad - 2.1$$

with $B = v/V_{ph}$, and forms a cone.

In the case of an ultra-relativistic particle the maximum angle of emission is reached,

$$A_{max} = \cos^{-1} (1/n) \qquad - 2.2$$

which in the case of air at N.T.P. is ~ 1.3 °

Cerenkov radiation will therefore only occur at those frequencies for which n in the medium is > 1. For air, at N.T.P. this corresponds to the microwave to ultraviolet region.

The detailed theory was developed from these classical arguments by Frank and Tamm (Frank and Tamm, 1937). Using this theory the rate of production of radiation, W ($ergs^{-1}$), for a path length, l (cm), and a particle of charge Ze, is given by,

$$\frac{dW}{dl} = \frac{Ze^2}{c^2} \int_{\beta n > 1} (1 - (1/Bn)^2) \, w.dw \qquad - 2.3$$

where w is the angular frequency (Hz).

This result reveals that the spectrum is continuous, and proportional to w.dw, i.e. more radiation is emitted at higher frequencies. For a particle moving through air at N.T.P. the typical number of photons produced in the wavelength range 3500 - 5500 Angstroms, per unit path length, is ~ 0.3 ($photons.cm^{-1}$). In this case the corresponding threshold energy (B = 1/n , A = 0) for the electron is ~ 20 MeV. It is important to note that this polarisation

process results in a much lower energy loss ($\sim 10^{-4}$) than the ionisation processes which are also associated with the particle.

A full quantum mechanical treatment by (Ginzburg, 1940) produces the same general features. The 'Cerenkov Effect' is essentially a macroscopic process with little radiation reaction, and so there is negligible quantum mechanical modification to the simple interpretation described above.

2.3: Cerenkov radiation from V.H.E. gamma-rays.

When a very high energy ($> 10^{11}$eV) photon enters the top of the atmosphere it's first interaction occurs at an atmospheric depth of $\sim$ 40 gcm^{-2}. This value is determined using Monte Carlo simulations of the behaviour of a 1000 GeV gamma-ray initiated cascade. On interaction it generates an electron and positron by pair production in the nuclear field of an atom. These electrons produce further gamma-rays by the Bremsstrahlung process and these photons in turn undergo pair production and so on. An electron - photon cascade develops with the maximum number of $\sim$ 1000 electrons occurring at an altitude of $\sim$ 10 km and at an atmospheric depth of 250 gcm^{-2} . A schematic representation is given in fig 2.4a. It is important to note that cosmic-ray particles produce similar cascades, these are described schematically in fig 2.4b. In the case of the energy of the primary particle/photon being $> 10^{13}$ eV the cascade of secondary particles survives to ground level and is termed an 'Extensive Air Shower'.

The large number of particles produced in these cascades ($\sim 10^{5}$ for a primary energy of 10^{12}eV), move at the very high velocities sufficient to produce Cerenkov radiation. For the particular case of a cascade initiated by a 10^{12} eV gamma-ray primary, the particle cascade dies out before reaching ground level, but the Cerenkov light survives with little atmospheric absorption and constitutes a short pulse of

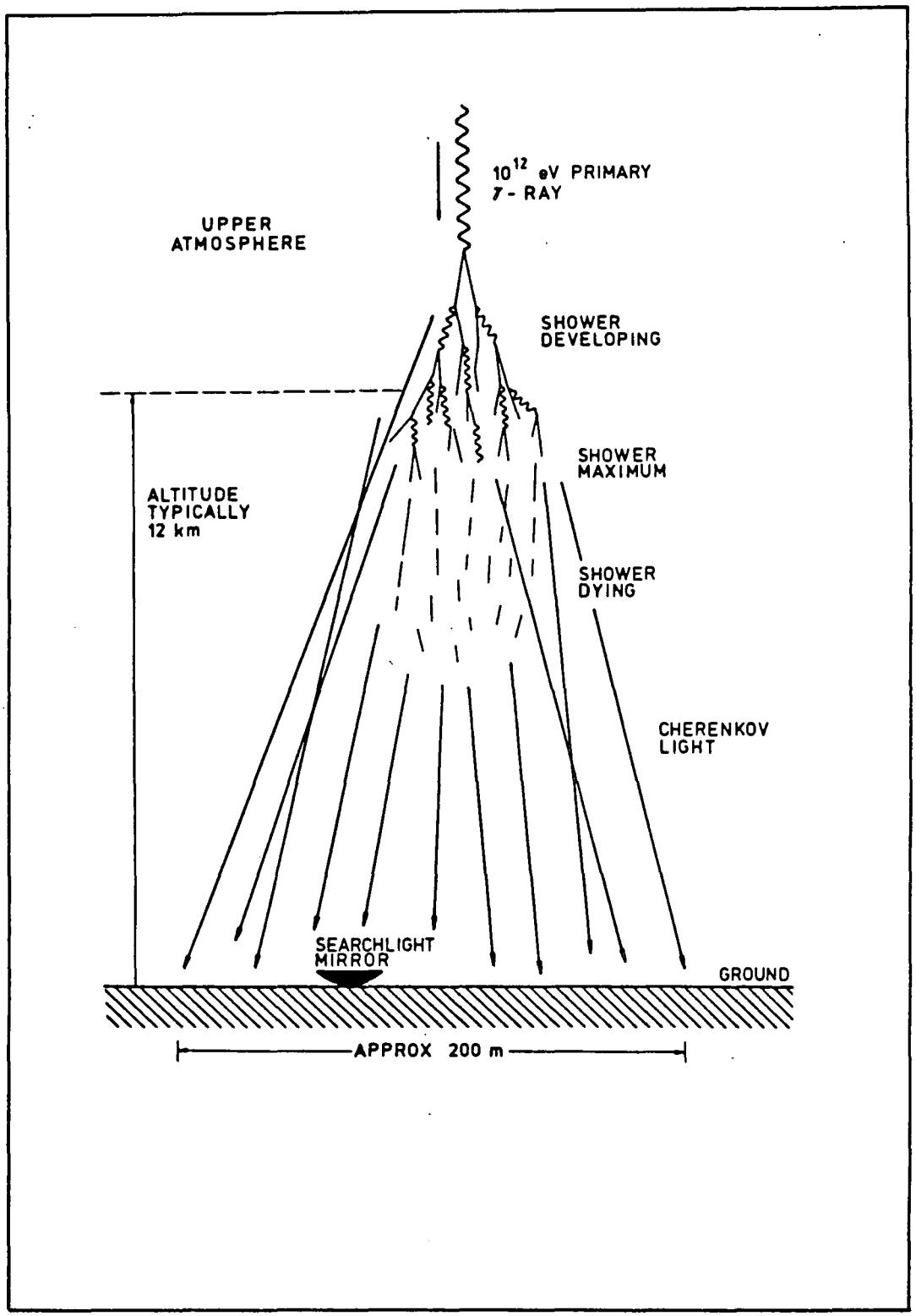

Figure 2.4a: A schematic description of a V.H.E. gamma-ray initiated cascade in the Earth's atmosphere.

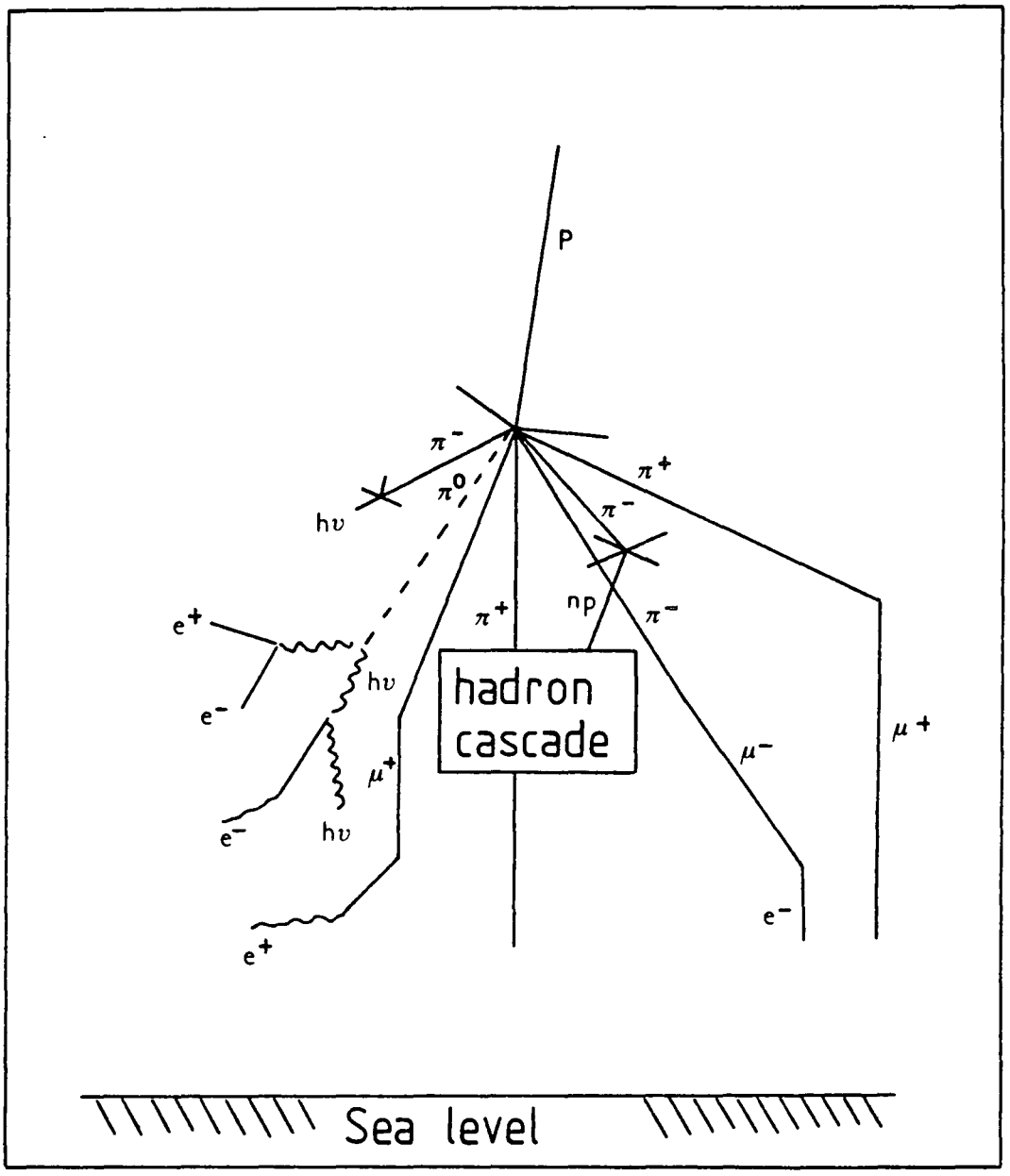

Figure 2.4b: A schematic description of a V.H.E. cosmic ray particle initiated cascade in the atmosphere.

blue-ultraviolet light.

Blackett indicated that there should be a contribution to the night sky brightness due to Cerenkov radiation from the cascade of particles (Blackett, 1948). He concluded that the Cerenkov contribution was as little as 10^{-4} of the total photon rate of 6.4 10^{7} $cm^{-2}s^{-1}$ sr^{-1}, and so would not be detectable by the usual techniques. Galbraith and Jelley showed that the Cerenkov light expected from a cascade arrives at the Earths surface in a pulse of very short duration, $\sim 10^{-8}$ s (Galbraith and Jelley, 1953). In this short time, the background would effectively be formed by fluctuations in the brightness of the sky and not its mean value. The Cerenkov signal should then be detectable by simple detectors coupled to fast electronics.

These early, simple detectors consisted of a small f-ratio mirror, which could be of quite poor optical quality, with a fast photomultiplier at the focus. The electronics coupled to this system included a fast amplifier and discriminator (time constant $\sim$ 10 ns), with the Cerenkov pulse displayed on a triggered oscilloscope. The height and duration of the pulse were then directly proportional to the intensity and duration of the Cerenkov flash. Such a system was limited by fluctuations in the sky brightness, but this problem was reduced by using faster amplifiers, and was removed completely by operating three such detectors in fast coincidence.

2.4: Details of the Cerenkov light pulse.

Over the last 20 years considerable effort has been made to measure and explain the detail of the Cerenkov pulse, and a brief review of the essential features is presented here.

The typical Cerenkov pulse detected at ground level from a 1000 GeV gamma-ray primary lasts 1 - 10 ns. This pulse consists of the continuous spectrum given in fig 2.5 and most of this light originates

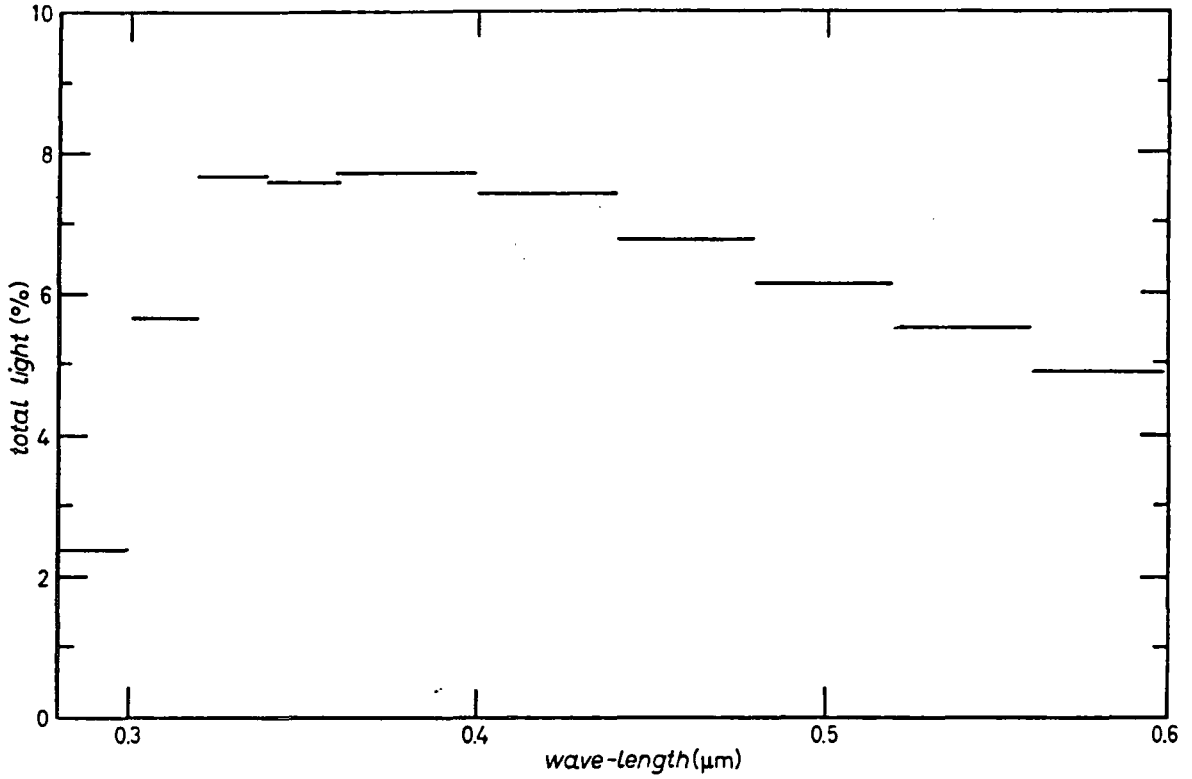

Figure 2.5: The spectrum of the Cerenkov light produced by a primary gamma-ray of energy 100 GeV - observed at sea-level.

near the cascade maximum (altitude ~ 10 km). The pulse represents a light spot on the sky about the arrival direction of the primary. The size and shape of the light spot are determined by many factors, important among these being multiple Coulomb scattering of the secondary particles in the atmosphere, and also fluctuations early in the shower development. As a result the angular spread of the flash exceeds the 1.3° suggested by simple Cerenkov theory.

2.4.1: The lateral extent of the Cerenkov flash and Computer simulations

Early calculations of this measure took multiple Coulomb scattering, and modifications due to the Earths magnetic field into account (Zatsepin and Chudakov , 1962). Fig. 2.6 gives the result. Clearly, the form of the lateral distribution is peaked within 200 m of the detector, but a finite intensity may exist out to distances of ~ 1 km.

The approximate analytical calculations are useful for a general appreciation of the basic features of the Cerenkov light signature from high energy particles. However, for the purposes of optimization in the design of detectors a more detailed shower investigation must be made using computer simulations. These simulations require a detailed knowledge of the nuclear physics involved in the cascade development and the absorption processes in the atmosphere. They are developed on large mainframe computers using the Monte-Carlo technique. The detector parameters such as height above sea-level and field of view are incorporated into the calculations, and so the simulated shower can be compared with direct measurements. Simulations have been made (Browning and Turver, 1977), and (Hartman et al, 1979) for both proton and gamma-ray initiated showers. These show good agreement with observations.

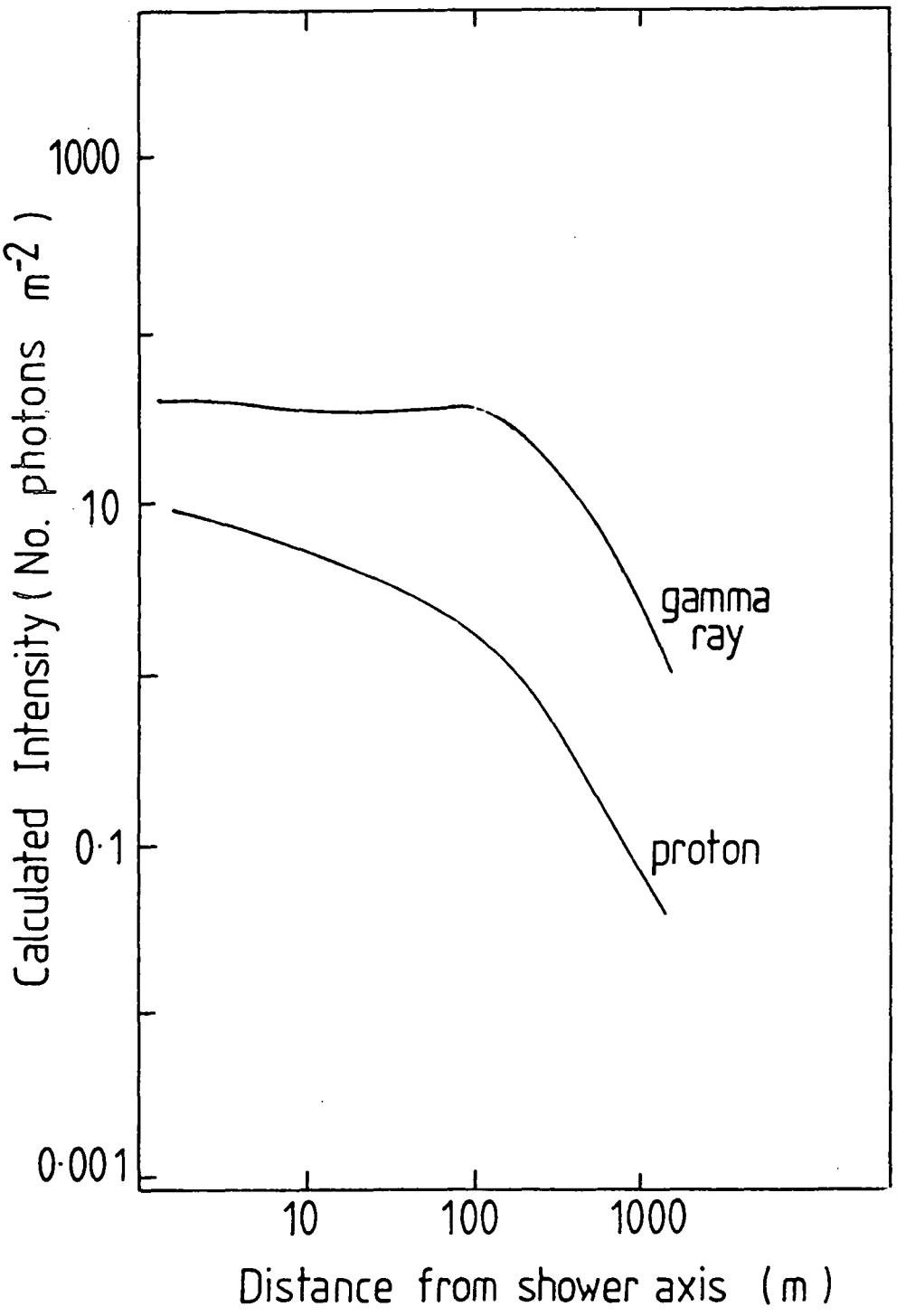

Figure 2.6: The calculated lateral extent of the Cerenkov 'flash' - initiated by a 1000 GeV gamma-ray.

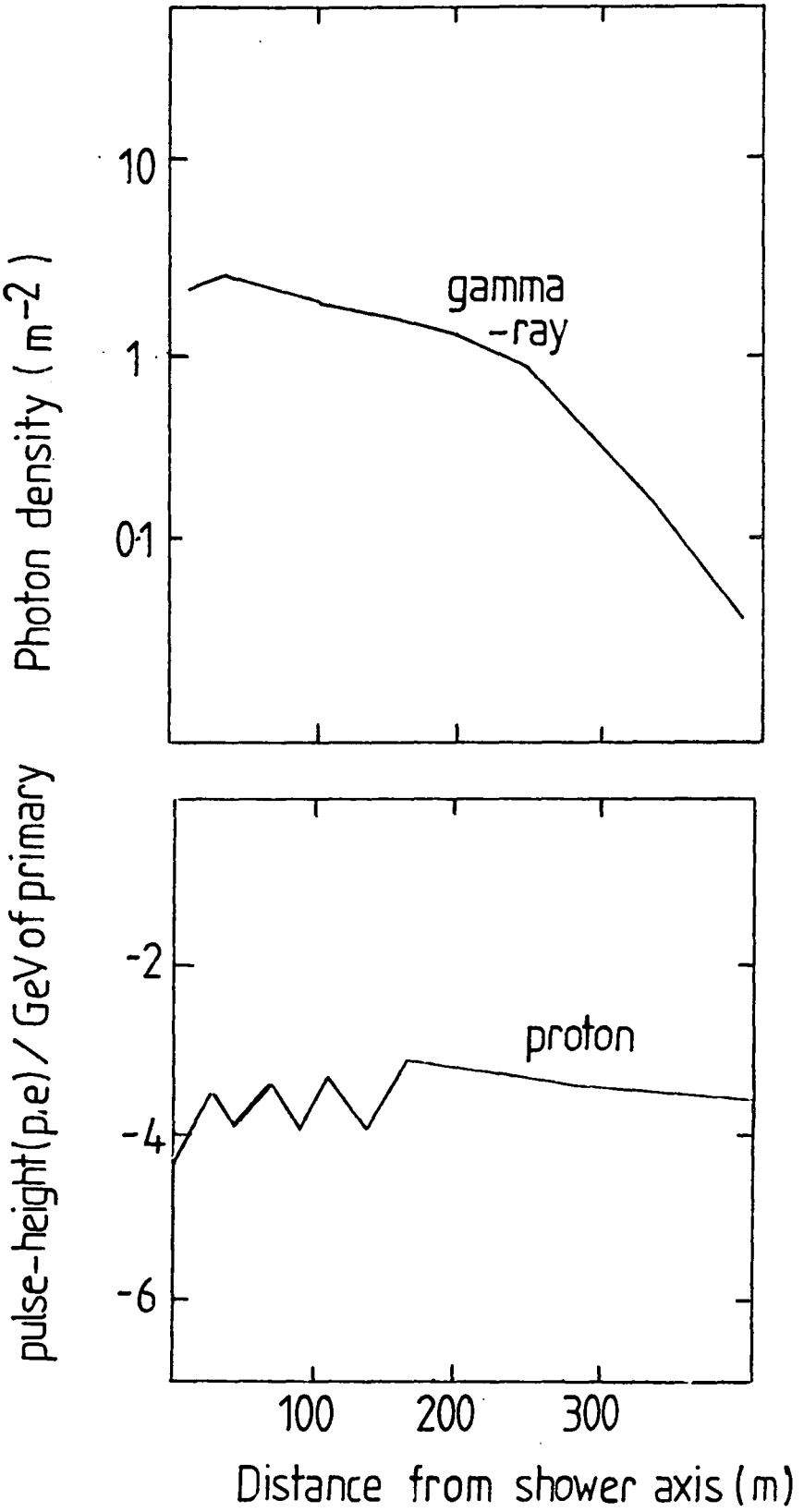

Figure 2.7: The lateral distribution of the Cerenkov radiation from a 1000 GeV gamma-ray and proton initiated cascade, derived from Monte-Carlo simulations.

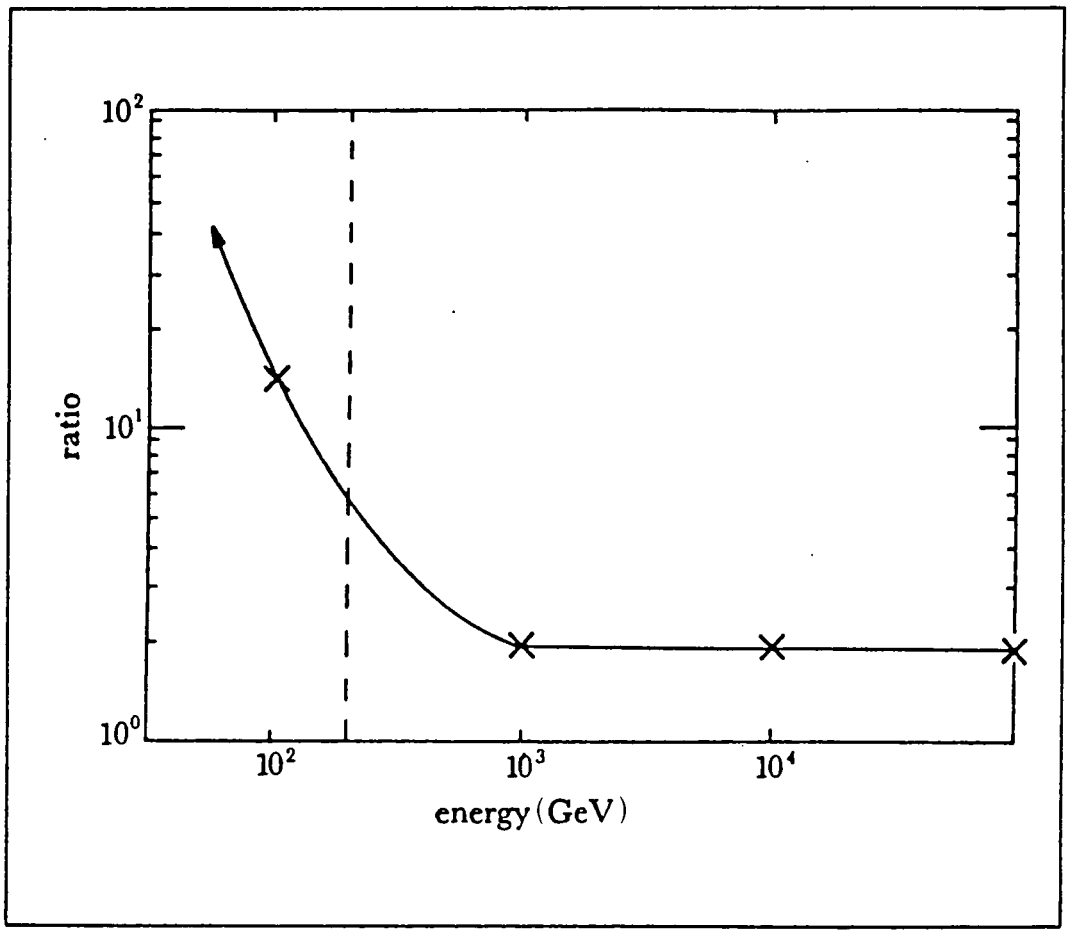

Figure 2.8: The ratio of the Cerenkov light yield from a gamma-ray initiated cascade to that from a proton cascade.

The typical lateral distributions for a 1000 GeV proton and a 1000 GeV photon are given in fig. 2.7. Perhaps the most significant result for Gamma-ray astronomy concerns the ratio of Cerenkov light from gamma-ray to that from proton showers of the same energy - see fig 2.8. This ratio is constant at ~ 2 for energies > 1000 GeV (the gamma-ray cascade is more efficient at producing Cerenkov photons) but as the energy falls below 1000 GeV this ratio rises dramatically. For a proton initiated shower most of the Cerenkov light comes from the secondary cascade of pions. Two-thirds of the energy goes to charged pions which may undergo collision or decay to muons. Muons are relatively poor Cerenkov emitters and the shape of fig. 2.8 can be explained as the probability of decay is increased at lower energy. The advantages for Gamma-ray astronomy of thresholds lower than 1000 GeV are obvious.

2.4.2: The Zenith angle distribution of the Cerenkov light intensity.

To understand the response of ground based Cerenkov detectors a knowledge of the variation of the pulse intensity with zenith angle is needed. This distribution was investigated at an early stage, and was found to depend markedly on the sensitivity and field of view of the detector. However, it has been shown that for a system of narrow field of view (a few °), the distribution takes the form,

$$N(Z) = \cos^{N} Z \qquad - 2.4$$

where N = (2.5 +/- 0.5) and Z is the zenith angle (Galbraith and Jelley, 1955).

This is appreciably flatter than the known distribution of particles from an E.A.S. surviving to ground level. This effect has

important implications for the observation of celestial objects, and generally restricts useful work to zenith angles < 45°.

2.5: Cerenkov light detectors.

A major improvement to the simple detectors used in the first experiments can be achieved by the use of fast coincidence between the mirror-phototube units. The careful application of this technique can reduce the effect of the fluctuations in the night sky brightness allowing only the Cerenkov pulses to be detected within the ~ 10 ns time-gate.

Improvements are also obtained by varying the combination of detector area, A, quantum efficiency, e, field of view, F and integration time, T of the electronic system. It can be shown (Porter and Weekes, 1978) that the ratio of signal/noise in the detector will be proportional to,

$$(A.e / F.T)^{1/2} \qquad - 2.5$$

Detector collecting area, A.

The original experiments were conducted using searchlight mirrors with apertures in the range 0.6 - 1.5 m, low f-ratios (f/0.5), and poor optics. Though very useful work can be done with such systems, efforts have been made to find an inexpensive method to produce more suitable mirrors.

The optical quality of the mirror is not critical but high reflectivity is important. In particular, the use of polished aluminium has been investigated, as this is more reflective than silver at the wavelengths where the Cerenkov spectrum peaks - this is discussed in greater detail in section 3.8.1.

The largest reflector, purpose built for Atmospheric Cerenkov work is the 10 m^2 Mount Hopkins telescope which operates at an energy threshold of ~ 100 GeV.

The field of view of the detector.

There is an optimum field of view for the normal operation in Gamma-ray astronomy (the search for emission from a point source). A particular combination of phototube and mirror f-number is needed, and the resulting field of view is generally chosen to lie in the range 1.1 - 3 °. In general the field of view for normal operation should be chosen to be close to the angular spread of the peak of the Cerenkov flash (> 1.1°).

The photomultiplier tube and detector electronics.

Most modern experiments use phototubes with cathodes efficient in the blue and ultraviolet regions i.e. optimising the performance at the strongest wavelengths in the Cerenkov spectrum.

The width of the Cerenkov pulse is dependent on the primary energy of the cascade and also the altitude of the observing site, as well as the field of view of the detector. For effective operation the electronic system should have integration times not much larger than the width of this pulse.

Details of the system used in the Durham University gamma-ray facility are given in the next chapter, including the refinements made to the design and optics over the last few years.

2.6: Gamma ray observations.

As it is not possible to directly distinguish gamma-ray and proton initiated showers, methods have been developed to extract the gamma-ray signal.

The two standard methods, used in the observations for this work are the 'drift-scan' and 'tracking' techniques described in Chapter 4. However, a number of other techniques have been developed and these are briefly reviewed below.

i: Fast annulus

The Cerenkov emission angle from gamma-ray showers changes within the first few radiation lengths, effectively focussing the light to an annulus of ~ 120 m radius about the shower axis. The pulse width is very short ~ 3ns , and an array of fast, narrow field of view detectors is expected to be biased in favour of detecting these showers. This technique has been used by at Glencullen (Fegan et al, 1968), but unfortunately reduces the effective collecting area of the array limiting its effectiveness.

ii: Array of detectors sampling the lateral distribution

With detectors spaced ~ 50 m apart the lateral distribution of the Cerenkov pulses can be investigated by studying the pulse height spectra in the detectors. This system has been developed by a group working at Maryland College (Tornabene, 1977).

iii: The double beam technique

If two detectors have their optic axes inclined to intersect at the shower maximum altitude - an increase in the coincidence rate is expected. This technique has been extended to include a second intersection at a lower altitude (Grindlay, 1971). A further enhancement of the coincidence rate is observed at this lower altitude and is interpreted as being due to the penetrating component of the nucleon induced showers (muons). With the two systems running in anticoincidence, a rejection of proton showers is possible. There is, however, a disadvantage, since this technique is only applicable to energies $> 10^{13}$ eV when a considerable number of muons are produced.

iv: Fast timing

The standard E.A.S. technique of inter-detector fast timing can be adapted to V.H.E. Gamma-ray astronomy. It is possible to resolve within the field of view of an array of detectors by examining the relative time of arrival of the shower front at each detector. Off-axis showers are then rejected as likely background. This technique has been used by the University of Maryland group (Tornabene and Cusimano, 1968) and was demonstrated in observations of the Crab pulsar by the Dugway array (Walmsley, PhD thesis in preparation).

v: The Whipple Observatory Imaging telescope.

The 10 m^2 optical reflector at the Whipple Observatory has been adapted for use as an imaging instrument. A 'Camera' consisting of 37,

5cm diameter phototubes is placed at the focus of the reflector. Each phototube provides a 0.36° pixel within the overall field of view of 3.5°, and so allows an image of the Cerenkov flash to be recorded.

An observation consists of i. tracking the region of the sky containing the object of interest and ii. performing a similar tracking observation of a region of the sky displaced 30 minutes in Right Ascension from the object (same zenith and azimuth range as i.). In this way a background estimation is possible.

Several Monte-Carlo simulations of the performance of the 'Camera' have been made, but with differing conclusions (Cawley et al, 1985a). The data analysis involves a software selection of events based on the results of such simulations. For instance, a selection of narrow angular width events as candidate gamma-ray initiated flashes was suggested by simulations performed at Leeds University, but other selections have also been used.

The telescopes effective energy threshold is estimated to be ~ 200 GeV with a gamma-ray collecting area of ~ 10^4 m^2.

vi: The Haleakala telescope.

The Universities of Hawaii, Purdue, Athens and Wisconsin operate a highly sensitive telescope with an energy threshold lower than 300 GeV. The instrument is situated at Haleakala, Maui, Hawaii and began operations in June 1985. The telescope has a 10 m^2 mirror and has an narrow aperture of 0.5°. Simultaneous observations are made of the object and a position displaced 3.6° in declination to allow a measure of the 'off-source' background. The essential feature of this telescope is the software selection of events. Each photoelectron is counted and chance fluctuations leading to coincidence are removed in the software analysis. This system allows energy cuts to be made at

the software stage and is expected to provide important results for V.H.E. Gamma-ray astronomy, (Resvanis et al, 1986).

The large numbers of experiments designed to investigate the Cerenkov effect for use in Gamma-ray astronomy are reviewed in table 2.1. The table indicates the wide interest in this technique since the early 1960's. It is unfortunate that many experiments have not achieved the significant increase in sensitivity for gamma-rays expected from the methods described above.

In all Cerenkov work the problem of the high proton background remains, making the identification of a source of gamma-rays very difficult. It is therefore essential to establish a database of observations, free from systematic effects, and to derive a series of suitable analysis procedures. Despite the special problems associated with work in this energy region, there is an increasing number of V.H.E. gamma-ray sources detected by many groups.

ATMOSPHERIC CERENKOV EFFECT EXPERIMENTS.

Institution	Location	Epoch	Reflector (No. x size /m)	Field of view (1/2 angle in deg)	Energy Threshold (GeV)
A.E.R.E. U.K.	Pic du Midi	1953	2 x 0.61	2.2 4.9	10,000
Lebedev Inst. U.S.S.R	Crimea	1960-64	12 x 1.5	1.75	5,000
A.E.R.E. + U.C.D.	Glencullen	1964-65	2 x 0.9	2.5	5,000
A.E.R.E. + U.C.D.	Glencullen + Malta	1966-70	4 x 0.9	0.5	2,000
Woodstock College	Maryland	1966-67	4 x 0.9	0.5	2,000
Smithsonian Inst. U.S.A	Mt. Hopkins (1.2 km)	1967-68	2 x 1.5	0.6	2,000
Smithsonian Inst. U.S.A	Mt. Hopkins (2.3 km)	1968-72	10	0.5	100
A.E.R.E. U.K.	Harwell	1968-69	2 x 0.9	1.5	13,000
Tata Inst. India	Mukurthi	1969-70	2 x 0.9	1.5	10,000
Crimean Astrophys. Obs., U.S.S.R	Crimea	1969-	4 x 1.5	0.9	2,000
Univ. of Sydney Australia	Narrabi	1968-69	2 x 6.5	0.6	1,000

Table 2.1: A selection of Gamma-ray experiments using the the 'Cerenkov Effect'.

Institution	Location	Epoch	Reflector (No. x size /m)	Field of view (1/2 angle in deg)	Energy Threshold (GeV)
Smithsonian Inst. U.S.A	Mt. Hopkins (2.3 km)	1970-72	3 x 1.5	0.5	1,000
Smithsonian Inst. U.S.A	Mt. Hopkins (2.3 km)	1972-74	1.5 + 10	0.5	700
U.C.D. Ireland Smithsonian Inst. U.S.A	Mt. Hopkins (2.3 km)	1972-73	2 x 1.5	2.5	5,000
Univ. of Sydney Australia Smithsonian Inst. U.S.A	Narrabri	1972-74	2 x 6.5	0.5	200
Smithsonian Inst. U.S.A	Mt. Hopkins (2.3 km)	1974-75	10	3 x 0.5 7 x 0.5	1,000
Iowa State Coll. U.S.A	Ames	1975	32 x 0.6	1.2	20,000
Bowie State Coll. U.S.A	Maryland	1972-75	10 x 1.6	7 x 3	10,000
Smithsonian Inst. U.S.A	Mt. Hopkins (2.3 km)	1974-77	10	10 x 0.5	200

Table 2.1: Continued.

Institution	Location	Epoch	Reflector (No. x size /m)	Field of view (1/2 angle in deg)	Energy Threshold (GeV)
Tata Inst. India	Ootacamund	1976-	10 x 0.9	0.5	500
Lebedev Inst. U.S.S.R	Tien Shan	1979-	2 x 1.2	-	1000
Durham Univ., U.K.	Dugway	1981-85	12 x 1.5	1.1	1000
Univ. of Hawaii, Purdu + Wisconsin	Haleakela	1986-	6 x 1.5	0.25	200
Durham Univ., U.K.	Narrabri	1986-	2 x 3.6	0.5	240
Univ. of Potchefstroom	Potchefs-troom		9 x 1.5	1.1	1400
Smithsonian Inst. U.S.A U.C.D., Hawaii, Iowa	Mt. Hopkins (2.3 km)	1984-	3.0 + 10	0.5	<100
Univ. of Adelaide	White Cliffs	1986-	3 x 5	2	5000

Table 2.1: Continued.

Chapter 3: The Dugway Experiment.

3.1: Introduction.

The Durham University V.H.E. Gamma-ray astronomy group conducted observations from May 1981 to October 1984 using an array of specially designed telescopes. In addition, this original array was used as a testing ground for the new generation of V.H.E. instrument discussed in section 3.8.

This chapter will describe the details of the Mark I detector which was used throughout the experiment. The Mark II detector - an improved telescope which replaced one of the older detectors after July 1983 will also be discussed. The development of a completely new Mark III system destined for operation in the Southern hemisphere will be described. In particular, the improvements in the optics of the Mark II and III telescopes will be explained.

3.2: The Choice of array dimension.

The arrangement of the four detectors is shown in fig. 3.1. They were placed at the apices and centre of a 100 m equilateral triangle. This arrangement was based on detailed computer simulations of the Cerenkov flash expected from a 1000 GeV gamma-ray (Macrae, 1985). There are conflicting requirements for the inter-detector spacing. The advantages of operating widely spaced (> 100m) detectors include increased overall counting rate, as the detectors count independently. However, in a system designed for fast inter-detector timing a closer spacing is appropriate. The variation of the overall sensitivity and angular resolution with detector spacing is shown in fig. 3.2. (This

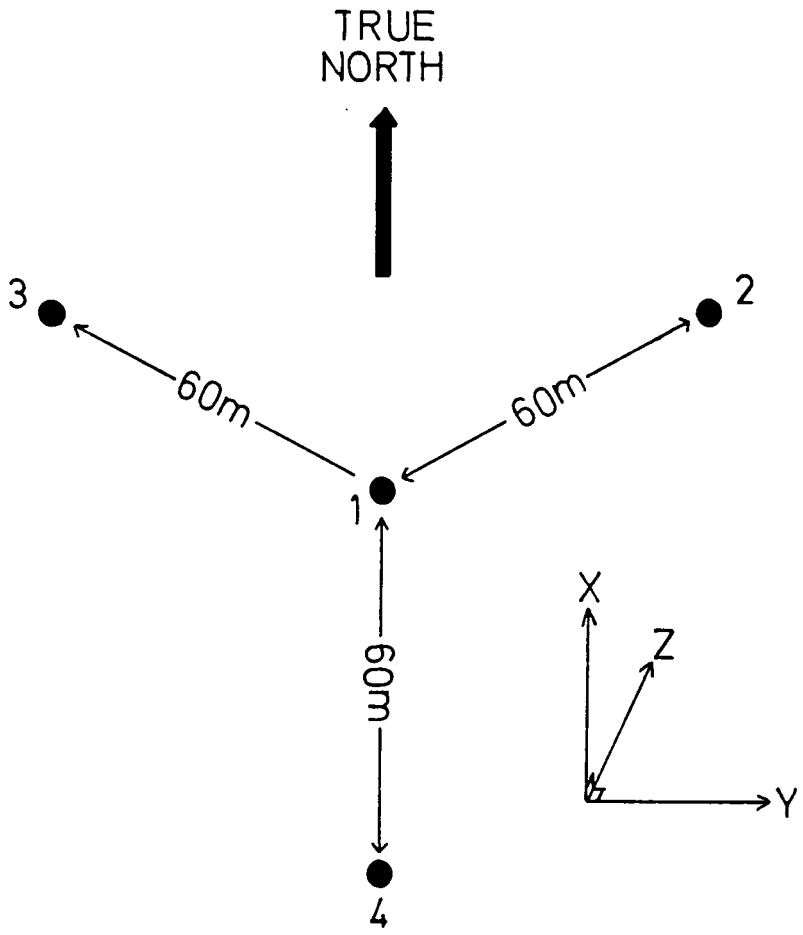

Figure 3.1: The arrangement of the four telescopes making up the Dugway array.

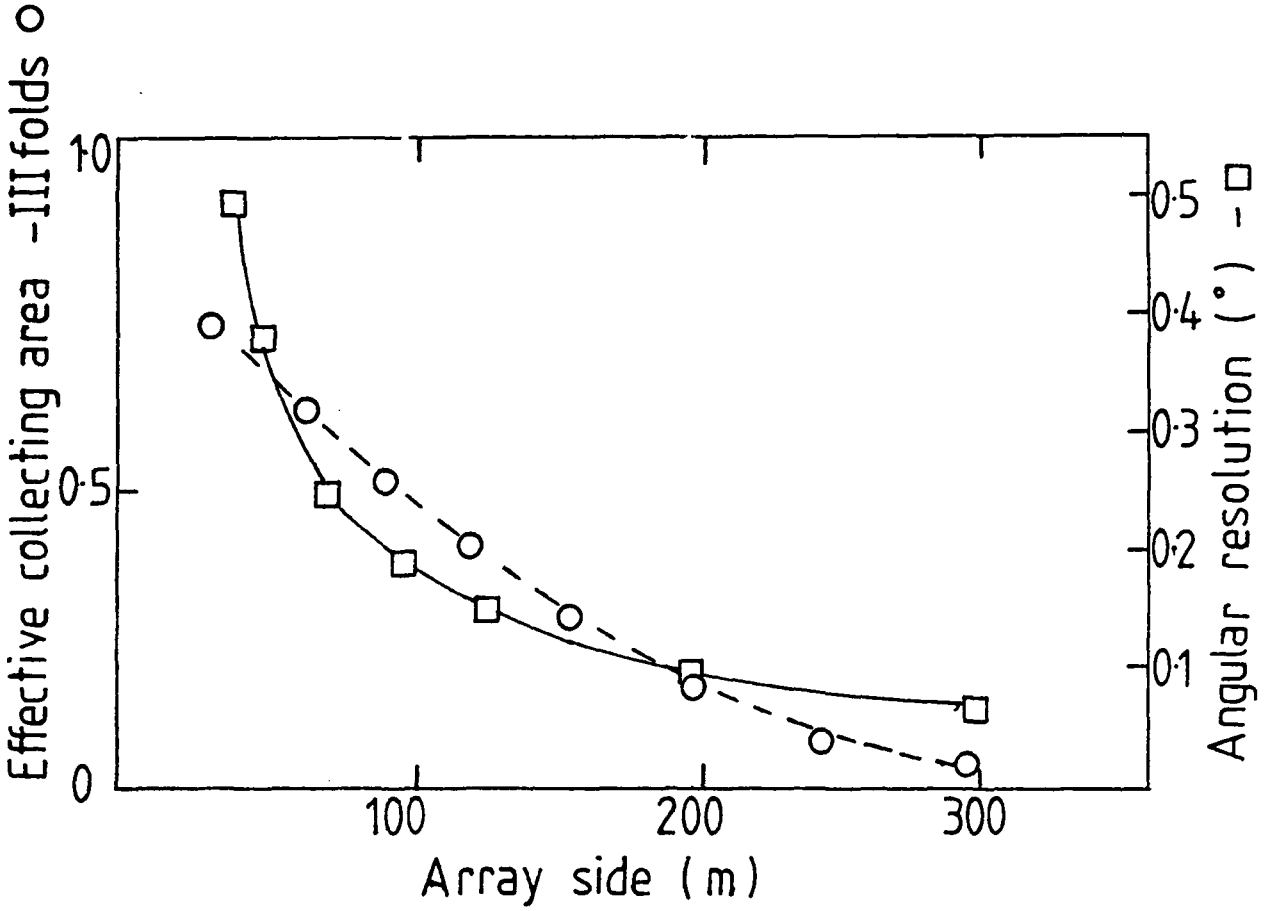

Figure 3.2: The variation of overall sensitivity and angular resolution with telescope spacing (adjacent telescopes).

figure is plotted for a simplified array of 3 adjacent detectors). Small spacing gives a large effective collecting area for the multiple fold events i.e. those triggering more than one detector. A larger spacing gives increased angular resolution from the inter-detector timing within the field of view, up to a maximum value after which the detectors start to operate independently.

A compromise spacing of ~ 60m was chosen for each outer-central detector combination. This leads to an angular resolution of ~ 0.2 °, and a threefold collecting area of ~ 0.5 of the maximum.

The operation of the array was controlled with an electronic system housed in a caravan situated close to the central detector (detector 1). The telescopes were usually operated by two observers using observing methods described in Chapter 4.

3.3: The Mark I telescope.

Each telescope in the original Dugway array consisted of three 1.5 m diameter paraxial parabolic searchlight mirrors. Each mirror focussed the Cerenkov light flash with Cassegrain optics onto a phototube. The whole telescope, 3 mirror-phototube systems, was operated in 3-fold coincidence and was computer steered on an alt-azimuth mount. The detector power supplies and the necessary cable junctions were enclosed in a weather-proof 'mother-box' placed a few metres to the side of the telescope. A number of useful features were built into the box, a telephone link to the control centre, a number of spot lights and a manual override to the detector steering.

A photograph of the Mark I telescope is given as figure 3.3. Cables ran from the 'mother box' to the central control room - a caravan which housed most of the electronics, a Tektronix 4051 computer, the recording device and the power transformers.

The telescope was supported by a robust concrete plinth, with an

Figure 3.3: The Mark I telescope.

aluminium framework holding the mirrors. It was steered in azimuth by a geared DC motor and was supported on three bearings. Movement in altitude was achieved using another rack mechanism and DC motor. The mirrors were held to the structure by six aluminium pads and six brass ball joints - see fig. 3.3. This system was suggested by Grubb Parsons Ltd. to reduce image distortion for all telescope orientations as the mirror weight would always act through its centre of gravity.

3.3.1: The Optical system.

The searchlight mirror system was far from ideal for this type of work, but similar large aperture telescopes with relatively poor optics had been used to good effect in the past (Jelley and Porter, 1963). For reasons of convenience and cost they were chosen for the Mark 1 facility. The optics are summarised in fig. 3.4.

Each primary mirror had an f-number of 0.43 and was made from electroformed brass, plated with rhodium.

A Cassegrain system was used to provide a more appropriate size of aperture for the 5" phototube chosen for this system. In addition, by choosing such an arrangement, there was a reduction in reflection off the photocathode - although losses in intensity at the secondary (~20%) worked against this. The secondary mirror was 12" in diameter and was made of aluminium.

The whole system defined a physical aperture to a point source of ~ 1.75° at Full Width Half Maximum (F.W.H.M.) - see section 3.5.5. The estimated overall reflectivity of the system was 65% at 500 nm.

The image size was found to be ~ 2 cm in diameter for a point object, and suffered large aberration, but was adequate for this type of work. The 5" fast photomultiplier tube was placed ~ 8 cm behind the focal plane, in a protective plastic tube. This ensured a defocussed

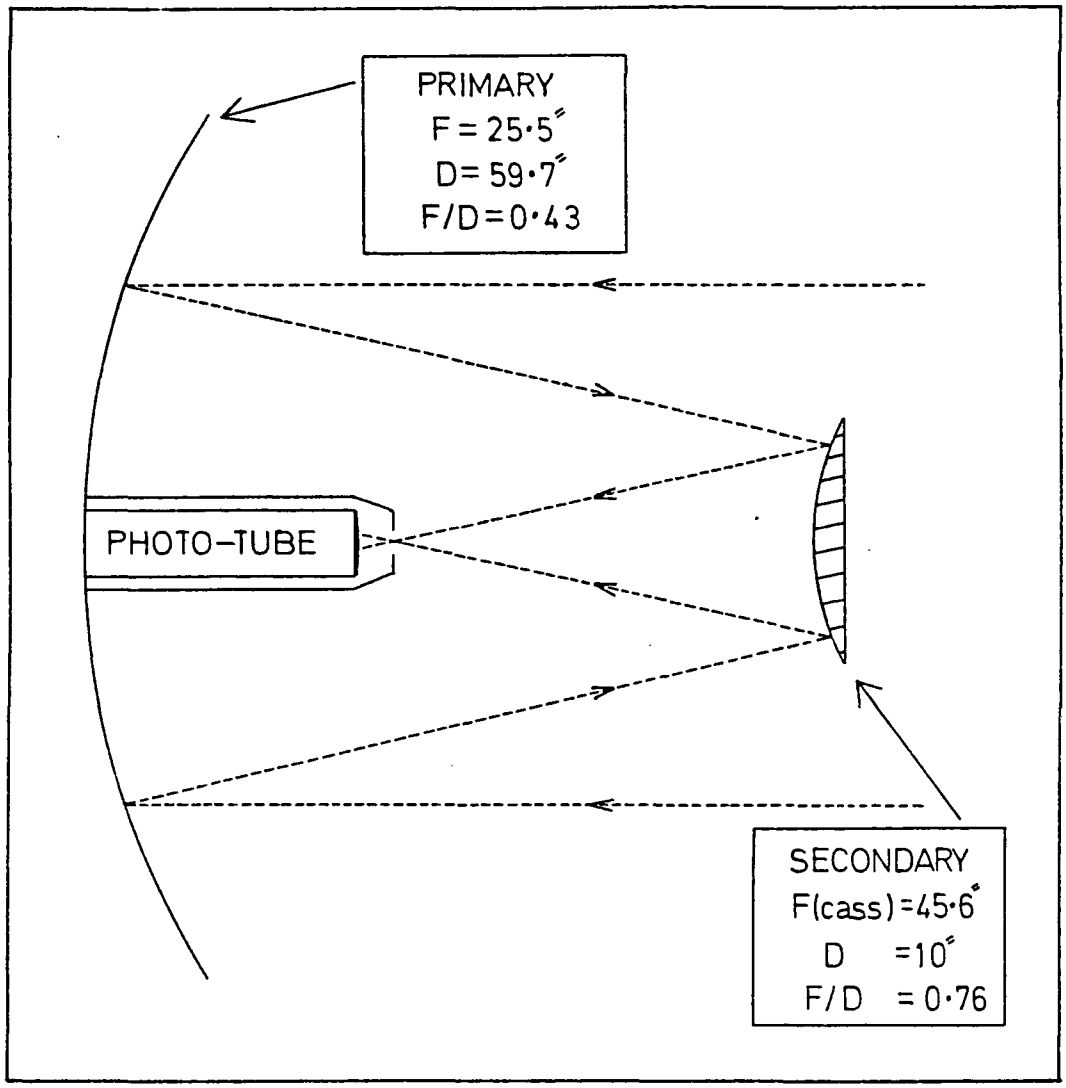

Figure 3.4: The Mark I telescope optical system.

image with no differential gains arising from stellar images on the photocathode (these would distort the electron optics). The problems caused by stray light from the night sky were reduced by using cylinderical baffles to surround the secondary mirrors.

3.3.2: Steering control.

Steering accuracy was achieved using incremental shaft encoders attached to the altitude and azimuth gears. The altitude encoder was used in conjunction with a pendulum attached to the telescope structure defining the vertical direction. Computer control of the telescope pointing was provided by a Tektronix 4051 computer situated in the control centre, and via four 'MOSTEK F8' microprocessors, one dedicated to each detector. A steering accuracy of better than 0.1° was expected. Magnetic cut-outs to the DC motors provided protection against steering past certain points, preventing motor damage if the telescope steered past altitude = 0, and cable damage for continuous steering in azimuth. As an extra precaution against high winds a number of clamps and pegs were fitted.

3.3.3: The photomultiplier system.

A suitable photomultiplier for the system was the RCA type 4522 (12.5 cm diameter), linear focussed tube which was fast and had a bialkali photocathode. Among the other characteristics of this phototube include a relatively high quantum efficiency of ~ 15% in the wavelength range of the Cerenkov flash. The tube was placed in a weatherproof plastic tube, behind a thin 'MYLAR' sheet, and was magnetically shielded by a mu-metal cylinder held at the cathode potential. The photomultiplier system was operated at a typical E.H.T. voltage of 1800 V to give the fast performance needed. Adjustment to

this value was possible at the 'mother box' which housed the EHT units. In the normal operating conditions only 11 dynodes were used, resulting in a gain of ~ 50,000. The anode currents of the working system were typically 5 μA at a telescope rate of ~ 10 kHz. The discriminator level was set to correspond to a threshold intensity of ~ 50-100 photons.m^{-2}. The response of the tubes was sufficiently fast in these operating conditions with the rise time corresponding to ~ 2 ns for a pulse of F.W.H.M. ~ 5 ns. As the 3 mirror-phototube systems operated in 3-fold coincidence, an almost accidental free signal was provided.

3.3.4: The Automatic Gain Control system.

The A.G.C., or 'Automatic Gain Control' system, consisted of a green LED placed in the field of view of each mirror - phototube unit and servoed with a time constant of ~ 10s to the phototube anode current. As the photocurrent varies with sky brightness the dynode voltage varies leading in turn to a varying gain. The A.G.C. system was used to stabilise the photoelectron emission rate (the chance of a random 3-fold coincidence increases with the number of photoelectrons emitted, and a stable rate ensures that a reliable measure of any accidental counts can be made for the observation). For many observations a stable gain was needed, e.g. observations where the suspected source drifted through the field of view (a drift scan) and so the A.G.C. system was used.

The initial measurement of the anode current and the setting of the required intensity of the LED emission was conducted by the Tektronix 4051 computer. Subsequent servoing to this value was carried out by Fairchild '741' operational amplifiers.

A demonstration of the effective operation of the A.G.C. system is given as fig. 3.5. In this observation the telescopes scanned the

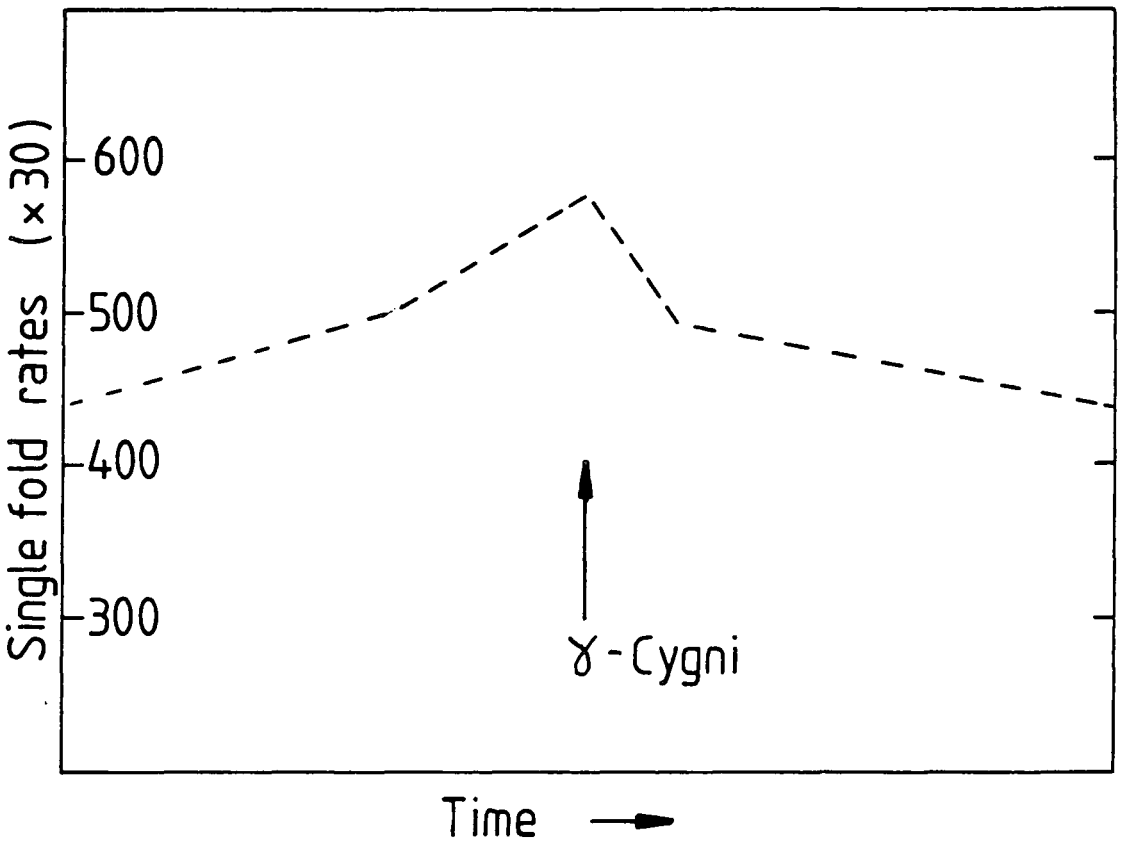

Figure 3.5: The variation of the photoelectron emission rate as γ-Cygni drifted through the telescope's field of view.

Galactic plane, with the 2nd magnitude star γ-Cygni entering the field of view. The plot of the rate of photoelectron emission from one of the phototubes in detector 3 indicates the stability of the system to this changing night sky background.

3.3.5: The Night-time TV Cameras.

Each telescope had a paraxial, highly sensitive night-time TV camera ('C.C.T.V.' camera) mounted on the aluminium structure. These cameras monitored a region of the night sky ~ 5° square about the source. They were sensitive to 5th magnitude stars and allowed a convenient check to be made on the detector steering from the control centre. In addition, each detector could be viewed in daytime from the caravan using less sensitive cameras mounted on nearby posts.

3.3.6: The transfer of data to and from the control room.

The basic cabling system is outlined in fig. 3.6. Short cables lead from the telescope to the 'mother box' junctions, and from the box along elevated cable runs to the control centre. In addition to supply cables the cabling system consisted of;

i. 3 heavy coaxial cables carrying the phototube signal to the control electronics.

ii. 3 medium weight coaxial cables; the EHT control from the centre.

iii. There were 8 steering cables, 4 to drive the motors, and 4 from the drive sensors.

iv. A 12-way signal cable including links to the TV cameras, the A.G.C. cables and various measures of the phototube performance.

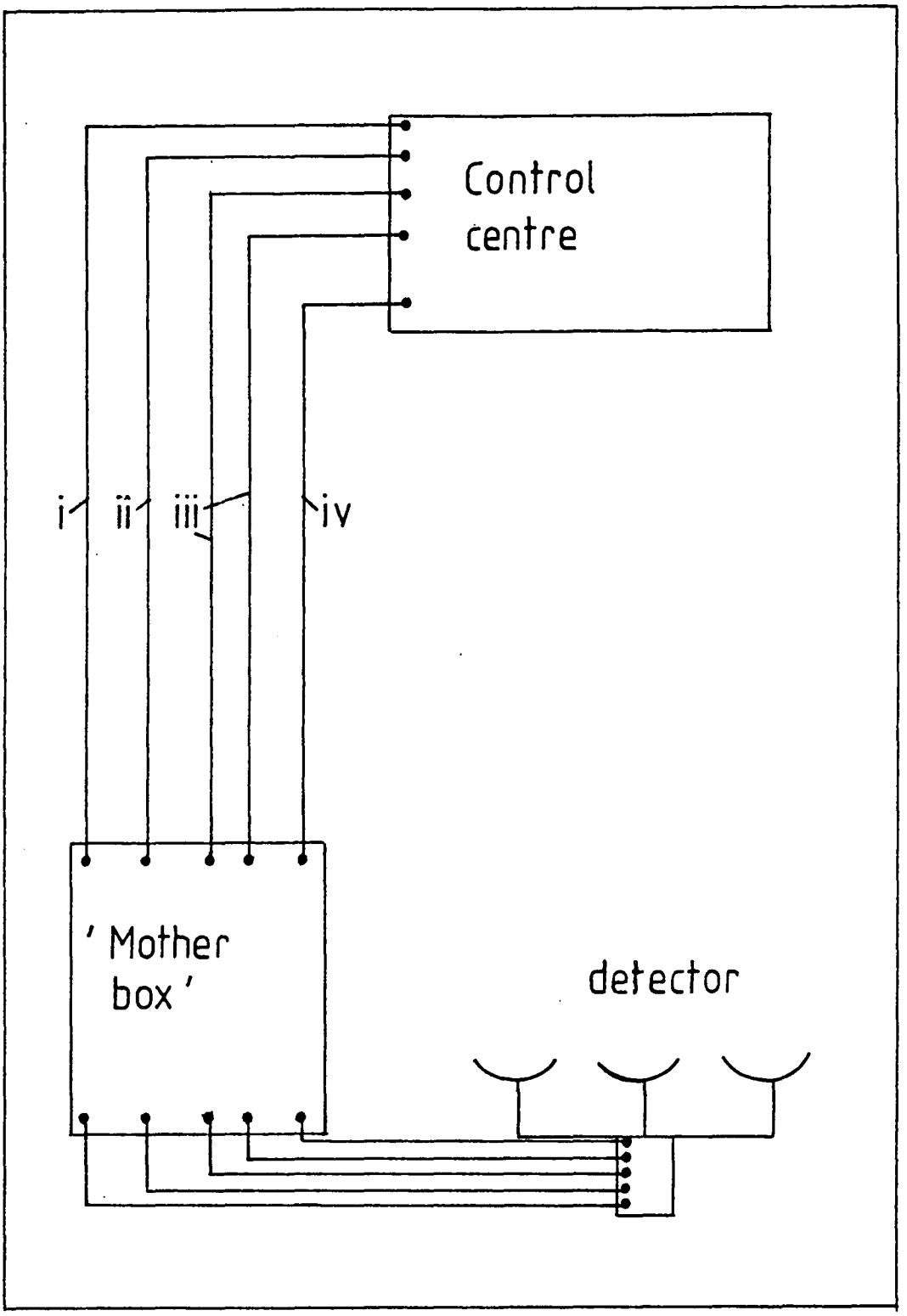

Figure 3.6: The Mark I telescope cabling arrangement.

(i - iv, refer to the text).

3.4: The electronic system.

3.4.1: Amplification and discrimination.

The electronic pulse from each photomultiplier was 'fed' to a LeCroy 'VV100' amplifier which gave an amplification by a factor 10 and fed the signal to a dual level discriminator system. In Cerenkov work, and especially in systems aiming to utilise fast inter-detector timing, it is important to use initial amplifiers and discriminators with short rise times, with suitable values corresponding to a few ns. The high level discriminator unit 'accepted' pulses of peak voltage > 100 mV, thereby removing much of the low level noise in the individual phototubes. The output from these three discriminators entered a coincidence unit. Each phototube needed to record a sufficiently large pulse for the event to be processed further. By using the three-fold coincidence within a 10 ns timegate, the accidental rate could be reduced to near zero.

The pulses from the three photomultiplier tubes entered the low level discriminator and were first 'fed' through a 'mixing unit' to improve the signal. The mixing resulted in much less 'jitter' on the pulse entering this unit compared with the pulse processed by the high level discriminator. Because of the relative stability of this pulse it was used by the inter-detector timing system.

3.4.2: The charge-to-time converters (LeCroy QT100B's).

After a 3-fold coincidence, the charge in the pulse was measured. The measurement was made, after the amplification and high level discrimination stages, by the LeCroy charge-to-time converters ('QT100B's'). From the converter the measured charge output was sent

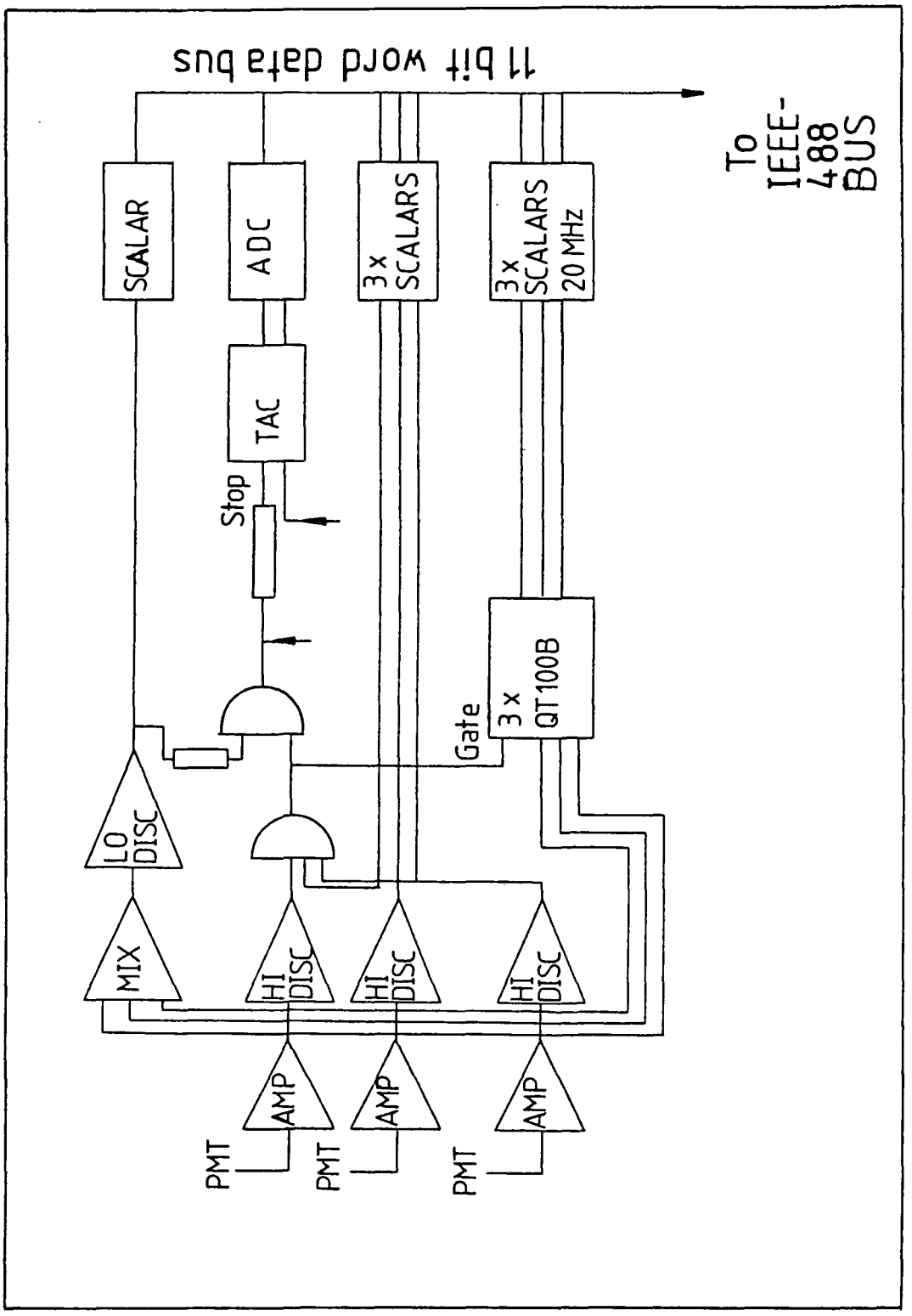

Figure 3.7: The Mark I telescope electronic system.

to an 11-bit scalar, and from there to the data bus - see fig.3.7.

The charge was measured over the range 0-256 pC with a resolution of 0.1 pC. The full output duration for a charge of 256 pC corresponded to 50 microseconds.

3.4.3: The Time to Amplitude converters (T.A.C.'s).

The relative arrival times of pulses detected in other telescopes within a set time interval were also recorded. These measures were used in the inter-detector timing analysis to provide information on the arrival direction of the shower. The electronic arrangement is shown in fig. 3.7. If any detector registered a coincidence, then all the Time to Amplitude Converter (T.A.C.) units commenced counting and stopped as their parent detectors registered the same shower. The stop pulse was developed from the low level discriminator. In this way the relative time delay across the array could be noted. If a detector did not record the shower then the T.A.C. unit was stopped and automatically reset after a delay of 200 ns. The dual level discrimination was employed to allow an accurate measure of the relative timing. The 'jitter' at the start of the measure was large - as the discrimination was set near the top of the pulse, but this was unimportant since the T.A.C.s started simultaneously. The low level discrimination on the stop pulse allowed a much more accurate response to the Cerenkov pulse. This was all done to an estimated timing resolution of 1 ns.

In addition to the inter-detector fast timing and pulse charge measures, the individual photomultiplier tube anode currents and photoelectron production rates were digitised. The outputs from temperature and atmospheric pressure sensors were also recorded.

Each digital output was sent to the 11-bit data bus and sampled by a MOSTEK F8 microprocesser with each 3-fold trigger.

With each event the time was noted to microsecond accuracy.

3.4.4: Data control and recording.

The schematic description of the control system is shown in fig. 3.8. The Tektronix 4051 computer provided the essential control and monitoring system for the array. The controlling computer and the MOSTEK F8 microprocessors, which acted as controllers to the data stream, were placed on an IEEE-488 bus along with the recording device - a 9-track magnetic tape unit, and a printer. The eight MOSTEK F8 processors were dedicated to the following operations;

i. The steering for each detector was controlled by the Tektronix computer in conjunction with processors P1 - P4 (see fig. 3.8).

ii. The Automatic Gain Control system was controlled by P5. This processor gave digital-to-analogue conversion (DAC), with 12 of the 16 channels running the A.G.C.

iii. A separate processor P6 was used to control the dot-matrix printer which provided a summary of the array performance at intervals of ~ 2 minutes throughout an observation.

iv. P7 represents the important processor which communicated with the data bus. Its main purpose was to compile the data record to be passed back along the IEEE - 488 bus to the 9 - track tape via an eighth processor P8.

3.4.5: The Crystal clock.

The relative timing system used in the Dugway array was based on an oven-stabilised 1 MHz crystal clock. The oscillations were regularly checked against a standard timing signal from Fort Collins, Colorado.

The calibrations and checks made on this clock unit formed an important part of each months observing program and will be reviewed in the next section. Each event was recorded to an accuracy 1 μs.

3.5: Calibrations of the system.

For an effective analysis of the data produced from this system a series of preliminary calibrations were needed. These procedures are described in the next sections.

3.5.1: Calibration of the crystal clock.

The crystal clock was initialised using a standard radio signal broadcast at 5, 10 and 15 MHz by the 'WWV' radio station at Fort Collins in Colorado, over 600 miles from the Dugway array. The timing signal consisted of 50 second tics for each minute, with 5 cycles of a 1 kHz modulation broadcast on each minute and synchronised to Coordinated Universal Time (U.T.C.). The exact synchronisation with U.T.C. occurred at the front edge of the 5 cycle variation, and this edge was used to initialise the clock unit.

The time of passage of the radio signal from Fort Collins to Dugway varies with atmospheric conditions, as does the quality of the radio signal, and these effects were important in reducing the accuracy of the clock initiation to 0.25 - 0.5 ms. These uncertainties effectively set the absolute timing accuracy of the Dugway experiment.

The Dugway clock was set to run faster than true U.T.C., and the extent of the error was checked regularly against the radio signal. This was done using an oscilliscope triggered by the clock unit whilst displaying the 'WWV' radio signal. The displacment of the radio pulse on the screen was then proportional to the error in the clock unit.

A typical crystal clock 'drift rate' was,

$15.94 +/- 0.02\ ms.day^{-1}$

for the November 1982 observations.

For observations of periodic objects, calibrations should be performed as often as possible, and at least daily to achieve an accurate 'drift rate'. Unfortunately the weather conditions did not always allow a clear radio signal and many months data were taken with accuracies much less than that quoted above.

In observations of sources with fast periods (e.g. the millisecond pulsar, 4C21) the clock calibration is most important and ideally only one initialisation should be performed for a months observation. This allows the maximum integration time as the large uncertainties in the initialiation effectively prevent data from different resets being related in time. A more detailed investigation of the crystal clock accuracy is discussed elsewhere (Kirkman, 1985).

3.5.2: Calibrations of the charge-to-time converter units.

Calibration of the charge-to-time units was made through a series of tests which supplied each LeCroy 'QT100B' unit with three pulses of different amplitude, (the pulses were produced by a Farnell pulse generator). The results of these tests are given as fig. 3.9 and show the differing response of each unit, (a) and the relation between the left centre and right hand channels for each detector, (b). These calibrations were sufficient to show that the output from the charge-to-time converter units was directly proportional to the input pulse size, though the response of individual detector units varied for the same pulse.

Further investigation relied on the record of real showers, and indicated a form of response consistent with the calibrations, excepting detectors 2 and 4 (fig. 3.9). Detailed work on the responses of the system has been complicated by the use of different E.H.T.

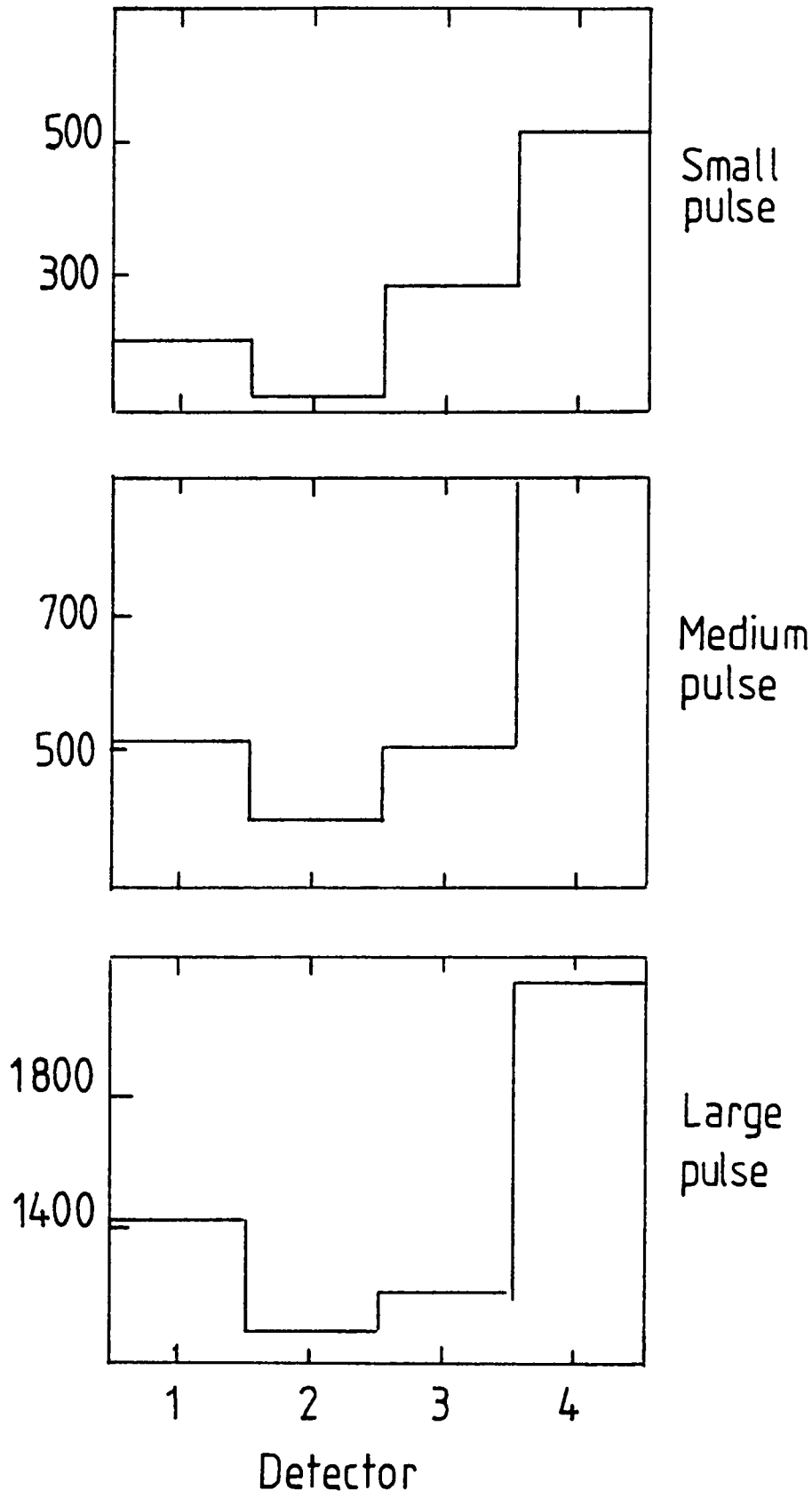

Figure 3.9a: The response of the centre tube of all four detectors to three different sized pulses.

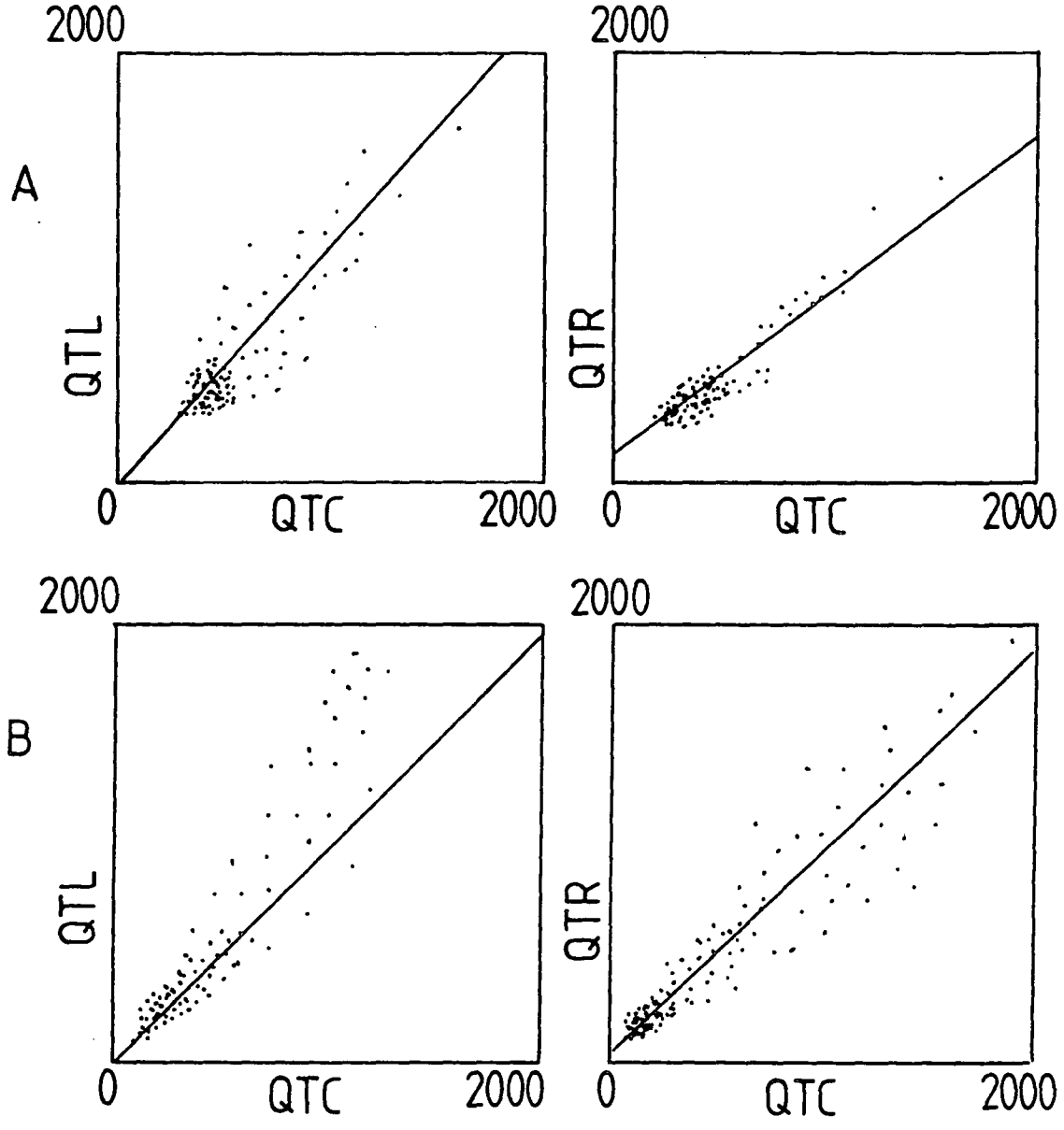

Figure 3.9b: The calibration of the LeCroy 'QT100B' units;
The left and right tubes plotted against the centre tube,
- the data points correspond to real showers.

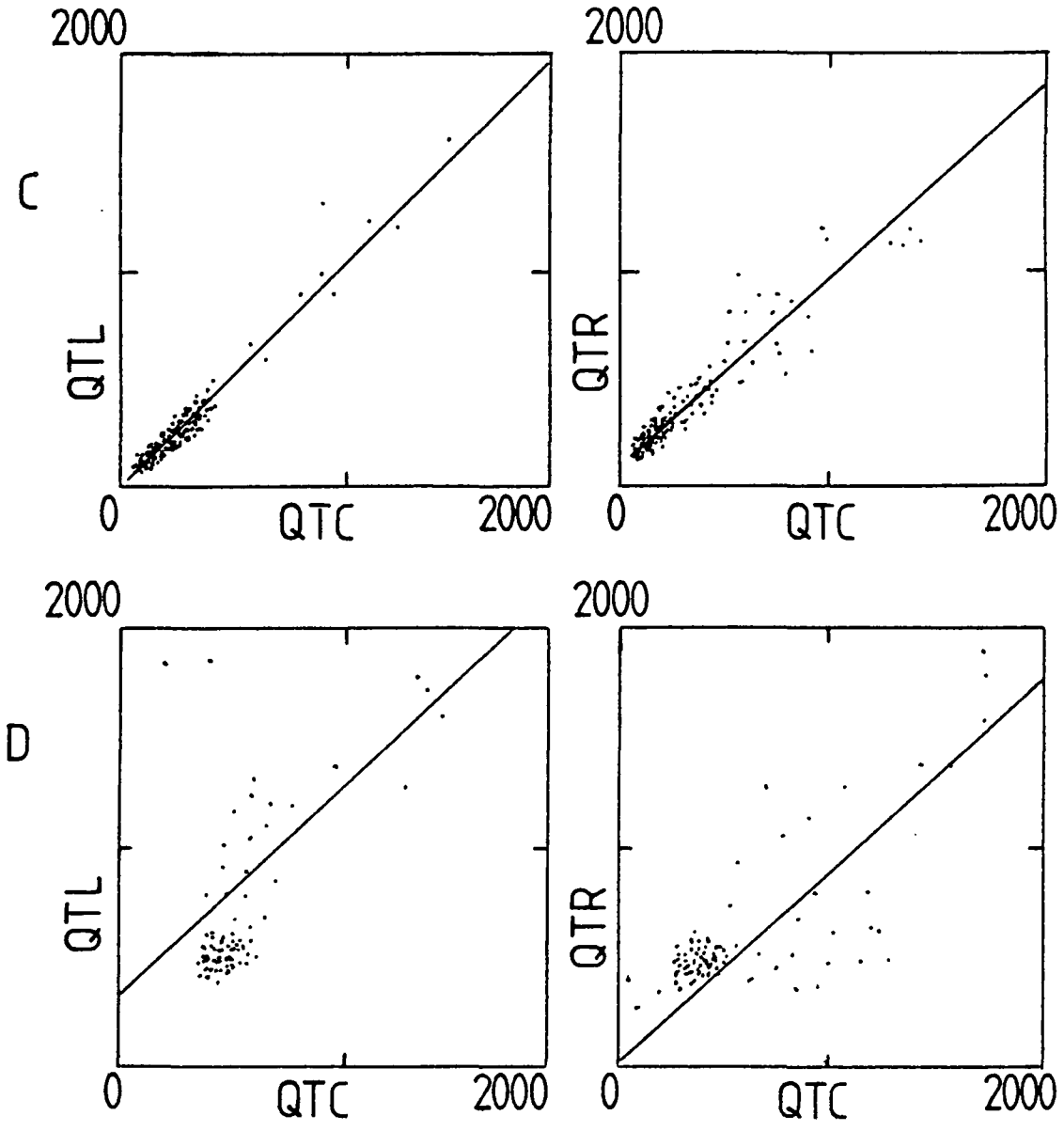

C = detector 3
D = detector 4

Figure 3.9b: continued.

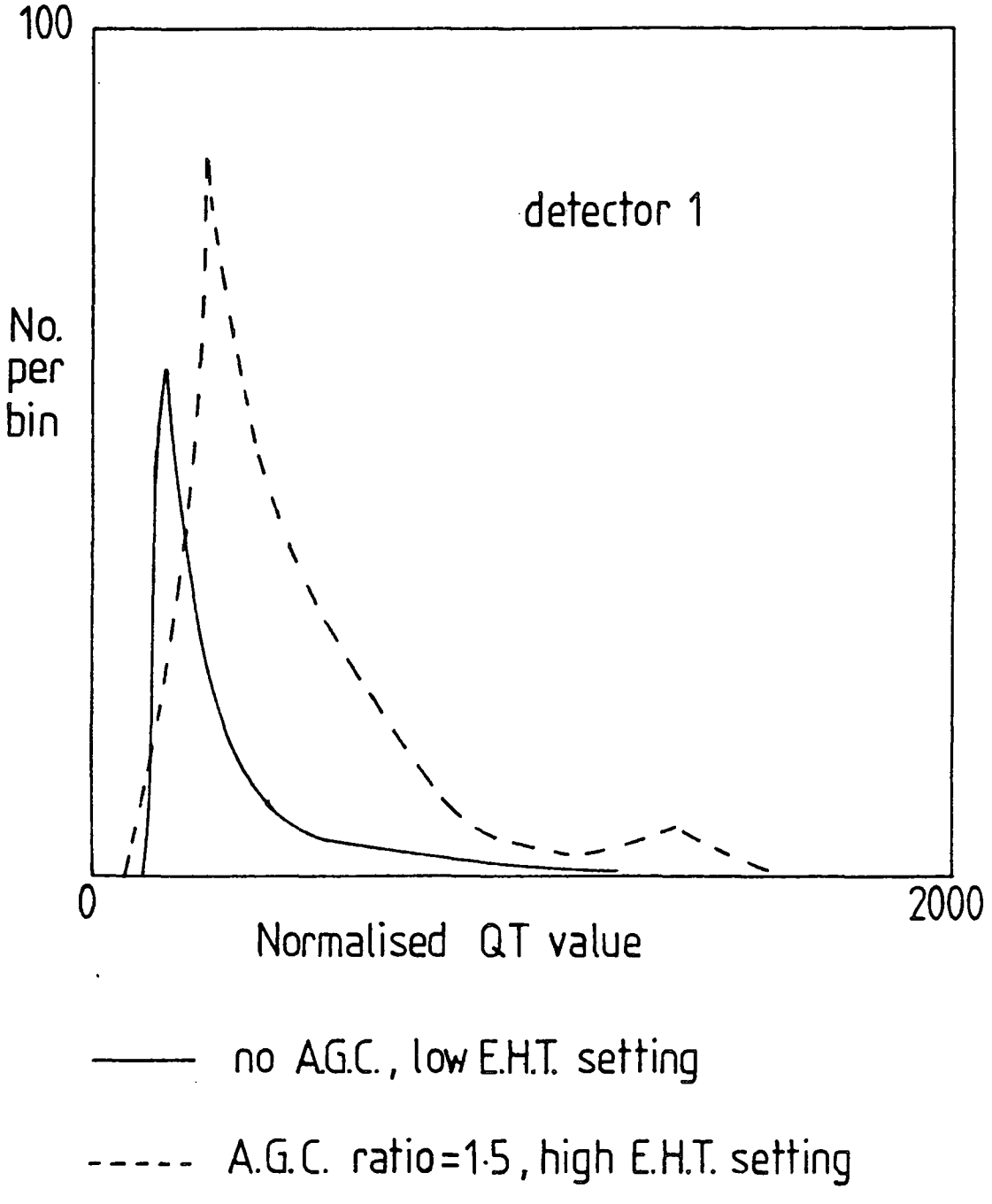

Figure 3.10: The pulse amplitude distributions from two nights with differing experimental conditions.

levels during observations and also by changes in the A.G.C. setting. The change in conditions in which the phototubes operated meant that the response to a given light pulse varied from night to night, and observation to observation - as shown in fig. 3.10.

3.5.3: Calibrations of the Time-to-Amplitude converters.

The relative timing calibration was performed by triggering each T.A.C. unit with an input pulse and then stopping the unit with another pulse separated from the first by a previously determined time interval. A record of the digitised output was then taken. Such measurements indicated that the T.A.C. output was directly proportional to the input delay.

More details of these calibrations are given in the extensive discussion of the fast inter-detector timing technique (Walmsley, PhD thesis in preparation).

3.5.4: A survey of the array.

In the fast inter-detector timing analysis of the showers an accurate knowledge of the relative positions of the detectors was needed. A reference point was chosen as the centre of the array, close to detector 1, and the orientation of each detector was then measured relative to true North. From the survey readings the detector positions, defined in a cartesian frame were calculated and are shown in Table 3.1. Each survey position has an estimated accuracy of +/- 0.1 m.

3.5.5: The measurement of the field of view.

Measurements of the Field Of View (F.O.V.) were conducted at an

Detector	Coordinates(m)		
	X	Y	Z
1	0·00	0·00	0·00
2	30·88	51·45	-1·83
3	28·43	-52·66	0·46
4	-60·13	0·66	1·82

Table 3.1: The relative positions of the four telescopes.

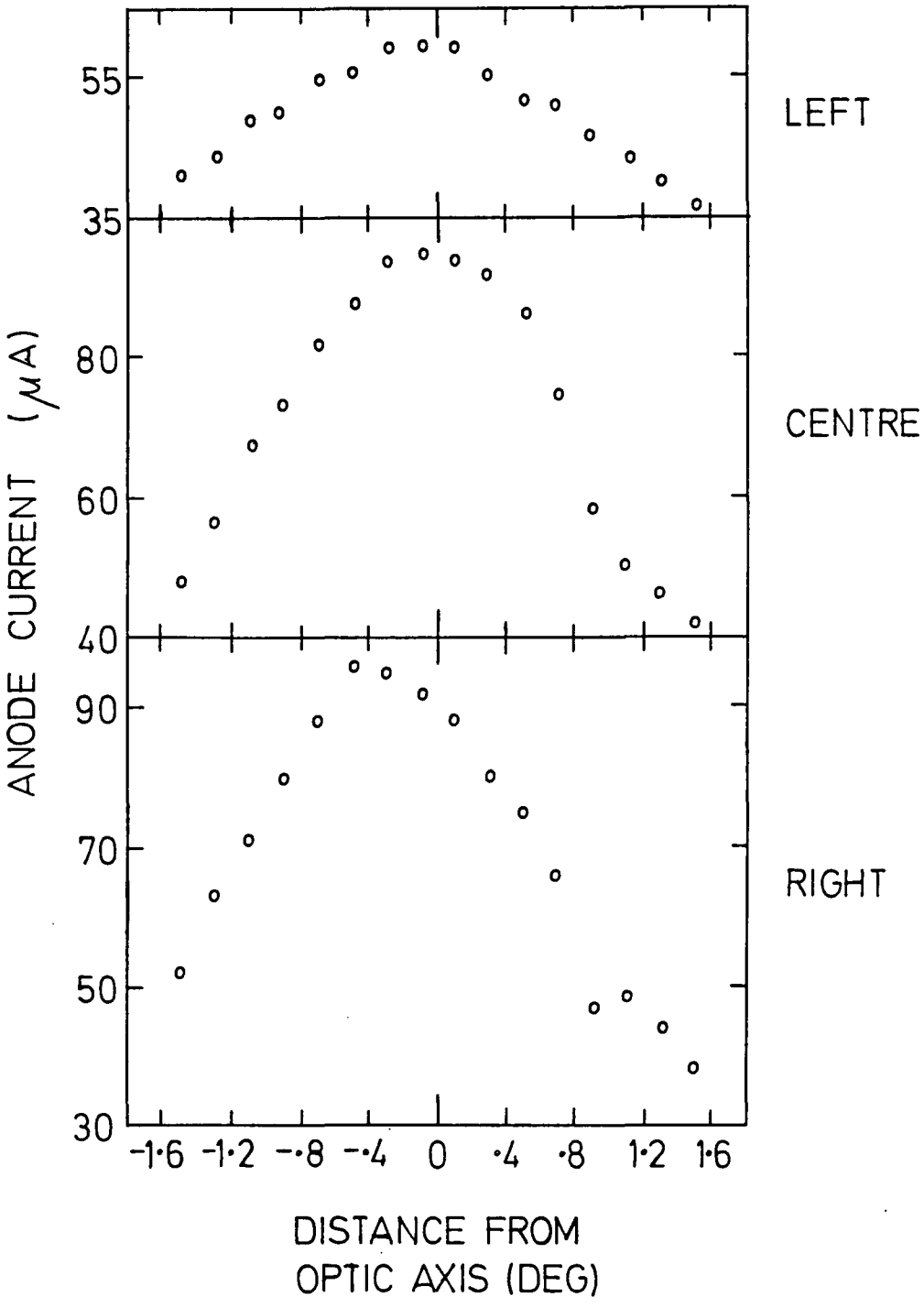

Figure 3.11a: A 'Raster scan' of Polaris - Mark I optics.

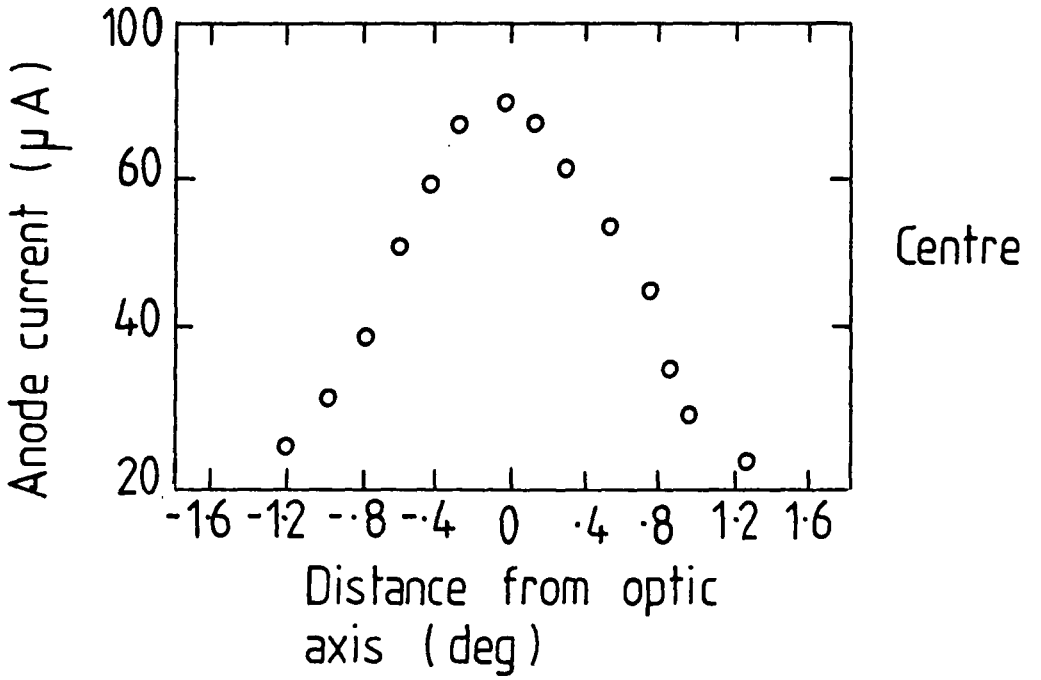

Figure 3.11b: A 'Raster scan' of Polaris - Mark II optics.

early stage of the telescopes construction by investigation of the mirror images using L.E.D.s. The resulting values for the Mark I and Mark II telescopes are given (at F.W.H.M.) as 1.75° and 1.3° respectively.

A different measure was provided from observations using the full Dugway system. The telescope mirrors were correctly aligned on each detector with the aid of a bright L.E.D. placed a considerable distance from the array. Once the optics were aligned, the variation of the anode current in the phototube could be used to plot out the response of the system to a 5° scan in small steps about a suitable small magnitude star. The star acts as a point object, and Polaris was used. These measurements were made for each of the mirrors on all detectors and checks were made over the 4 years of operation.

The results of two such scans are given as fig. 3.11a and fig. 3.11b for the Mark I and Mark II systems respectively. The respective F.O.V.s, at F.W.H.M. were measured as;

Mark I F.O.V. = 1.75°

Mark II F.O.V. = 1.3°

3.6: The array performance.

3.6.1: The array counting rate.

The basic performance of the array is measured by the counting rate of the individual detectors. An investigation of the variation of the rate with zenith angle has been made for all the years of operation. For the night of 31st of August 1981 the telescopes were used to conduct a 'drift scan' of the Cygnus X-3 region at various zenith angles. The variation of the count rate is given in fig 3.12 for 1981, fig.3.13 for a night in 1982, and the variation for 1983 is

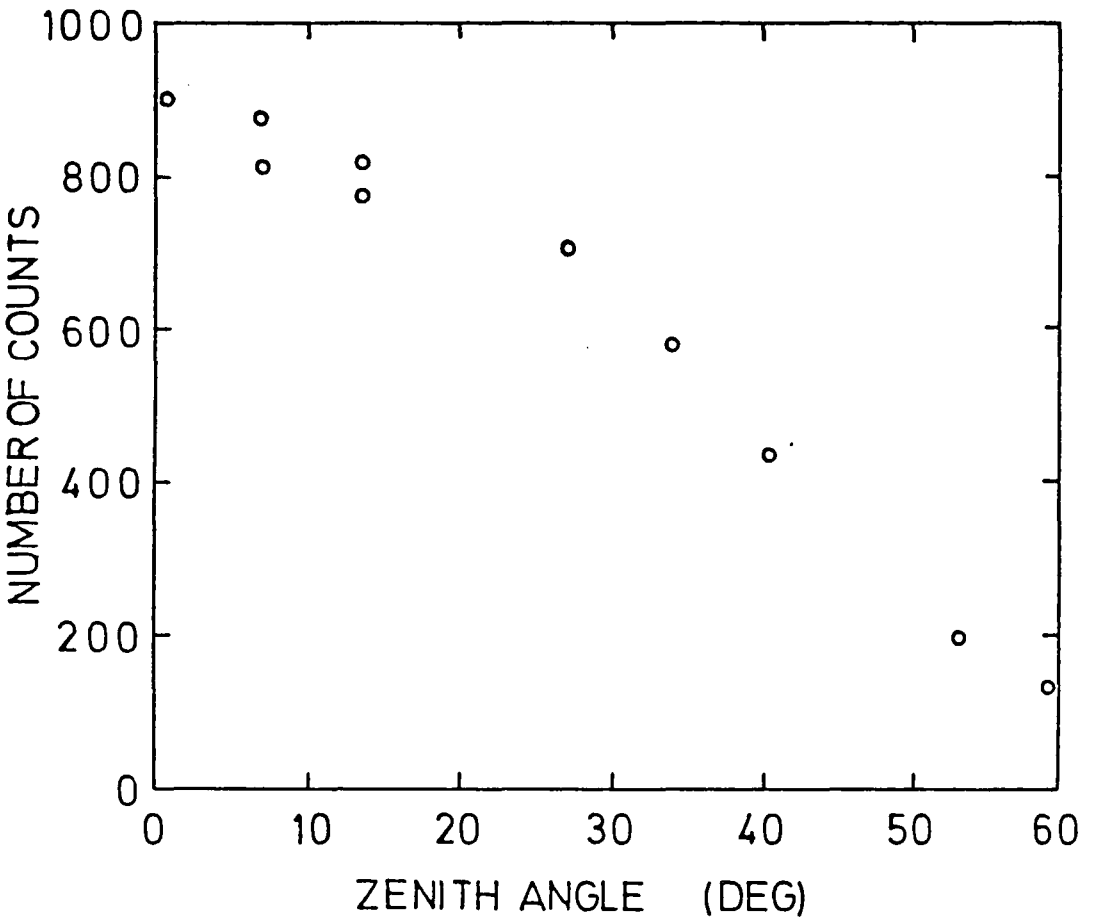

Figure 3.12: The variation of counting rate with Zenith angle for data taken in 1981.

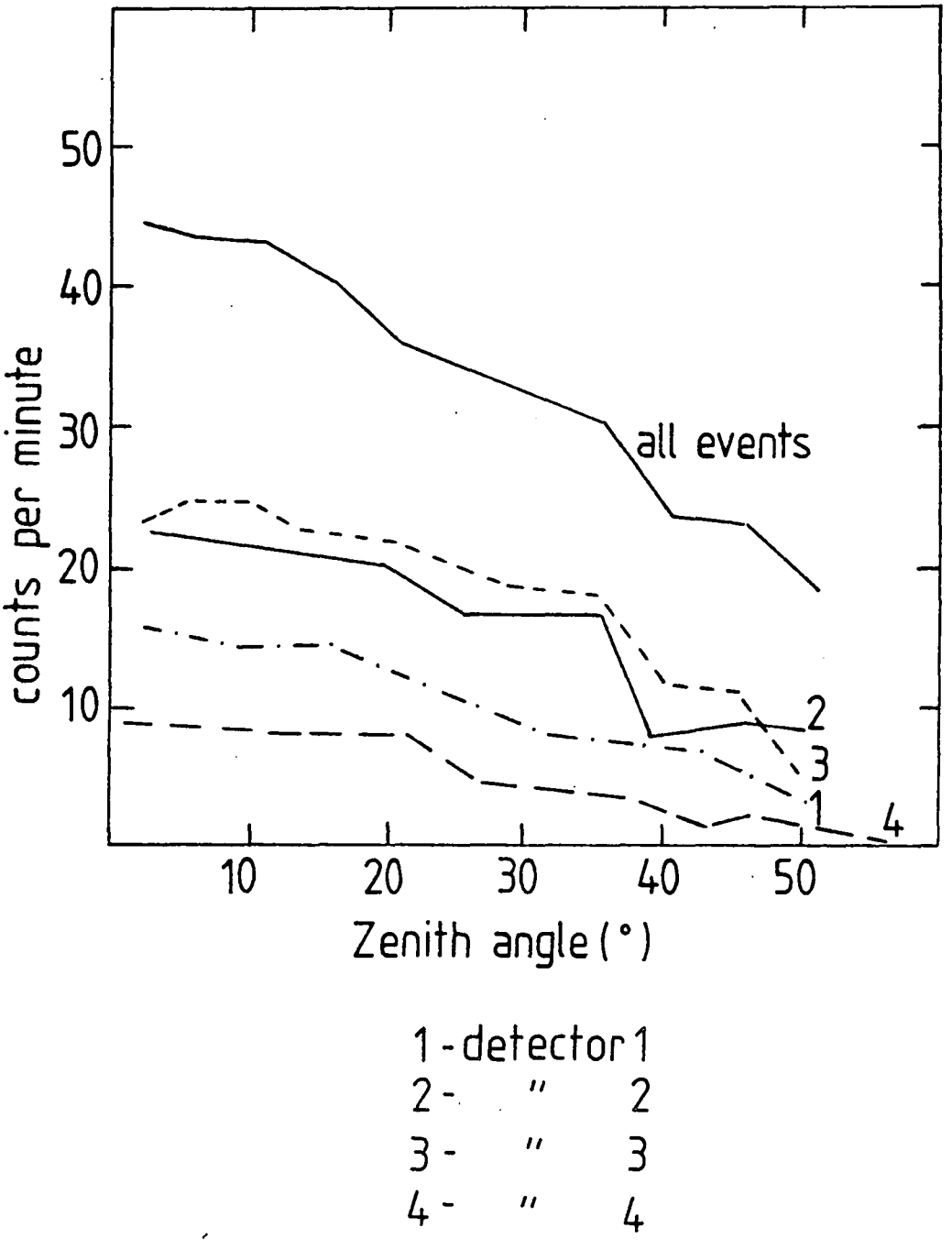

Figure 3.13: The variation of counting rate with Zenith angle for data taken in 1982.

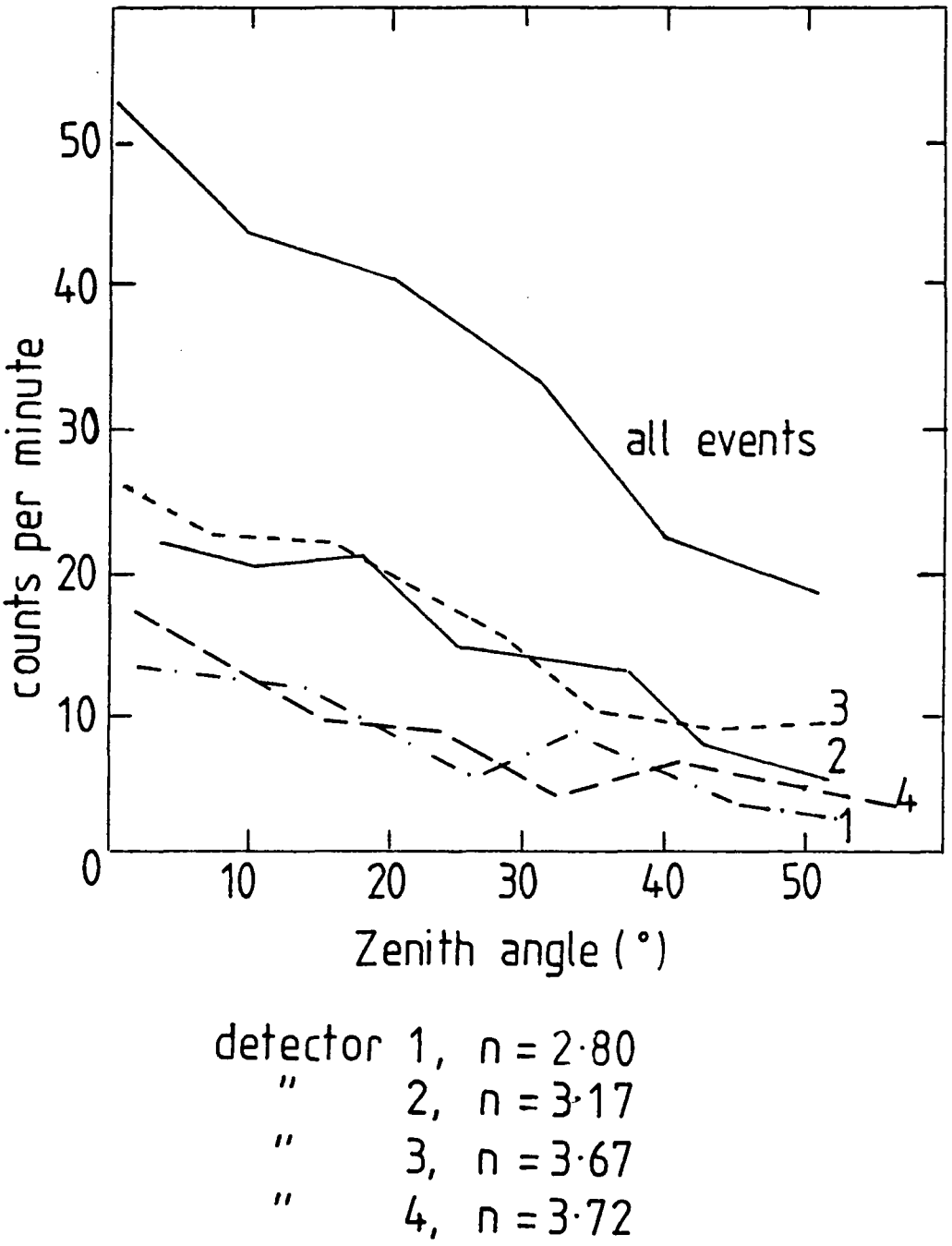

Figure 3.14: The variation of counting rate with Zenith angle for data taken in 1983.

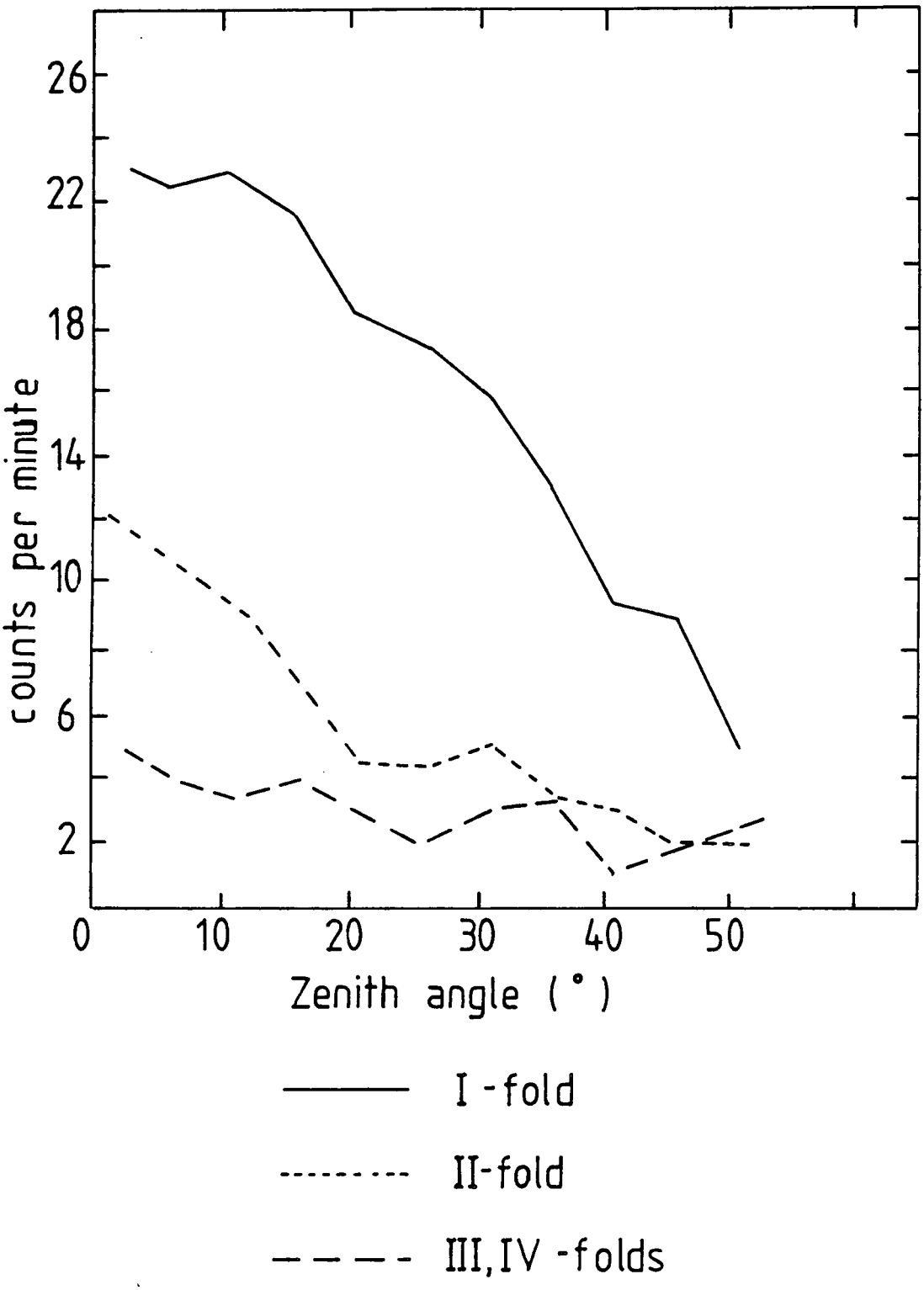

Figure 3.15: The variation of counting rate with Zenith angle for I, II, III and IV - fold detector responses.

shown in fig 3.14 (all measurements were taken with the telescopes pointing at Cygnus X-3). The distributions can be summarised by a function of the form;

Count rate = C. $\cos^n$(Zenith angle)

The exponent is found to vary from 2.47 for 1981 data, to 3.02 for the 1983 data (both values corresponding to the overall array rate). Individual detectors perform differently, with values of n as shown in fig. 3.14. In fact, because of the poor rates found in 1981, all detectors other than number 3 required a full realignment of the mirrors and fine tuning, early in 1982. The improved counting rate of detector 2 resulted from this adjustment. After July 1983 the improved Mark II detector 4 system was installed; the enhanced performance of this system is evident from fig. 3.14.

The combinations of detector responses also differ greatly in their zenith angle behaviour. Fig 3.15 shows the rapid fall in the II, III and IV fold rates with zenith angle for the 6th September 1983 'tracking' data. This rapid decline has an unfortunate effect on the power of the fast inter-detector timing technique.

3.6.2: The Pulse amplitude distributions.

The computer simulations have indicated that the intensity of the Cerenkov flash is related to the energy in the particle cascade, and so will have some relation to the primary energy.

A plot of the distribution of the detected pulse amplitudes (the LeCroy'QT100B'outputs) is given as figure 3.16, with the various features of the plot indicated. The different contributions to the distribution of I, II, III and IV fold events should be noted. The distribution is positively skewed and so for much of the analysis the median pulse amplitude was taken as the most useful measure of the central tendency of the distribution. This value is shown to vary

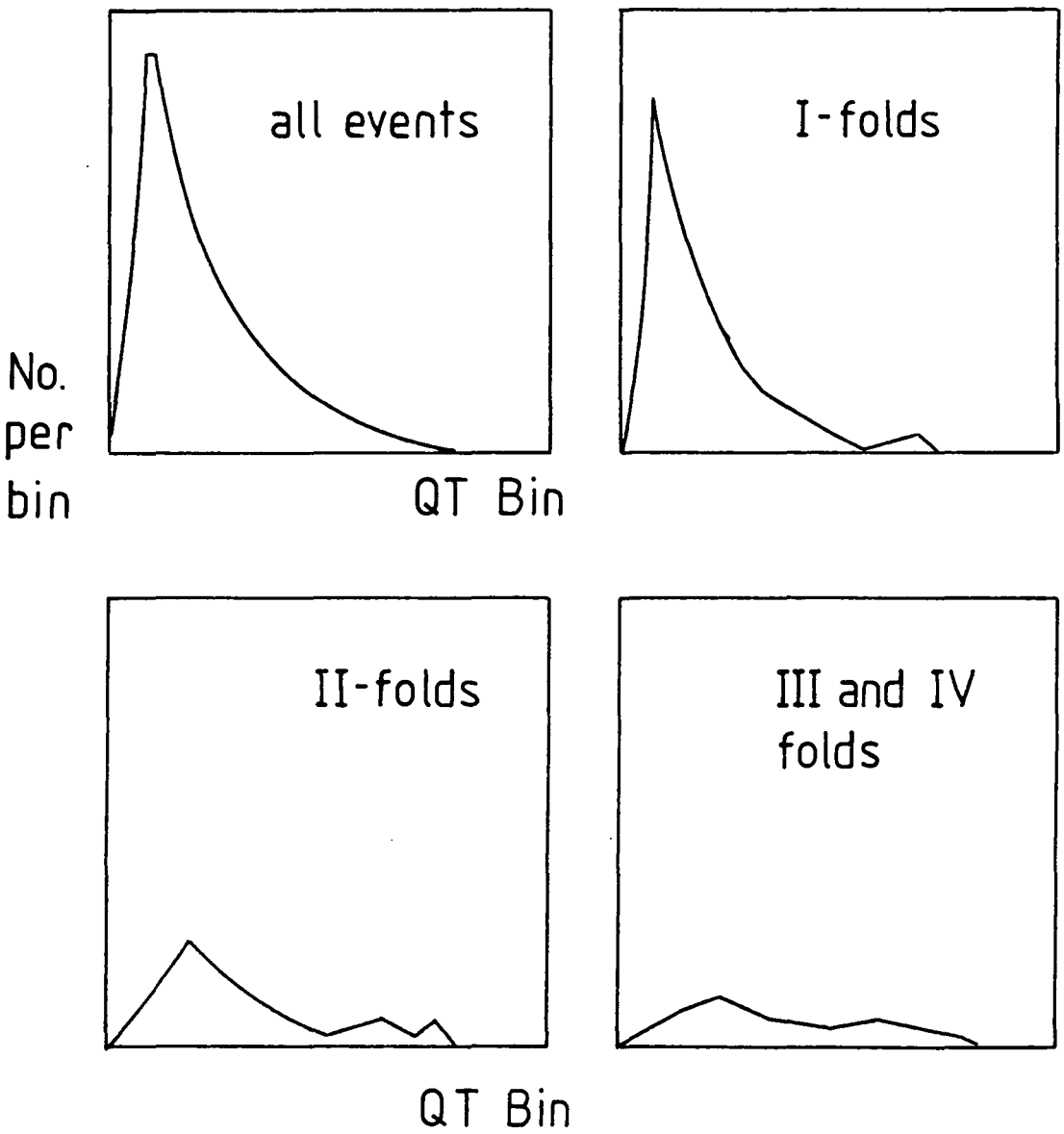

Figure 3.16: The pulse amplitude distribution - showing the contributions of I, II, III and IV - fold detector responses.

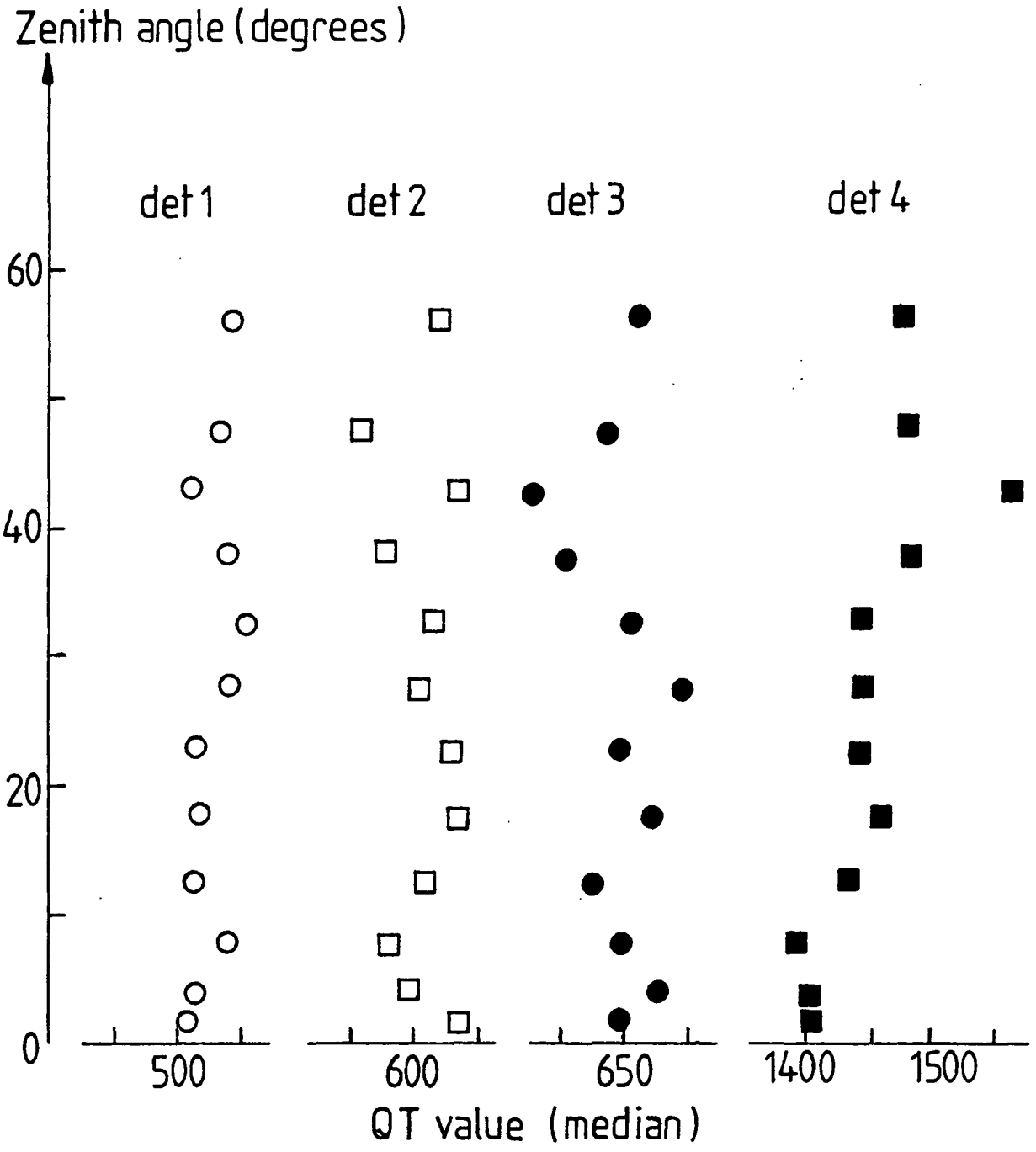

Figure 3.17: The variation of the median pulse amplitude value over a range of zenith angles.

little over the zenith angle range 0 - 50° in 1983 tracking data, see fig 3.17. This indicates that the basic distribution of the light intensity in the detected showers remains similar over the full range of detector pointing directions. The only variation would seem to be in the numbers of such events.

Direct calibration of each LeCroy 'QT100B' output was not attempted, analysis of this measure simply compared distributions from background and potentially enriched gamma-ray samples, see section 5.5.

3.6.3: Telescope aperture functions.

The telescope field of view has been well defined by calibrations from scans of bright stars - see section 3.5.5, and from the geometric optics of the mirror system.

The above measures give the response of the system to a point source. However, the angular extent of the Cerenkov flash is found to be ~ 1° see section 2.4 , and this extended source must be added to the estimation of the detector aperture function. Detailed computer simulations, discussed elsewhere (Macrae, 1985) indicate that the response function for a Mark I detector is Gaussian in form, i.e. similar to that shown in fig 3.18. The aperture may be defined at F.W.H.M. to be;

(2.2 +/- 0.2)°

- for a shower initiated by a 1000 GeV gamma-ray.

The aperture function of the Mark II detector has not been accurately determined, but should be of the order of ~ 1.8, if it follows the same relationship between the computed, and point-source fields of view found above for the Mark I system.

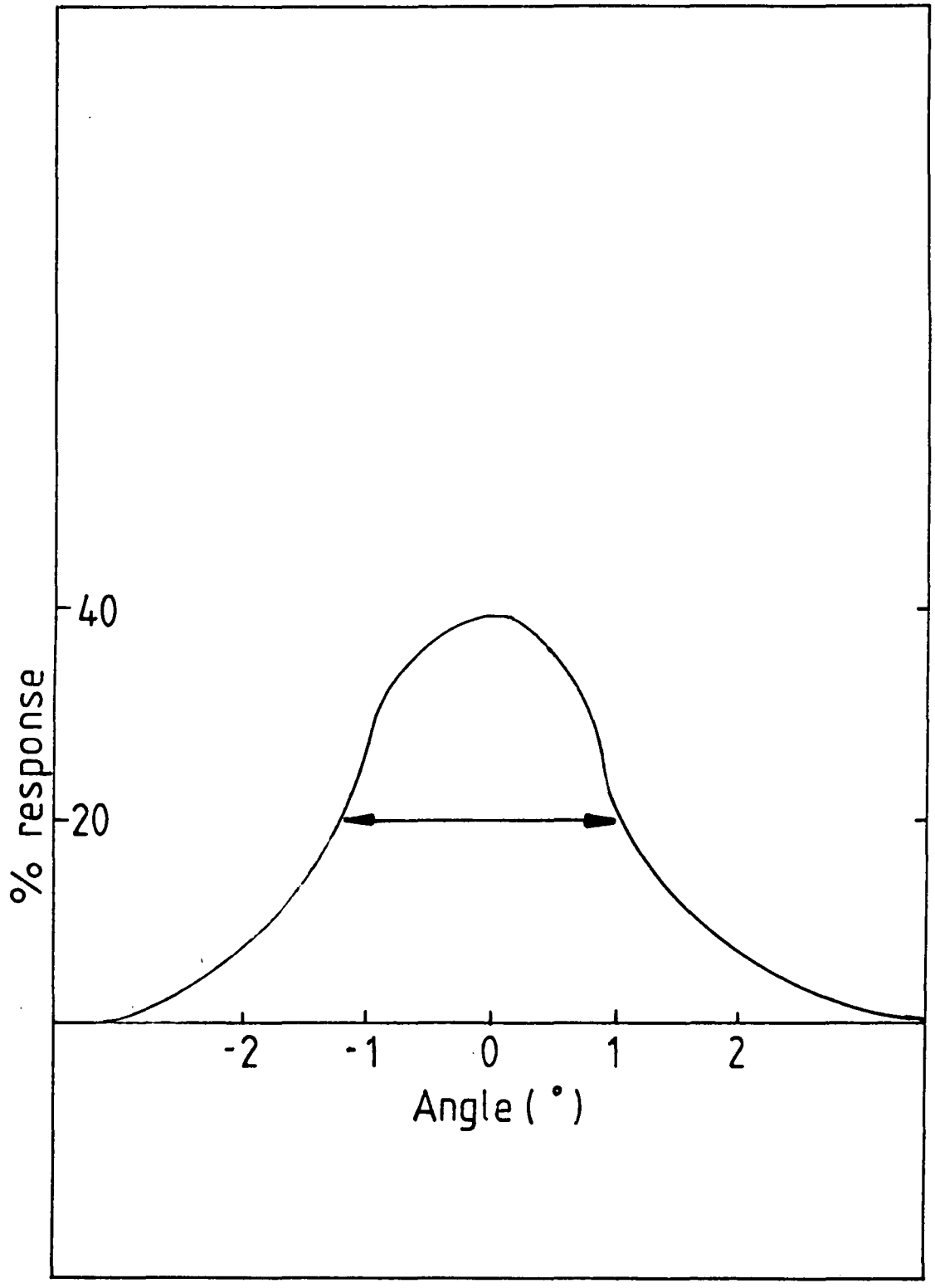

Figure 3.18: The Mark I telescope aperture function.

3.6.4: Energy Threshold.

The indirect form of gamma-ray detection employed in the Atmospheric Cerenkov technique makes an accurate determination of the energy threshold difficult. The procedure used in this work and others involves approximations to the threshold based on the response of the detectors to real showers and computer simulations of the shower development for gamma-ray and proton primaries. Among the many complicating factors affecting the energy threshold for real observations is the zenith angle, and the collecting area itself is a function of the primary energy.

To determine the threshold for a detector the following quantities must be known;

i. The collecting area of the telescope

ii. The field of view of the telescope

iii. The counting rate of the telescope (at a given zenith angle)

iv. Computer simulations of the relative response of the telescope to gamma-ray and proton initiated showers.

i. Collecting area.

This is difficult to measure accurately but a reasonable estimate is obtained by noting the detailed performance of the array. As an example, most of the showers that trigger detector 3 are not recorded by the nearest detector (i.e. detector 1). It is therefore possible to estimate that the collecting radius is less than 60 m (the detector separation). A reasonable estimate of the radius would then seem to be 45 +/- 10 m, leading to the collecting area for detector 3 single fold responses;

$$(6362 + 3141 - 2513)\ m^2$$

Complications to this simplistic approach arise when multiple fold responses are added. This is particularly true for detector 4 in 1981/82 where the much higher energy threshold resulted in a larger proportion of multiple fold events being detected.

ii. Field of view.

The aperture function of a telescope is given by a Gaussian function of F.W.H.M. (2.2 +/- 0.2)° as discussed in section 3.6.3. An estimate of the field of view of a telescope leads to a value of;

$(1.67 + 0.32 - 0.29) . 10^{-3}$ str.

This value can be applied to all detectors, apart from the Mark II detector 4 used since mid 1983, where a smaller value is appropriate;

$\sim 1.11 . 10^{-3}$ str.

iii. Counting rate.

The counting rates of the four detectors are summarised in fig. 3.12, fig. 3.13 and fig. 3.14.

iv. Simulations.

The discussion of the relative yields of Cerenkov photons from proton and gamma-ray initiated showers was given in section 2.4.1. In general for energies greater than 1000 GeV gamma rays are 1.4 - 2.0 times as efficient.

Example.

For detector 3 in 1982 the counting rate within 1° of the zenith is estimated as 16.9 min^{-1}, and so the average flux seen with the telescope pointing at the zenith is;

$2.65\ (+2.62\ -1.17)\ 10^{-2}\ m^{-2}\ s^{-1}\ str^{-1}$

The flux at the top of the atmosphere due to protons is estimated

Year	Detector	Energy threshold (GeV)
1982	1	2417 ± 800
	2	1800 ± 700
	3	1742 ± 700
	4	4200 ± 1300
1983	1	2700 ± 900
	2	1800 ± 700
	3	1400 ± 450
	4	1500 ± 500

Table 3.2: Approximate telescope energy thresholds from 1982 - 1983.

from figure 2.1 as $1.14 \cdot 10^{-1}$ m^{-2} s^{-1} str^{-1} at an energy of 1000 Gev. With the integral spectral slope of -1.6 the energy threshold for protons is,

2489 (+ 1093 - 869) GeV

- appropriate for detector 3. Including the results of the detailed simulations, the threshold for gamma-rays is,

1742 (+ 765 - 608) GeV

For most of the 1982 observations an energy threshold for gamma-rays of ~ 1300 GeV has been used. This value is in good agreement with the value suggested from computer simulations of the array performance (Macrae, 1985). Table 3.2 summarises the energy thresholds for all four detectors for the 1982 and 1983 observing seasons.

3.7: The Mark II telescope.

In the Mark I array, detector 4 carried the lowest quality searchlight mirrors and its performance was always significantly below that of the other three, so an improved detector was clearly desirable and work began on its construction in the autumn of 1982. In addition, the Mark II telescope was used as an important stage in the long term development of a purpose built gamma-ray detector.

A new method was used to produce cheap, robust mirrors from aluminium plate, and some new investigations were made into the optimum mirror-phototube combination. The Mark II telescope is shown in fig 3.19, and was operated on the Mark I mount using modified Mark I electronics.

After a series of tests in Durham the new telescope was deployed in July 1983 and began to take data later in that month.

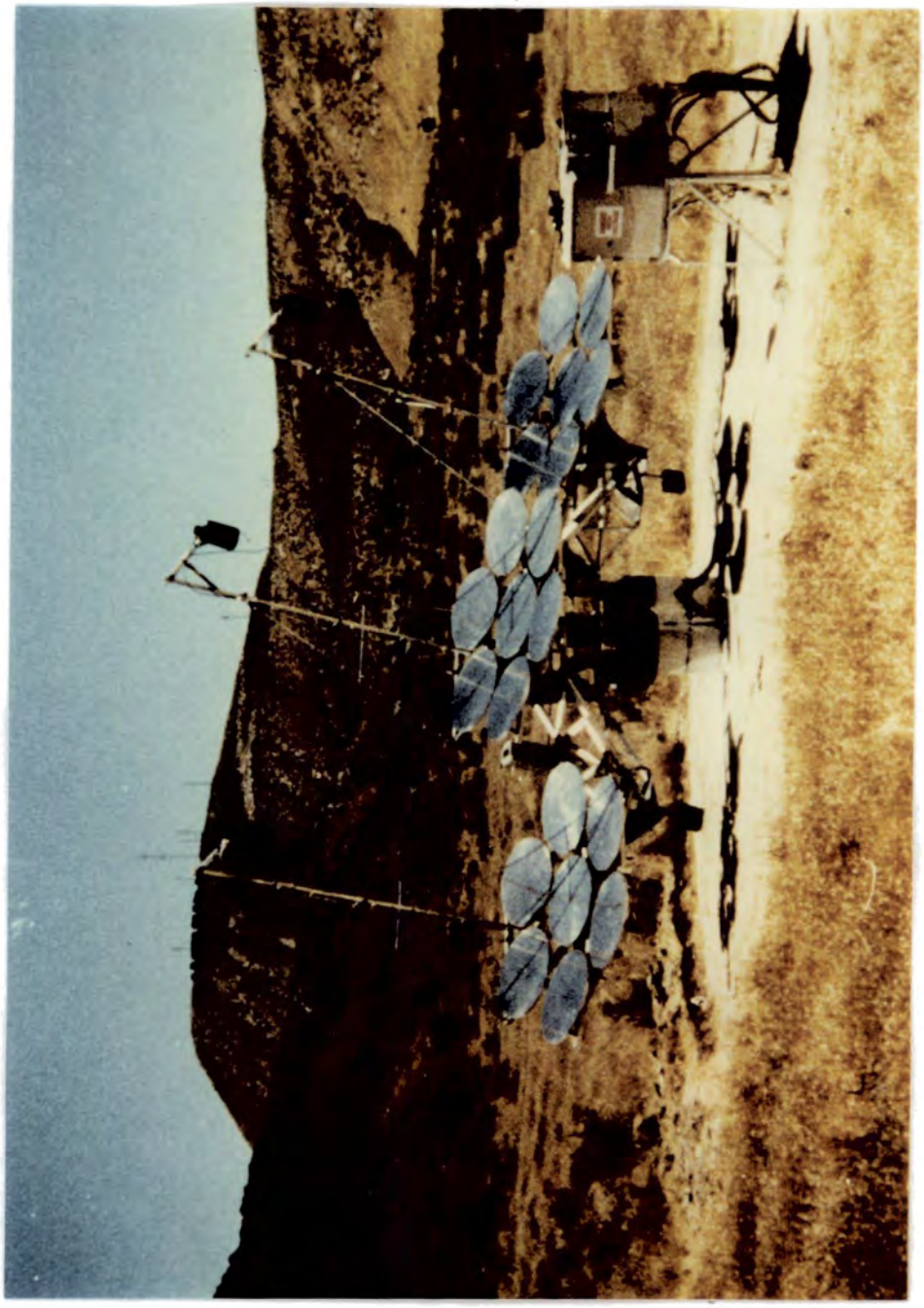

Figure 3.19: The Mark II telescope.

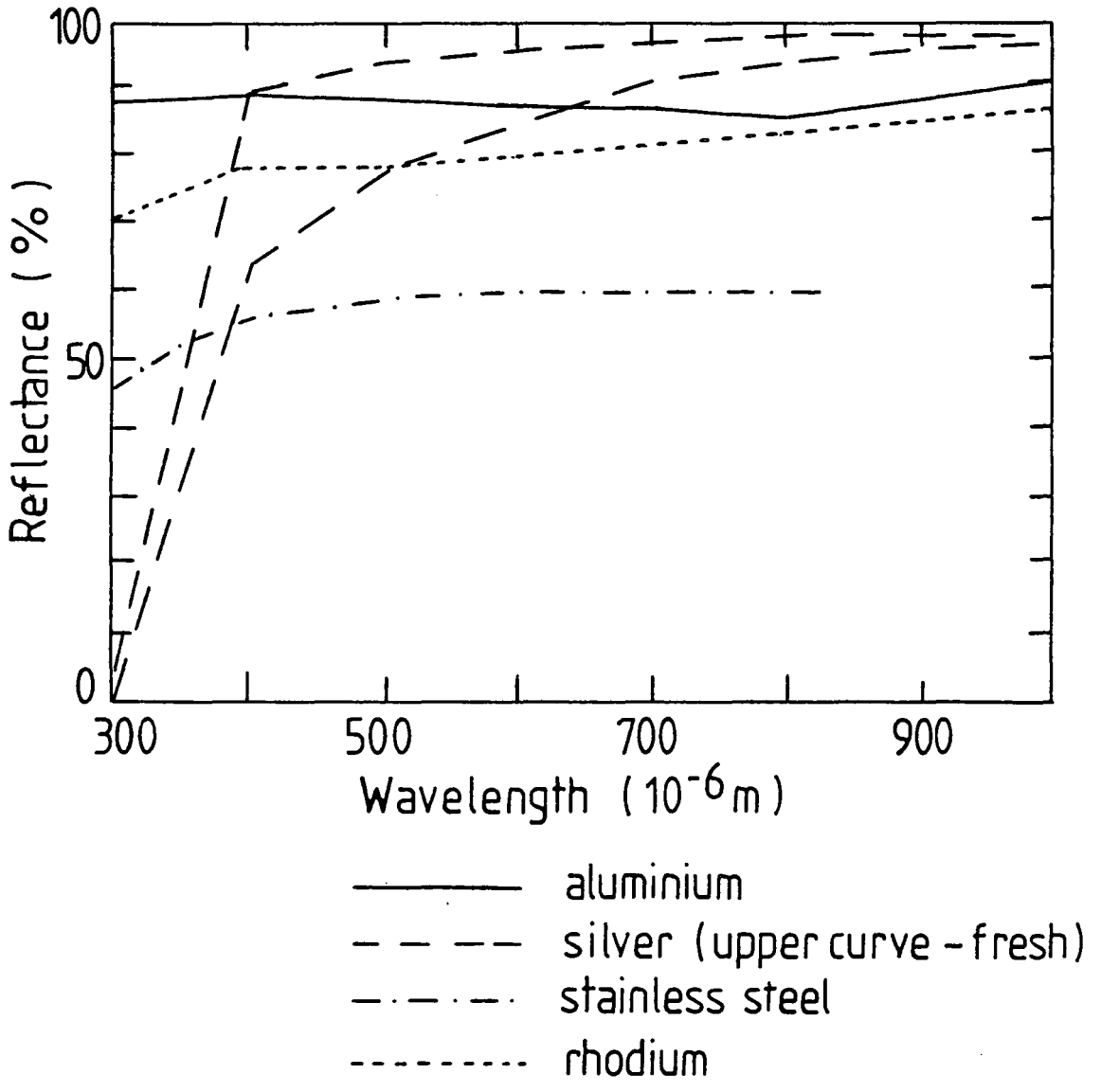

Figure 3.20: The reflectance of aluminium, rhodium and silver in the visible and near ultraviolet region.

3.7.1: The Optical System.

The 3 Mark I searchlight mirrors were replaced with 21, 2ft diameter aluminium mirrors. Aluminium was chosen as its reflectivity is considerably better than rhodium, especially over the wavelengths at which the Cerenkov spectrum peaks, see fig 3.20. In addition, aluminium corrodes to form a clear oxide, protecting the mirror surface from serious deterioration, and providing a more robust reflective surface than traditional 'metal-on-glass' mirrors.

Each mirror was made from 3/4" thick aluminium discs, cut first on a lathe to the required focal length and then ground and polished to a mirror finish. This process was lengthy but resulted in an acceptable mirror quality and excellent control of the mirror parameters. Twenty-eight mirrors were produced, the seven not used in the new detector remaining in Durham for test purposes. The size of the image produced was adequate, at 4cm diameter (measured at the radius of curvature) and suffered some aberration. The optics of the Mark II mirrors are summarised as fig. 3.21 and below;

Diameter = 0.61 m

Focal Length = 2.21 m

Image scale = 0.026°/mm

The Cassegrain system was not adopted. This in itself, represented a major improvement in system reflectivity over the Mark I telescope, as the mirrors focussed Cerenkov flashes directly onto the face of the phototube.

Each mirror weighed roughly 21 lbs and necessitated the design of a robust adaptor to fit to the Mark I mount. Despite this extra weight, and with careful balancing, the steering motors were able to function satisfactorily.

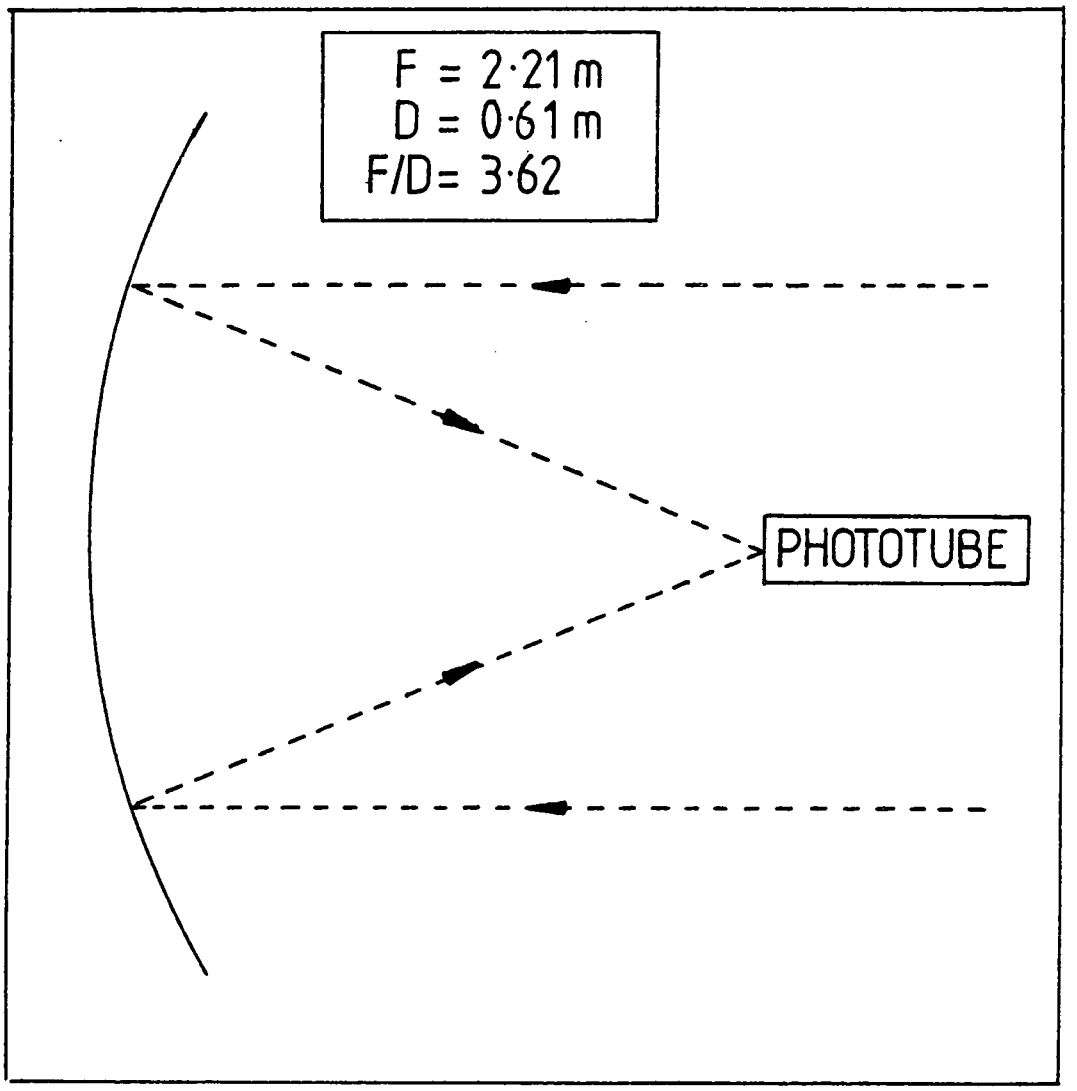

Figure 3.21: The Mark II telescope optical system.

3.7.2: The Mark II Phototubes.

The angular extent of the Cerenkov flash is $< 2^{o}$ as discussed in section 2.4, and so the large field of view used for the Mark I telescopes was not at an optimum. The new system used 2" diameter RCA type '8575' tubes with a bialkali photocathode of good quantum efficiency in the Cerenkov light region of the spectrum, and fast anode pulse rise time at < 2.5 ns.

With this combination of mirror and phototube, the field of view is estimated as 1.3^{o} and was expected to be closer to the optimum for the Cerenkov flash than the old combination. 'Raster' scans of Polaris were carried out (see section 3.5.5), and indicated that the field of view to a point source was indeed 1.3^{o} at F.W.H.M. Although no simulations of the performance of this system were made, we can estimate a field of view to real showers as,

$$= 1.8^{o} \text{ at F.W.H.M.}$$

by comparing with the Mark I result.

3.7.3: Other Modifications.

The new telescope was designed to require few modifications to the existing electronic system, however, some changes were needed, and the main ones are summarised below;

i. The new 2" phototubes were able to operate at much higher E.H.T. voltages than the RCA type '4522' tubes, without developing an excessive accidental counting rate. For the 2 years of operation, the E.H.T. system was set at its maximum voltage to give the maximum sensitivity to Cerenkov light flashes.

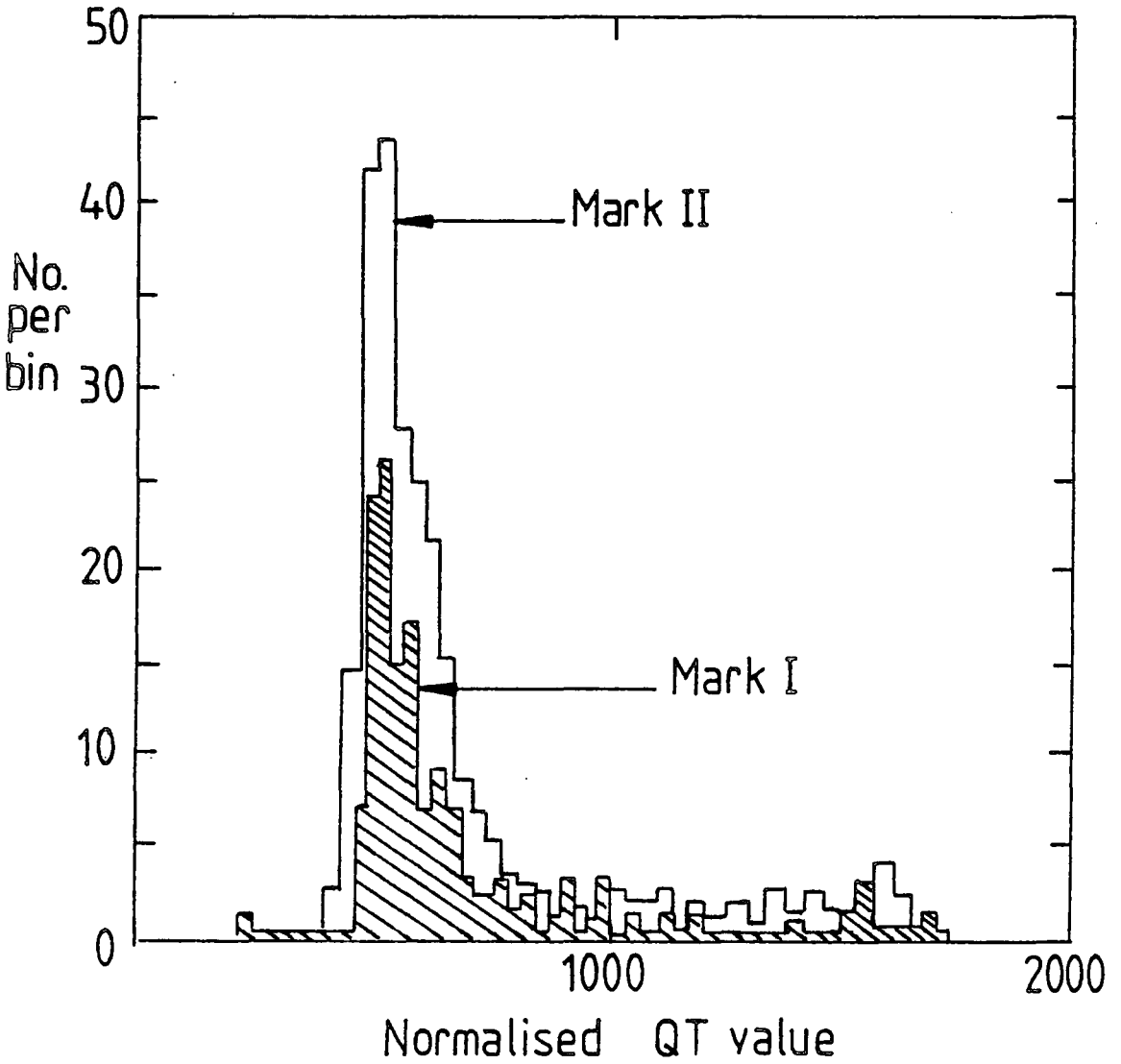

Figure 3.22: A comparison of the Mark I and Mark II pulse amplitude distributions.

ii. In addition, the cable lengths to the control centre were adjusted, again to ensure optimum counting rate, and to minimise accidentals.

3.7.4: Mark II Performance.

It is possible to look at the difference in the pulse amplitude distributions for the Mark I and II versions of detector 4. Little quantitative comparison can be made, due to differences in for instance, the E.H.T. levels. Fig 3.22 represents a plot of the two distributions showing the different response due to the upgrade.

A considerable increase in detector counting rate was achieved as indicated in fig. 3.14. The improved telescope parameters lead to a better 'Signal to Noise' ratio by lowering the telescope energy threshold.

In conclusion, the new, smaller aperture telescope represented the most sensitive telescope in the array, and allowed some significant analysis to be performed on this detector alone. Many of the lessons learnt in building and operating the new telescope were extended to the programme of design and observation for the Mark III Southern hemisphere telescope.

3.8: The Mark III telescope.

With the success of the Mark I array and the advances made using a Mark II design, it became evident that a purpose-built Atmospheric Cerenkov telescope would provide the major improvements in sensitivity necessary to discover more V.H.E. gamma-ray objects.

A new telescope has been developed to operate in three modes;

i. A survey instrument

ii. A telescope capable of tracking an object with high data

collection rate.

iii. A telescope capable of operation in the conventional 'drift scan' mode (see section 4.3).

Each of these considerations require different mirror - phototube combinations. A system with a large field of view is needed for survey work, but modes ii. and iii. require a smaller opening angle - a system similar to the Mark II telescope. These problems are overcome by using four phototubes in a cluster. One central tube is surrounded by the three arranged in a ring, each phototube viewing a small region of the sky - near the optimum of 1.3°, but the whole sampling a wide region suitable for survey work. The area surveyed can be increased by expanding the number of phototubes in the cluster. The arrangement is capable of operating as a 'tracking' (see section 4.3) instrument with the central 'on-axis' tube viewing the region around the object, the others providing a background estimation from adjacent regions of the sky. In the 'drift scan' mode (see section 4.3), the source may pass through the field of view of several tubes in the cluster, once again providing a good estimate of the background. An A.G.C. system is incorporated into the design.

The system is shown in fig. 3.23, with the three mirror-phototube systems operating in 3-fold coincidence. The whole structure will be steered by servoed D.C. motors. The steering control is achieved using a system including absolute encoders in contrast to the Mark I system which gave a relative position. The accuracy in steering is similar to the Mark I system, i.e. ~ 0.1°. Unlike the Mark I telescopes, the steering is continuous, and is computer controlled by a separate system from that collecting the data.

A detailed investigation of the performance of the phototubes indicated that the old Mark I RCA type '4522' tubes were not suitable for this type of work. For the new telescope, a 2" tube, the RCA type '8575' has been chosen. These tubes have a stable performance and

Figure 3.23: The Mark III telescope.

worked well with the Mark II telescope. Full details of the phototube tests are given elsewhere (Chadwick, PhD thesis in preparation).

The electronic control and data logging have been extensively changed from the Mark I system. The new experiment requires much larger amounts of data to be recorded quickly and reliably, and so the data logging is performed by a dedicated Motorola '68000' microprocessor. The system is specifically designed for the Mark III experiment and runs on a LeCroy '3500C CAMAC' databus giving a short 'dead time' between recording events of ~ 0.3 ms. This facility is important in the observation of rapidly periodic objects.

The relative timing in the new experiment is achieved using a rubidium clock which is capable of a highly stable performance (~ 1 part in 10^{11}). This will allow a further improvement in the relative timing resolution, though the problem of clock initialisation remains.

A feature of the new control centre will be the extensive use of BBC microcomputors communicating on an 'ECONET' local area network. Six computers will be used, one dedicated as the master control of the experiment, one for the steering control and the other four acting as a computer monitoring system (Anode currents, Steering position etc).

The recording of the data is achieved using a 3M cartridge tape drive, the event parameters (event time, pulse amplitude and anode currents) and measures of the array conditions are registered. In addition the recording system incorporates a facility which notes only the event time for events occurring within the 'dead time' of the system - in this way short bursts of gamma-rays may be detected.

3.8.1: Mirror Development.

The requirements for the new optical system are a large collecting area, with a field of view near the optimum value of ~ 1.3°. The 2"

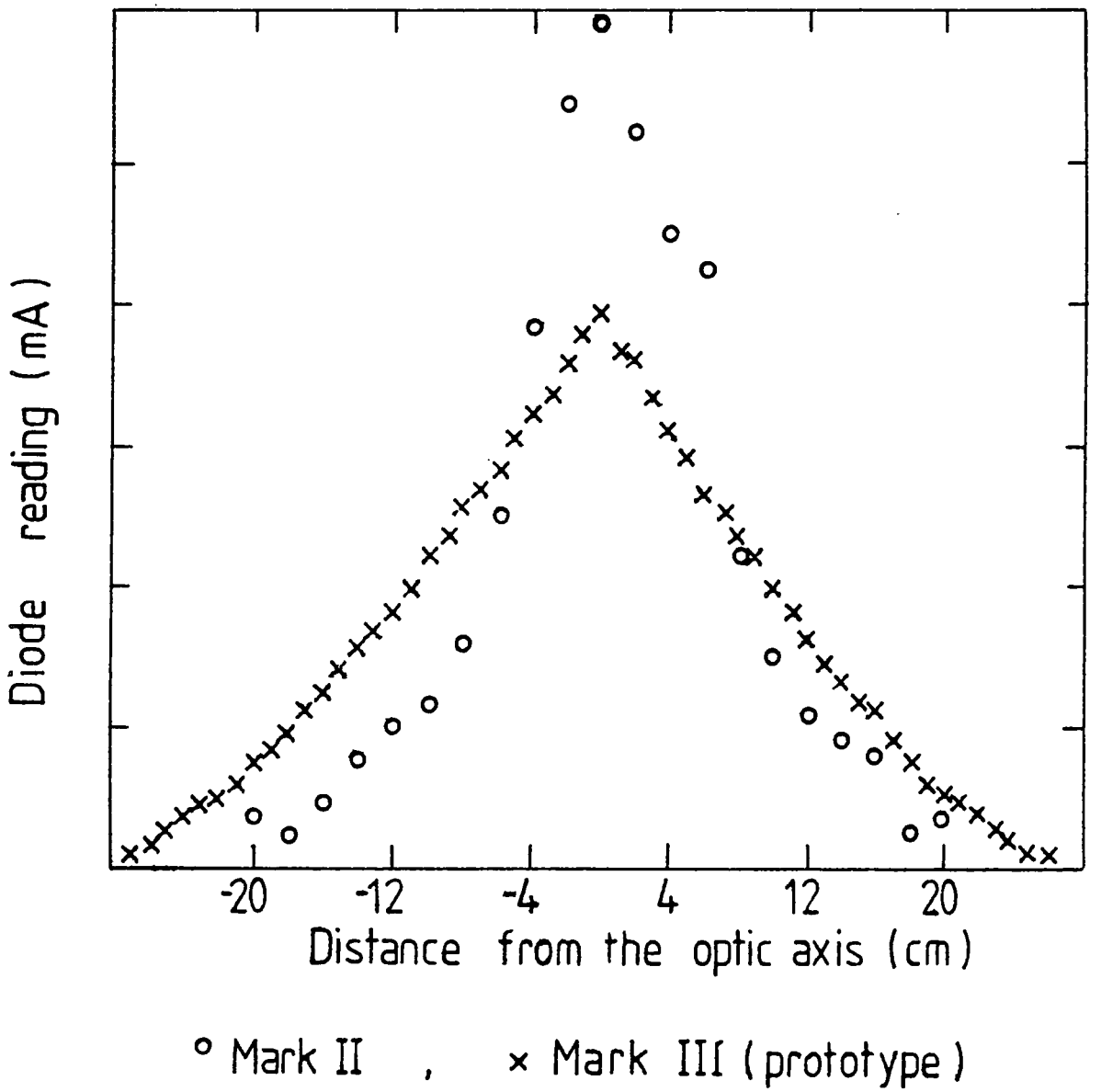

Figure 3.24: The images produced by a Mark II and a prototype Mark III mirror (measurements performed at the radius of curvature).

phototubes define a telescope of focal length ~ 2.5 m. The Mark III mirrors needed to be of adequate optical quality, with weight and size suited to the new design, and in view of limited funding, they needed to be cheap to produce.

Mark II mirrors are cheap and simple to produce, but their weight and time of manufacture mean that they were unsuitable for a system with a large collecting area. Several alternative methods of production have been investigated;

i. Pressing thin aluminium sheet between 'male' and 'female' formers figured to the correct mirror dimensions.

The necessary quality control of image size and focal length - essential for a useful telescope was found to be low. However, a prototype batch of mirrors was produced and compared directly with the Mark II mirrors. Images were large (> 40mm diameter in the focal plane) and with large aberration. A comparison of a scan using a photodiode across the Mark II and Mark III (i) mirror images is given in fig 3.24 with the Mark II mirror clearly superior.

ii. Mirrors may be produced by thermoforming PERSPEX, a process in which thin (3-5mm) discs of extruded PERSPEX are heated and either pressed, 'blow formed' or 'drape formed' against an accurately figured mould. The temperature behaviour of the expansion of the PERSPEX polymer is given in fig. 3.25 and indicates that the shaping process should be conducted in the narrow temperature range 150 - 165°C in order to achieve reproducability. The resulting mirror blanks had to be supported on a concentric ring of aluminium to maintain the accurate shape (n.b. aluminium is chosen as it has a similar expansion coefficient to PERSPEX).

Many different methods of forming the mirror blanks were tried, but all the results were poor.

The essential requirement for thermoforming PERSPEX is an accurate control of the temperature of the plastic, allowing the thermoelastic

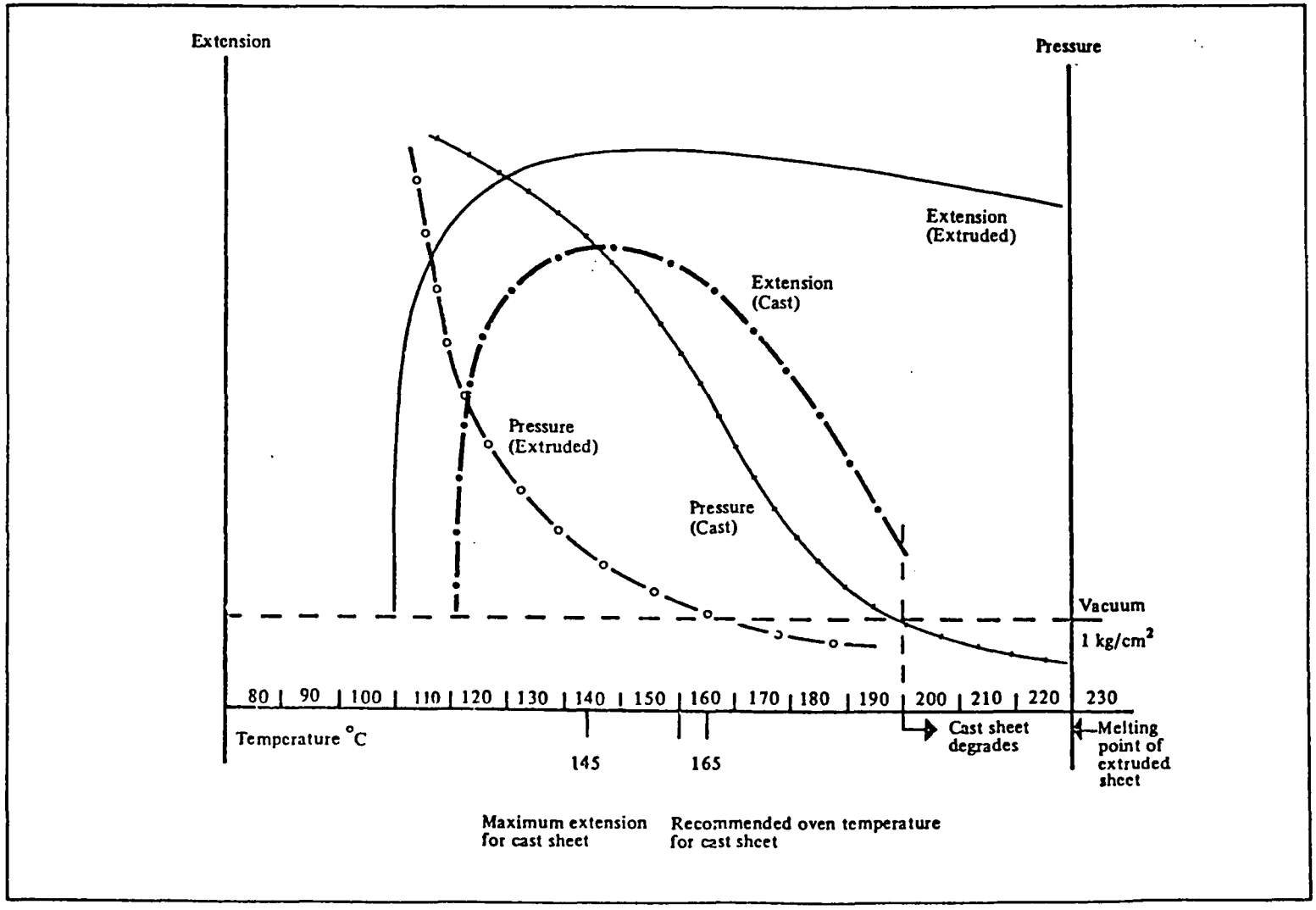

Figure 3.25: The expansion of PERSPEX.
(ICI PX132)

flow of the material. After this the controlled cooling of the moulded disc is necessary. It is important to reduce temperature differences throughout the procedure to a minimum thereby preventing differential flow or cooling which would introduce stress in the plastic and would ruin the accurate mirror figuring. To achieve this a computer controlled oven was developed allowing uniform heating to within +/- 5° C.

The clear thermoformed mirror blank is then coated with aluminium, using either an anodising or a sputtering process. Once again consideration must be given to the form of the coating, there is a conflict between front aluminised mirrors with a higher reflectivity, and back aluminised ones that are more robust.

Image sizes typical of this process were not good; ~ 5" for the drape forming process and ~ 3.5" for blow forming and pressing (all measurements of image size were made at the radius of curvature). The images suffered large aberration, and there was a wide variation in mirror quality.

Unfortunately, the critical dependence on temperature mitigates against the use of this process. It may be possible to exploit this method more successfully with an investment in a fully controlled development rig.

Several other methods were attempted, including spinning aluminium sheet, and pressing thin glass mirrors. Both of these processes are derived from commercially available techniques, but were found to be inadequate for gamma-ray work.

3.8.2: The Mark III mirrors.

The most successful procedure of all was adapted by Tim Currell from the method used to construct the antennae for the United Kingdom

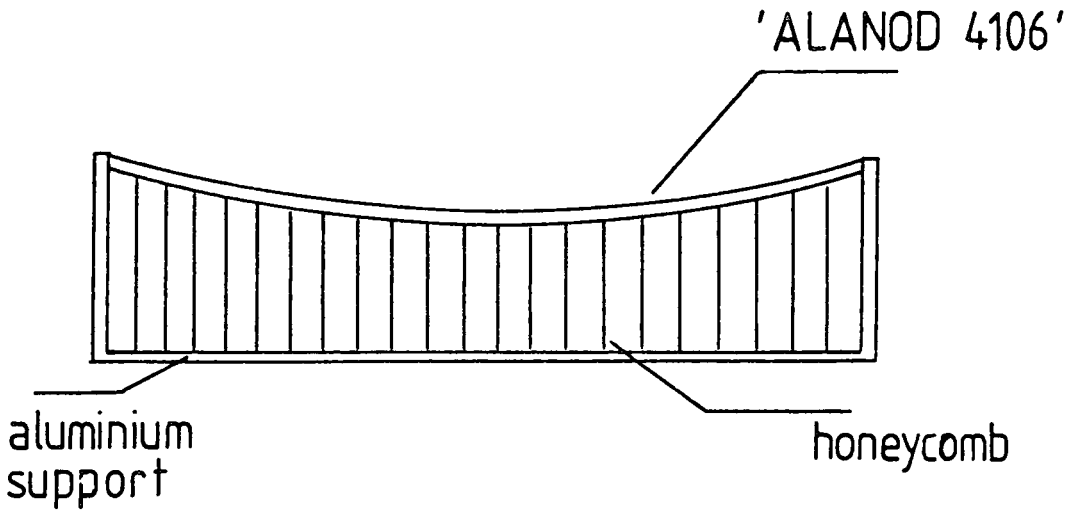

Figure 3.26: The construction of the Mark III mirrors.

millimetre wavelength telescope. It involves the bonding of thin (0.5mm) anodised aluminium sheet ('ALANOD 4106') onto a honeycombed aluminium support - see fig.3.26. The mirrored aluminium sheet has excellent reflectivity (> 75%) in the wavelength range of interest (300 - 500nm), and the honeycomb with aluminium plates provides a satisfactory rigid support.

3.8.3: Method of Manufacture.

The first step in all of these procedures is the manufacture of an accurately figured mould. In this case a steel 'male' mould was made. First the steel blank was cut using a lathe, and then it was more accurately figured by grinding.

i. The honeycomb used as a support in these mirrors is first crushed against the mould to form the required shape, and it is then bonded to an aluminium plate - see fig 3.26.

ii. The anodised aluminium sheet is stretched across the mould and clamped in position, the honeycombed support is then glued onto the mirrored sheet. The whole apparatus is heated to 150°C to promote curing.

The resultant mirrors have excellent reproducibility. The estimated range of focal length is +/-20mm in 2.5 m, the mirrors provide an 'on-axis' image size of less than 10mm in the focal plane, defining a spot size of ~ 0.2°.

The full telescope comprises 130 of these mirrors and provides a large increase in effective collecting area, once reflectivity and direct optics are taken into account, over the original array. The new telescope underwent extensive tests in 1985 and was deployed to Narrabri, New South Wales in 1986 - a site suitable for Atmospheric Cerenkov work.

Further details of the design and operation of this experiment are given elsewhere (Chadwick, PhD thesis in preparation).

Chapter 4: Observation techniques.

4.1: Introduction.

This chapter will explain in some detail the observation methods used in this experiment. It will also give a general outline of the data preparation prior to analysis.

The experimental techniques were designed to enable the observers to monitor and to make allowance for the many possible changes in conditions that affect the smooth running of the equipment.

Details of the analysis procedures are given in the next chapter. In this chapter an explanation is given of the process of transforming the data recorded in compact format in Dugway to a form suitable for analysis by Fortran programs.

4.2: General features of the site.

The Dugway array recorded data for well over 1000 hours from August 1981 to October 1985. This extensive observation required the development of standard methods of operation, both to safeguard the equipment and to select data for analysis.

The Dugway array was favourably situated for observations of the two main candidate V.H.E. gamma-ray sources (Cygnus X-3 and the Crab pulsar) at small zenith angles;.

latitude = 40.2° N

longitude = 112.825° W

The altitude of the array was 1450 m.

The weather record for the Dugway Proving Grounds was readily available from US government sources, and showed the site to be

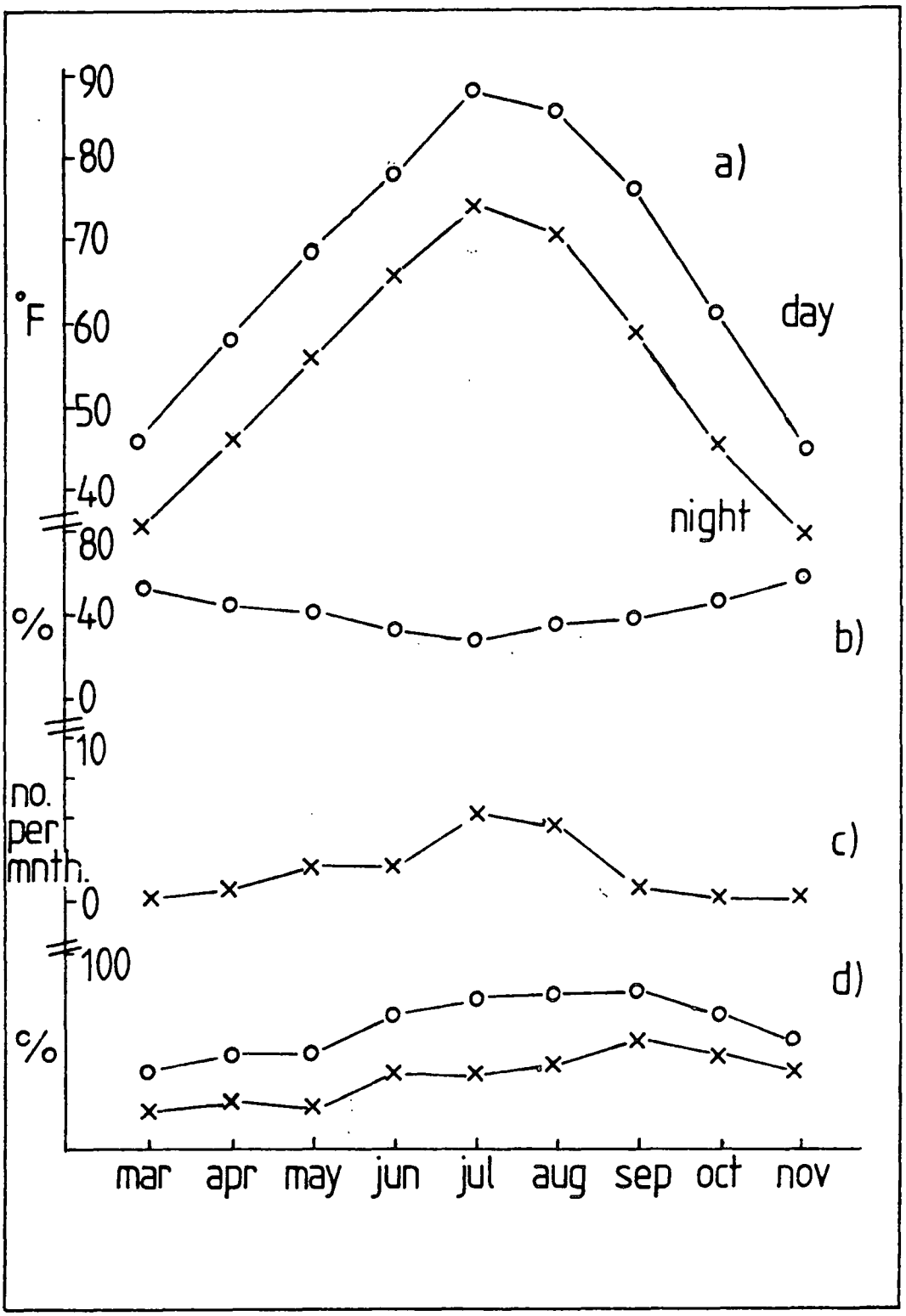

a) Average Temperature
b) Humidity
c) Thunderstorms
d) × - clear sky : o - clear sky + scattered cloud

Figure 4.1: The Dugway weather record.

suitable for this type of work. The climate in this part of Utah has a high percentage of clear skies and in addition, the 'seeing' is relatively good as the nearest city lights (Salt Lake city) are situated over 80 miles away. A summary of the weather conditions is given as figure 4.1 showing the monthly variations.

With the weather constraints evident from fig. 4.1 the observing season was set to start in July and run to November, with more observations conducted in March and April as required. This programme allowed a full coverage of the target sources. Over the 4 years of operation only 2 months were spoilt due to bad weather - September 1982 (lightning) and March/April 1983. In the next section the two main modes of operation are reviewed.

4.3: Observation techniques.

4.3.1: 'Drift scan' observations.

This simple mode of observation is favoured for the investigation of sources suspected of constant emission. The detectors remain stationary as the object drifts through their field of view with the Earths rotation. The technique comprises three distinct sections; the collection of 'OFF' source data, before the transit, an 'ON' source period, with the source in the field of view and another 'OFF' source section after the transit. Each 'OFF' section is chosen to last the same time as the 'ON' section.

With the detectors pointing at a constant zenith angle and with the instrument settings fixed, the background data collected should be governed by statistical fluctuations - assuming the sky conditions do not change. However, the inclusion of data taken 'OFF' source (before and after) allows a check to be made for systematic changes in the experiments performance due to any sky brightness or atmospheric

changes or instrumental drifts.

The duration of the scan depends on the objects declination and the field of view of the detector, but for the Dugway Mark I telescope with a field of view ~ 2.2° it takes Cygnus X-3 (Declination : 40 53 57) ~ 12 minutes to drift through, and so a drift scan of 36 minutes was used.

The correct interpretation of the technique uses the Gaussian form of the response of the system to a source, but this is difficult to determine exactly, and the analysis of drift scans made using the Dugway system involves a different approach.

The 'ON' source measurement is taken as the time during the scan with the object completely inside the field of view, and in the 'OFF' source sections the object is completely outside the field of view - see fig. 4.2. The response is therefore approximated more closely by a 'Top-hat' function, and the data taken with the object on the edge of the field of view is discarded.

The simplicity of the observation is matched by the straight-forward and easily interpreted analysis procedure described in section 5.2, but the inefficiency is apparent since the source spends most of the time out of the telescope's field of view.

4.3.2: 'Tracking' observations.

When it is important to maximise the amount of time that an object spends in the field of view of the detectors, and in particular, for the investigation of objects suspected of periodicity, the telescopes track the object across the sky. The Dugway system tracked an object by a series of short detector steers and not by a continuous movement. Between steers the object drifts in the field of view of the telescope, the interval between steers is set to ensure that the object remains near the centre of the field.

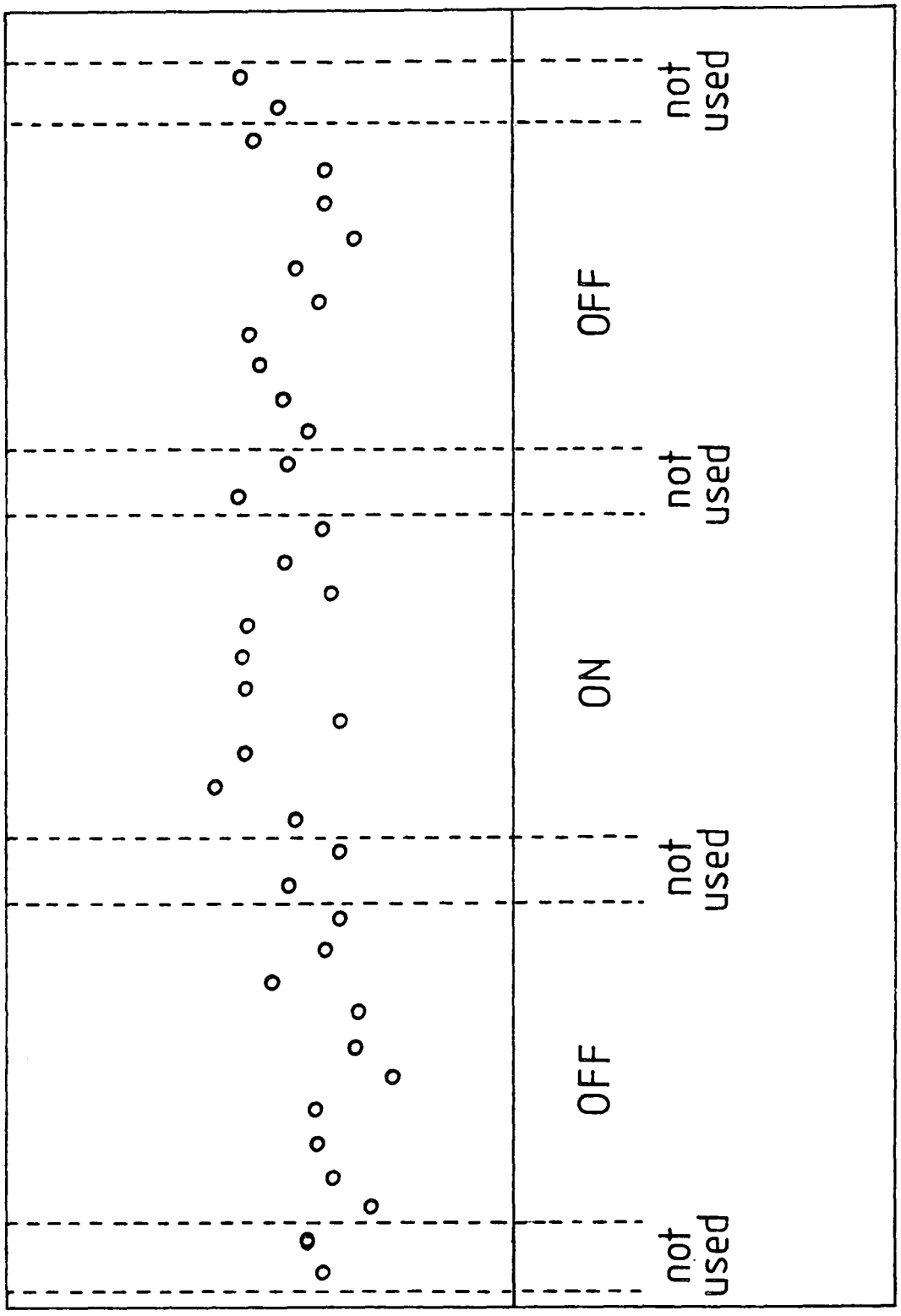

Figure 4.2: A schematic description of a 'drift scan' observation.

There are disadvantages to this method of observation. The need to steer every few minutes, often in extreme conditions, allows an increased probability of telescope steering failure. The tracking over a range of zenith angles results in a changing background counting rate, which can complicate the interpretation of the results. The changing background may be eliminated by the use of the servoed AGC lights (see section 3.3.4), however there is a consequent increase in threshold.

With an array of telescopes it is possible to operate pairs of units independently i.e. using the array to simultaneously monitor 2 objects. This form of observation has not been used extensively at Dugway as the detection of a source usually requires the maximum number of events to be detected to extract the small gamma-ray signal from the background. However, it may be used in the future for survey work.

The analysis procedures are described in section 5.4 and basically search for a periodicity in the data. Other forms of analysis can be performed on the tracking data, in particular the fast timing between detectors, and the pulse amplitude distributions have been investigated in an attempt to enhance the gamma-ray 'signal-to-noise' ratio.

4.4: The observational database.

The priority for the gamma-ray experiment in 1981 and 1982 was to collect data from the Crab pulsar and Cygnus X-3, regarded as the two strongest V.H.E. gamma-ray candidate sources in the Northern Hemisphere. With the detection at high significance of both of these objects (Dowthwaite et al, 1984b) ,(Dowthwaite et al, 1983), a more extensive observation of other objects was possible. A brief description of the observational database is now given.

Mode of observation	1981	1982	1983	1984
Tracking (hours)	27·5	141	43	-
Drift scan (hours)	85	9	1·5	-

Table 4.1: Observations of Cygnus X-3 from 1981 - 1983.

4.4.1: Cygnus X-3

A total of 307 hours of data were taken from this object, the details are summarised in table 4.1. In 1981 data were recorded in the 'drift scan' mode (76, 36 minute scans), with the telescopes sampling the 4.8 hour phase range, with the scans centred at 0.125 phase intervals from phase 0.0. In addition, further drift scans were made at phases offset by 0.03 from these values. A full description of the analysis of these data is given elsewhere (Kirkman, 1985). The 1982 observations were made using the tracking mode, the aim being to discover the duration of a large excess detected in the 1981 data at phase 0.63 (Gibson et al, 1982b). There were 28 nights suitable for analysis yielding 78520 recorded events. As in 1981 the data were analysed by first separating into distinct sections centred on the following phases,

phase	coverage (hours)
0.0	6.6
0.125	9.0
0.25	6.6
0.375	2.4
0.5	4.8
0.625	12.0
0.75	10.8
0.875	10.8

note: most nights did not cover the whole phase range.

Observations of Cygnus X-3 were conducted in 1983, but with only five of the nights suitable for count rate analysis. There were three drift scans of the object and two long nights of tracking data taken

in September covering the full phase range. These two nights included data taken with the improved Mark II detector 4, discussed in section 3.7.

These data were analysed using a method derived from the drift scan analysis to enable comparison with the earlier results - called a 'pseudo-drift-scan'. This method is described in greater detail in section 5.2.3.

Despite the smaller coverage, useful observations were conducted in September 1983. These were particularly significant due to the improvements in the array performance made in the first half of the 1983 season. No observations were made in 1984.

4.4.2: The Crab Pulsar.

Observations of this object were made throughout the 1981, 1982 and 1983 observing seasons, with the 1982 database by far the most extensive. In total over 137 hours of data were taken. All observations were made using the tracking mode without the servoed AGC system as maximum sensitivity was required rather than a stable data rate. The observations of November 1982 (> 70 hours) were particularly important. In this month the crystal clock timing was determined to high accuracy as it was based on a single reset (see section 3.5.1). This accuracy enabled a detailed investigation of the width of the mainpulse emission to be made (Kirkman, 1985).

4.4.3: Hercules X-1.

Over 32 hours of data were taken from this object, including a number of drift scans in April 1983. The drift scans were followed by tracking data recorded during July and August of 1983 and 1984. In particular the July 1983 data were contemporary with the strong

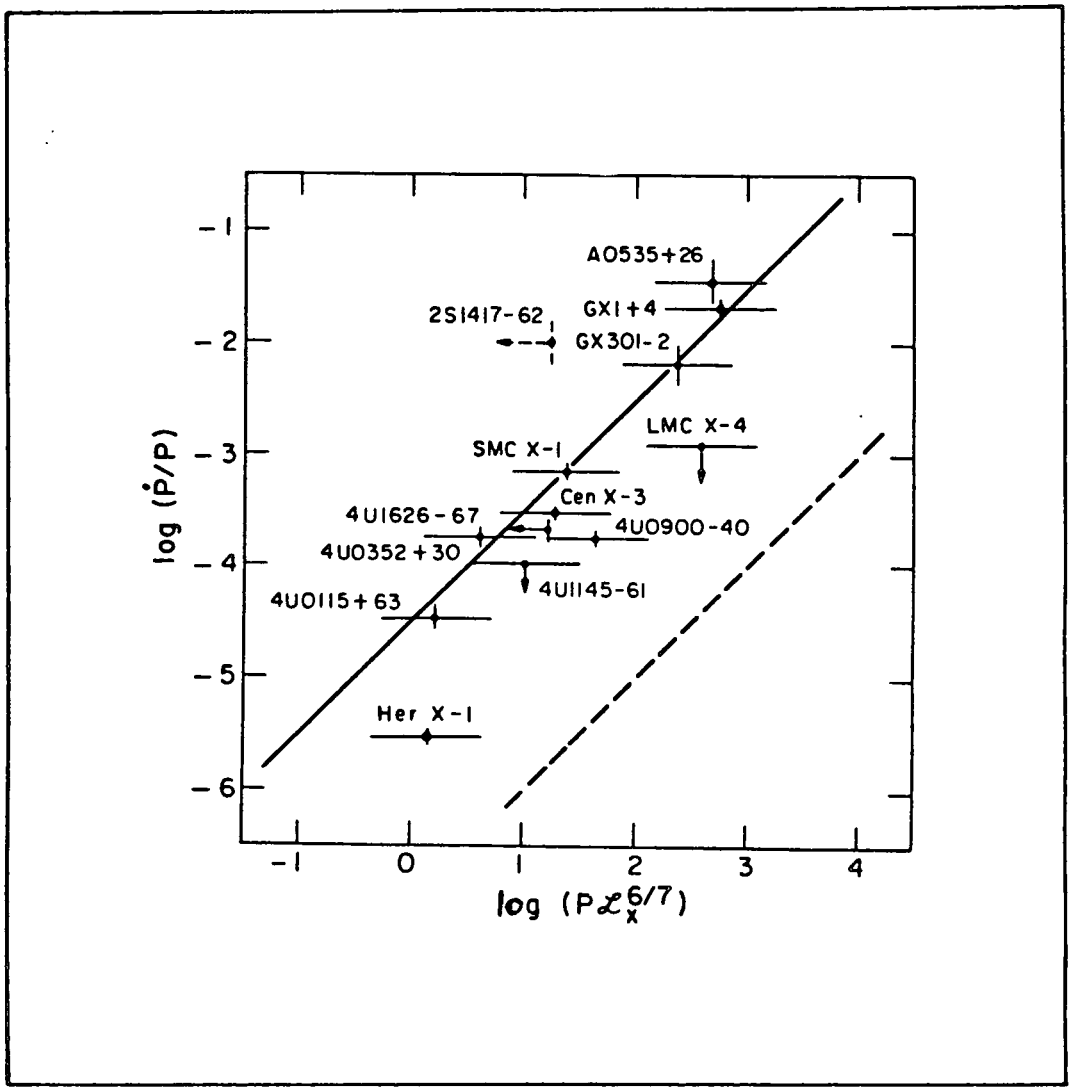

Figure 4.3: The relationship between age and luminosity for binary X-ray pulsars.

Object	Total (hours)
PSR0531	137
HER X-1	32
4U0115	25
GAL. PLANE	4
M31	5
2CG195	63
2CG065	64
4C21	132
CYG X-1	4
SS433	3
PER X-1	2
2CG135	11
3C273	13
NGC4151	3
CAS-A	3
PSR0950	47
PSR1929	11
PSR1133	27
PSR2233	69
PSR0355	36
PSR1508	33
PSR1930	4
PSR1913	15
PSR0655	10

Table 4.2: Observation totals 1981 - 1984.

detection at energies > 10^{14} eV by the University of Utah's 'Flys eye' detector. A full discussion of the results is given in section 6.4.

4.4.4: 4U0115 + 63.

With the detection of V.H.E. gamma-rays from Hercules X-1 (Dowthwaite et al, 1984a), a search was made for similar objects as candidate V.H.E. gamma-ray emitters.

The properties of binary X-ray pulsars can be summarised in the relationship (Rappaport and Joss, 1977)

$$\dot{P}/P = -3.\ 10^{-5} \cdot f \cdot (P/\ 1s) \cdot (L/\ 10^{37}\ ergs^{-1})^{6/7} - 4.1$$

i.e. relating the age of the pulsar, $P/\dot{P}$ to the period, P and luminosity, L (f is a dimensionless function ~ 1)

This function is plotted in fig.4.3 for a number of binary X-ray sources. The pulsar with the properties most resembling Hercules X-1 is then 4U0115+63. With the discovery of Hercules X-1 at V.H.E., 4U0115+63 was observed throughout the September/ October 1984 dark period. A total of 25 hours of data recorded using the tracking mode.

4.4.5: The Galactic plane.

One long drift scan, lasting 4 hours was made across the Galactic plane in the Cygnus region. Three of the detectors were operational, as detector 4 was being re-fitted with Mark II mirrors. The whole system was monitored closely during this observation to ensure stability. The servoed A.G.C.s were used and frequent checks on weather conditions, steering etc, were made.

The Dugway array observed many more objects in the period from 1981 to 1984, and these are summarised in table 4.2. In total, 1080 hours of useful data were recorded, comprising an extensive database.

4.5: The Computer database.

Analysis of the data taken at Dugway was conducted on two large computer facilities. For the initial work (1981) an IBM 4341 computer running the 'Michigan Terminal System' was used - the Durham University node of the 'NUMAC' computer service. But most of the data reduction, and most of the analysis reported in this work was performed using a DEC VAX 11/750 minicomputer running the VMS operating system - the Durham University Physics department node of the Science and Engineering Research councils 'STARLINK' network for astronomers. A description is now given of the database established on this system.

At Dugway, the data was recorded onto a 1600 ft, 9-track master-tape in a compacted form and then 'un-packed' into a format suitable for analysis. The overall procedure is summarised in flow diagram form in fig 4.4.

The data on the master tape were first converted to a format compatible with the VAX 11/750, then to a form suitable for analysis (see below) - in a separate stage. The data were then separated into each nights observation. At this stage the 'un-packed' data were edited into 'source' files i.e. separated into observations of each object and for each night. These source files form the main database and the 'unpacked' files were recorded as an 'archive' onto more 9-track tapes.

A source file exists for all objects observed for more than 10 hours, with other observations collected on a 'miscellaneous source' tape. In all there are 21 of these tapes, and they were the only tapes that needed to be accessed regularly.

4.5.1: The contents of the main files.

Each 'source' file then contains the following information;

i. A record of the start of the file, and a series of comments on the weather, name of object observed, observing method (i.e. drift scan or tracking mode), the start time in Mountain Standard Time, (M.S.T.) and a microsecond clock time along with the projected stop time. A note was made of the E.H.T. and A.G.C. status.

ii. At the start of an observation the equatorial coordinates of the object were recorded, along with the microsecond start time, E.H.T. and A.G.C. status.

iii. With every steer of the telescopes each detector's zenith and azimuthal angle was written to the 9-track tape, along with the microsecond time of the steer.

iv. For every event detected by any telescope the following measures were recorded;

The time of the event, recorded in microseconds.

A note of the mode of operation of the array (i.e. a 'normal' mode detection with the telescopes stationary, or an event recorded as the telescopes were steering).

The T.A.C. and 3 LeCroy 'QT100B' outputs for each detector involved in the event were also recorded (see section 3.4).

In addition, the anode currents in each phototube were recorded. A detailed summary of the experimental conditions was noted every minute, including measurements of the accumulated single-fold (photoelectron emission) rates, anode currents, phototube temperatures and pressures. The error in the steering of each detector was recorded as was the the microsecond time of these measurements.

4.5.2: The DASD database.

Much of the analysis of the 'tracking' data involves a search for periodicity and so requires only the event arrival times and a note of the combination of detectors involved. Such a database can be derived from the 'source' files and stored permanently on a DASD, the 'COSMOS' disc attached to the VAX 11/750 computer. The V.H.E. gamma-ray data has been allocated 10 Mbytes on this device, sufficient to store most of the event times recorded on all objects except for Cygnus X-3 and The Crab pulsar. This data is then accessible quickly and speeds the analysis procedure considerably.

Usually the event arrival times must be reduced to the Solar System barycentre before any analysis for periodicity is possible and the Durham University Barycentre routine must be applied to the source files to establish this database. A description of the Barycentring process is given in section 5.3.1. The barycentred times are then converted from Julian ephemeris time to a microsecond time and stored as mentioned above on the 'COSMOS' disc.

For objects known to be binary systems it is necessary to further reduce the event arrival times to the focus of the orbit and the results of this procedure may also be stored on the 'COSMOS' disc for easy periodicity analysis. Details of these focussing procedures are given in section 5.3.2.

With this database established, the wide range of analysis programmes, which were developed and stored on another part of the hard-disc, can be utilised. For instance 'PERIOD' is a powerful program written in FORTRAN77 to apply various statistical tests in a search for periodicity in sections of the data.

The preliminary analysis involves an investigation of the counting rate for the array. The number of events recorded in, for instance,

each minute is computed for all combinations of telescopes. This record is then printed to provide a useful summary of the array performance and may be used to search for bursts of gamma-ray events on the timescale of minutes.

4.6: The Pulse amplitude analysis

For analysis of the intensity of the Cerenkov flash the amplitude of the pulses registered by the phototubes is investigated. The use of this measure has been found to be limited and so an extensive, general database was not needed. The investigation is restricted to sections of data thought to be rich in candidate gamma-ray events as determined by more powerful analyses. Programs have been developed to set up small databases extracting the information in the source file to produce a normalised pulse height value and microsecond time for each detector, with each event.

For data taken over a relatively short time ~ 1 hour the systematic effects of changes in zenith angle are small (see section 3.6.1) and a normalised pulse amplitude value is derived for each detector using a linear least squares fit for each phototube normalised to the centre tube. In cases where an analysis is made over a longer period e.g. several hours in the case of the November 1982 Crab pulsar data, the normalised pulse amplitude is simply derived by adding all three detector values (left, centre and right). The database is then stored on 9-track tape for detailed analysis using programs written to search for differences in the pulse amplitude distributions by applying the statistical tests described in section 5.5.

The detailed investigation of the inter-detector fast timing also requires a large magnetic tape database of the event time, but this database is not discussed here (see Walmsley, PhD thesis in

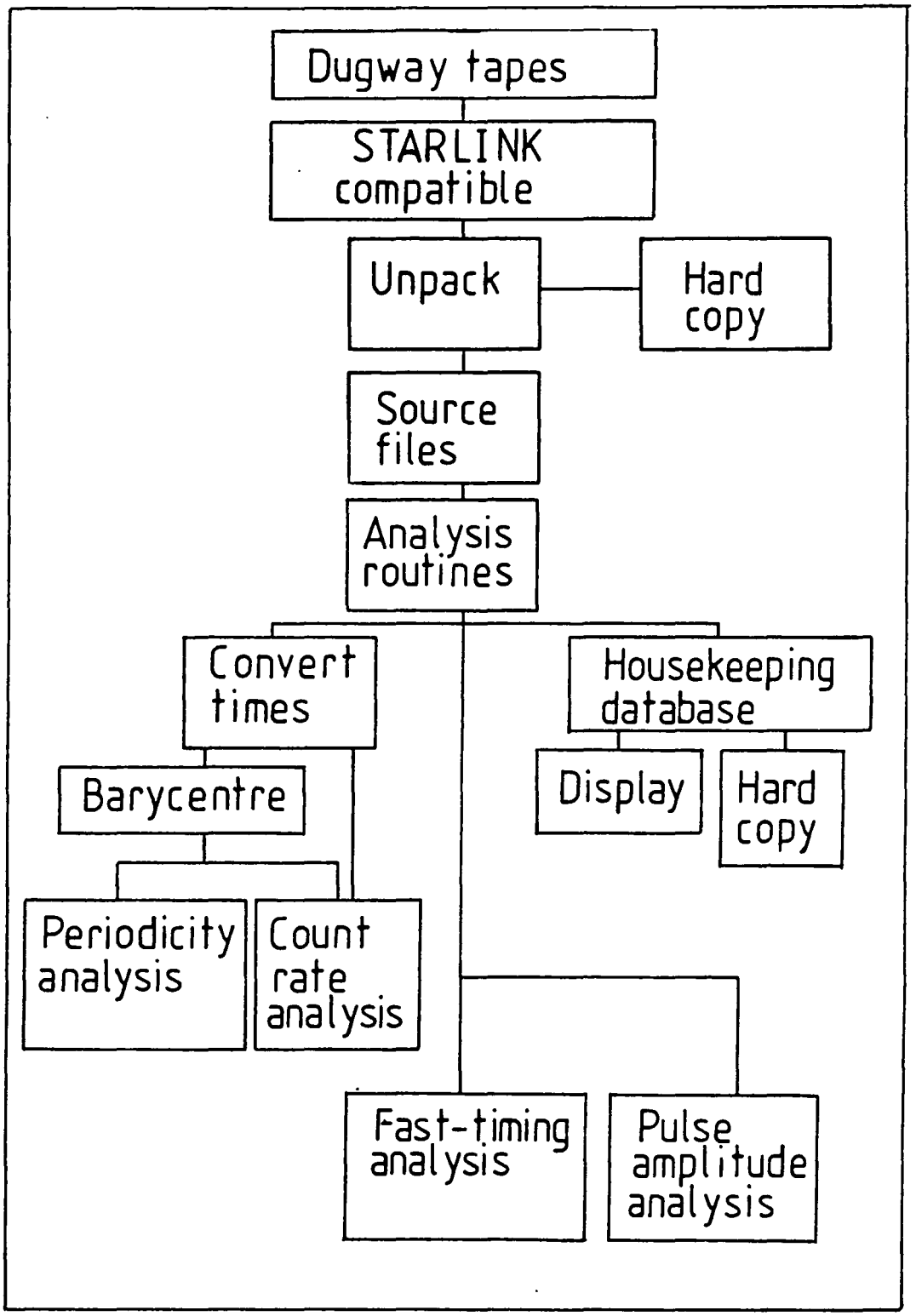

Figure 4.4: A summary of the analysis procedure.

preparation).

The full analysis procedure is summarised in schematic form in fig. 4.4. The detailed discussion of some of these procedures is given in the next chapter.

Chapter 5: Data Analysis Techniques.

5.1: Introduction:

The interpretation of data taken with ground-based Cerenkov telescopes is not straightforward. This is due to the very high background or 'noise-level' from cosmic ray protons. Efforts have been made to identify a difference in the signatures of the flashes caused by protons and gamma-rays, but with little success. Recently, results have indicated that the showers may differ slightly in intensity (Cawley et al, 1985b), (Stepanian et al, 1983) and see section 6.2.6, but present knowledge does not allow a significant direct increase in the signal-to-noise ratio.

Despite these difficulties it is possible to enrich the gamma-ray sample by the use of the fast inter-detector timing technique. This does not directly distinguish gamma-ray showers, but rejects off-axis ones within a large field of view system as likely background. The technique has been employed with success in the analysis of the data taken at Dugway from the Crab pulsar (Dowthwaite et al, 1984b), and from Hercules X-1 (Dowthwaite et al, 1984a).

In general, the approach adopted must be based on the temporal or spatial anisotropy in the data, as the proton initiated showers are randomly distributed. The data recorded with the telescopes tracking a periodic source can be analysed using statistical techniques designed to extract the periodic content from the data - see section 5.3. The simple observing technique known as the 'drift scan', and described in section 4.3.1 lends itself to the form of analysis outlined in the next two sections. The tests look for an increase in count rate when the object is in the field of view of the telescope.

5.2: The analysis of 'drift scan' data.

5.2.1: The 'Top Hat' analysis - likelihood ratio.

A suitable analysis of 'drift scan' data can be made, the method is due to K.J. Orford and is also described elsewhere (Dowthwaite et al, 1983).

If 'O' counts are recorded with the suspected source in the field of view and 'b' counts are recorded before and 'a' counts after this, then the maximum likelihood estimate of the signal from the object is given by;

$$s = O - (a+b)/2 \qquad - 5.1$$

The simple case used in the analysis presented in this thesis assigns data taken with the source fully in the field of view as the 'ON source' data, and takes events recorded with the source completely outside of the field of view as the 'OFF source' data. The data recorded with the source on the edge of the field of view are ignored. This type of analysis can be termed a 'Top hat' procedure. The aperture function of a Mark I telescope is a Gaussian function of full width half maximum = 2.2°, and a suitable procedure for making more efficient use of the data is described in section 5.2.2.

Investigations of the counting rate of the array show that the temporal distribution of these events is essentially Poissonian and it is therefore possible to use the statistical approach outlined below.

If a signal from the source S and a background rate B are suspected from a prior knowledge of the exact situation, then the Neyman-Pearson Lemma can be used to select the most powerful test for distinguishing between the two hypotheses,

H_1 (S = some value S')

H_0 (S = 0)

A suitable test statistic to use is,

$$l\ (N,S) = \frac{L\ (\ N\ |\ S = S'\ )}{L\ (\ N\ |\ S = 0\ )} > = C \qquad - 5.2$$

where it is assumed the background is known exactly, N counts are recorded during the ON source time, the signal detected is represented by S counts, and C is some confidence level.

In the case of ground-based 'Cerenkov Effect' astronomy the background is not known and there is no most powerful test. However an estimate of the true background rate can be made from a probability distribution of the observed background. One way to proceed, is to identify the maximum likelihood ratio;

$$M = \frac{\max L\ (\ N\ |\ S = 0\ )}{\max L\ (\ N\ |\ S\ )} \qquad - 5.3$$

as a suitable test statistic for H_0.

In this analysis the following assumptions are made.

i. N counts are recorded during the ON source part of the scan.

ii. B counts are recorded in the OFF source part of the scan which lasts R times as long as the ON source period.

iii. The signal detected is S and the true background is T.

n.b. these are both unknown.

Now suppose that the signal S = 0, in which case N and B are simple

statistical fluctuations from T. The probability is given by;

$$L_{\varnothing}(T) = L\,(N,B \mid S = \varnothing, T) = \frac{e^{-(1+R).T} \cdot T^{(N+B)} \cdot R^{B}}{N! \cdot B!} \qquad - 5.4$$

If there is a signal, S detected by the equipment, and therefore N is not a statistical fluctuation then the probability is given by;

$$L_{S}(S,T) = L\,(N,B \mid S, T) = \frac{e^{-((1+R).(T+S)} \cdot (T+S)^{N} \cdot (R.T)^{B}}{N! \cdot B!} \qquad - 5.5$$

Given the two expressions the maximum likelihood ratio M can be reduced from equations 5.4 and 5.5 by setting $dL_{\varnothing}(T)/dT = \varnothing$ to find $\max(L_{\varnothing}(T))$, and from $d^2L_S(S,T)/dSdT = \varnothing$ to find $\max(L_S(S,T))$ The resultant ratio is then,

$$M = \left(\frac{N+B}{(1+R) \cdot N}\right)^{N} \left(\frac{R.(N+B)}{(1+R) \cdot B}\right)^{B} \qquad - 5.6$$

For the particular case of the drift scan observations conducted using the Dugway array the ratio, R = 2, and so,

$$M = \left(\frac{N+B}{3N}\right)^{N} \left(\frac{2.(N+B)}{3B}\right)^{B} \qquad - 5.7$$

This last expression gives the relative likelihood of N, the number of ON source counts being a statistical fluctuation from T, the 'true' background rate, i.e. of $H_{\varnothing}$ being true to H_1 being true. Note that the

most likely source strength is S_1, where,

$$S_1 = S' = N - T' = N - B/R \qquad - 5.8$$

this is taken as the best estimate of the source strength available from this analysis. The limits on S_1 are obtained by relaxing the value of M to S+ and S-, which correspond to the 68% confidence regions for S_1. This analysis is considered to give a 'conservative' likelihood estimate of source strength.

The use of this method has been discussed in recent papers (Li and Ma, 1983), (Protheroe, 1984). It has been shown to be preferable to earlier estimates of a source strength (Hearn, 1969), (O'Mongain, 1973) and (Cherry et al, 1980).

5.2.2: Cross-correlation analysis of 'drift scan' data.

This method is due to Hermsen and its application to the Durham data is described elsewhere (Kirkman, 1985). The basic feature of this procedure is a correlation of the signal over and above the background which is consistent with the 'point spread function' of the telescope. It is therefore a more refined analysis than the simple 'Top hat' approach outlined in the previous section, and used in this thesis. The cross correlation technique was used in the analysis of the gamma-ray data taken with the COSB satellite (Hermsen, 1980). It should be adapted for the analysis of 'drift scan' observations from future generations of ground-based arrays.

5.2.3: The likelihood ratio analysis of 'tracking' data.

In 1982 the data from Cygnus X-3 were taken with the detectors in the 'tracking' mode i.e. the source of gamma-rays was never out of the

field of view. The data were analysed by analogy with the 'drift scan' methods. This procedure was used to investigate the 1982 Cygnus X-3 data, taking 10 minutes centred on the required phase and comparing this to 10 minutes of data taken before and after this using an adaptation of the maximum likelihood technique described above.

The problem with this procedure concerns the evaluation of the background counts. In the 'tracking' mode the zenith angle of the object is constantly changing, as is the background counting rate (see fig.3.13), and so one of the basic requirements of the maximum likelihood technique, i.e. a constant background is not met. However, it can be shown that the decrease in counting rate with zenith angle is 1.5% around a zenith angle of 10°, 5% around 30° and 9% at 45° for say 25 minutes and so the method outlined in section 5.2.1 may be used, as the non-linearity in the count-rate change with zenith angle is small (< 0.15%).

5.3: The analysis of the tracking data:

In the majority of the observations taken with the Dugway array the telescopes followed the object across the sky. This form of observation allows a more efficient use of the recording time than the drift scan technique and the tracking method is more suited to the detection of periodic sources, such as X-ray and radio pulsars. The analysis procedure adopted is summarised below.

5.3.1: The Barycentring process

The phase errors caused by both the spin of the Earth on its axis and its orbit around the Sun mean that the period of any object e.g.

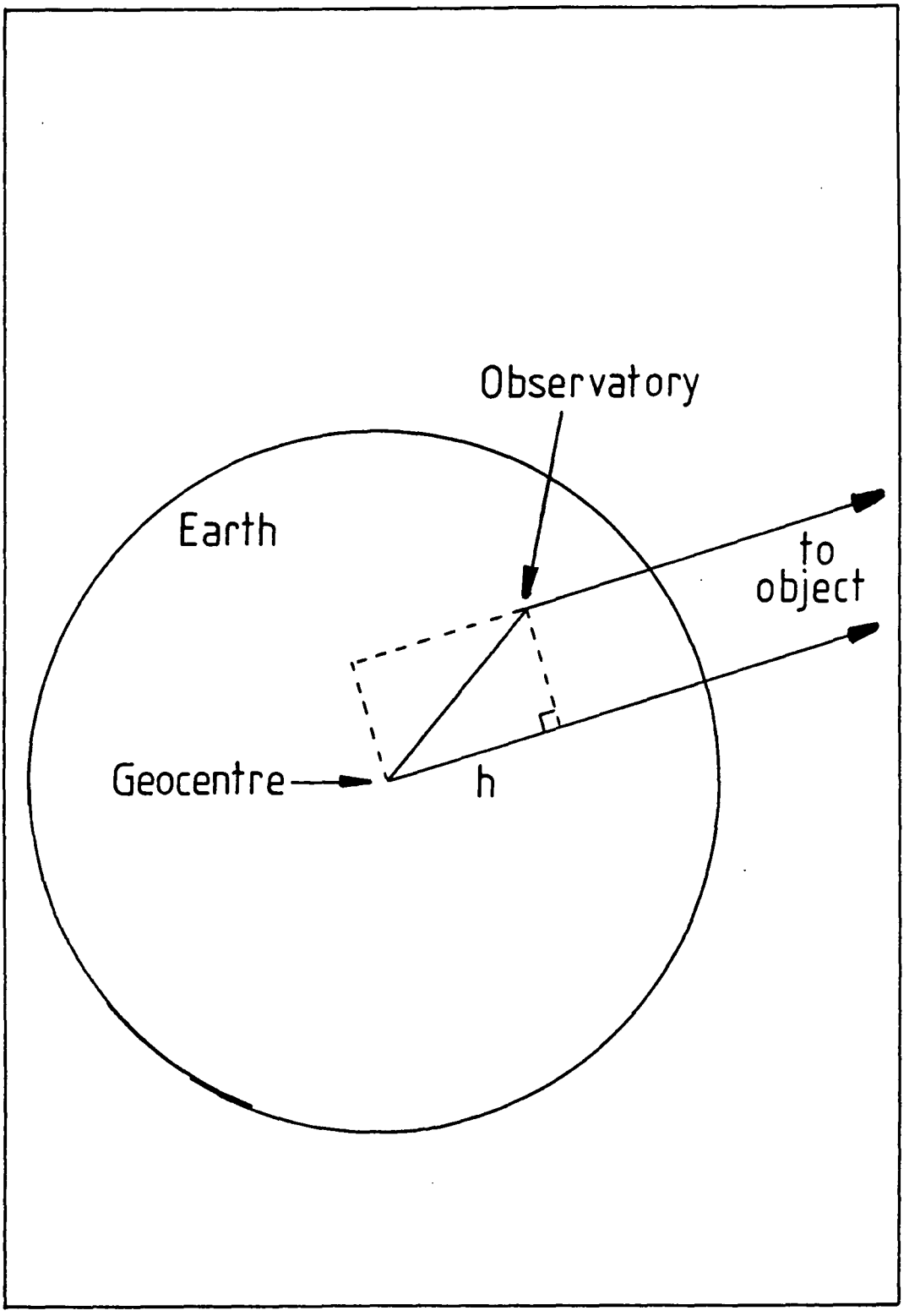

Figure 5.1: The reduction of event times to the Earth's centre.

the Crab pulsar, as measured in the laboratory frame, change in a predictable manner modulated with the periods of these rotations. In practise, the time of arrival of each event should be corrected to the time at which the event would have arrived at the Solar System Barycentre (the suitable inertial reference frame). This is important as ephemerides usually refer to the Barycentre.

There are five main stages to the barycentring process;

i. The event arrival time must be corrected for changes in the system clock rate. This is achieved by making regular spot measurements of the drift - see section 3.5.1.

ii. A correction must be made for the delay in the propagation of the WWV radio signal used to calibrate the system clock.

After these two corrections have been made the event times are in Coordinated Universal time (UTC), absolutely accurate to ~ 0.5 ms and to a resolution of ~ 1 μs.

iii. Correction to the centre of the Earth.

Refering to fig. 5.1.

The site coordinates are taken as,

R.sinL and R.cosL

where R is the radius of the earth at the particular site, and L is the site latitude.

It is usual to continue in a coordinate system, x,y,z defined as follows; with x pointing to A, the First Point of Aries, z to the pole, and y at right angles to these. We can then evaluate the vector from the centre of the Earth to the site at the time of the event. The right ascension and declination of the object are usually known to high accuracy from measurements made at other (lower) energies, and since the site coordinates are in the same frame of reference the scalar product can be performed to give the distance h in terms of R. The value h/c gives the correction time which is added to the event arrival time to give its arrival at the centre of the Earth.

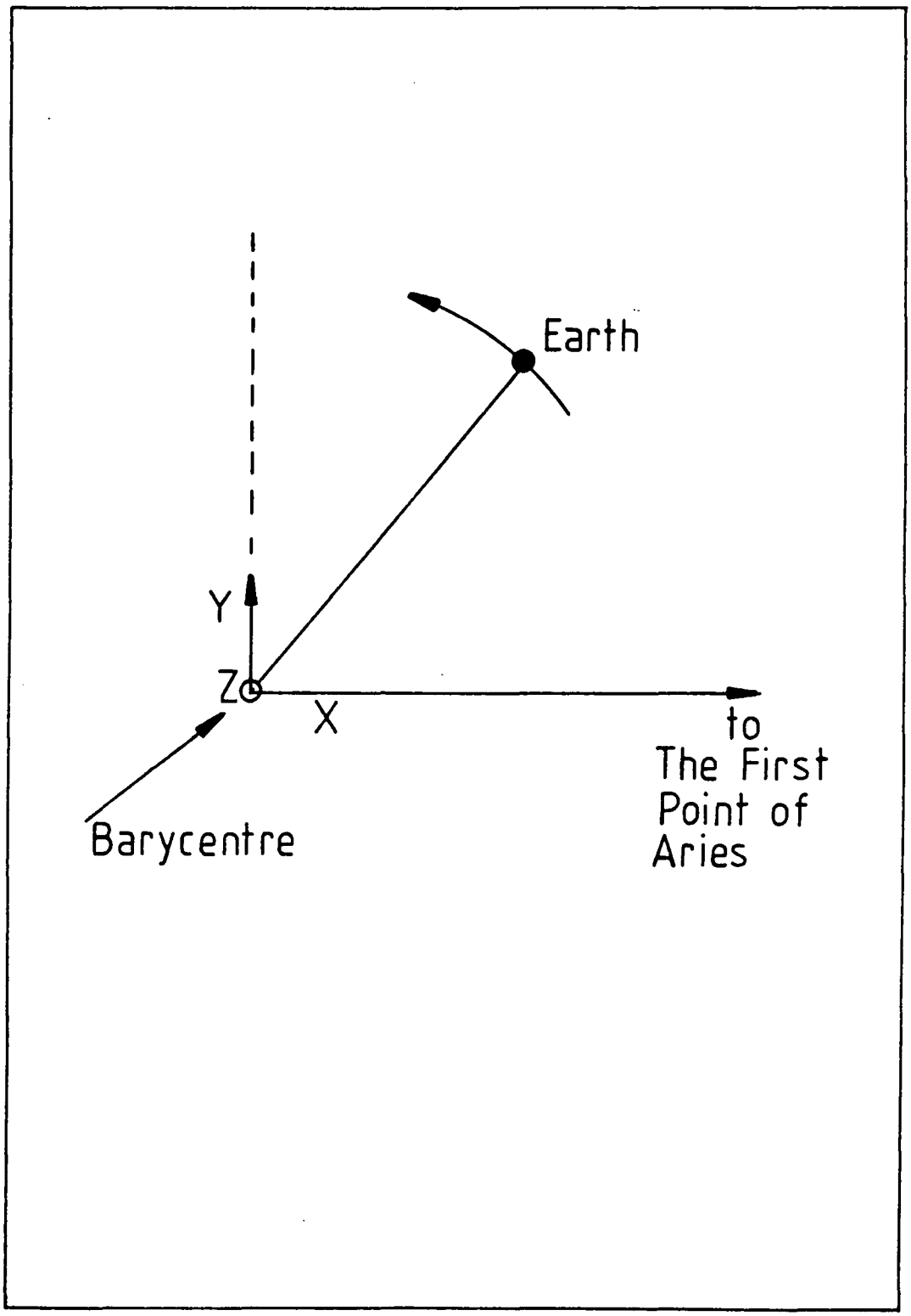

Figure 5.2: The reduction of event times to the Solar System Barycentre.

n.b. h is evaluated for each event.

iv. Correction to the Barycentre.

Refer to fig. 5.2.

Accurate ephemerides such as that derived by the Massechusetts Institute of Technology, MIT have been used (Ash et al, 1967). This ephemeris provides the coordinates of the centre of the Earth relative to the Barycentre (X,Y,Z and $\dot{X},\dot{Y},\dot{Z}$ values) tabulated every 2 hours. In order to deduce the accurate position of the Earth a polynomial fit was made to the separate X,Y and Z coordinates (13 in the case of MIT) for a day about the event arrival time at the geocentre. Knowledge of this resultant vector and the position of the observed object allows the required correction to be made. This correction is converted to seconds and added to the event arrival time.

v. A small relativistic correction must be made to the times due to the orbital motion of the Earth.

The event arrival times are then recorded in 'Barycentred Julian Ephemeris Time'. A check on the accuracy of the correction was made by comparison with the routine used to barycentre data from the Anglo-Australian telescope (Kirkman, 1985). The maximum difference in the values from the two procedures was found to be 200 μs in 500 s - adequate for all the analysis presented in this work.

5.3.2: The reduction of event times to the focus of an orbit.

Many of the objects observed by this experiment are binary systems e.g. Hercules X-1 and 4U0115 + 63. For analysis of data taken over a substantial part of the binary orbit it is essential to remove the orbital doppler shift of the period. This is only possible if accurate orbital elements are known. The basic parameters that are needed to

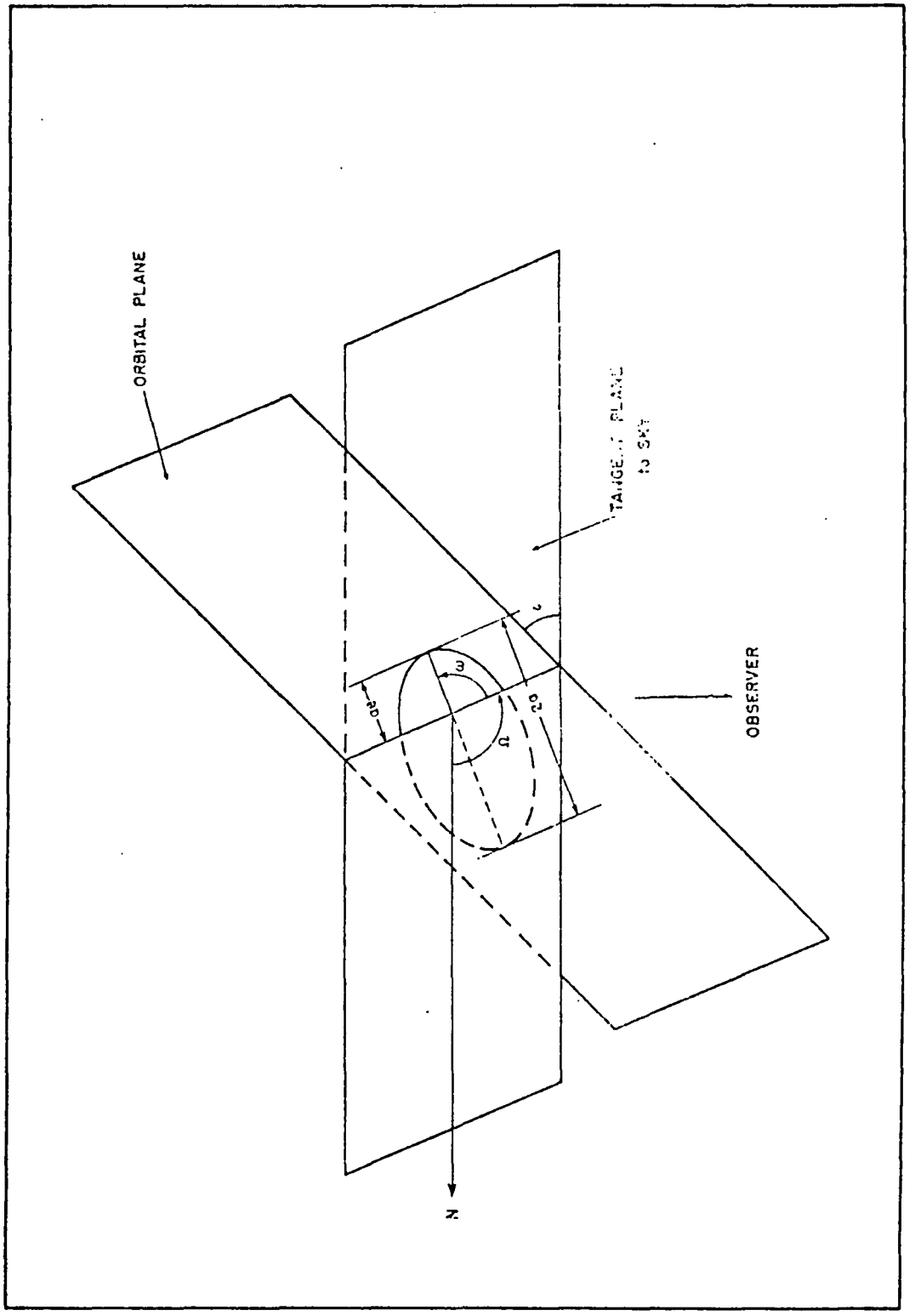

Figure 5.3: A representation of a binary system showing some of the orbital elements.

completely specify a binary orbit are (see Fig. 5.3);

a : semi-major axis

e : eccentricity

P_b : Orbital period

i : inclination of the orbital plane to the line of sight

Ω : position angle of the node

W : longitude of periastron

TP : time of periastron passage

For the X-ray binary pulsars no complete set of values are available but it is possible to focus the event times given P_b, e and a from an estimate of the 'mass function', f,

$$f(M_1, M_2) = \frac{M_2^3 . \sin^3 i}{(M_1 + M_2)^2}$$

where M_1 and M_2 are the component masses.

The methods used to focus the arrival times for one of the binary pulsars PSR1913+16, are explained elsewhere (Blandford and Teukolsky, 1976) and (Taylor et al, 1979) and will not be explained in great detail here.

The expression giving the phase at time t, A(t) is;

$$A(t) = A_\omega + \upsilon_\omega (t - TP_\omega) + \frac{1}{2} \dot{\upsilon}(t - TP_\omega)^2 + \upsilon_\omega . Q (2\pi . R . S . P_b^{-1} - 1) - \dot{\upsilon} . Q (t - TP_\omega) \quad - 5.9$$

where,

υ = pulsar frequency

Q = fg + h.sinE

R = -g.sinE + h.cosE

S = $(1 - e.\cos E)^{-1}$

f = cosE - e

g = a.sini.sinW

h = $(1 - e^2)^{1/2}$ a.sini.cosW

and the values of P_b, e, and $W = W_\omega + \dot{W} (t - TP_\omega)$ are initial

estimates of the binary period, eccentricity, and the longitude of periastron. E is the eccentric anomaly defined by,

$$2\pi \frac{(t - TP_{\omega})}{P_b} = E - e.\sin E$$

TP_{ω} is a reference time of periastron passage. The pulsar frequency ν_{ω} and a reference longitude W_{ω} are also defined at this epoch. Corrections to the terms are obtained by a least squares fit to the residuals.

The Durham data for binary sources have been focussed using procedures developed by Pat Wallace (Rutherford-Appleton laboratory).

5.3.3: The search for periodicity - A known ephemeris.

An exact ephemeris has not been usual in the analysis of the Dugway data. Indeed, only for the Crab pulsar has an accurate ephemeris been available derived from radio measurements at Jodrell Bank contempory with the gamma-ray observations. Such measurements provide the following quantities;

t_{ω} : the Epoch of the observations

P_{ω} : the period at t_{ω}

P' : the rate of change of P_{ω} with time

p'': the second derivative of P_{ω}

A_{ω} : the phase of the mainpulse in the 'duty cycle' at P_{ω}

A summary of the 1982 Crab pulsar ephemeris provided by Jodrell Bank is given in Table 5.1.

The period at time t is then given by;

$$P(t) = P_{\omega} + P' (t-t_{\omega}) + \frac{P'' . (t-t_{\omega})^2}{2} + ... \qquad - 5.10$$

Month	Arrival time (days from 240000·0)	Period (ms)	error	$\dot{P}$ (μs/day)	error
JUNE	5135·500000202839	33·2720301004	1559	0·036426060	11185
JULY	5165·5 " 076191	" 31229251	" 1	" 6667	" 27
AUGUST	5196·5 " 264996	" 42521549	" 1	" 7312	" 21
SEPTEMBER	5226·5 " 217493	" 53449776	" 4	" 7882	"115
OCTOBER	5257·5 " 091210	" 64741818	" 4	" 7886	" 41
NOVEMBER	5288·5 " 120274	" 77603410	" 3	" 6444	" 57
DECEMBER	5318·5 " 269889	" 86961934	" 2	" 5918	" 28

Table 5.1: The Crab Pulsar ephemeris - 1982.

In cases where the value of the phase of emission in the duty cycle is important it is easier to convert the ephemeris into a frequency form;

$$f_o = \frac{1}{P_o}$$

$$f' = -\frac{P'}{P_o^2}$$

$$f'' = \frac{2.P'^2}{P_o^3} - \frac{P''}{P_o^2}$$

with the frequency of emission at time t given by,

$$f(t) = f_o + f'(t-t_o) + \frac{f''.(t-t_o)^2}{2} + \text{other terms}$$

The absolute phase of emission is then simply the integral of the frequency,

$$A(t) = A_o + f_o(t-t_o) + \frac{f'.(t-t_o)^2}{2} + \frac{f''.(t-t_o)^3}{6} \qquad - 5.11$$

Errors in the original ephemeris (relevant to t_o) cause an increasing uncertainty in the value of the period, and more seriously the phase with time t. For instance, the ephemeris for November 1982 for the Crab pulsar is adequate for almost one year in the case of the progressive error in the period. However, if the phase information needs to be retained to a tolerance of one tenth of the period then the ephemeris above can only be relied on for about one month after t_o. In the case of the Crab pulsar an update to the ephemeris was provided for each month in 1982. The phase of each event can then be determined accurately. Each dataset can then be tested for non-uniformity of phase using one of the statistical tests described below.

5.3.4: Epoch folding

The phase of each event is calculated using equation 5.11 above,

the distribution of phases is then binned. The binned distribution is then tested for non-uniformity using Pearsons χ^2 test (Leahy et al, 1983). The Epoch folding technique is most effective if the width and phase of the pulsed emission are known. In this case the bin width can be chosen accordingly and a very powerful Binomial test can be made on the favoured bin in comparison to the others. A discussion of the relative power of this technique when applied to the general case of unknown pulse phase and duration is given in section 5.3.10.

5.3.5: The Rayleigh test.

The events are assigned a phase in just the same way as for the Epoch folding technique, but instead of binning, each event is interpreted as a unit vector with a particular direction in a phasogram. The resultant of the N vectors in the datasample is then taken as a measure of the non-uniformity in phase, and evidence of a periodic content to the data.

In general, for the analysis of the Dugway data the Rayleigh test has been used. The procedure adopted is as follows;

i. Each event is assigned a phase, A using equation 5.11 and the accurate ephemeris.

$$A_i = 2\ \pi\ f.t_i \ (\mathrm{mod}\ 2\ \pi\ ) \qquad - 5.12$$

where f, the frequency = 1/period

ii. The resultant of the phases for the N events is recorded. If C and S are taken as the orthogonal components of the resultant vector then,

$$C = \sum \frac{\cos A_i}{N}$$

$$S = \sum \frac{\sin A_i}{N}$$

and the length of the resultant, R is simply,

$$R = \sqrt{C^2 + S^2} \qquad - 5.13$$

n.b. the resultant, R represents the % pulsed content in the sample.

The quantity $2NR^2$ is asymptotically distributed as a χ^2 statistic with two degrees of freedom, and it can be shown (Mardia, 1972) that the probability of NR^2 exceeding some value K is given by,

$$\text{Prob.}(NR^2 > K) = e^{-K}.\left[1+\frac{(2K-K^2)}{4N} - \frac{(24K-132K^2+76K^3-9K^4)}{228N^2}\right] \qquad - 5.14$$

with a useful approximation given by the first term, e^{-NR^2} .

The Rayleigh test can be understood as a correlation of a sine wave at the ephemeris period with the phased event distribution, and has some advantages over other χ^2 tests in that there is no requirement to set up arbitrary bins. There are also disadvantages, and a discussion of the power of the technique is given in section 5.3.10.

5.3.6: A Search over a range of periods.

Some searching about an inaccurate period was necessary to extract any periodic content in the data taken from objects for which an accurate ephemeris was not available. This is more complicated than the simple case outlined in the previous sections because it introduces 'degrees of freedom' into the analysis.

Among the reasons for the search are,

i. Uncertainties in quoted Epoch, period and period derivatives.

ii. Uncertainties in the orbital parameters, and so inaccuracies in the focussing technique.

In this form of analysis each independent period in the search range must be tested. The separation of independent periods is termed a 'fourier' or 'harmonic' interval.

If the duration of the observation is T seconds and the trial

period is P_1, then the phase of the last event relative to the first is,

$$A_1 = \frac{T}{P_1} \qquad - 5.15$$

as P_1 is increased to P_1+p' the phase slips relative to that defined by P_1, and at a period P_2 the phase slippage is equal to a whole period i.e. the phase coherence is totally destroyed. P_2 is then the next independent period, and P_2-P_1 the harmonic interval.

The number of independent periods that need to be tested as above in a period search between P_x and P_y is given by,

$$N_p = \frac{T}{P_x} - \frac{T}{P_y} \quad \text{(approx.)} \qquad - 5.16$$

where T is the time interval of the observation. The size of the harmonic interval is then given by;

$$N_p \sim= \frac{P_x^2}{T} \qquad - 5.17$$

- assuming $P_x \sim P_y$

It is evident that for a given observation the size of the interval depends on the period tested. As an example we can investigate a wide search in period, say from 1 ms to 1 second in a datasample taken over 10 minutes. The number of independent periods is then;

$$N_p = 6 \times 10^5$$

with 5.4×10^5 periods between 1ms and 10ms, only 6×10^4 between 10ms and 1 second.

The detailed analysis of a range of periods involves the application of the Rayleigh test as described in section 5.3.5 to each independent period.

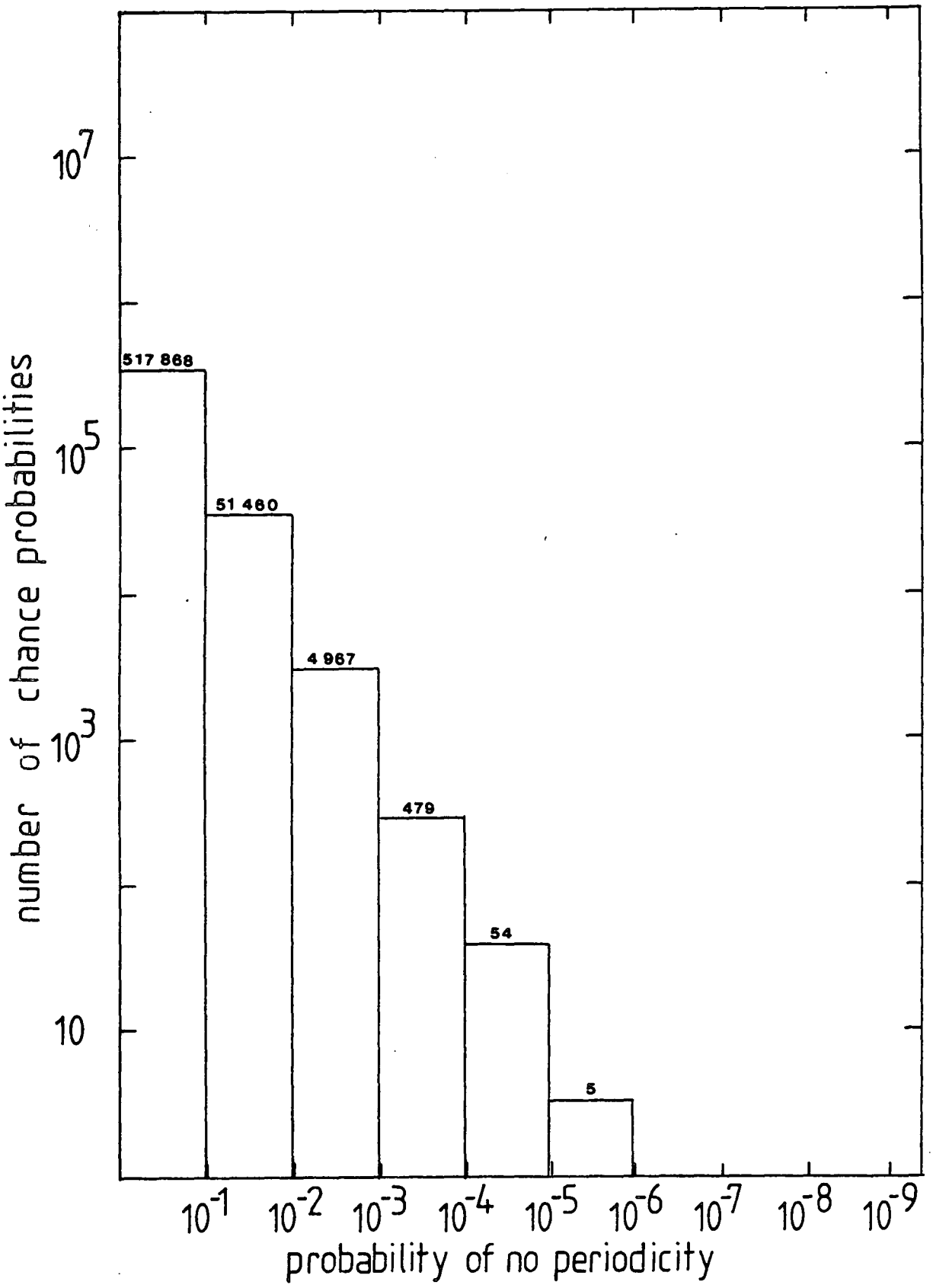

Figure 5.4: The distribution of chance probabilities produced by using the Rayleigh test to search for a period in random data. Search range = 10 ms - 1 s in data taken over 10 minutes.

5.3.7: 'Degrees of freedom'.

In a search for periodicity it is important to note the number of 'degrees of freedom' expended in the repeated use of the statistical test. For instance in a search from 10ms to 1s in 600 s of data, i.e. 6×10^4 independent periods, only probabilities considerably less than 10^{-5} should be considered to be indications of significant periodicity. Figure 5.4 represents a plot of the performance of the Fortran program searching for periodicity in random data using the Rayleigh test. In addition, it has been usual to perform the above test a number of times within the harmonic interval, introducing further 'degrees of freedom'. In all probabilities of no periodicity quoted in this work the 'degrees of freedom' have been noted and allowed for.

5.3.8: Simulated results of the periodicity analysis.

The probability function used in the above analysis has been extensively checked by;

i. Performing the periodicity analysis on a time series simulated by a 14-digit pseudo-random number generator.

ii. Investigating the performance of the above algorithm to real data analysed within a range of randomly chosen periods.

An example of this analysis is given as fig 5.4, a plot of the probability distribution for 100000 periods between 10ms and 1 s.

In both cases the probability distribution agrees well with expectation for probabilities as small as 10^{-5}. For probabilities greater than 10^{-7} the expression is thought to be valid for reasonable values of K, but for values less than this no information is given.

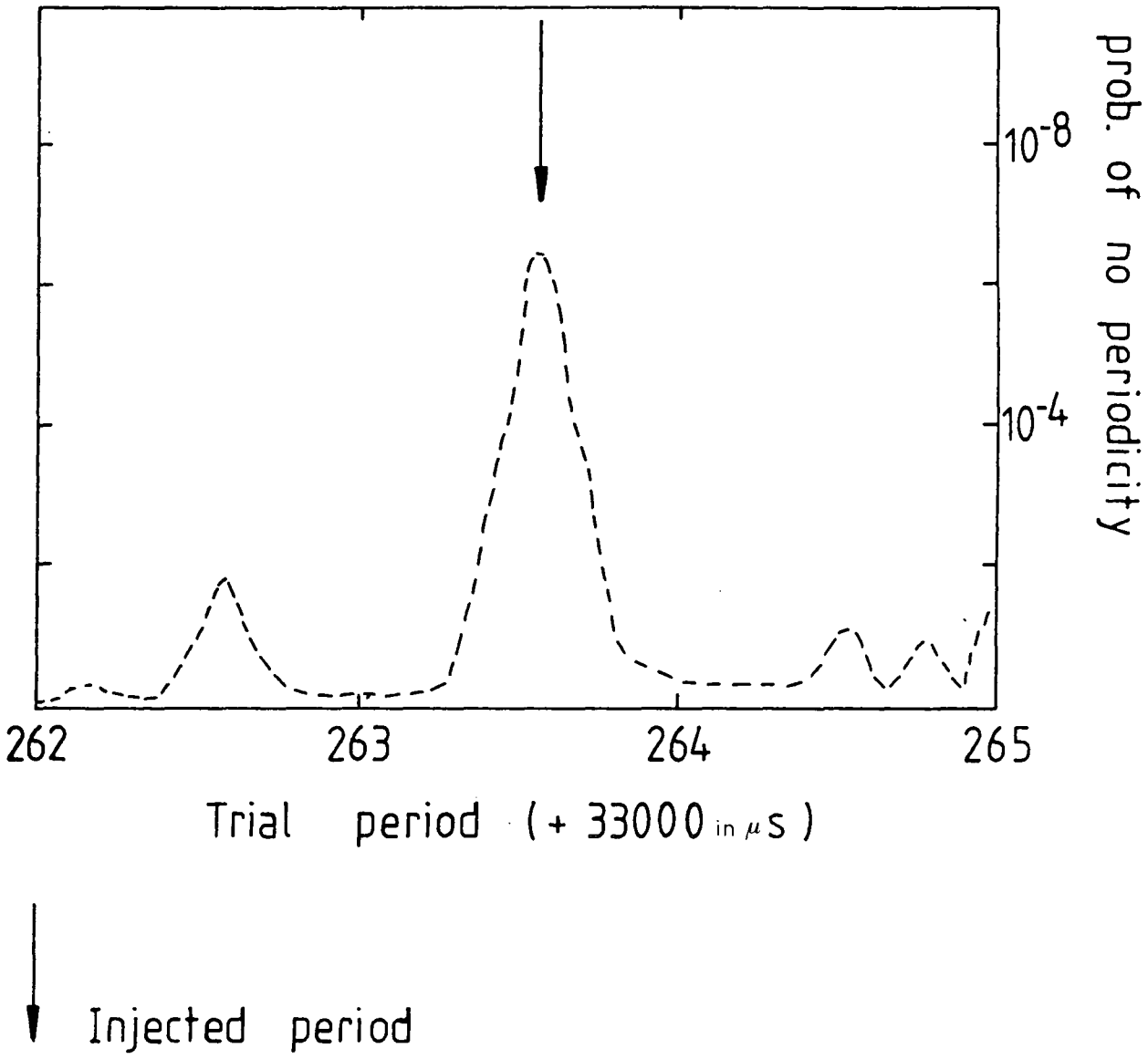

Figure 5.5: Sampling about an 'injected' period - pulsed events distributed evenly.

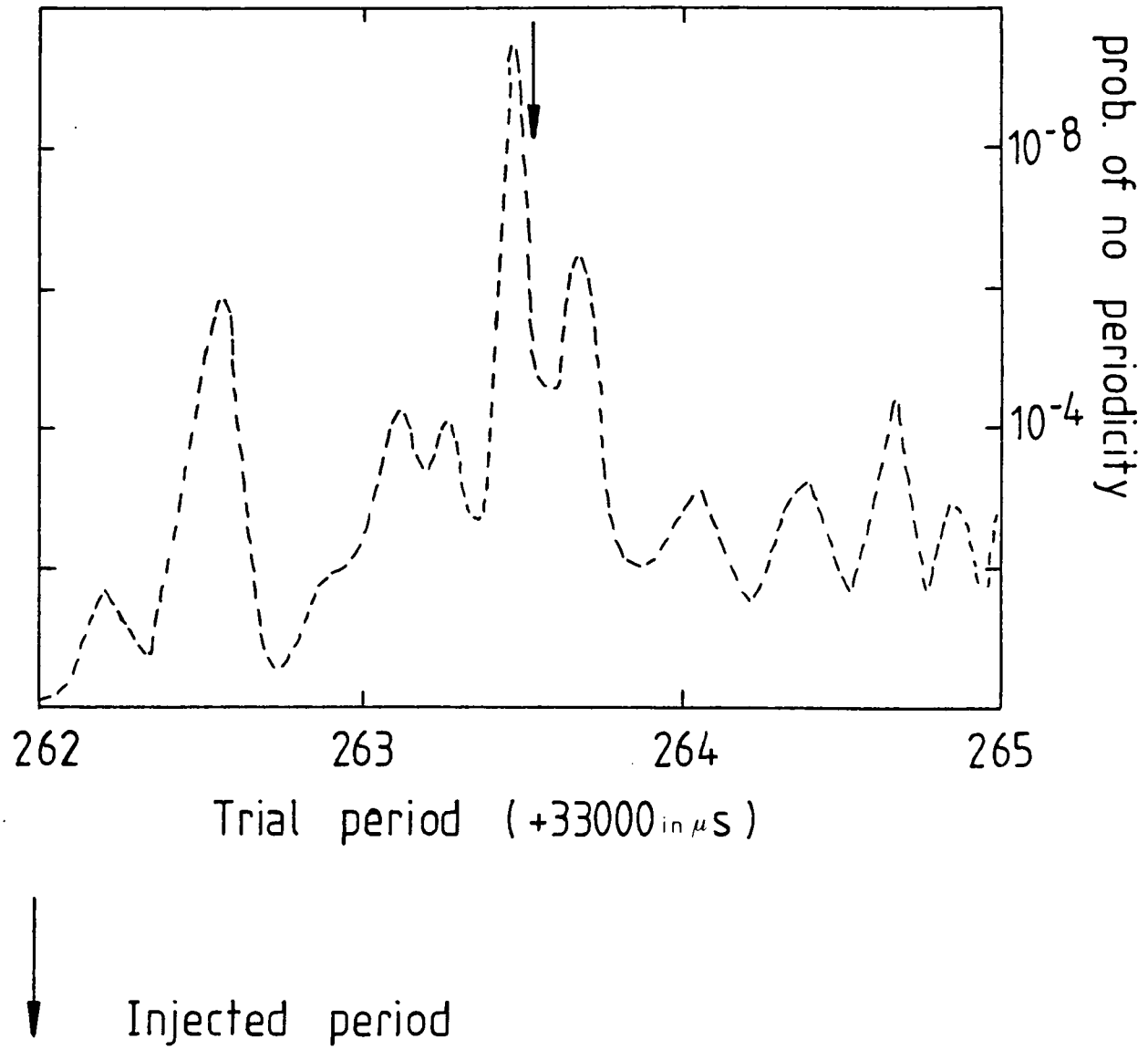

Figure 5.6: Sampling about an 'injected' period - pulsed events distributed over the first 10 % of the data.

5.3.9: Sampling effects.

Extensive simulations have been performed to investigate the effect of injecting an 8% pulsed content to a random time series (average counting rate of ~ 15 min^{-1}). The results of a scan about the injected period are given in fig 5.5. Here, the pulsed events are uniformly distributed through the data. By comparison, it is important to note (see fig 5.6) the effect of injecting the pulsed events over only the first 10% of the data. The above algorithm recovers the injected period at the adjacent sampling interval ~ one 'harmonic interval' from the True period. So, it is important to note that displacements in the detected period can occur in cases where the periodic content is localised to a short interval in the data sample.

In addition, the varied counting rate with zenith angle results in a need for some extra spreading of the sampling range for periodicity.

These considerations must be noted in the analysis of periodic data, and allow periodicity to be recovered close, but not coincident with the barycentred ephemeris value.

5.3.10: The relative powers of the two main tests for periodicity.

In a recent paper (Leahy et al, 1983) the use of the Rayleigh test and the method of Epoch folding in the analysis of a time series for periodicity has been investigated. The relative power is seen to depend on two factors;

i. The 'duty cycle' of the pulse. The Rayleigh test is more powerful for broad 'duty cycles' (square waves and sine waves). However, Epoch folding is definitely more powerful for narrower pulses.

ii. The number of periods tested. In searches over 1000 independent

periods, the Rayleigh test is more sensitive for sine waves and for broad duty cycles, but the relative sensitivity (Epoch folding/Rayleigh test) increases regardless of pulse shape as the number of periods tested increases. Once again Epoch folding is more sensitive to short duration pulses with the sensitivity increasing as the number of bins increases.

Other statistics have been suggested for testing for a known period in data (Protheroe, 1985). If the width and phase of the pulsed events are known (from an ephemeris or from theory) then a specific test can be developed which will be very powerful. Such a test is the Epoch folding technique in the case of the Durham analysis of the November 1982 Crab pulsar data - see section 6.6.1. If the width of the pulse is known, or expected from theory, but the phase is unknown, then a suitable powerful test can be applied (Hillas, 1975). In the more general case, where neither phase nor width of the pulse of periodic events are known, there are a number of tests that can be used. For broad pulses, the Rayleigh test and the 'Hodges and Ajnes test' are powerful. These tests are not suitable for detecting very narrow pulses and various other statistics have been proposed, (Bucherri and Sacco, 1984), (Kuiper, 1960), (Watson, 1961) and (Protheroe, 1985).

In general, the Rayleigh test has been used in this work, especially for X-ray sources thought to be undergoing accretion. These objects may well have a relatively large 'duty cycle' as the particle beam producing the gamma-rays may be deflected and 'spread' by interactions with infalling matter. The Epoch folding method has been used for radio pulsars where the emission beam may be expected to remain more collimated and the pulsations may be narrower.

5.4: The search for transient emission.

The techniques described above work best if there is a continuous pulsed content in the data. If the periodic events are restricted to a time much shorter than the observation time T, the periodic effect as deduced by tests such as the Rayleigh test is diluted. In addition simulations of the perfomance of the programs written to implement the Rayleigh test indicate that a concentration of pulsed events can cause a significant shift in the detected period from an injected period. It is therefore necessary to look for procedures sensitive to transient pulsed emission.

A choice exists between analysing sections of data split into equal numbers of events, or equal time durations. In this thesis the latter procedure is investigated. The search through the data on the Crab pulsar in sections of equal numbers of events is discussed elsewhere (Kirkman, 1985), and will not be covered here.

Two main statistical tests were used, the V-test which is sensitive to bursts with a broad duty cycle, and a binomial test of the mainpulse bin, sensitive to single bin (narrow) bursts.

5.4.1: The V-Test.

The V-test is used if a particular direction or phase Θ is predicted theoretically in a sample of n angular values

$$A^1 \ldots . A^n$$

The procedure performs a Rayleigh test on the data producing a resultant m of length r and polar angle P resolved onto the preferred direction. The null hypothesis to be tested is a random distribution, the alternative hypothesis tests for a significant resultant vector, information would be lost if knowledge of the preferred direction were ignored. If v is the projection of m onto the preferred direction,

then,

$$v = r.\cos (A - O) \qquad - 5.18$$

The test statistic used is,

$$u = (2n)^{1/2}. v \qquad - 5.19$$

Tables, (e.g. Batschelet, 1981) provide the critical values $u(\sigma)$, of the test statistic u for various significance levels σ.

The mainpulse phase (as derived from radio measurements) is specified as the preferred direction. This test resolves the phase of each event onto this predicted vector. Summing over all events the resultant gives a measure of the periodicity at the radio mainpulse.

5.4.2: The Binomial test.

In the case of a periodic source with an accurate ephemeris an even more effective test is a Binomial test of the number of events in a bin centred on the mainpulse, compared with the number predicted from other parts of the light curve.

The Vtest has the advantage of being sensitive to broad peaked duty cycles such as those observed in the 1981 bursts of gamma-rays from the Crab pulsar (Gibson et al, 1982a). In addition, any interpulse burst may be detected as a large negative effect (provided such emission did not coincide with a mainpulse effect, the two tending to cancel).

So the V-test looks for broad peaked bursts at the mainpulse OR at the interpulse and will probably give a better indication of burst activity at an unknown phase. The binomial procedure is a specific test for bursts confined to a single bin at the mainpulse phase - and in this case is expected to be more powerful than the Vtest.

5.5:Pulse amplitude analysis procedures.

The intensity of the light pulse constituting an event is measured by the LeCroy 'QT100B' units, as described in section 3.4.2. As indicated in the introduction to this chapter there may be some difference in the light pulse characteristics of proton and gamma-ray initiated showers, but any effect is likely to be small, and so to develop the analysis procedures only data known to be rich in candidate gamma-ray showers have been investigated. Such data is chosen using more powerful and established methods such as the likelihood analysis of 'drift scan' data or strong indications of periodicity. The basic test of a rich sample involves finding the number of events with pulse amplitudes < a median value predicted from a background dataset. If a difference is found then there is a choice of statistical tests to assign significance to the result - the choice is made depending on the number of events in the sample.

5.5.1: Analysis of a drift Scan excess.

The pulse amplitude analysis is conducted by analogy to the procedure for 'drift scans' themselves, outlined in section 5.2.

i. The observation is separated into three distinct sections; X minutes before, X minutes about, and X minutes after the time of interest.

ii. The mean, median and standard deviation for each of these three pulse amplitude distributions are computed.

iii. A check is made to ensure that there is no systematic variation over the 3X minute period by requiring the median, before and after to be consistent (i.e within 1 standard error on the median value of each other - section 5.5.2.).

iv. The two OFF samples (before and after) are added, and a median

for this combined OFF distribution is computed - MEDoff. The median of the ON sample (about the time of interest) is also computed - MEDon.

The null hypothesis requires proton initiated flashes to be indistinguishable from the gamma-ray initiated flashes i.e. the two distributions are from the same population.

v. The number of event pulse amplitudes in the ON sample $<$ the predicted median (MEDoff) = N_-, and the number $>$ the predicted median = N_+ are then calculated.

There should be an equal chance of a light-pulse falling either side of the predicted median, assuming the intensity of the flashes is uniformly distributed over this time.

Obviously if there were no difference in the distributions we would observe

$$N_- = N_+$$

but for cases where there is a difference, the significance can be determined as outlined in the following sections.

5.5.2: Statistical tests of the pulse amplitude distribution.

The significance of the result is not easy to determine using the usual techniques of error analysis as the pulse amplitude distributions are not normal - see fig 3.16. However, a consistent statistical approach may adopted.

It is, difficult to relate the errors on the median for distributions of differing shape (i.e.skewness). Of the several possible measures of dispersion of data of this type, inter-quartile range, and the standard error on the median Smed, are the most commonly used. The pulse amplitude distributions are not too highly skewed and so the standard error on the median Smed,

$$Smed = 1.2533\ Sdev$$

may be computed, where Sdev = standard deviation on the mean. It is this value that has been used in this work to ensure that there is no systematic variation over the period analysed -see section 5.5.1.

It is possible to combine the errors on the distributions to assign significance levels, but there are non-parametric tests well suited to this analysis - The Median Test, and The Mann-Whitney U-test have been used.

5.5.3: The Median Test.

The Median Test is a procedure for testing whether two independent samples differ in their central tendencies, or more precisely, whether the two independent groups have been drawn from populations with the same median. The null hypothesis requires the two groups to come from populations with the same median; the alternative hypothesis could be that the medians differ (two-tailed test) or that the median of one population is higher or lower than the other (one-tailed test).

To perform the Median test, a 'Grand median' for the combined group, (containing the candidate gamma-rays, Group I and the assumed background, Group II) is evaluated. Both groups are then dichotomized at this Grand median.

	Group I	Group II
>= Grand median	A	B
< Grand median	C	D

It can be shown (Mood, 1950) that the sampling distribution of I and II under the null hypothesis, $H_\varnothing$ (i.e. that $A = n_1/2$ and $B = n_2/2$) is a hypergeometric distribution, and the validity of $H_\varnothing$ can be tested by calculating the appropriate χ^2 statistic for 1 degree of freedom as,

$$\chi^2 = \frac{N(|AD - BC| - N/2)^2}{(A+B)(C+D)(A+C)(B+D)} \quad - 5.20$$

where, n_1 is the number of events in Group I

n_2 is the number of events in Group II

$N = n_1 + n_2$, which should be > 20

The significance can then be determined by reference to statistical tables.

5.5.4: The Mann-Whitney U-test.

This test determines if two subsets of events (one containing the candidate gamma-rays the other containing the background events), say I and II are drawn from the same population by using the ranks of the pulse amplitudes. The null hypothesis H_0 is generally chosen as the case where groups A and B are from the same population. The alternative hypothesis H_1 could be that one group is stochastically larger than the other.

The procedure used is well established (Siegel, 1956) and involves ranking each events pulse amplitude value (with tied values taking the average of the tied ranks). The candidate gamma-ray events are tested for predominantly low or high ranks. For a large enough sample of candidate gamma-ray events (i.e. > 20 , and always the case in the application of this test in this work), the value of a suitable normal deviate can be found, z_U

$$z_U = \frac{U - n_1 \cdot n_2/2}{((n_1)(n_2)(n_1 + n_2 + 1)/12)^{1/2}} \quad - 5.21$$

where,

n_1 is the number of events in the time of interest i.e. group I,

n_2 is the number of outside the time of interest i.e. group II,

R_1 is the sum of the ranks of the pulse amplitudes in group I,

U_1 is the U - test statistic calculated from;

$$U_1 = n_1.n_2 + \frac{n_1(n_1 + 1)}{2} - R_1 \qquad - 5.22$$

z_U is 'almost normally distributed' and has a mean value of zero and unit variance. Tables (Siegel, 1956) can be used to assign a probability to the value z_U under the hypothesis, H_∞ mentioned above.

5.5.5: Analysis of periodic data.

The detection of periodicity in data allows an examination of the "light curve", of the periodic emission and opens up the possibility of extracting the periodic events (e.g. candidate gamma-ray events in the main pulse of the Crab pulsar). These events can then be compared to the assumed background events making up the rest of the 'light curve'. The simplest method and the one used in this thesis involves performing the Median test to compare the two pulse amplitude distributions, main-pulse and other phases. The median test is particularly suited to this form of analysis, as the large numbers of events involved can be easily manipulated.

5.5.6: Use of the tests of the pulse amplitude distributions.

The Mann-Whitney U-test is about 95% as powerful as the equivalent parametric tests, t, and the analysis of variance (Siegel, 1956). The Median test is not very powerful in that it takes no account of the magnitude of the difference of an event pulse amplitude value from the Grand median value merely the number values above and below it. The median test is equivalent in power to the 'rank' tests for very small samples, but its relative power declines to about 66% as the sample size increases. It does have the distinct advantage that the test is

easy to calculate for large numbers of events.

The performance of the pulse amplitude tests has been investigated by analysing assumed background data i.e. data taken in the 'drift scan' mode with the object outside the field of view of the telescope. The results are consistent with there being no difference in the pulse amplitude distributions for this backgound data (section 6.2.6).

In this work these techniques have been applied to the objects detected at large signal strengths i.e. Hercules X-1 and Cygnus X-3, with an additional analysis performed on the periodic emission from the Crab pulsar by comparing mainpulse events with events recorded at different phases.

5.6: The calculation of flux values.

The likelihood ratio analysis (section 5.2.1) yields a percentage excess of events over the cosmic ray background. To convert this raw measure into a flux value several factors must be determined;

i. The threshold of the detectors for cosmic rays and for gamma-rays (see section 3.6.4). The calculation of thresholds requires a knowledge of the spectral index of the integral cosmic ray spectrum.

ii. The integral cosmic ray flux at threshold. This can be found from the known spectrum of cosmic rays.

iii. The field of view of the telescopes to real showers;

Mark I = $(2.2 \pm 0.2)^{\circ}$

Mark II $\sim 1.8^{\circ}$

An example of the calculation is given below for the particular case of the overall 1983 excess of counts (I-folds telescopes 2,3,4) taken with the telescopes pointing at Cygnus X-3.

The total number of events detected in 10 minutes about 0.625 phase

was 1060, the number detected in adjacent 10 minute intervals was 1957. The maximum likelihood number of excess counts gives 81.5, i.e. 8.33 % of the cosmic ray background.

From fig.2.1. the integral cosmic ray flux at a threshold of 2000GeV (equivalent to a gamma-ray threshold of ~ 1400 GeV) is 3.8 10^{-6} cm^{-2} s^{-1} str^{-1}.

The field of view of the Mark I telescopes is,

~ 1.67 10^{-3} str

and for the Mark II telescope,

~ 1.12 10^{-3} str

So the cosmic ray flux at this threshold is calculated as 6.34 10^{-7} cm^{-2} s^{-1} , and the gamma ray flux corresponding to 8.33 % of this background is thus 5.3 10^{-10} cm^{-2} s^{-1} (calculated for the Mark I field of view).

For calculations at other thresholds, the integral cosmic ray spectral index can be taken as -1.6 in the energy region of this experiment (Craig, 1984).

The calculation of flux for a pulsar.

The special case of a pulsar with the emission limited to a main and occasionally an interpulse the duty cycle of the pulsed emission must be taken into account i.e an allowance is made for the percentage of the period over which the excess gamma-rays are detected.

5.7: The calculation of upper limits.

There are several objects which have been observed for a limited time using the 'drift scan' technique, and they show no significant enhancement of the count rate with the source in the field of view of the telescopes. However, the flux which would have given a 3 standard

deviation detection for the particular length of observation can be calculated. This is illustrated below, for the example of the Dugway observation of the strong COSB source, 2CG135.

There were 2003 counts ON source, and 4072 counts OFF source. So the signal from the suspected source is -33 counts +/- 45.3 ,or 0.984 +/- ~ 0.02 % of the cosmic ray flux.

The 3σ limit therefore corresponds to a flux of 6.67 % and a knowledge of the integral cosmic ray flux at the energy threshold of the array of telescopes (~ $8 . 10^{-10}$ cm^{-2} s^{-1}) enables the flux limit corresponding to a 3σ detection to be calculated as,

$5.3\ 10^{-11}\ cm^{-2}\ s^{-1}$

n.b. the energy threshold for gamma-rays is considerably lower than that for protons, with a value of 1300 GeV suggested by computer simulations (Macrae, 1985).

5.8: Source luminosity

The flux,F and luminosity, L are related by the formula,

$$L = 4 \pi . F . d^2 . E_\gamma \qquad - 5.23$$

where d, is the distance to the source (in cm) and E_γ is the average photon energy detected from the object. This last factor, E_γ is unknown, but may be calculated as follows,

The differential cosmic ray spectrum is assumed to be of the form,

$$C(E) = \text{constant}(A) . E^{-x} \qquad - 5.24$$

where,

C(E)dE = the number of gamma-rays of energy between E and E + dE

E = the gamma-ray energy

X = the spectral index

from these values the integral spectrum can be calculated as the

number of gamma-rays above threshold energy E_t

$$N(>E_t) = \frac{(A.E_t)^{(1-x)}}{(1 - X)} \qquad - 5.25$$

and the total energy above the threshold is then given by,

$$E(>E_t) = E(E)dE = C(E)EdE$$

$$= \int A.E^{(1-x)}dE$$

$$= (A.E_t)^{(2-x)}/(2-X)$$

$$E(>E_t) = N(>E_t).E_t.\frac{(1 - X)}{(2 - X)}$$

$$E_\omega = E_t.\frac{(1 - X)}{(2 - X)} \qquad - 5.26$$

and so the luminosity given above as equation 5.23 becomes;

$$L = 4\pi . F .d^2. E_t.\frac{(1 - X)}{(2 - X)} \qquad - 5.27$$

The analysis procedures outlined above have been used to test for gamma-ray emission from the observations listed in chapter 4. The results are given in the next chapter.

Chapter 6: The results of the gamma-ray observations.

6.1: Introduction.

The results of the analysis of observations conducted with the Dugway experiment are presented in this chapter.

An attempt has been made to find similarities in any V.H.E. gamma-ray flux detected from Cygnus X-3, Hercules X-1 and 4U0115+63. In particular, strong positive detections have been investigated for evidence of a difference in the pulse amplitude characteristics of the candidate gamma-ray events. A new search for transient emission from the Crab Pulsar is also described. In addition, upper limits to the gamma-ray emission from 7 radio pulsars and 7 other miscellaneous sources have been derived.

A discussion of the implications of these results is presented in chapter 7.

6.2: Cygnus X-3.

This source was extensively observed over the 1981-1983 observing seasons. The acceptable data - see section 4.4.1, have been analysed in a search for periodic modulation on several timescales.

In the analysis of Cygnus X-3 some note of the ephemeris used must be made. The Dugway observations were interpreted using an ephemeris derived from X-ray data (Van der Klis and Bonnet-Bidaud, 1981), listed below

$$T_{\odot} = JD.2440949.8986 \pm 0.0030$$

$$P_{\odot} = 0.1996830 \pm 0.0000004 \text{ days}$$

$$pdot = (1.18 \pm 0.14) \times 10^{-9}$$

It is important to establish the accuracy of this ephemeris,

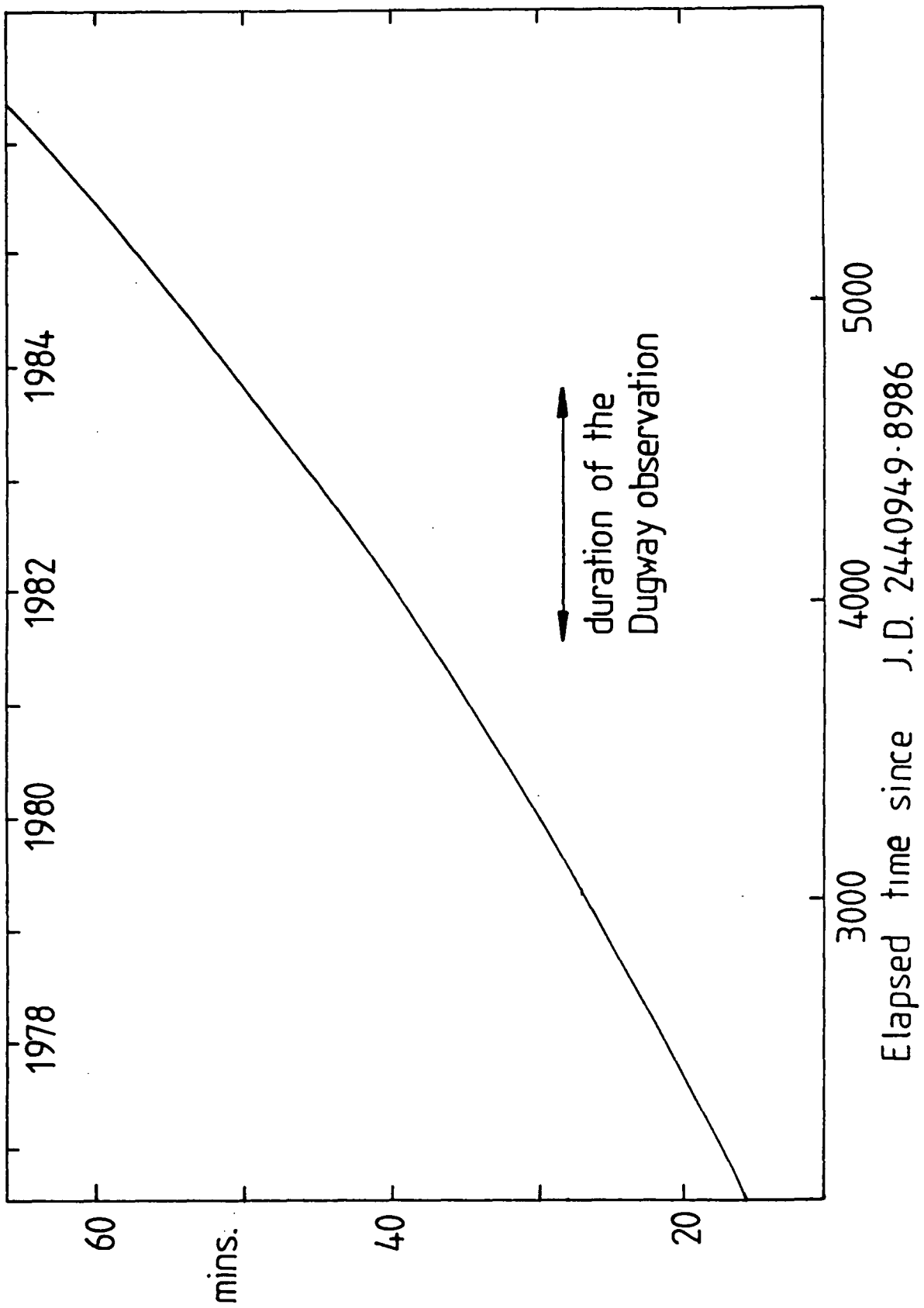

Figure 6.1: The progressive uncertainty in 4.8 hour phase due to the errors quoted in the Van der Klis and Bonnet-Bidaud ephemeris.

particularly for observations spanning a number of years such as those made at Dugway (Ramana Murthy, 1983).

The accuracy can be determined by calculating the progressive uncertainty in phase with time from T_0. The phase at time t is given by,

$$A(t) = A_0 + \frac{(t - T_0)}{P} - \frac{P' (t - T_0)^2}{P^2} + ... \quad - 6.1$$

Using the values of the Van der Klis ephemeris it is then possible to calculate the phase uncertainty throughout the Dugway observation for this object i.e. August 1981 until November 1983. A plot of the progressive phase error over this time is given as fig.6.1.

The results indicate that there is a relative uncertainty of as much as 12 minutes over the full observation (~ 2 years). This means that data from different years may not be reliably combined in phase even if they are split into relatively wide 10 minute (phase width = 0.03) sections, any 3-minute by 3-minute superposition (-see section 6.2.2) is restricted to data taken over < 3 months.

An additional uncertainty may be introduced if the ~ 20 day periodicity of the emission at X and gamma-ray wavelengths is assumed to be due to the systems apsidal motion. In this case a further modulation in phase of +/- 0.01 over the 20 days is introduced. Care has been taken to ensure that the results presented here keep within these restrictions.

The Durham data taken in 1981 and 1982 have been analysed at all phases in the 4.8 hour light curve for signs of an enhancement of the count rate above the cosmic ray background. The results are reported elsewhere (Kirkman, 1985) and will be summarised in the next two sections. Most of the 1981 observations were made in the 'drift scan' mode, comprising 76, 36 minute scans taken under acceptable conditions.

The results of the analysis of these data (see section 5.2) show a

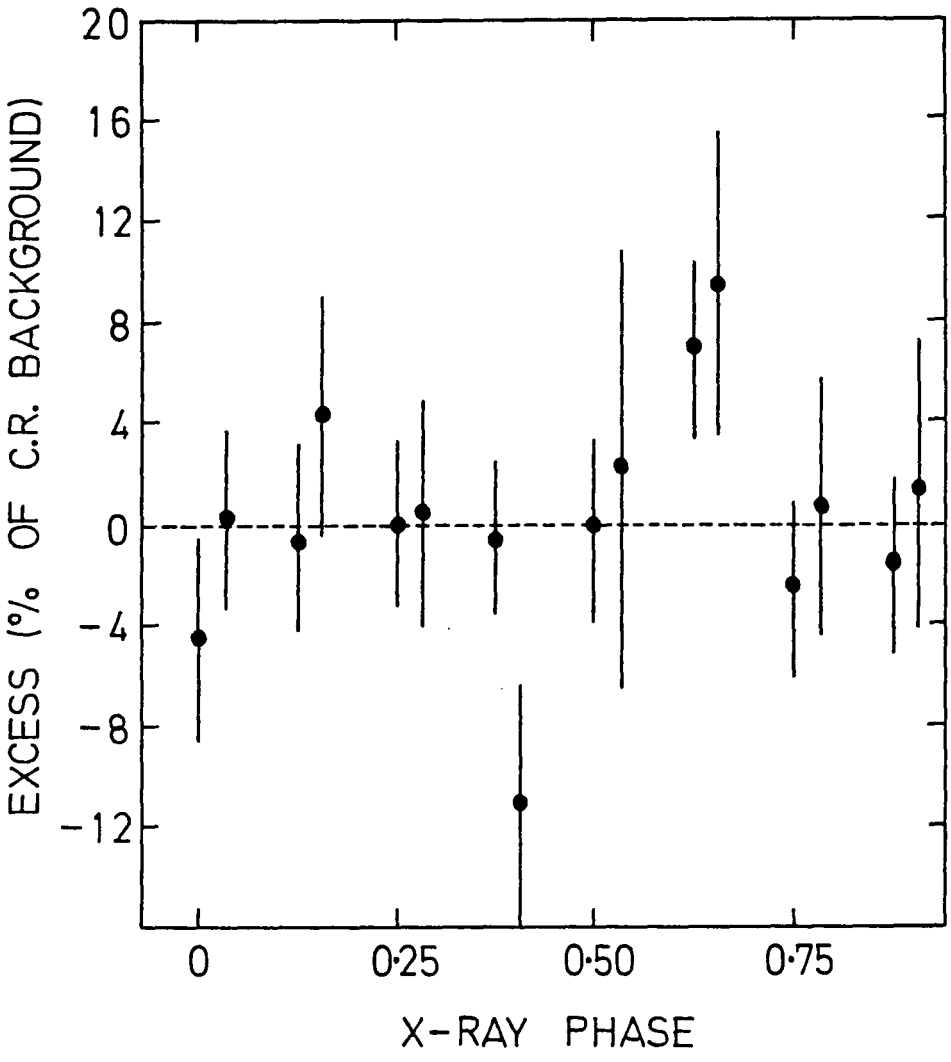

Figure 6.2: The 4.8 hour modulation in the data taken in 1981.

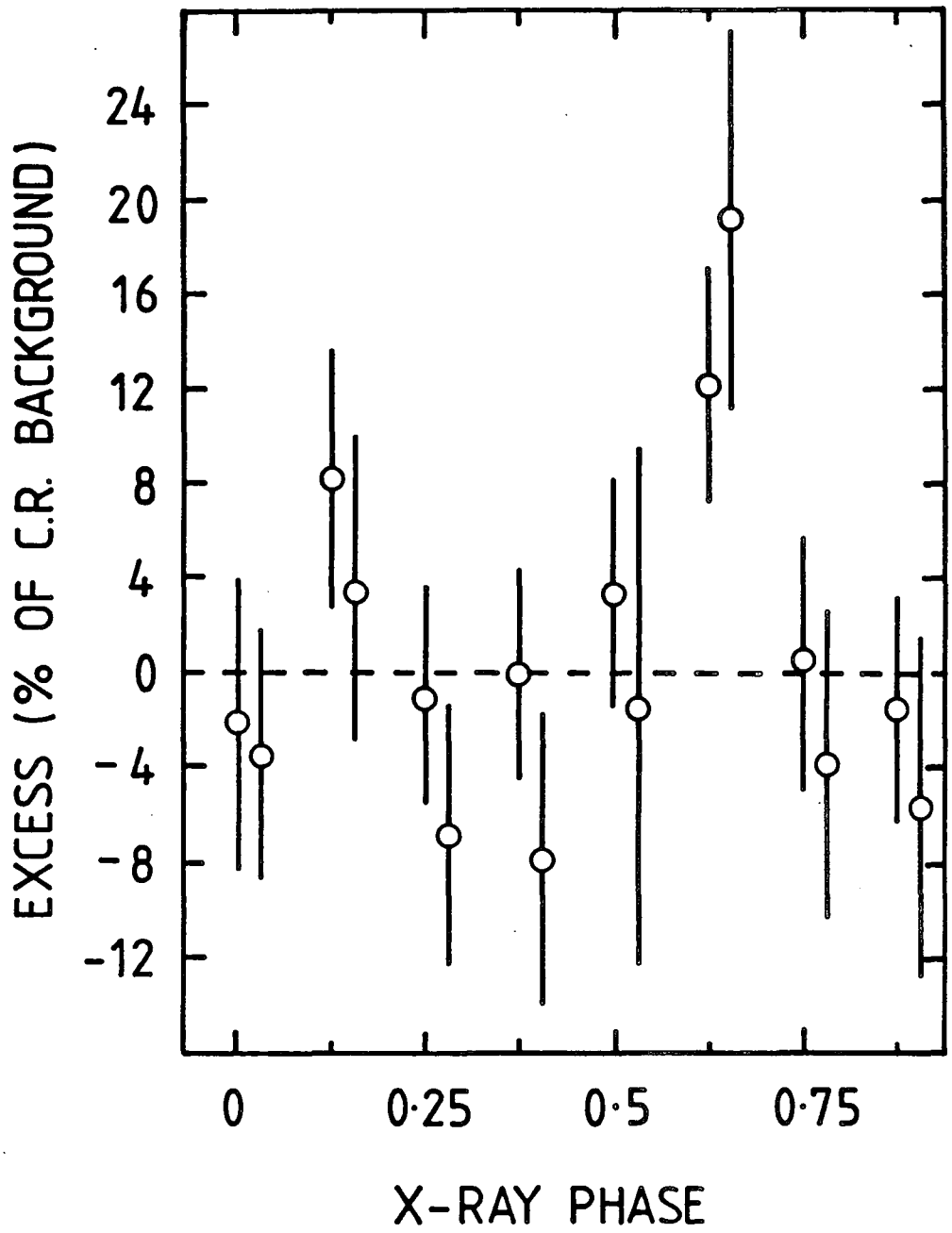

Figure 6.3: The 4.8 hour modulation in the low energy data (1-fold responses from telescope 3) taken in 1981.

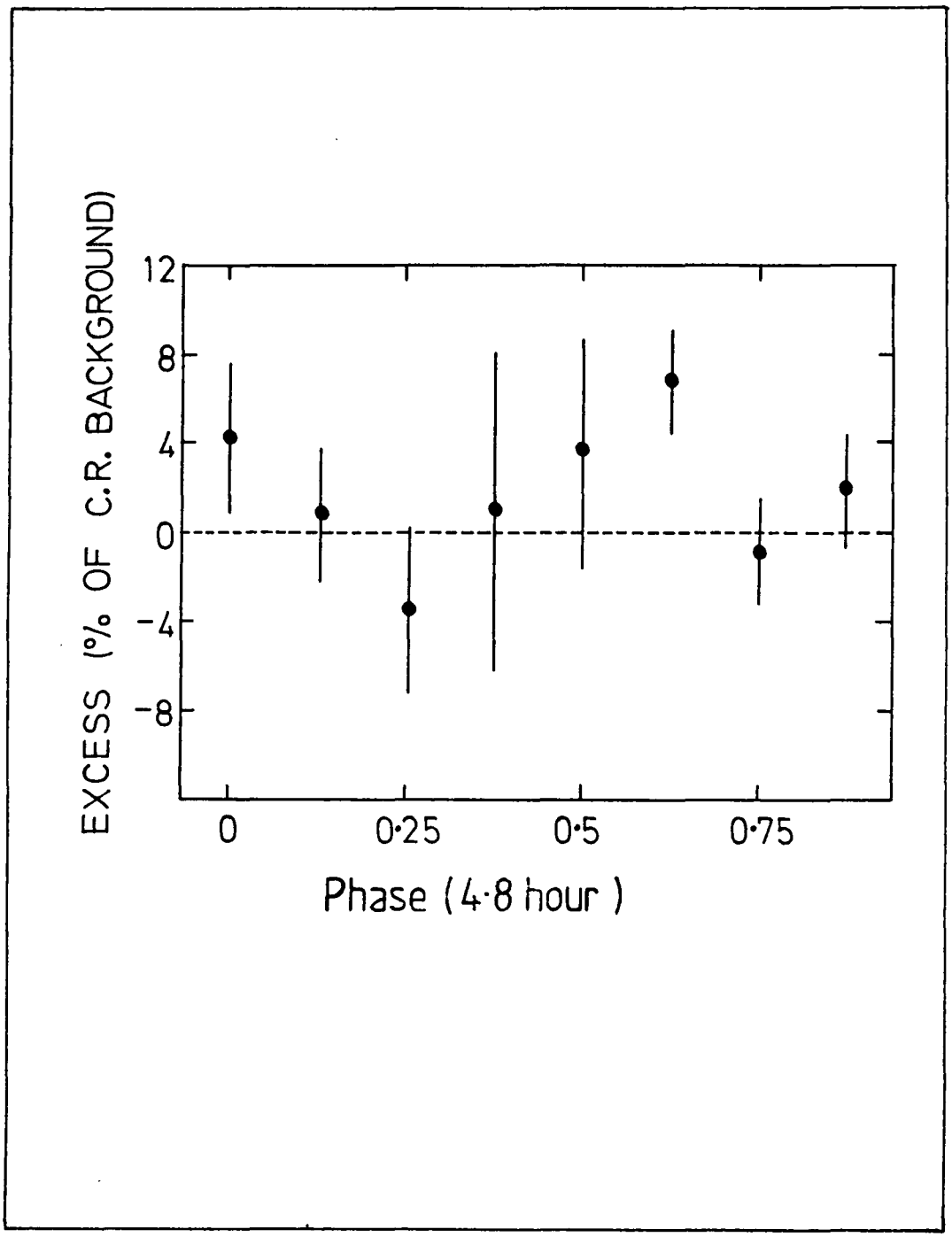

Figure 6.4: The 4.8 hour modulation in the low energy data (1-fold responses from telescopes 2 and 3) taken in 1982.

strong excess of events at the orbital phase = 0.625/0.655, significant at the 2.4 σ level. The results are summarised in fig.6.2. An additional analysis of the data taken with the low energy threshold telescope (telescope 3 in 1981) is summarised in fig.6.3, and shows a stronger enhancement at phase 0.625/0.655 corresponding to ~ 14% , (or 3.35 σ) of the cosmic ray background with some additional evidence of emission at phase ~ 0.13.

6.2.1: 4.8 hour modulation.

With the significant detection of V.H.E. gamma-ray emission in the 1981 'drift scan' data, a different approach was adopted for the 1982 observations. The object was tracked and a 'pseudo drift scan' analysis was performed as outlined in section 5.3. In 1982, telescopes 2 and 3 were found to operate at a lower energy threshold than the others and the data from these two detectors were investigated in the light of the 1981 excess. The results of the 'pseudo drift scan' analysis are given in figure 6.4, and show once again an excess at phase ~ 0.63, in this case significant at the 2.7 σ level, 6.8 % of the cosmic ray background.

The detailed investigation of the nightly contribution to the 6.8 % excess at phase ~ 0.63 reveals that there are four nights contributing strongly i.e. the 14th of July, 18th of July, 16th of August and the 24th of August. These nights have an excess above the cosmic ray background of between 20% and 35%, and they form a very useful enriched dataset on which to perform more detailed analyses.

The combined minute by minute count rate for these four nights in the ten minutes about phase = 0.625 is given as fig. 6.5. This analysis indicates that there is some evidence to suggest that the significant excess about phase = 0.63 is restricted to intervals of 4 and 3 minutes duration centred on phases 0.61 and 0.63.

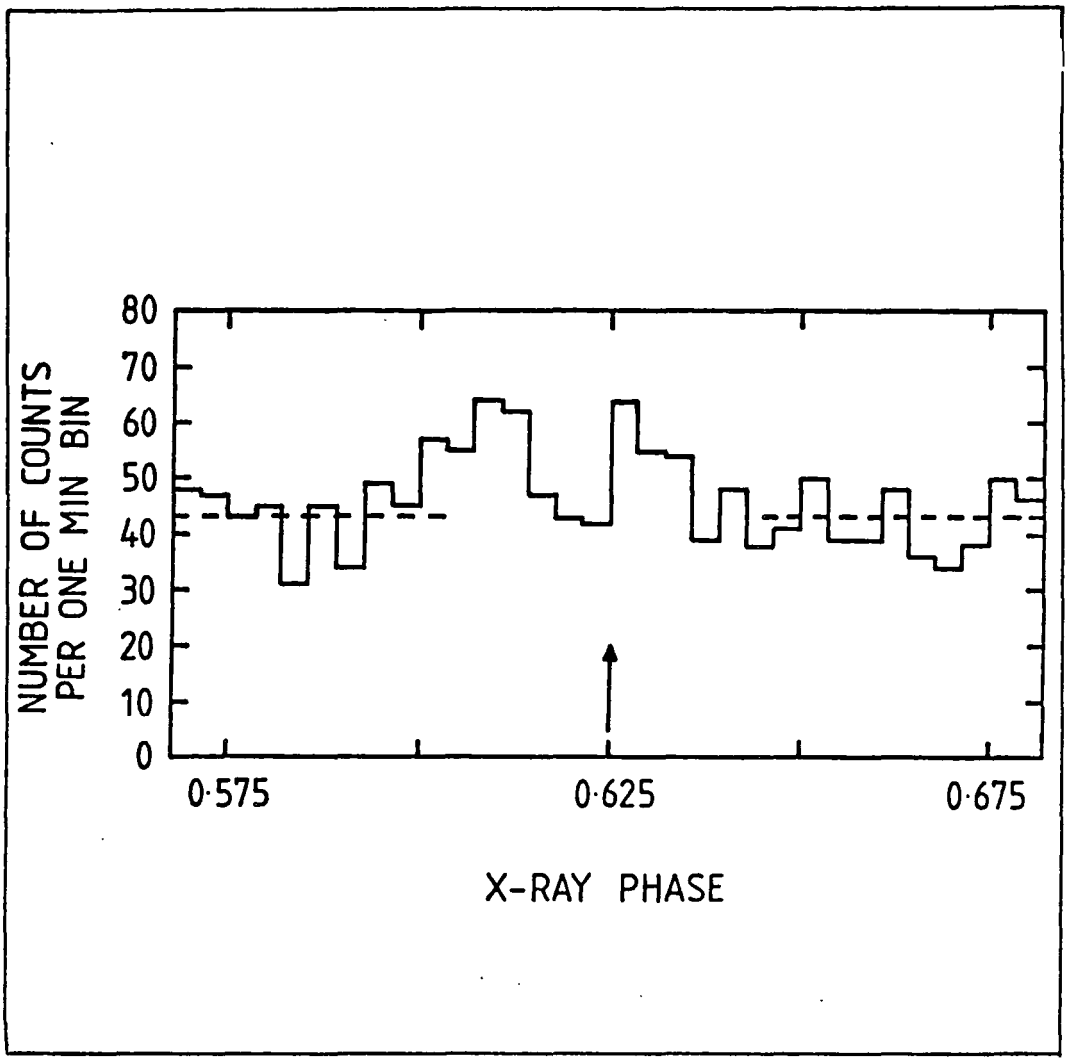

Figure 6.5: The variation of counting rate per minute in the 0.625 phase region for the four strongest excesses detected in the 1982 dataset.

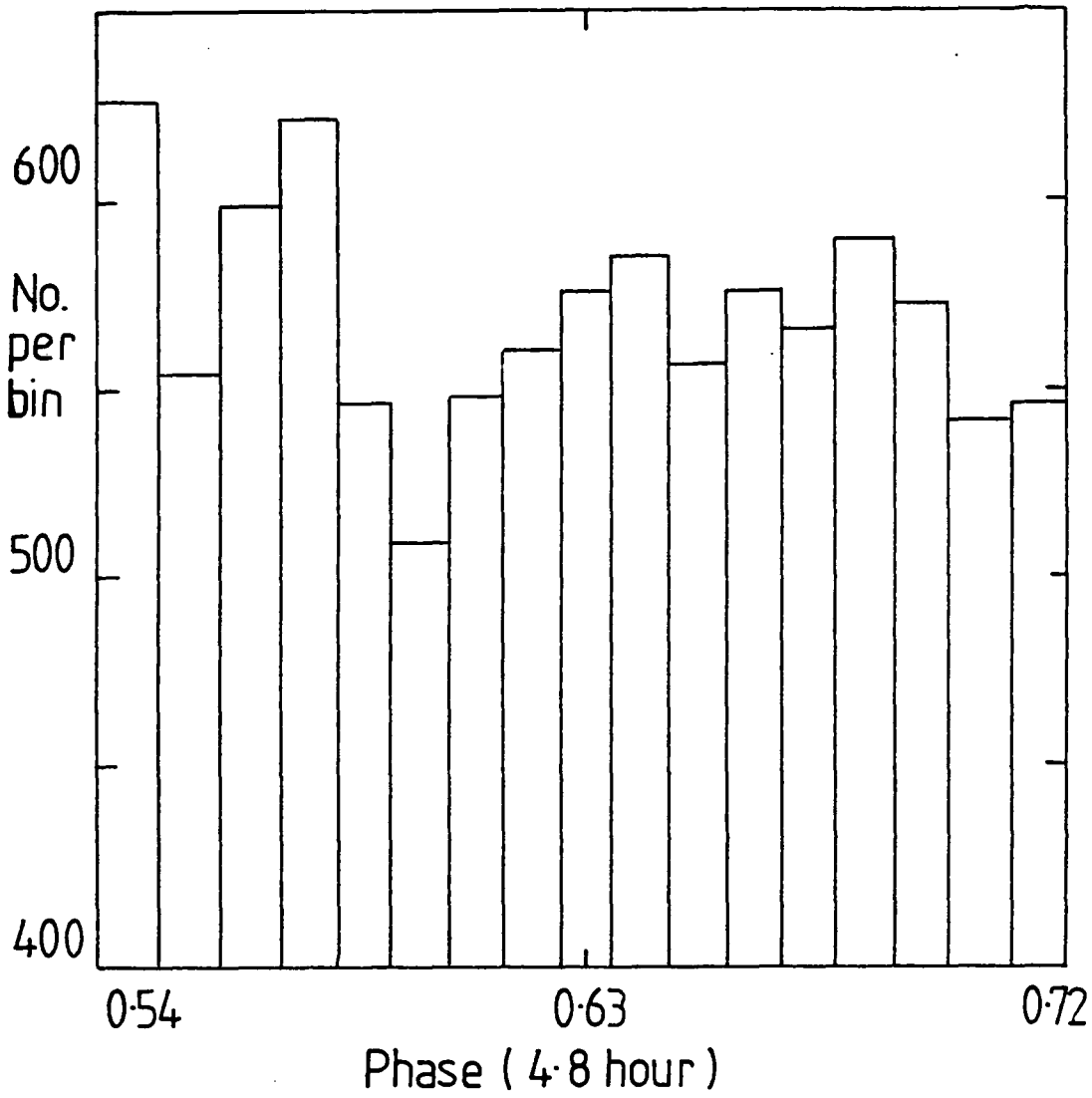

Figure 6.6: A plot of the I-fold data taken in 1982 for 51 minutes about phase = 0.625.

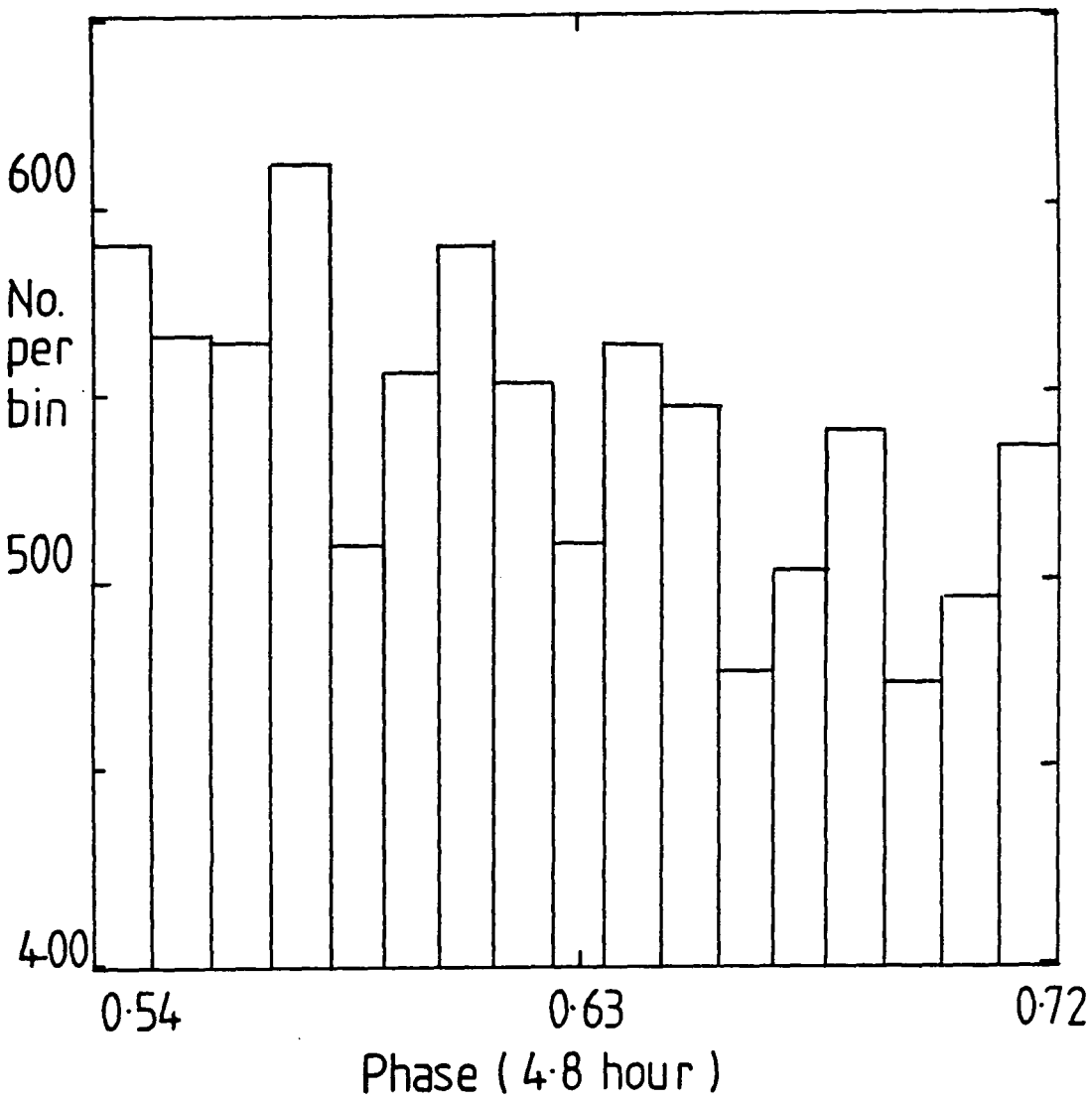

Figure 6.7: A plot of the low-energy I-fold data taken in 1982 for 51 minutes about phase = 0.625 (telescopes 2 and 3).

6.2.2: The detailed analysis of the 0.63 phase region.

The I-fold data.

The data taken about the 0.63 orbital phase have been analysed further. The I-fold responses have been added (bin width of 3 minutes) for 51 minutes about the significant excess. The combined results are given as fig. 6.6 showing that there is no significant evidence of emission in this phase range on the 3 minute timescale.

Since the 'drift scan' excess arises in the main in the data from the two lowest energy threshold telescopes (detectors 2 and 3), it is important to investigate this low energy cut in the data - the results are summarised as fig. 6.7. The reported structure from the four nights showing the strong drift scan excess around phase = 0.63 is evident, but no significant peaks occur at other phases. It seems that the double peaked emission appears only for the four nights showing the strongest excesses and is restricted to the 10 minutes about the 0.63 phase region.

The II-Fold data.

The II-fold sample was given the same extended coverage over the 0.63 phase region as for the I-fold dataset above, the results are presented as fig.6.8.

There is no evidence for an excess at any phase in this range. There is no evidence to suggest an enhancement of the signal/noise ratio in the II-fold sample and since II-fold events correspond to a subset of the data due to higher energy primaries (see section 3.6.1), this is consistent with a steep spectrum for gamma-ray emission from this object (Dowthwaite et al, 1983).

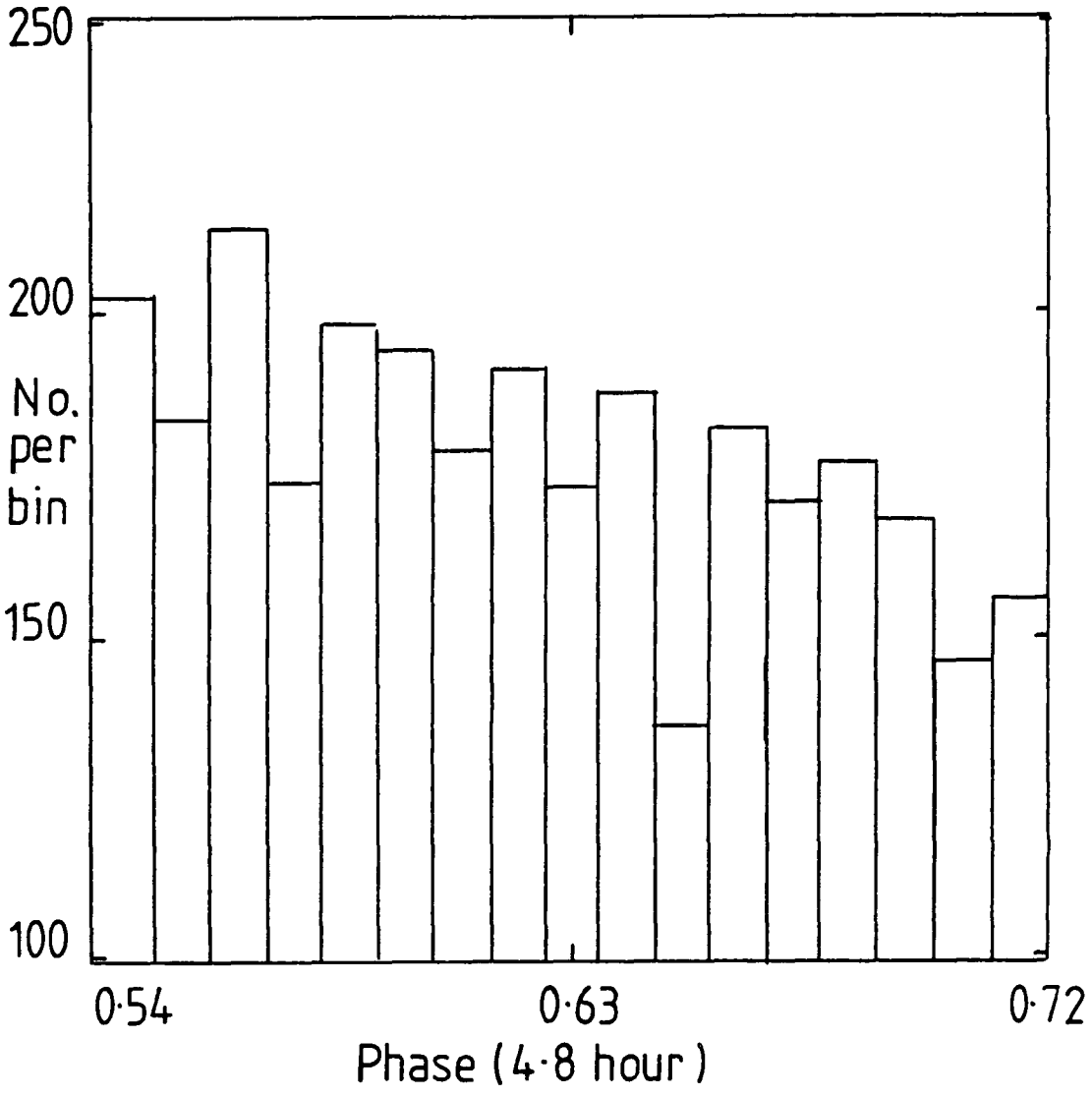

Figure 6.8: A plot of the II-fold data taken in 1982 for 51 minutes about phase = 0.625.

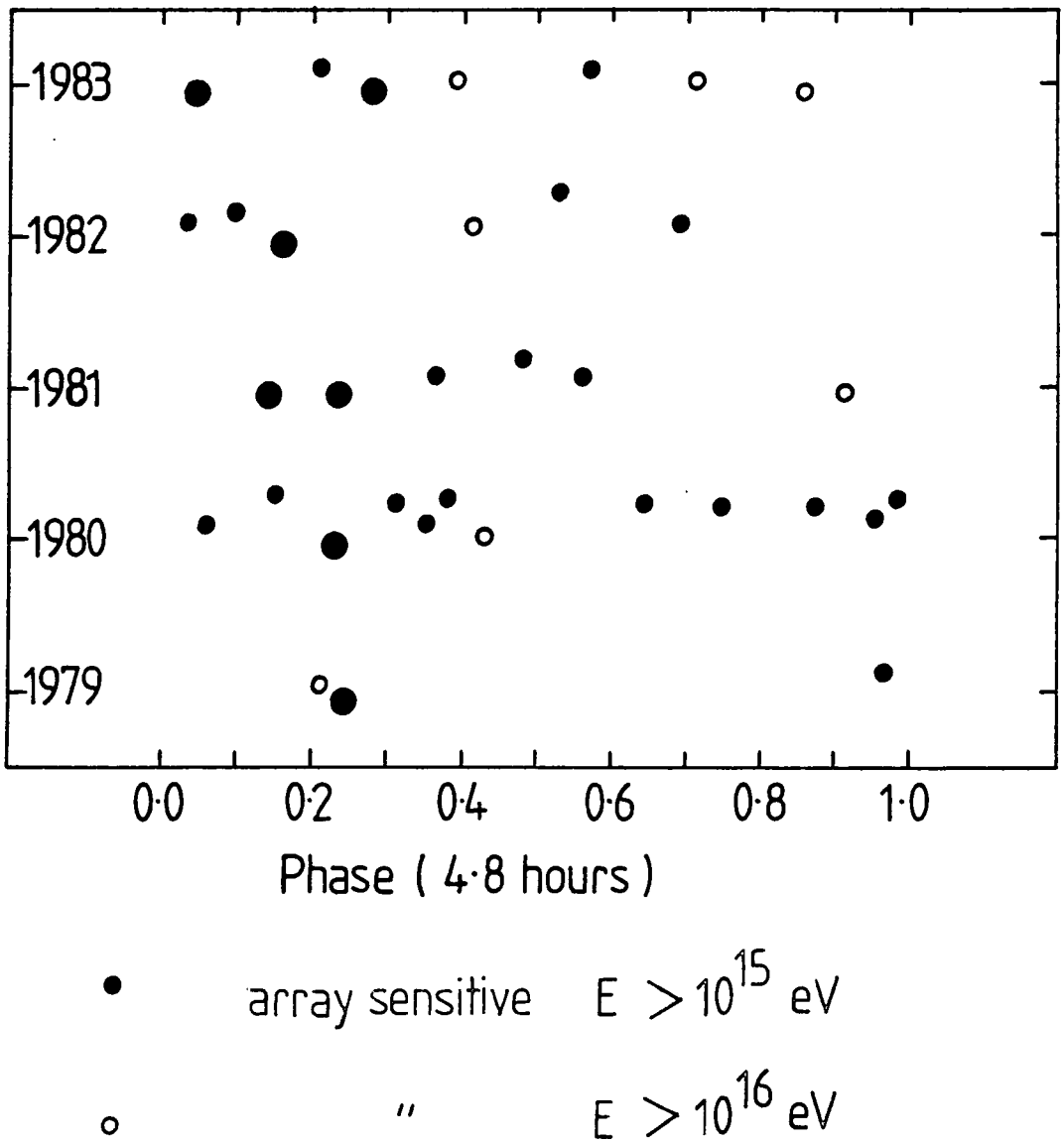

Figure 6.9: A plot of the 4.8 hour phase distribution of the U.H.E. results obtained at Haverah Park from 1979 until 1983 (The size of the dot indicates the magnitude of the excess) - Watson, A.A., private communication.

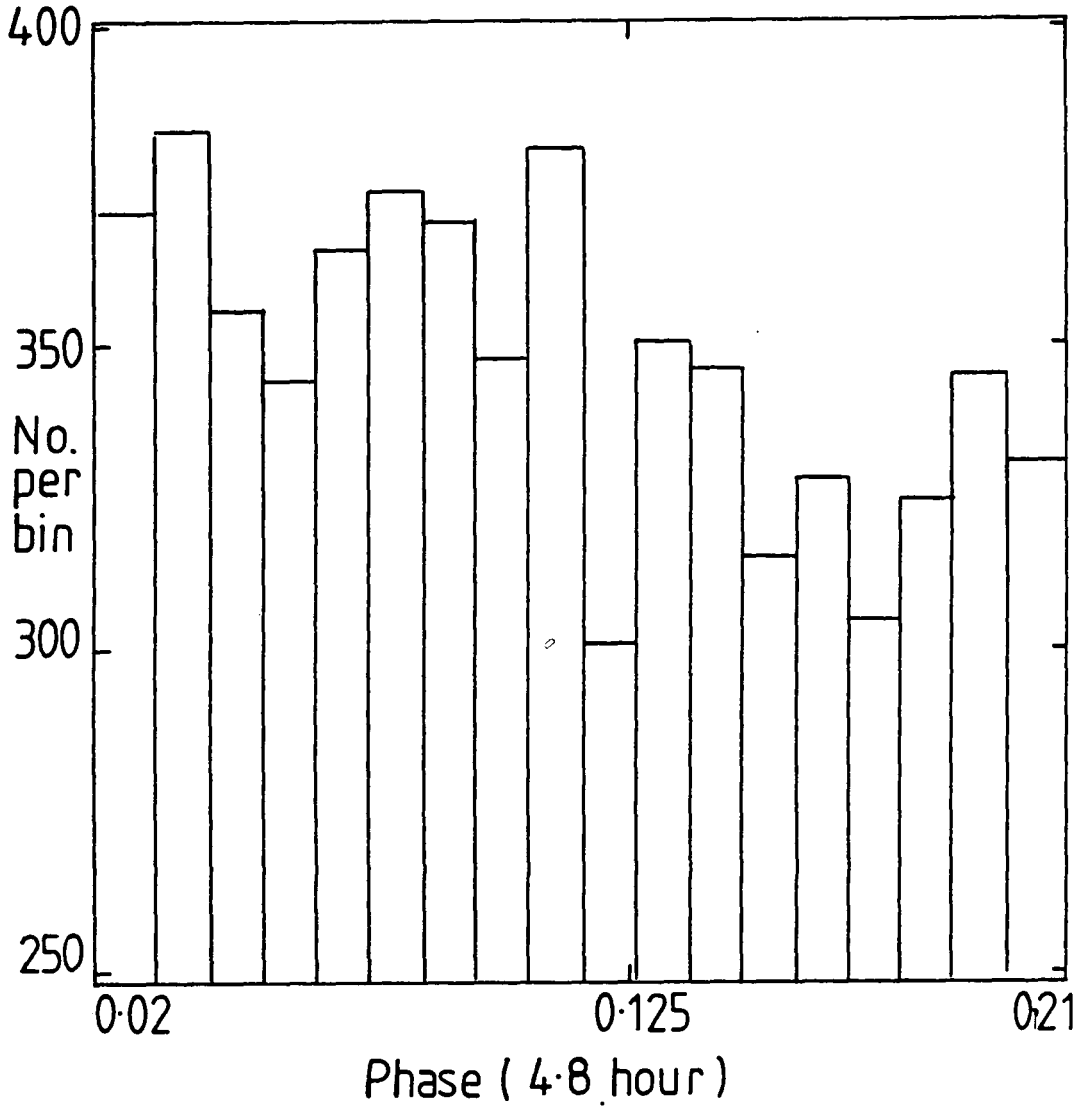

Figure 6.10: A plot of the I-fold data taken in 1982 for 51 minutes about phase = 0.125.

6.2.3: The detailed analysis of the 0.13 phase region.

In view of the binary nature of this source and the recent U.H.E. gamma-ray measurements, (Lloyd-Evans et al, 1983) - see fig.6.9, it is important to scrutinise the 0.0-0.3 phase region. There were 8 nights suitable for analysis in the 1982 dataset. The Dugway observing program was planned to give maximum coverage to the favoured 0.63 phase region at small zenith angles and so the 0.13 phase transit occurred at larger angles, with correspondingly fewer events in the dataset.

The I-fold data.

The single telescope responses for detectors 2 and 3 are presented for 51 minutes about phase 0.13 (3 minute bin size), in fig.6.10. There are no significant peaks, and an analysis of I-folds from all the detectors gives a similar result.

The II-fold data.

The II-fold data taken over the same phase range as above (3 minute bin size) are shown in fig.6.11.

There are very few events in this subset, and no significant peaks can be seen.

It is therefore not possible to confirm the U.H.E. result for emission in the 0-0.3 phase range. However, the fluxes that might be expected from an extrapolation of the U.H.E. result are probably below the limits of detection for the Dugway array operating at these count rates. It is possible, even with this limited observation to rule out any substantial emission of the type seen around phase = 0.63.

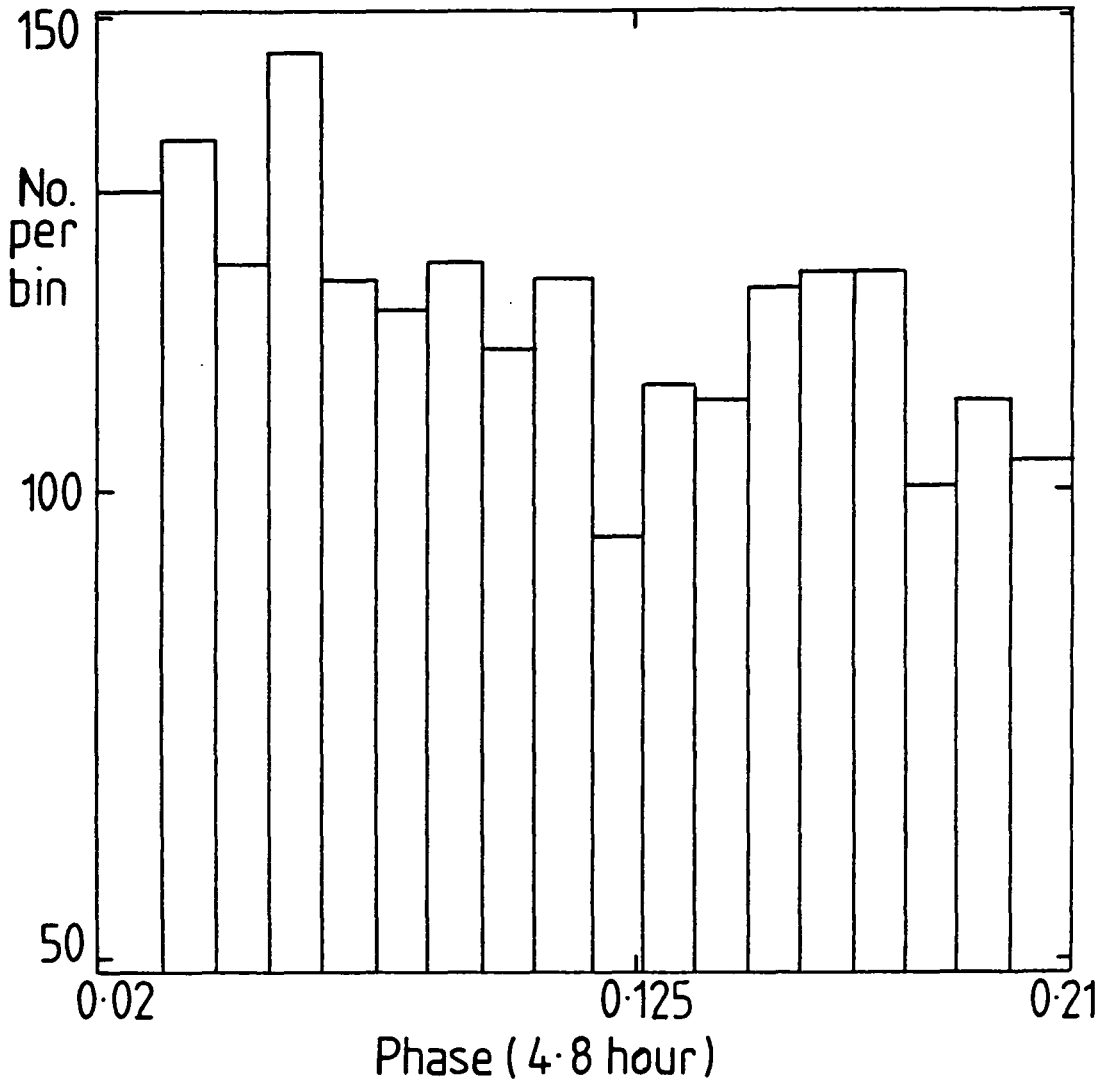

Figure 6.11: A plot of the II-fold data taken in 1982 for 51 minutes about phase = 0.125.

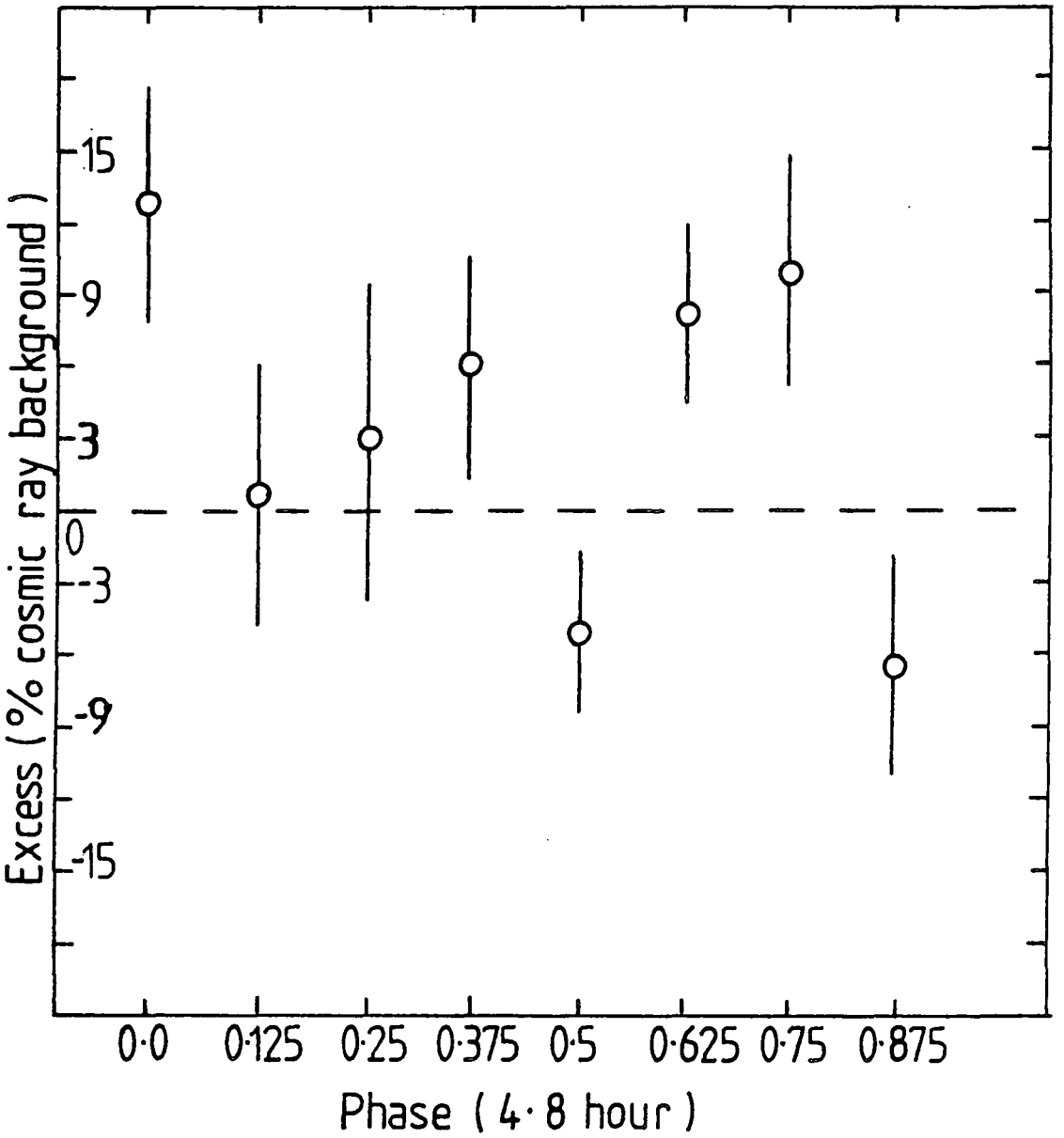

Figure 6.12: The 4.8 hour modulation in the low energy data (I-fold responses from telescopes 2,3 and 4) taken in 1983.

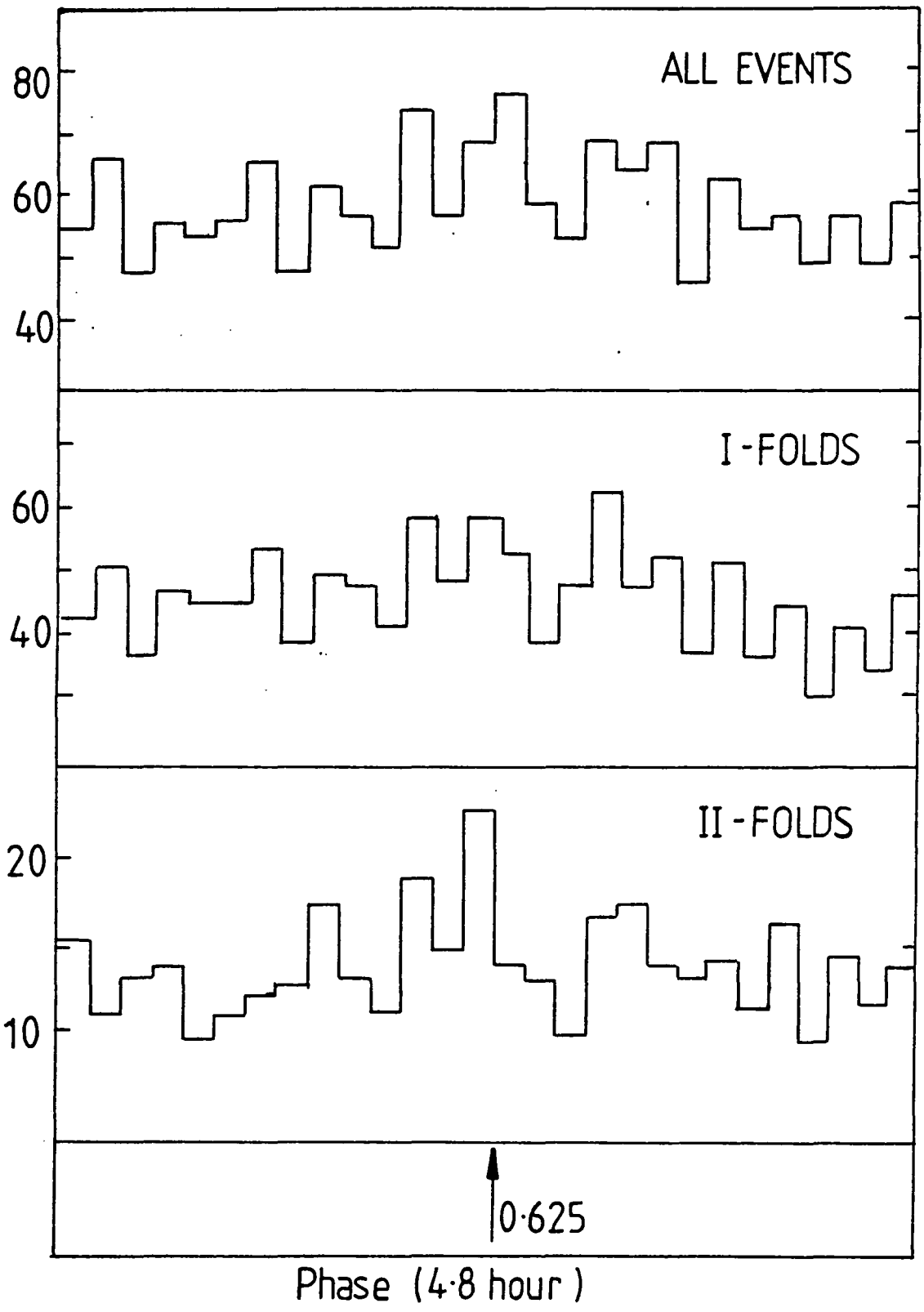

Figure 6.13: The variation of counting rate per minute in the 0.625 phase region - data taken on the 12th of September 1983.

6.2.4: The analysis of the 1983 data

The analysis of the 1983 data was performed using the techniques outlined in section 5.2 and those used for the 1981 and 1982 observations. The data from the 'drift scans' were analysed and added to the results of the 'pseudo-drift scan' output from the 'tracking' observations. The results for the I-fold, low energy data (detectors 2,3 and 4) are shown in fig. 6.12.

The I-fold data show excesses at phases 0.0, 0.625 and 0.75, significant at ~ 2.0 standard deviations. The result for the ~ 0.63 phase region confirms the similar effect seen in the 1981 and 1982 data. The excess at phase = 0.75 has not been observed in previous years. There was some evidence of an excess at phase = 0.0 in the 1982 data (see fig.6.4). Along with the previously noted effects at phase = 0.13 (see fig.6.3) the 1983 results give some confirmation to the results from U.H.E. produced by the Haverah Park array (see fig.6.9).

A more detailed analysis of the 1983 excess at phase 0.63 indicates that the night of the 12th of September gave a 18 % enhancement above the proton background around phase = 0.63 in the I-fold data. A minute by minute investigation of this phase region indicates that the excess comprises two peaks of 2-3 minute duration about the 0.625 transit - see fig.6.13. This is in agreement with the double peak to the emission noted in the large 1982 excesses.

6.2.5: Long term periodicity.

In the 1981 and 1982 observing seasons the Dugway array monitored the 0.63 phase region on 28 occasions see Table 6.1 (here the excess is expressed as a percentage of the cosmic ray background). There have been several reports of a long term (> 10 day) periodicity in the

Date	% of the cosmic-ray background
04·08·81	22·1 ± 11·5
27·08·81	0·8 ± 10·6
31·08·81	14·2 ± 8·3
01·09·81	5·7 ± 13·1
02·09·81	14·3 ± 12·5
25·09·81	40·9 ± 20·5
26·09·81	5·7 ± 18·6
27·09·81	16·2 ± 20·8
21·10·81	17·0 ± 11·0
14·07·82	35·1 ± 20·1
16·07·82	12·1 ± 18·2
17·07·82	6·5 ± 19·7
18·07·82	30·1 ± 16·8
20·07·82	-8·2 ± 21·7
16·08·82	20·1 ± 9·6
24·08·82	30·1 ± 16·8
25·08·82	3·5 ± 16·2
13·11·82	9·9 ± 7·9
14·11·82	1·5 ± 7·9
16·11·82	-2·1 ± 7·2
19·11·82	0·1 ± 6·5

Table 6.1: The 'drift scan' excesses detected at phase = 0.625 in the 1981 and 1982 data.

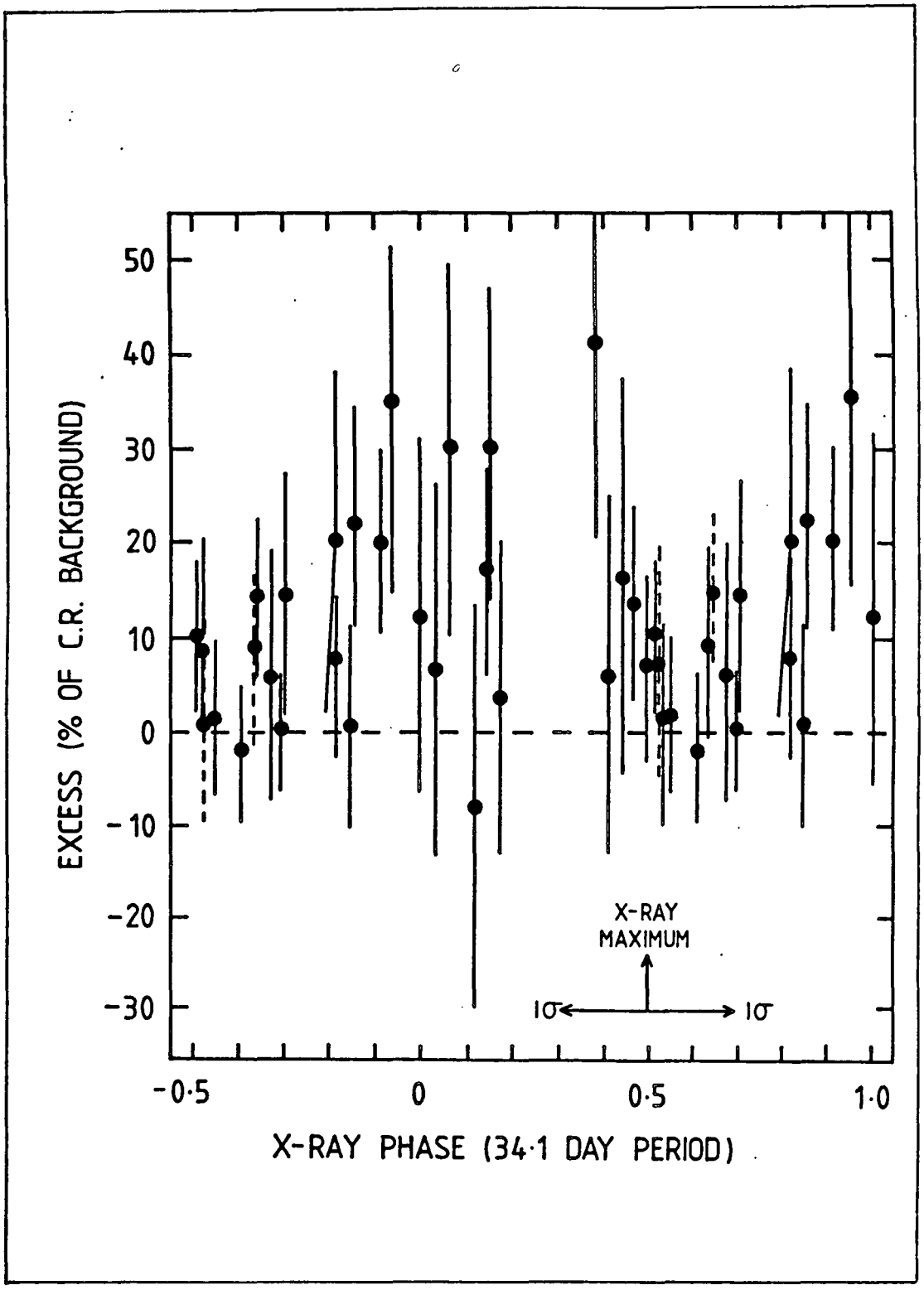

Figure 6.14: The 1981 and 1982 excesses obtained at phase = 0.625 folded modulo 34.1d.

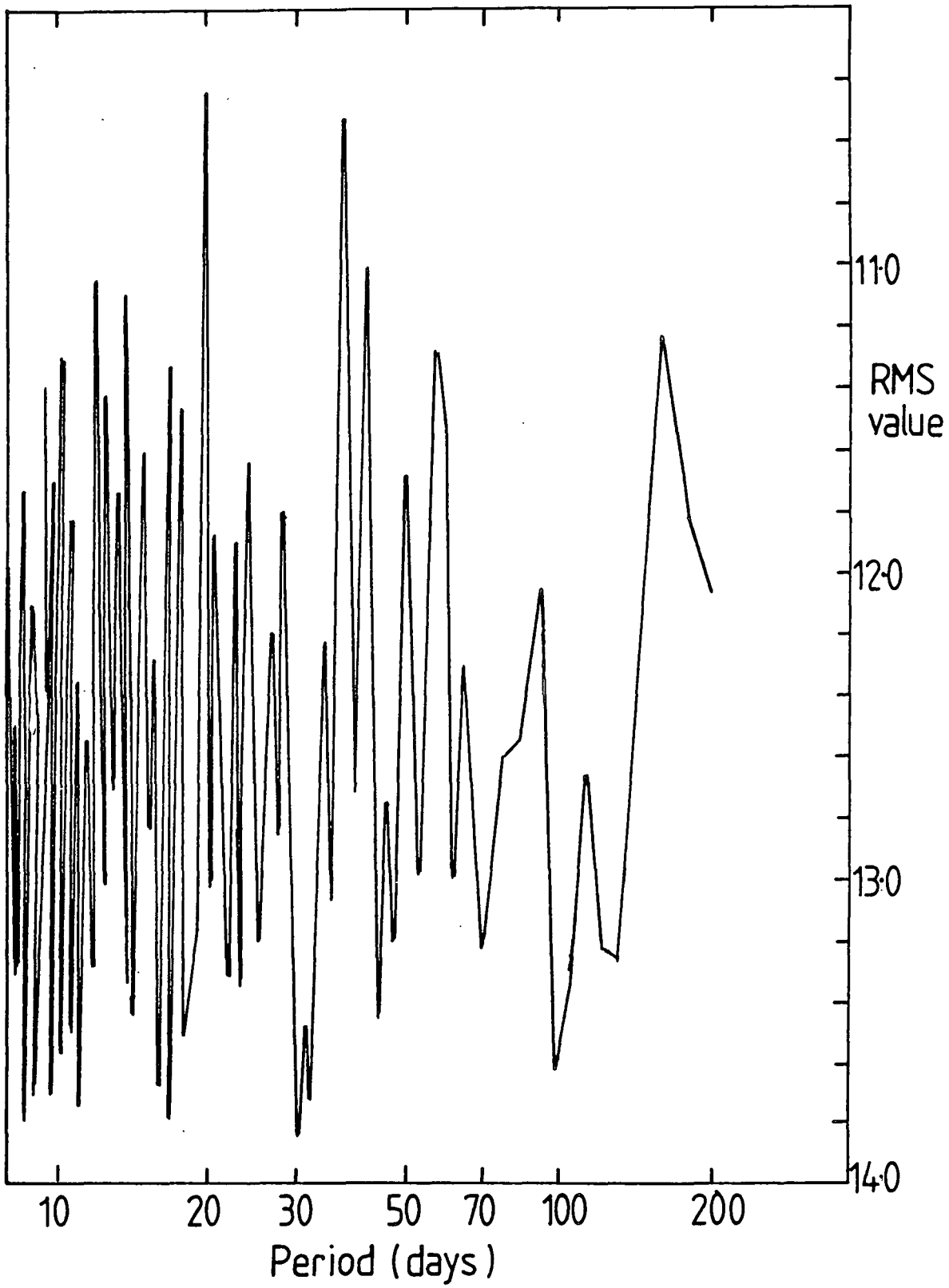

Figure 6.15: The deviations from sinusoidal periodicity in the 1981 and 1982 excesses at phase = 0.625 over the period range 8 - 500 days.

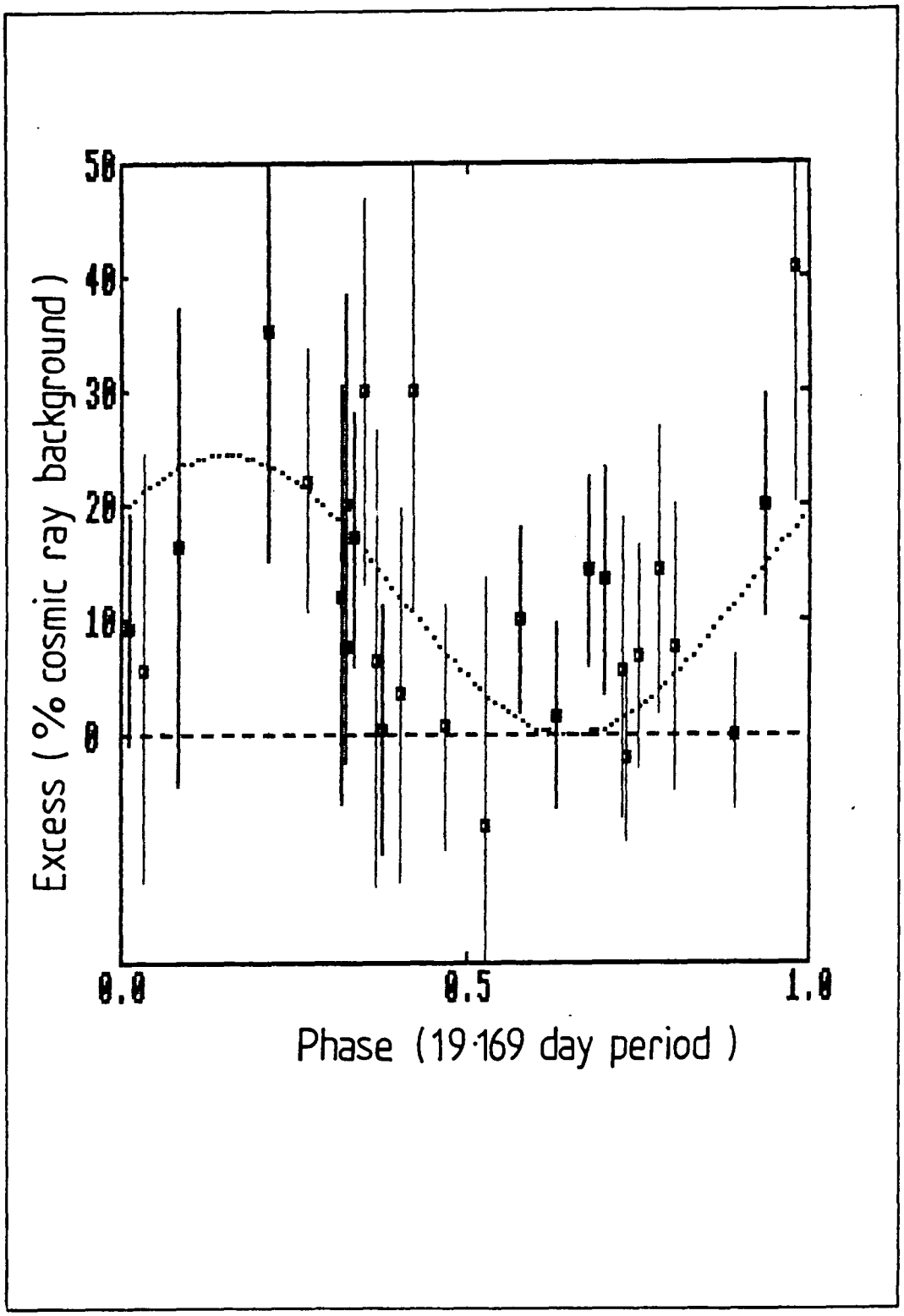

Figure 6.16: The 1981 and 1982 excesses obtained at phase = 0.625 folded modulo 19.2d.

X-ray flux from the object (Molteni et al, 1980), (Holt et al, 1976) and (Bonnet-Bidaud and Van der Klis, 1981). Initially, the data taken at phase = 0.63 were folded modulo 34.1 days in accordance with a predicted variation noted by Molteni et al. These results are shown in fig. 6.14, and were reported elsewhere (Dowthwaite et al, 1983).

It is possible to conduct a search for other long periods. The procedure that was adopted is outlined below.

i. An arbitrary day number was assigned to each 0.63 scan (taking 00.00 hours UT on January 1 1981 as Day=0).

ii. The average level of emission was fixed at the value of 8.8% of the cosmic ray background, (the average of the 1981 and 1982 'drift scan' excesses at this phase).

iii. A sine wave was fitted to the data for all independent periods between 8 days and 500 days.

A measure of the 'goodness of fit' is given by the Root Mean Square (RMS) deviation of the data points from the sine wave. Small deviations are a suitable indication of the extent to which the data conform to a real sinusoidal periodicity. The best fit is given by a period of 19.2 +/- 0.4 days (with a harmonic at 36.8 +/- 1.5 days) see fig. 6.15. The data when folded modulo 19.2 are plotted in fig.6.16.

It is difficult to assign an exact probability to this period but the distribution of the RMS deviations shows the average deviation to be 12.5647 with a standard deviation on this value of ~ 0.767. With these assumptions the observed 19 day period is significant at the ~ 2.7 σ level.

This result is in agreement with previous reports of an approximately 20 day variation in the X-ray data (Bonnet-Bidaud and Van der Klis, 1981). The 20 day X-ray modulation was explained as apsidal motion in the Cygnus X-3 system - see section 7.4.

Phase	Date (1982)	Detector							
		1		2		3		4	
		N_	N+	N_	N+	N_	N+	N_	N+
0·5	14/07	18	27	49	32	20	26	17	18
	18/07	23	37	29	37	27	21	19	17
	16/08	59	57	75	68	79	81	24	36
	24/08								
0·625	14/07	54	30	56	29	33	49	45	10
	18/07	47	41	31	41	36	41	35	10
	16/08	77	46	64	76	105	65	29	24
	24/08	20	22	42	19	24	29	19	6
0·75	14/07	53	39	37	47	61	53	37	26
	18/07	46	35	45	52	52	53	29	25
	16/08	73	49	70	61	51	76	28	40
	24/08								

Table 6.2: The initial analysis of the pulse amplitude values. (data taken about phases 0.5 and 0.75 on 24/08/82 was not suitable for this analysis).

6.2.6: Pulse amplitude Analysis.

The four nights showing the largest 'drift scan' excesses at phase 0.63 (section 6.2.1) can be investigated in greater detail. These nights, rich in gamma-ray candidate events can be analysed in a search for a difference in the characteristics of the pulse amplitudes between the 'ON', 0.63 phase events and the two adjacent 'OFF' phases. The analysis procedure was outlined in section 5.5.

The initial analysis searched for a difference in the number of events with pulse amplitudes above (N_+) and below (N_-) a median value predicted from background data. This analysis was applied separately to the data taken from each detector and for each night and the results are summarised as Table 6.2.

There is a noticeable difference in the pulse amplitude values for this data in favour of small intensity showers.

i.e. Median(ON phase) < Median(OFF phase)

and $N_- > N_+$

The difference is present for all the detectors, but is most marked for detector 4 which had the highest energy threshold (see section 3.6.4).

To check these results the same nights were analysed in exactly the same way at the adjacent phases 0.5 and 0.75 - see Table 6.2. There is no indication from these samples of the large difference in the light-pulse characteristics detected at phase 0.63.

The pulse amplitude distribution may be sensitive to changes in the experimental conditions, and therefore checks were made to ensure that the experimental conditions were stable throughout the time under investigation. The median of the pulse amplitude distributions for the data taken in the two 'OFF' and the 'ON' phase regions about phase = 0.63 have been computed. There is no significant deviation in

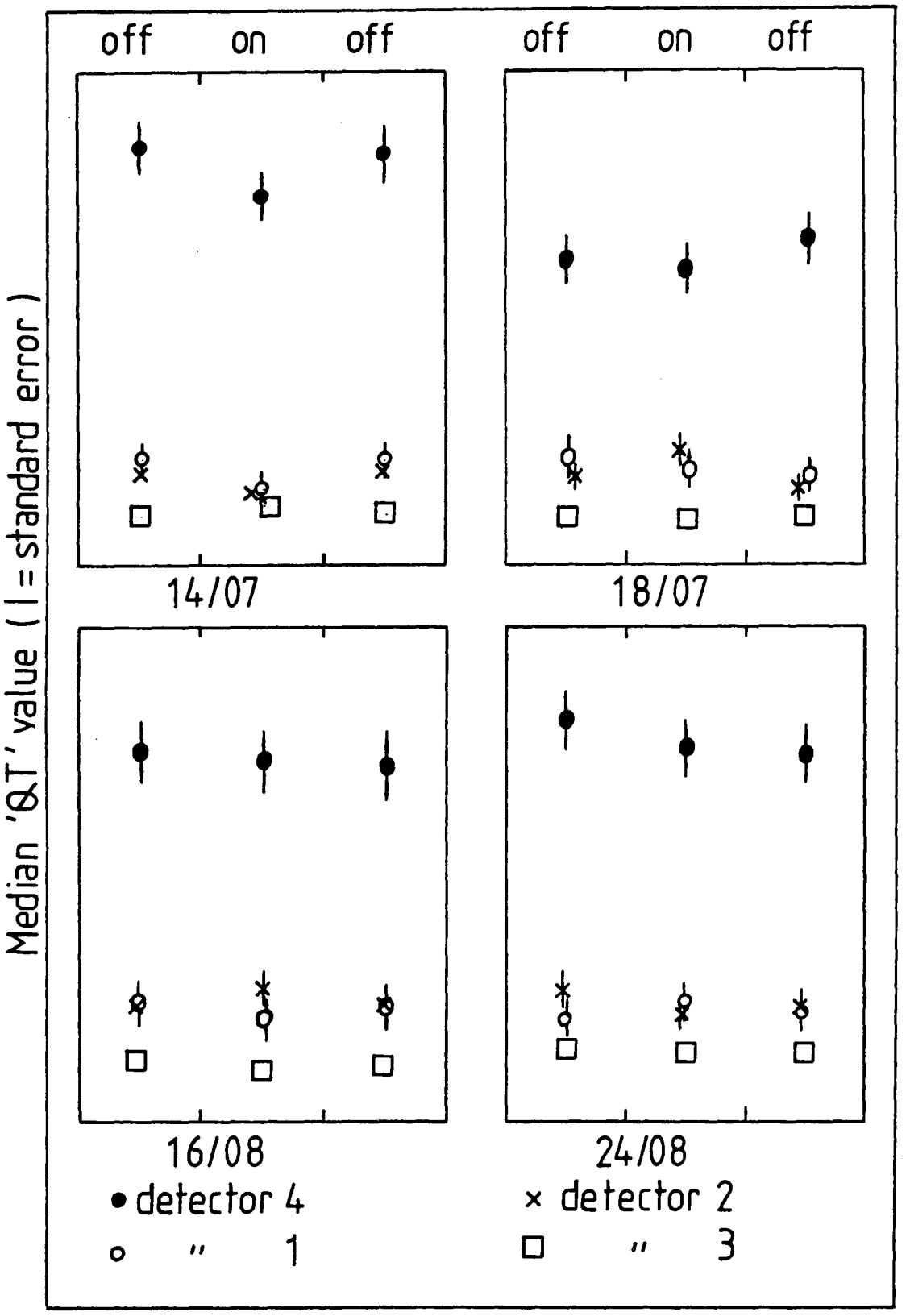

Figure 6.17: The variation of the median pulse amplitude values over the 0.63 phase region for the four nights showing the strongest excess in 1982.

Phase	detector	Mann-Whitney probability
0·5	1	0·09
	2	0·12
	3	0·97
	4	0·04
0·625	1	0·006
	2	0·03
	3	0·1
	4	0·005
0·75	1	0·06
	2	0·99
	3	0·7
	4	0·6

Table 6.3: The difference in the pulse amplitude characteristics for each detector at phases 0.5, 0.625 and 0.75.

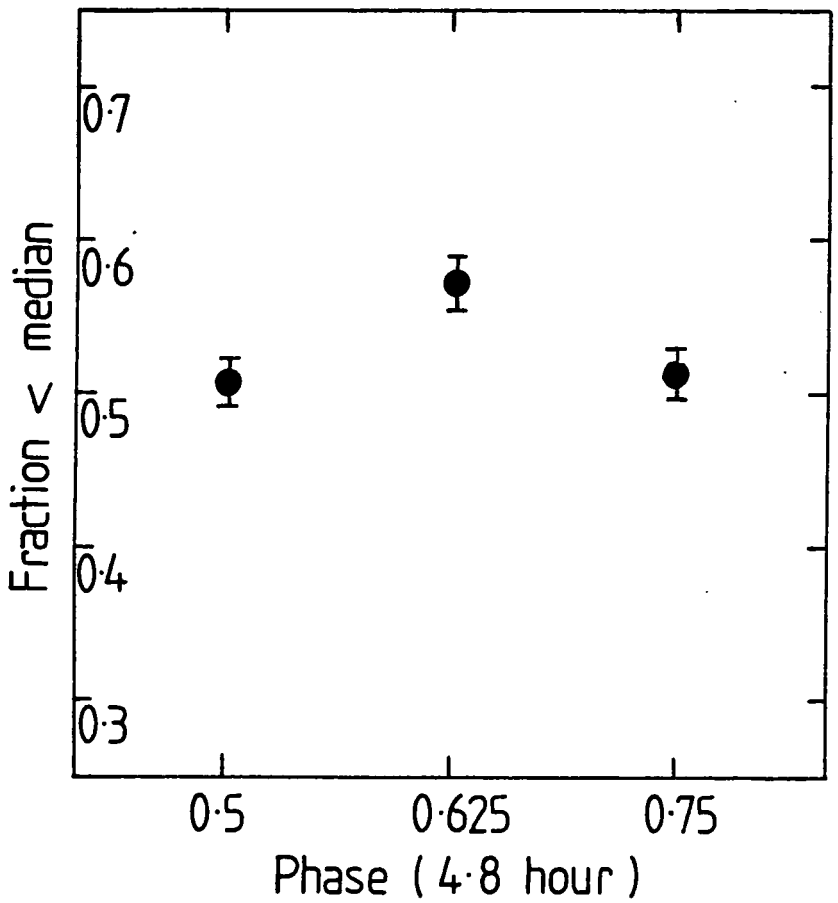

Figure 6.18: The results of the pulse amplitude analysis presented in Table 6.3.

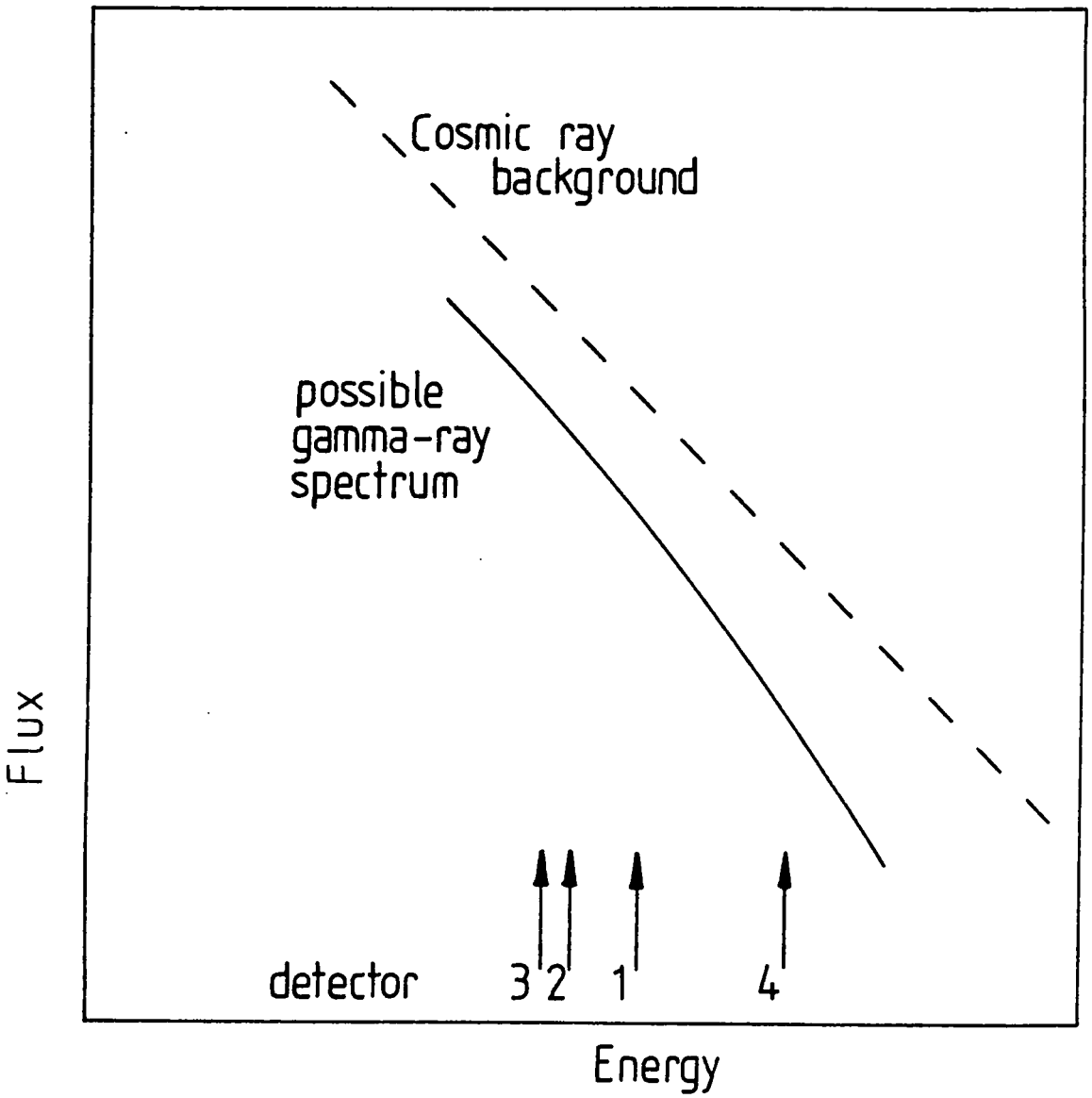

Figure 6.19: A possible V.H.E. spectrum for Cygnus X-3 - suggested by the results of the pulse amplitude analysis.

the median values for the 'OFF' sections for each night as indicated graphically in fig. 6.17, and so a reliable analysis can be performed.

The significance levels for the pulse amplitude effects for each night have been calculated as described in section 5.5.4 using the powerful Mann-Whitney U-test. The full results are presented as Table 6.3, and given graphically as fig.6.18.

This result is explained by noting that in 1982 the array consisted of four telescopes of differing energy threshold - see section 3.6.4, detector 3 having the lowest, detector 4 the highest. The response to gamma-rays would then be significantly different.

A steepening spectrum compared to the proton background, as shown in figure 6.19 could explain these observations. For detector 3 with its low relative energy threshold, and narrow response a smaller imbalance above and below the predicted median would be observed than for detector 4 with a much higher relative threshold and a wider response (see Table 3.2).

The observations do seem to indicate that the spectrum in the 1 TeV region may be curving away from the cosmic ray background i.e. steepening. This result is rather difficult to explain when compared with the U.H.E. measurements and will be discussed in Chapter 7.

6.2.7: Pulsar periodicity - the range of the period search.

Some of the models proposed for Cygnus X-3 involve particle acceleration by a pulsar (see section 7.4.3). The Dugway array has an accurate timing system, essential for a search for short (ms) periods, and so subsets of the data showing the strongest excess over the background cosmic rays i.e. containing the strongest concentration of gamma-ray candidate events have been searched for evidence of pulsar periodicity. The Rayleigh test was chosen as a suitable test for this

analysis (see section 5.3.10).

Cygnus X-3 is a binary system and some account must be made of the modulation of the event arrival times due to the orbit. The motion of the supposed pulsar around the companion star introduces a 'Doppler shift' to the periodic emission varying with the 'line of sight' velocity. This shift 'smears' the periodic signal from the object, and may prevent the detection of a signal for faster periods.

For other binary sources observed by the Durham array (e.g. Hercules X-1, 4U0115+63), accurate orbital parameters are available from measurements made at other energies, and so this orbital modulation can be removed from the data as described in section 5.3.2. In the case of Cygnus X-3 there is no complete orbital information and so some estimate of the range of periods that can be scanned, limited by this ambiguity must be made.

The first assumption made in this calculation is that the orbit is nearly circular. This will serve for the purpose of an 'order of magnitude' estimate. The projected separation of the components of the system is usually taken to be $\sim 10^{11}$ cm (= asini), and so the radial velocity is given by;

$$\frac{V_r}{c} = \frac{(2.\pi . a.\sin i)}{T.c} \qquad - 6.2$$

where, T = orbital period i.e. 4.8 hours

$$\frac{V_r}{c} \sim 1 . 10^{-3}$$

Therefore, any relativistic effects can be ignored in this estimate.

For a roughly circular orbit the period, P_ω of a pulsar will vary

according to,

$$P = P_\omega \left(1 + \frac{V_r}{c} . \cos \frac{(2.\pi .t)}{T} \right) \qquad - 6.3$$

and the change in period per unit time is then,

$$\frac{dP}{dt} = \frac{- P_\omega . V_c . \sin i . 2.\pi}{c.T} . \sin \left(\frac{2.\pi .t}{T} \right)$$

over the 10 minutes of data constituting a 'drift scan' excess the cosine term can vary between ~ 1 and ~ 0.1. So since velocity variations are proportional to the variations in period it is possible to calculate a change in the period DP over the 10 minutes of the observation from;

$$P = P_\omega + \frac{dP}{dt} . t \qquad - 6.4$$

or $DP = \sim 4.3\ 10^{-7} . P_\omega . (0.1 - 1.0) . 600s$

i.e. the best case corresponds to;

$$DP \sim 2.6\ 10^{-5} . P_\omega$$

and the worst case corresponds to:

$$DP \sim 2.6\ 10^{-4} . P_\omega$$

It is this value that must remain less than the 'harmonic interval' (see section 5.3.6) for the period search to be valid.

If this calculation is performed it is clear that at best only periods greater than

~ 10 ms

should be tested for true periodicity.

To cover this possibility all periods from 10 ms upwards were analysed.

Date	No. of counts	% excess	Predicted probability if all excess pulsed
14·07·82	110	35·1	1.10^{-6}
18·07·82	83	30·1	5.10^{-4}
16·08·82	193	20·1	4.10^{-4}
24·08·82	87	30·1	3.10^{-4}
12·09·83	450	18	4.10^{-7}

Table 6.4: The probabilities recovered by the Rayleigh test assuming all the count-rate excess is pulsed.

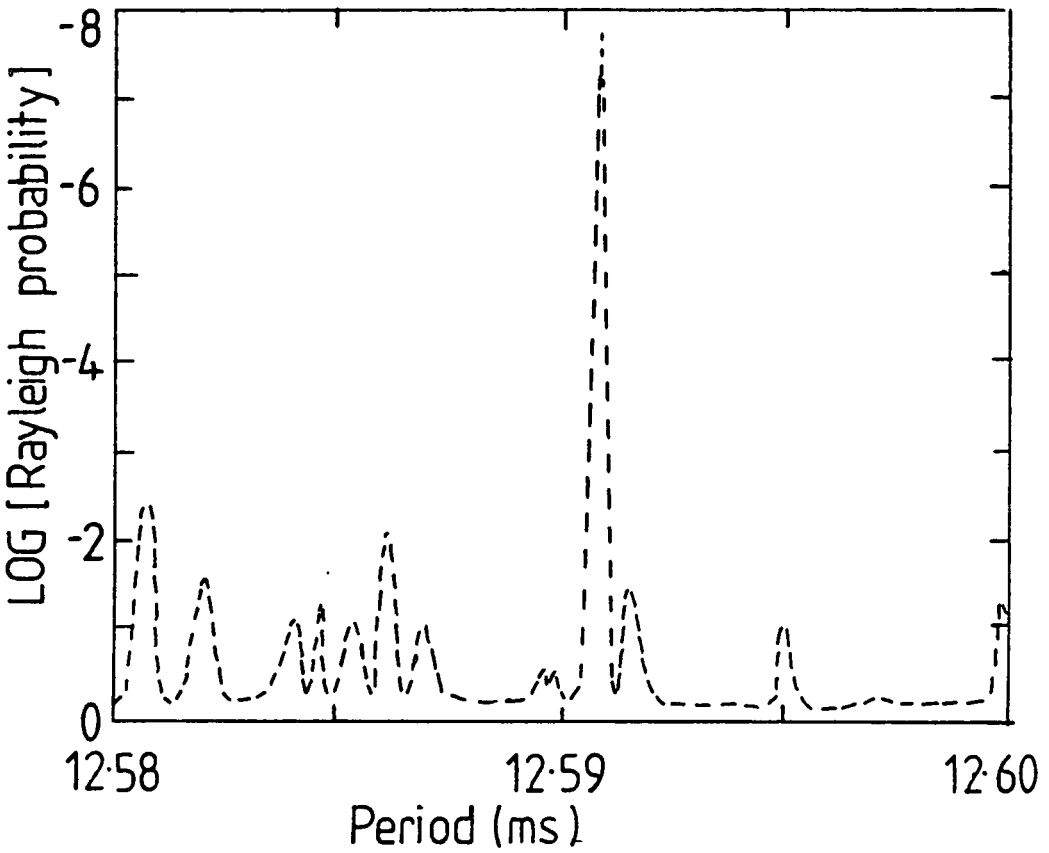

Figure 6.20: i, The chance probability at 12.59 ms in the data taken on September 12th, 1983.

6.2.8: The Systematic search.

To have a chance of detecting a significant periodicity in the sparse data taken in the V.H.E. observations using the Rayleigh test, there are two important prerequisites.

The data must exhibit a large excess over the cosmic ray background, R, and the overall counting rate, N, must be high. The probability of no periodicity in the data must be less than the reciprocal of the number of degrees of freedom expended in the search for this analysis to be valid.

The number of degrees of freedom used is roughly equal to the number of periods tested - see section 5.3.7. For the search for periods from 10 ms to 50 s the number of degrees of freedom expended is $\sim 6 \cdot 10^4$. The probabilities of no periodicity for the strongest excesses in the 1982 - 1983 observing seasons (assuming all the excess is periodic) are listed in Table 6.4.

Initially this analysis was performed on the 1982 data and no significant periodicity was found. However, the increased counting rate of the array in 1983 meant that the one night with a significantly excess of $\sim$ 18 % over the cosmic ray background (12th September) gave the best opportunity for a successful search for millisecond periodicity over the 7 minutes of the excess. A period of 12.5905 ms was seen in the data taken around phase = 0.63 (see fig.6.20.i). The probability of no periodicity for this period was found to be $\sim 4.8 \cdot 10^{-6}$.

Once degrees of freedom have been taken into account this detection is at a probability level of $\sim 2.6 \cdot 10^{-3}$ - a significant indication of pulsar periodicity.

The form of this detection has been analysed for each of the detectors in the array and for the II-fold detector responses with the

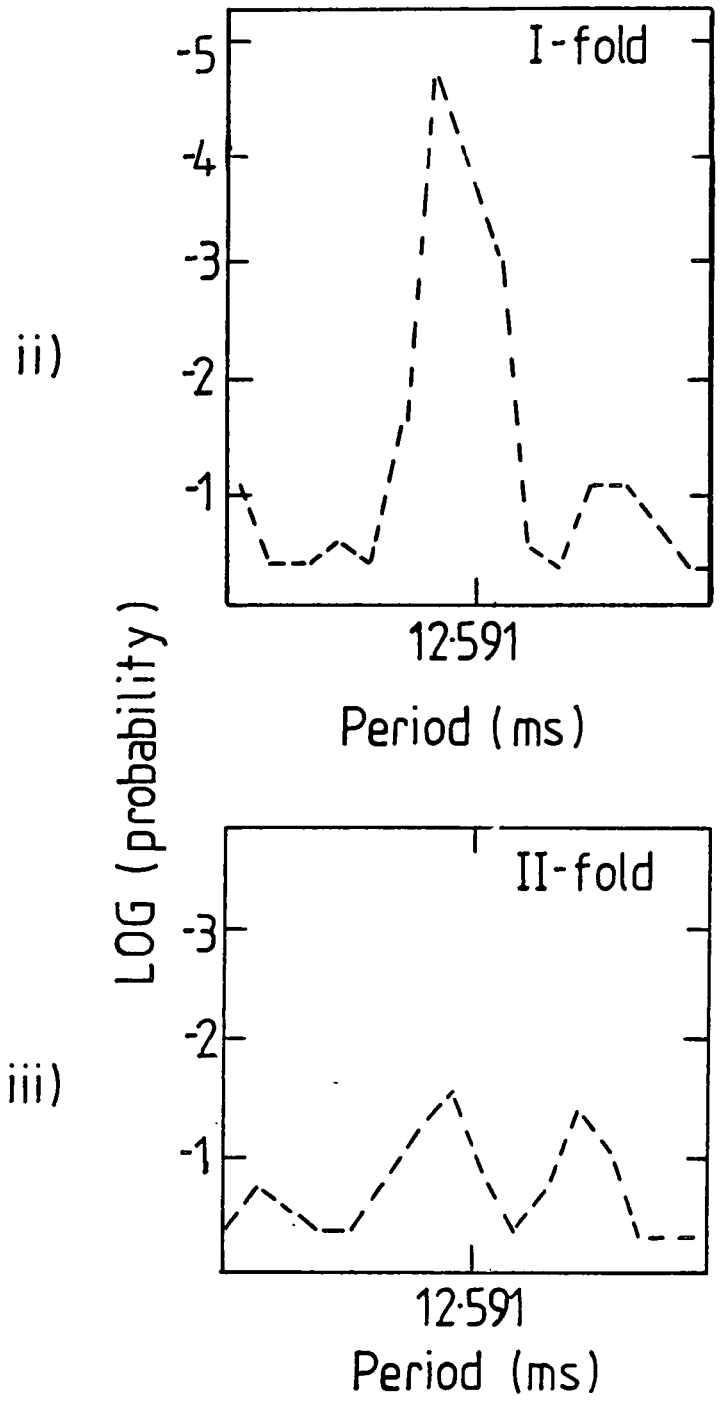

Figure 6.20: ii - vi, The periodic content in the data taken on September 12th, 1983 - various detector combinations.

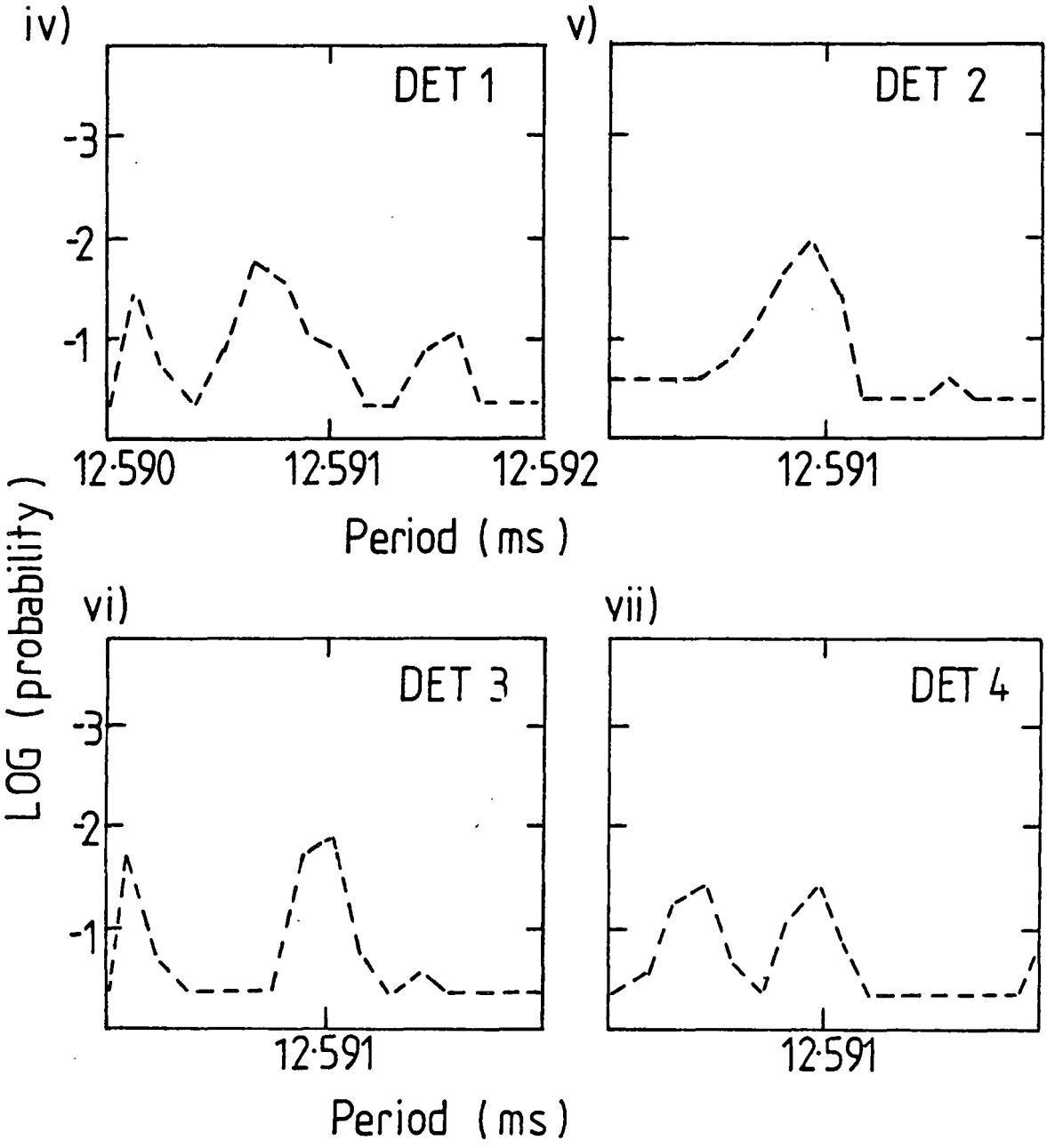

Figure 6.20: continued.

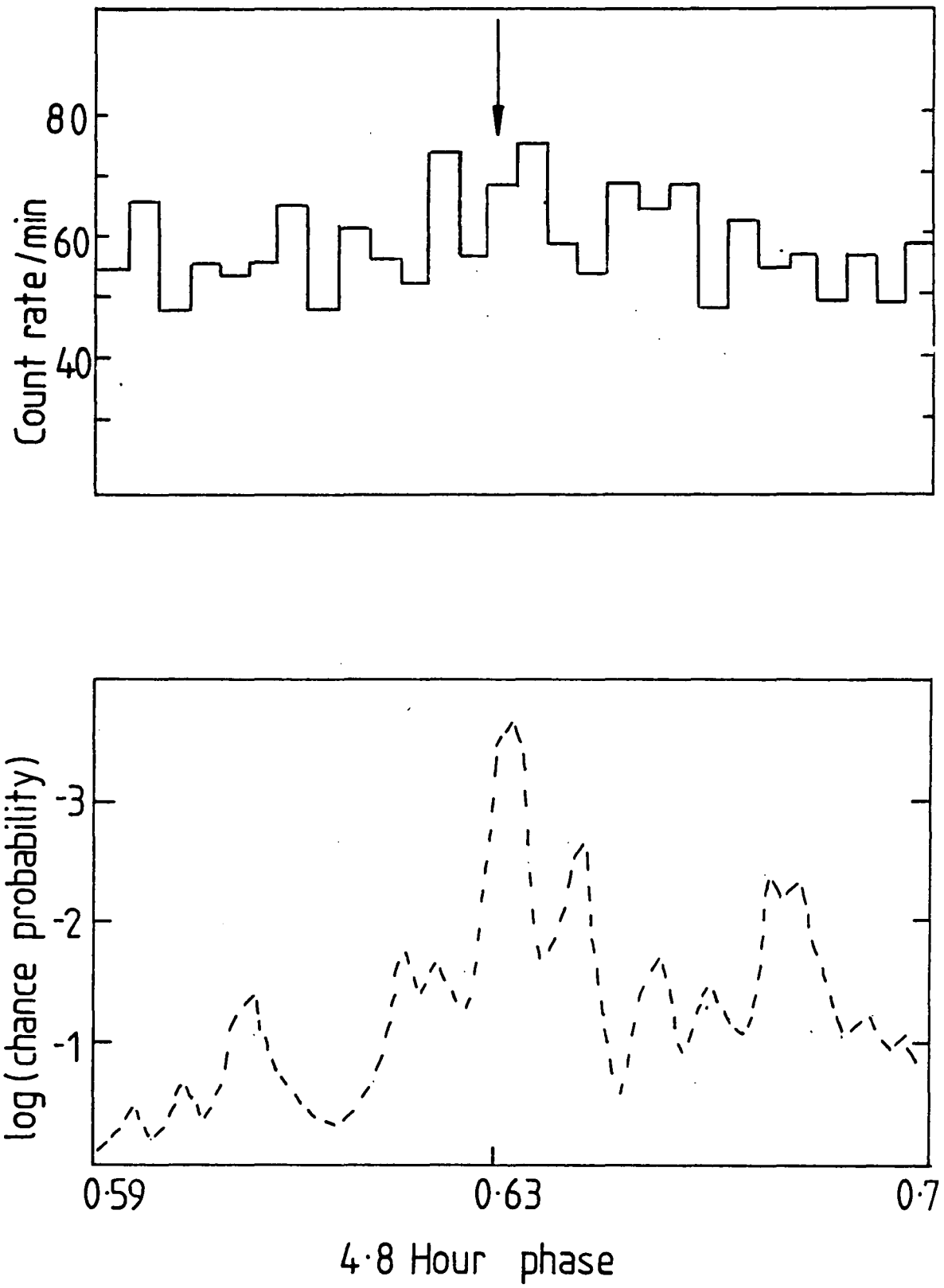

Figure 6.21: The periodic content in the data taken about phase = 0.63 mapped to the count rate excess.

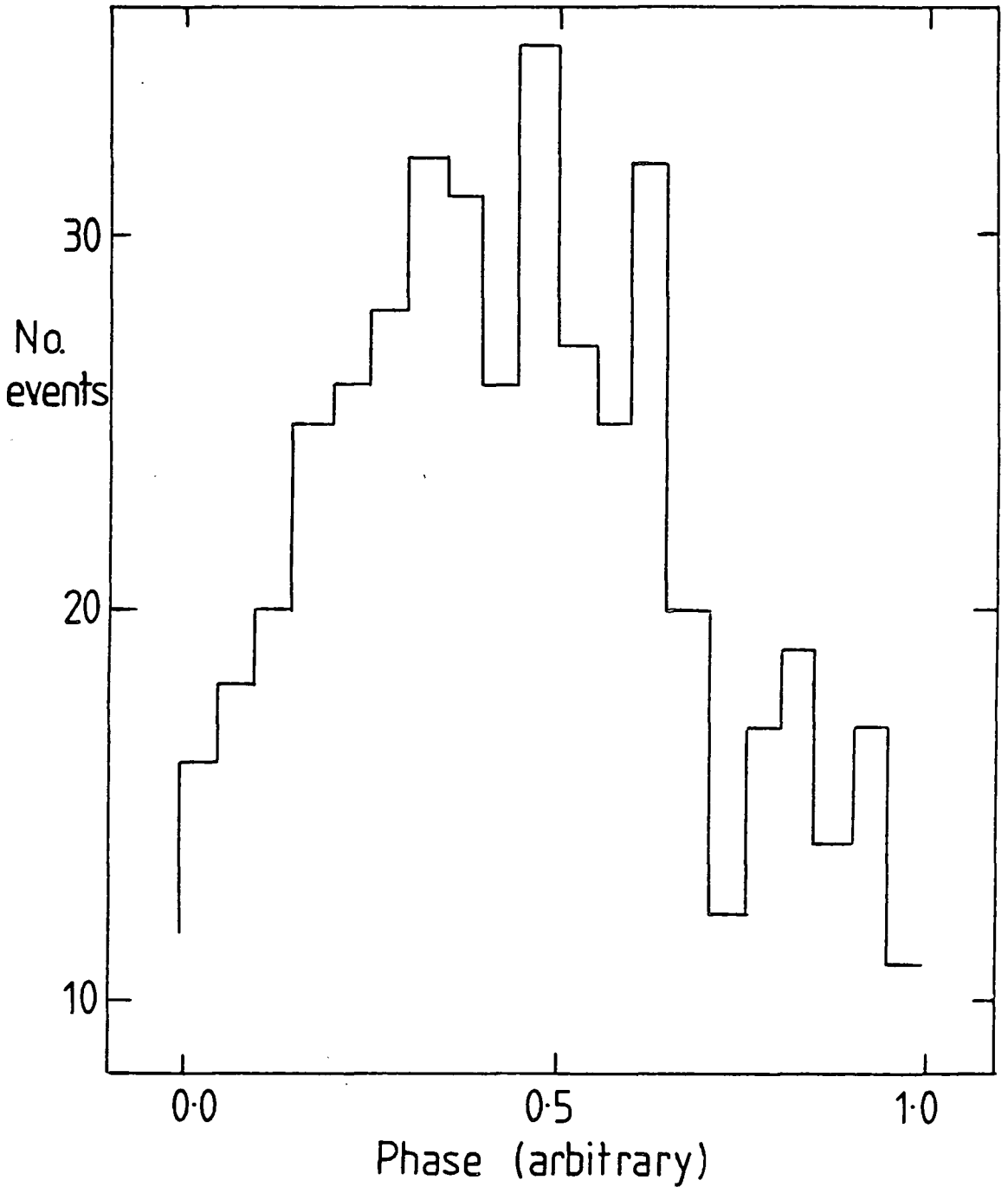

Figure 6.22: The 'light curve' at 12.59 ms.

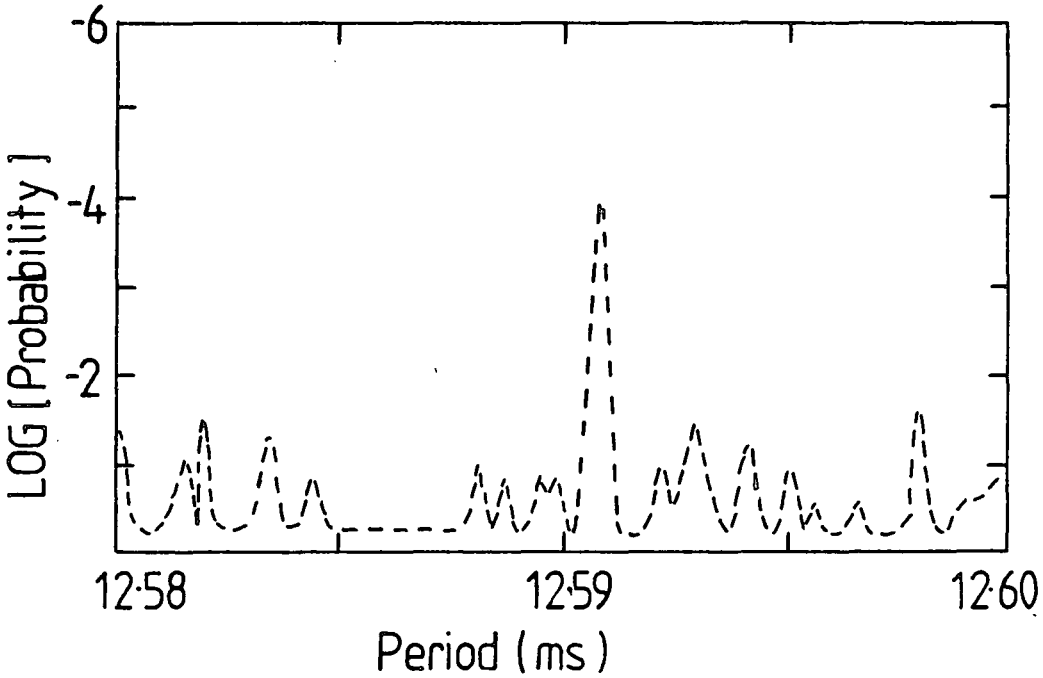

Figure 6.23: The detection of 12.59 ms periodicity in the data taken on October 2nd 1983.

results given as fig.6.20.ii to fig.6.20.vii. The ~ 12.59 ms period is evident in the events detected by all telescopes, and is also present in the II-fold data. In addition, the strength of the periodic content in the data maps the structure noted in this count rate excess (fig.6.21). The 'light curve' is plotted in fig.6.22.

To check for any instrumental effects present in the system, the data taken from other sources observed in this month have been analysed at this period. No evidence of ~ 12 ms periodicity was found. No other objects were observed on the night of the 12th of September and so a close check with similar experimental conditions was not possible.

Given the ~ 12 ms period, other suitable data can be analysed for evidence of emission at this period. The rest of the 1983 data were analysed, including nights when the sky conditions were not ideal. The 12 ms period was found in ~ 7 minutes of data taken on the 2nd of October 1983 at phase ~ 0.63 i.e. ~ 20 days after the 12th of September (see fig 6.23). This detection occurred at a probability of no periodicity of ~ $4.0 \cdot 10^{-4}$ and provided further evidence for a 19-20 day long-term modulation to the data. The 6 other nights searched did not yield any significant positive detection. If the null results are taken into account the evidence for periodicity at ~ 12.59 ms was at a chance probability of ~ $2 \cdot 10^{-5}$ for the 1983 data. The combination of the separate probabilities was calculated from,

$$\chi^2_{combined} = -2. \ln \cdot \Pi \text{ Probability}_i \qquad - 6.5$$

with 2n degrees of freedom

(Eadie et al, 1971)

The strongest excesses detected in 1982 did not show strong evidence of periodicity at this period. However, further more detailed analysis has discovered some confirmation of the ~ 12ms periodicity at phases close to 0.63. These results will be presented elsewhere

(Chadwick, PhD thesis, in preparation).

The detection of a pulsar period in the data from Cygnus X-3 has important implications for the models suggested for this system, and will be discussed in section 7.4.6.

6.2.9: Second-minute periodicity.

There has been recent evidence of 'quasi-periodic' X-ray signals from the Cygnus X-3 system at periods greater than 1 second (Van der Klis and Jansen, 1985). The 1982 large 'drift scan' excess nights have been analysed for periodicity in the range 0.1 seconds to 100 seconds in a search for similar emission from the gamma-ray data.

In this case there are 6000 independent periods to be tested for a 10 minute dataset, and so we would expect only those periods detected with probabilities of no periodicity less than $1.66\ 10^{-4}$ to be significant.

No highly significant periods were detected in the data for any of these nights.

Despite the absence of significant detections it may be possible to infer a periodicity in the data by looking for patterns in the most significant results of this analysis. No detectable pattern to these periodic effects was found.

6.2.10: The Cygnus X-3 V.H.E. gamma-ray spectrum.

The data for 1981 and 1982 show an average integral peak flux of 11 % of the cosmic ray background restricted to the narrow (0.035) phase region around phase 0.63. This peak of the emission corresponds to a flux of $4\ .\ 10^{-10}$ cm^{-2} s^{-1} at E > 1000 GeV, and may exceed 10^{-9} cm^{-2} s^{-1} at the peak of both the 4.8 hour and 19 day modulations. The flux

Legend for figure 6·24

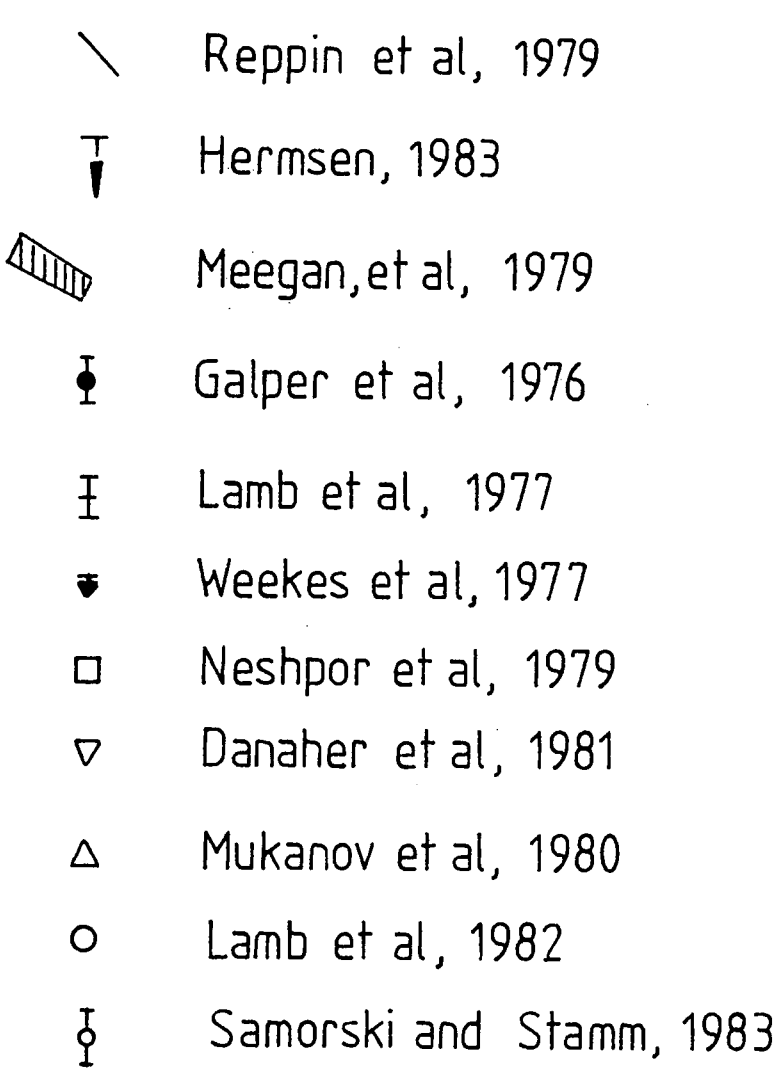

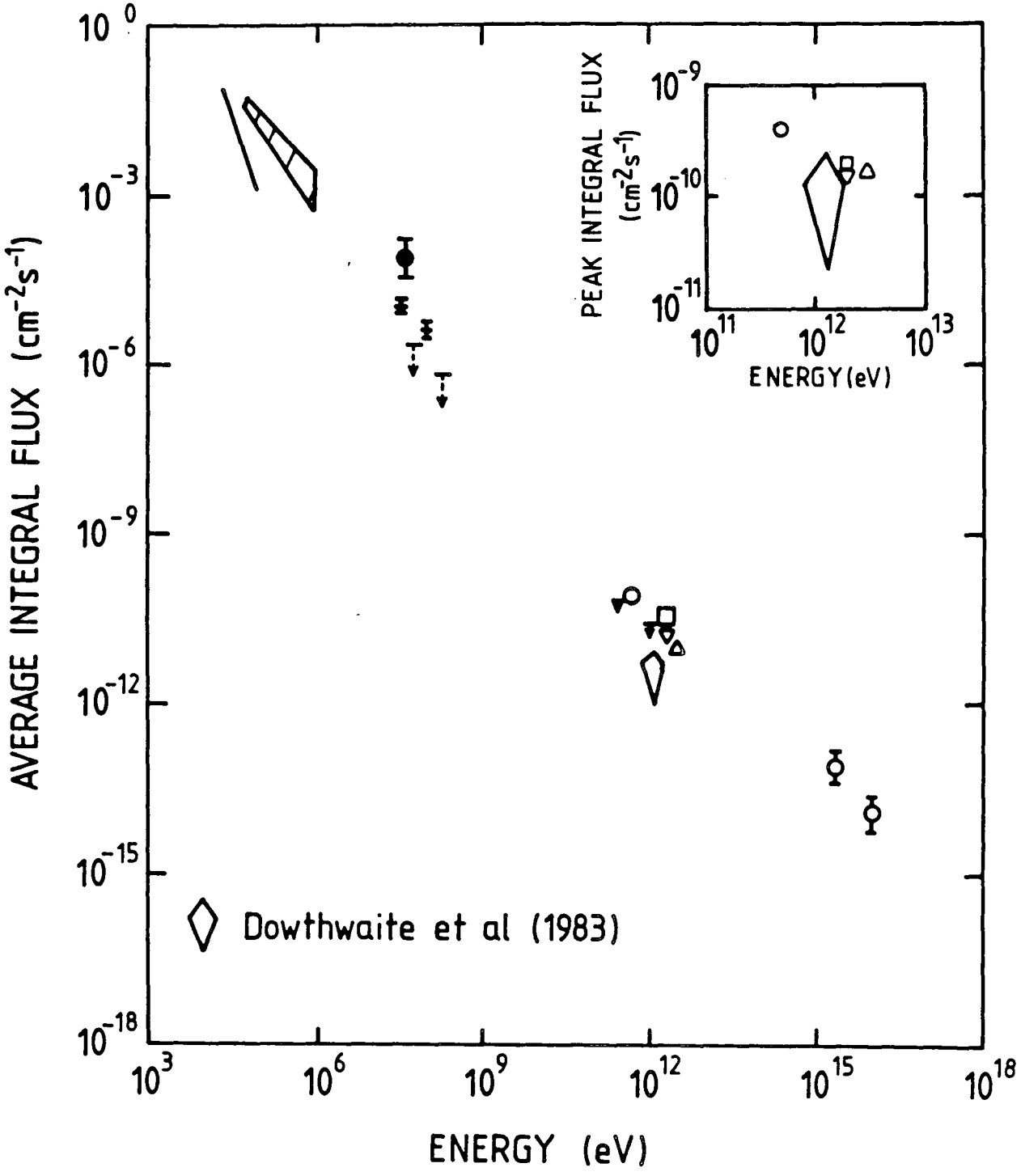

Figure 6.24: The V.H.E. gamma-ray spectrum from Cygnus X-3.

averaged over the full 4.8 hour cycle then corresponds to $\sim$ 5 . 10^{-12} cm^{-2} s^{-1}. These values are in close agreement with those from other experiments - see fig.6.24.

The low energy threshold telescopes detect a larger excess over the background than those operating at higher thresholds. This indicates that the gamma-ray spectrum is more steep than the cosmic ray spectrum by $\sim$ 0.8 +/- 0.5 (Dowthwaite et al, 1983).

There is some evidence to confirm this picture in the 1981 and 1983 data. An estimate of the peak V.H.E. flux (averaged over 10 minutes) from this object detected on the night of the 12th of September is given below,

Low energy data (I-fold, Dets 2,3,4)

2.4 . 10^{-7} $cm^{-2}s^{-1}$ str^{-1} at E > 1000 GeV

Higher energy (II-fold, Dets 1,2,3,4)

3.3 . 10^{-10} $cm^{-2}s^{-1}$ str^{-1} at E > 2500 GeV

(3 σ upper limit)

Results from the pulse amplitude measurements made in 1982 (see section 6.2.6) also indicate a steep spectrum in the V.H.E. region, though a similar analysis of the 1983, 12th of September burst did not show any imbalance in the pulse amplitude values. The shape of the spectrum between the V.H.E. and U.H.E. regions is discussed in section 7.4.6.

6.3: The Galactic Plane.

The long 'drift scan' observation of the Galactic plane (see section 4.4.5) was made in the Cygnus region (l = 79.9; b = 0.7). The result is given as fig.6.25, and shows that there is evidence of

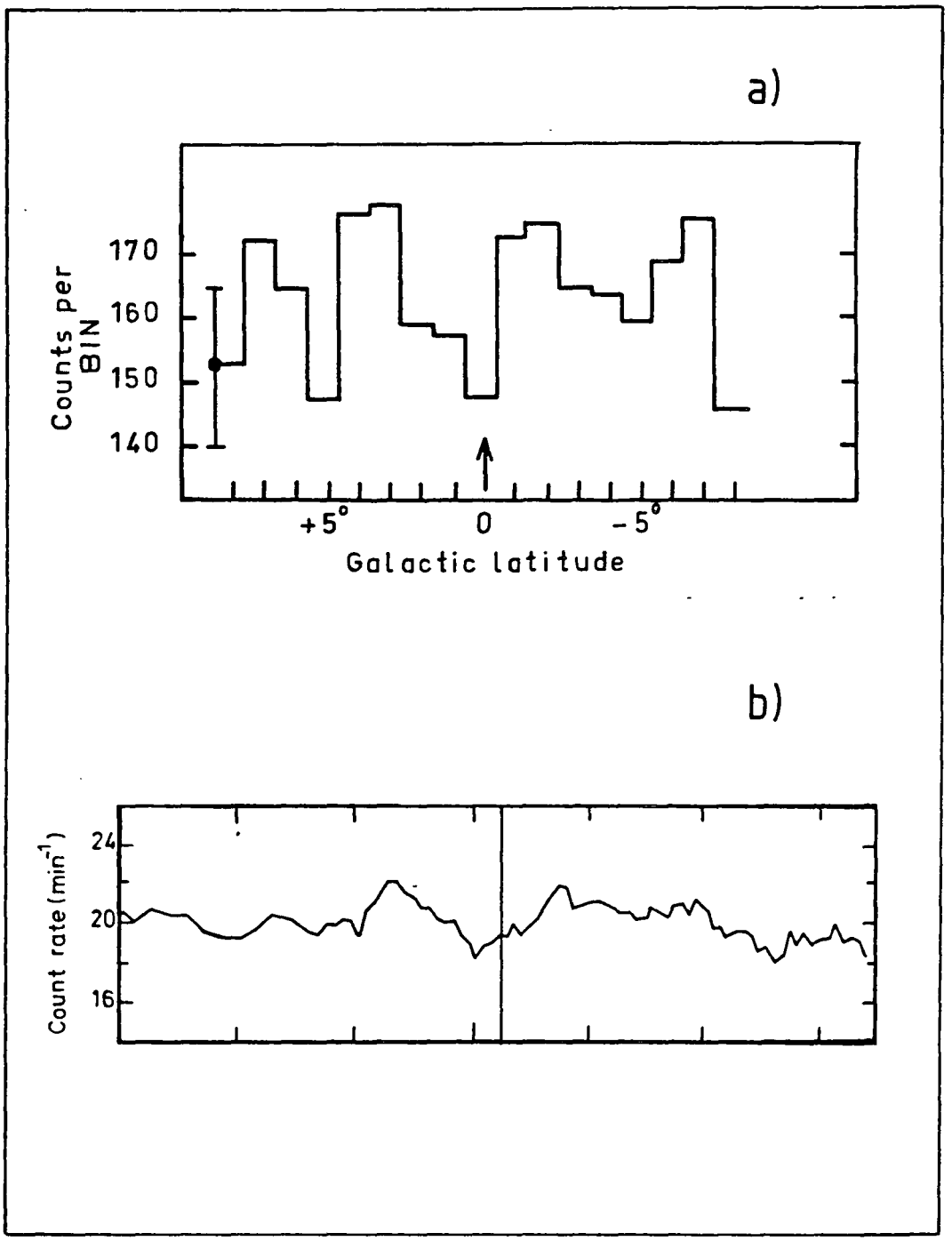

a) count rate per 8 min. (low energy telescopes)

b) count rate per min. ("

- averaged over 20 min.)

Figure 6.25: The 'drift scan' across the Galactic Plane (l=79.9, b=0.7).

emission from the Galactic plane itself. The details of this observation are discussed elsewhere (Dowthwaite et al, 1985), but it is important to note that the structure of the emission exhibits a 'dip' around the Cygnus X-3 region. If this structure is confirmed it means that the 1981 drift scans were conducted against a varying background, with the minimum coinciding with the transit of the V.H.E. source. The detected flux at all phases should then be increased by ~ 2 % of the background rate in fig.6.3 to account for the higher 'OFF' source background. This increases the significance of the excess at phase = 0.63 to ~ 5 standard deviations and the excess at phase = 0.13 to ~ 2 standard deviations.

The Galactic plane measurement indicates that the detection, in 1981 at phase = 0.63 corresponds to a flux of 6 . 10^{-10} photons cm^{-2} s^{-1}. It provides further evidence for the emission at two phases in the orbit i.e. 0.13 and 0.63. This will be discussed in relation to the models for suggested from this system in section 7.4.

6.4: Hercules X-1.

6.4.1: The analysis of the 'drift scan' observations of Hercules X-1.

Four 40 minute 'drift scan' observations were made of the binary X-ray pulsar, Hercules X-1 on the 17th of April 1983. The data were barycentred and reduced to the focus of the orbit using the X-ray ephemeris provided by observations made using the UHURU satellite (Tananbaum et al, 1972).

Each of the scans was analysed using the technique described in section 5.2 for evidence of an excess while the object was in the field of view of the telescopes. The last scan did show a significant excess of events equivalent to 14 +/- 7 % of the cosmic ray background over the full 'ON' source time. A more detailed investigation of this

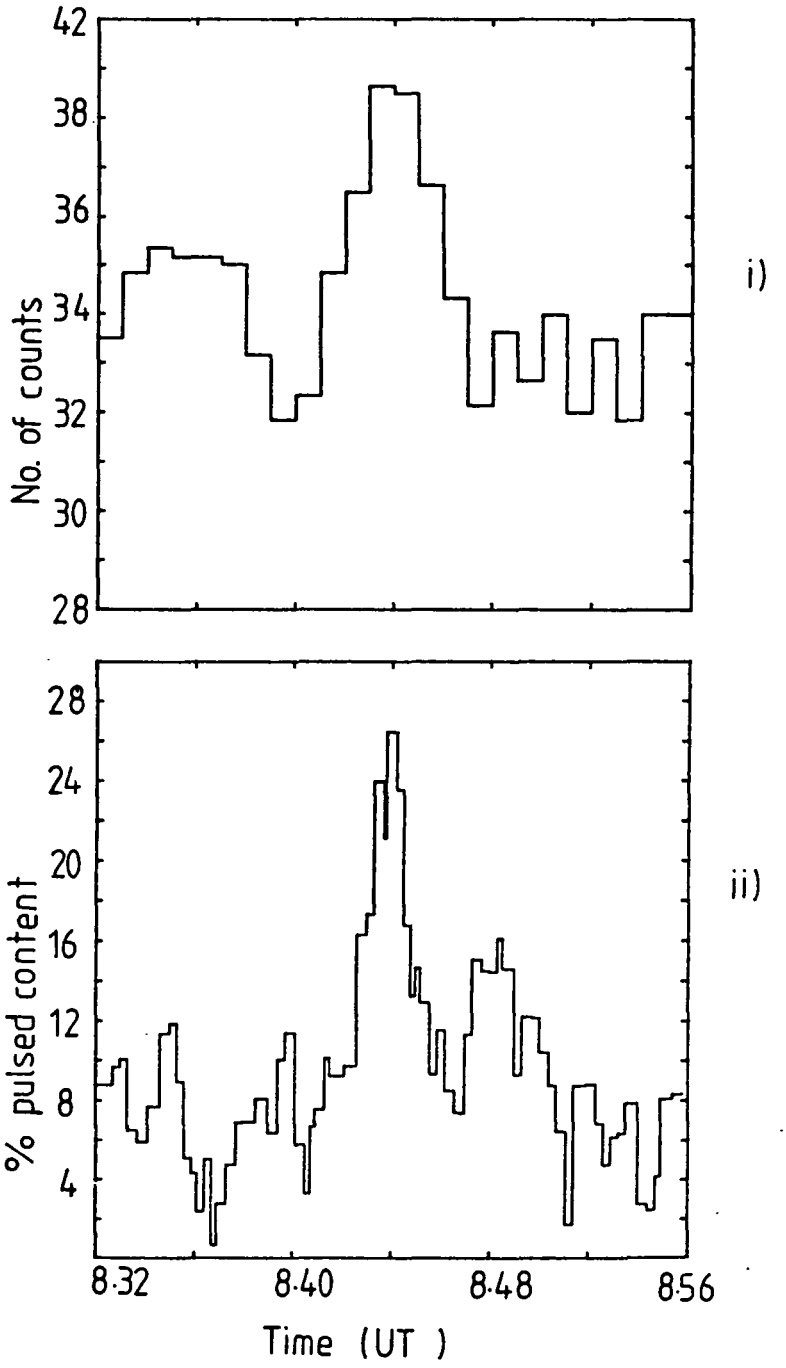

Figure 6.26: The periodic content in the V.H.E. burst from Hercules X-1 mapped to the count-rate excess.

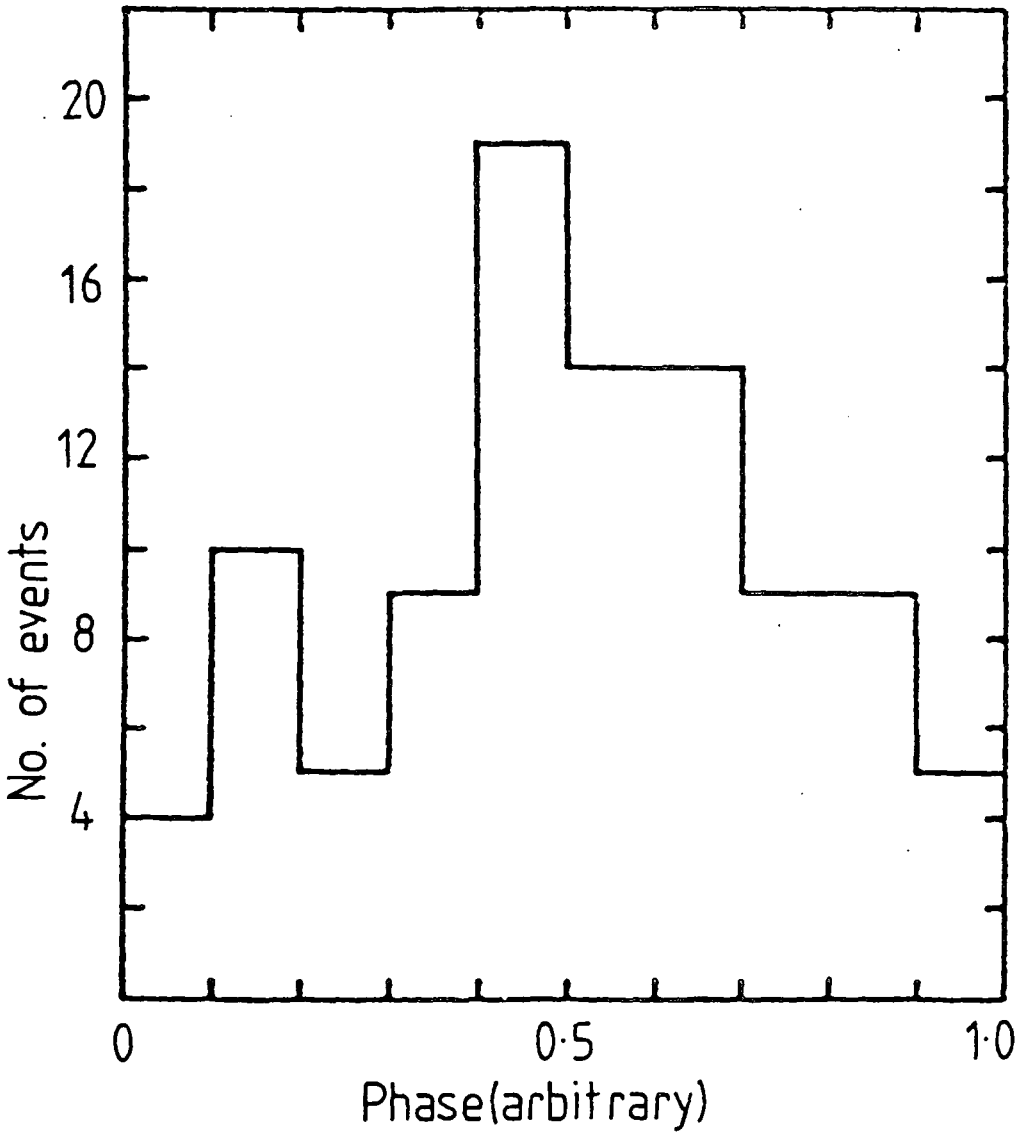

Figure 6.27: The 'light curve' of the burst events.

effect shows that the excess events were limited to a three minute section occurring ~ 5 minutes before the centre of the scan. In these three minutes the telescopes detected an excess of 33 +/- 10 % of the background.

The excess events were tested for periodicity at the X-ray pulsar period, ~ 1.237 s. The Rayleigh test, as outlined in section 5.3.5 was used. The 3 minute burst was effectively 100 % pulsed at this period, and corresponded to a probability of $4.0 \cdot 10^{-4}$ for the effect arising by chance. The profile of the burst is shown in fig.6.26i with the percentage of the periodic content in the data shown as fig.6.26ii for comparison.

Evidence for the X-ray period was found in the independent I and II-fold data. In addition, the 'fast inter-detector timing' technique was applied to the data and indicated that the pulsed events came from the centre of the field of view of the telescopes i.e. from Hercules X-1.

The 'light curve' for the pulsed events is shown in fig. 6.27. The light curve consists of a broad peak, ~ 30 % of the width of the full 'duty cycle'.

6.4.2: Analysis of the pulse amplitude values.

The strong 3 minute excess is a suitable subset of the data, rich in gamma-ray candidate events, for other analyses to be performed. The events can be investigated to determine if there are differences in the pulse amplitude values between the burst and the rest of the scan. A similar analysis to that used for Cygnus X-3 was performed. The 'OFF' source data from the 'drift scan' were used to establish the median of the background pulse amplitude distribution. The burst events can be split about this background median into the number below (N_-) and above (N_+) this value. The results are presented in Table

Detector	Background median		Median test probability
	N+	N_	
1	19	11	0·19
2	13	11	0·8
3	18	19	0·72
4	4	2	0·6

Table 6.5: The results of the pulse amplitude analysis of the burst events.

6.5.

The significance levels in Table 6.5 were calculated using the Median Test as outlined in section 5.5.3.

The overall probability for a difference in the pulse amplitude values for all detectors was calculated by combining those from the four detectors using equation 6.5, and results in an overall value of ~ 0.7.

So there is no evidence for significantly different signature to the burst events.

6.4.3: Further observations of Hercules X-1.

This object was observed in subsequent months, July and October 1983. These were tracking observations, and the data were combined for each month independently and analysed in a search for pulsed content at the pulsar period. The Rayleigh test was used as it is powerful in detecting broad light curve periodicity. There was evidence of a low level of pulsed emission in the data taken between July the 3rd and 13th 1983 at the ~ 2 σ level. The period detected was in agreement with the roughly contemporary Tenma X-ray satellite detection of 1.2377873 s (Nagase et al, 1983).

This low level of detection corresponds to 0.84 +/- 0.4 % of the cosmic ray background, and so the time averaged flux from the object may be calculated as (3 +/-1.5) . 10^{-11} cm^{-2} s^{-1} assuming the array operated at energies > 1000 GeV.

The 3 minute burst of 33 +/- 10 % of the background indicates that the peak flux from Hercules X-1 is ~ 1.2 . 10^{-7} cm^{-2} s^{-1}.

It is important to note that the V.H.E. burst occurred at phase = 0.76 in the 1.7 day orbit i.e. at one of the favoured phases (0.2 and 0.7) for the X-ray 'turn on'. This result will be discussed in detail in section 7.5.

6.5: 4U0115+63

The binary X-ray pulsar, 4U0115 + 63 is a sporadic X-ray source with the most recently derived Ariel VI orbital and pulsar parameters listed in Table 6.6.

6.5.1: Gamma ray observations.

The Dugway array observed this object in 1984 (see section 4.4.4). Each individual observation lasted about three hours and occurred at roughly the same sidereal time. These regular observations introduce a 'pseudo-periodicity' in the data of ~ 24 hours and associated harmonics, and so the data are not completely random. Care must be taken to ensure that such periodicity is not confused with any periodic effect from the object. The 'sidebands' due to the regular observations are shown in fig.6.28.i , from the data taken pointing at 4U0115+63. They are also evident in data from PSR2223 (see fig.6.28.ii), which was observed for the same nights as 4U0115+63, and which provides a useful set of background data. These plots indicate that the 'sidebands' are not significant for frequencies $>> 10^{-4}$ Hz, and should not produce any spurious periodicity in the range of the X-ray pulsations (~ 3.6s). Further details of the observations of this object are presented elsewhere (Chadwick et al, 1985c)

6.5.2: Periodicity analysis.

The data were barycentred, and focussed to the binary orbit using the parameters listed in Table 6.6. The quoted errors in the X-ray ephemeris necessitate a period search about the 3.614664 s period. In particular the period derivative of the pulsar is large and has varied

Characteristics of the 4U0115+63 system	
Pulsar period	3·614664 ± 0·0000011 s
Period derivative	$-0{\cdot}000272 \pm 0{\cdot}000007\ yr^{-1}$
Epoch of orbit	MJD 44586·008
Periastron angle	47·08 ± 0·20 deg
A. sin i	140·130 ls
Orbital period	24·3154 ± 0·0004 days
Eccentricity	0·3402 ± 0·0004

Table 6.6: The orbital and pulsar parameters of the 4U0115 + 63 system (Ariel VI)

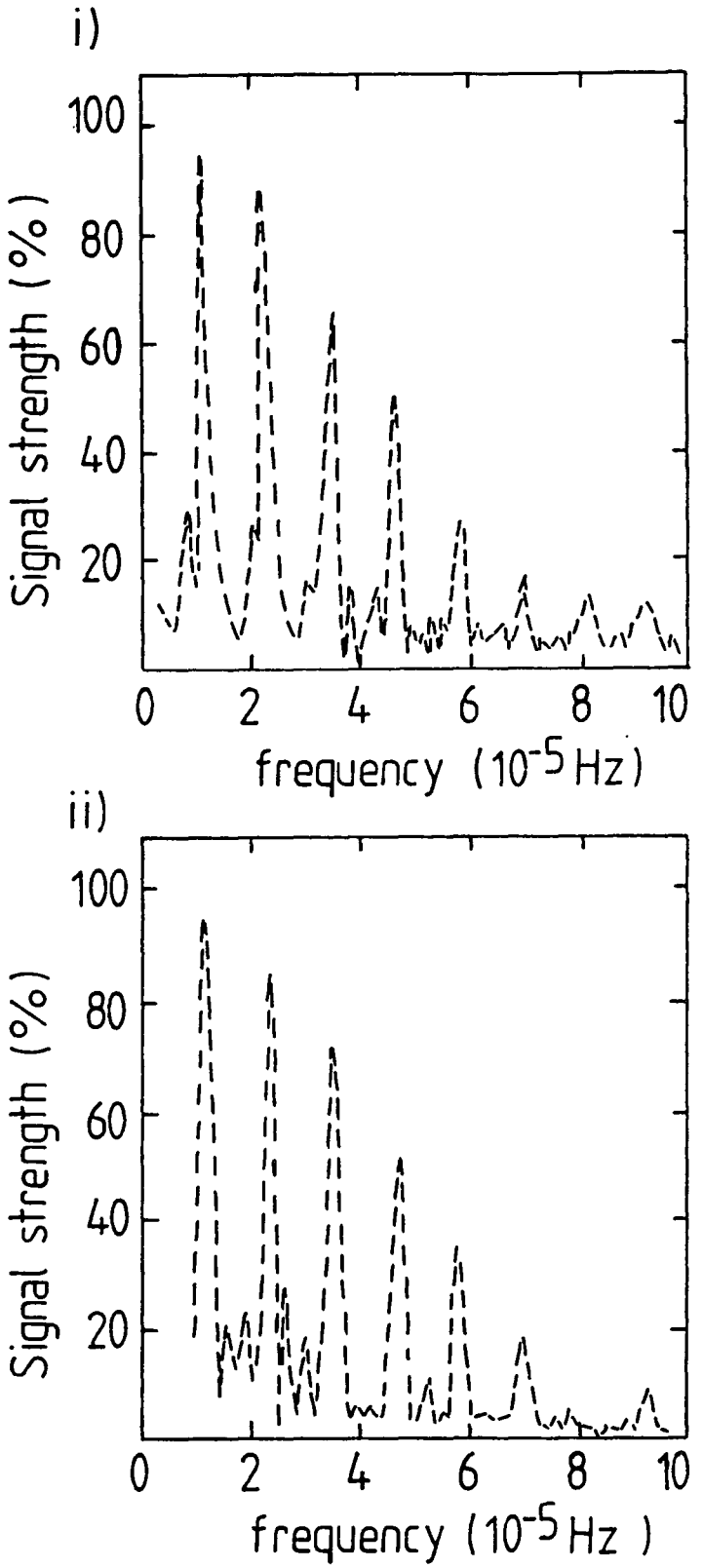

Figure 6.28: The 'Sidebands' introduced by regular observations of an object (i - 4U0115+63, ii - PSR2223).

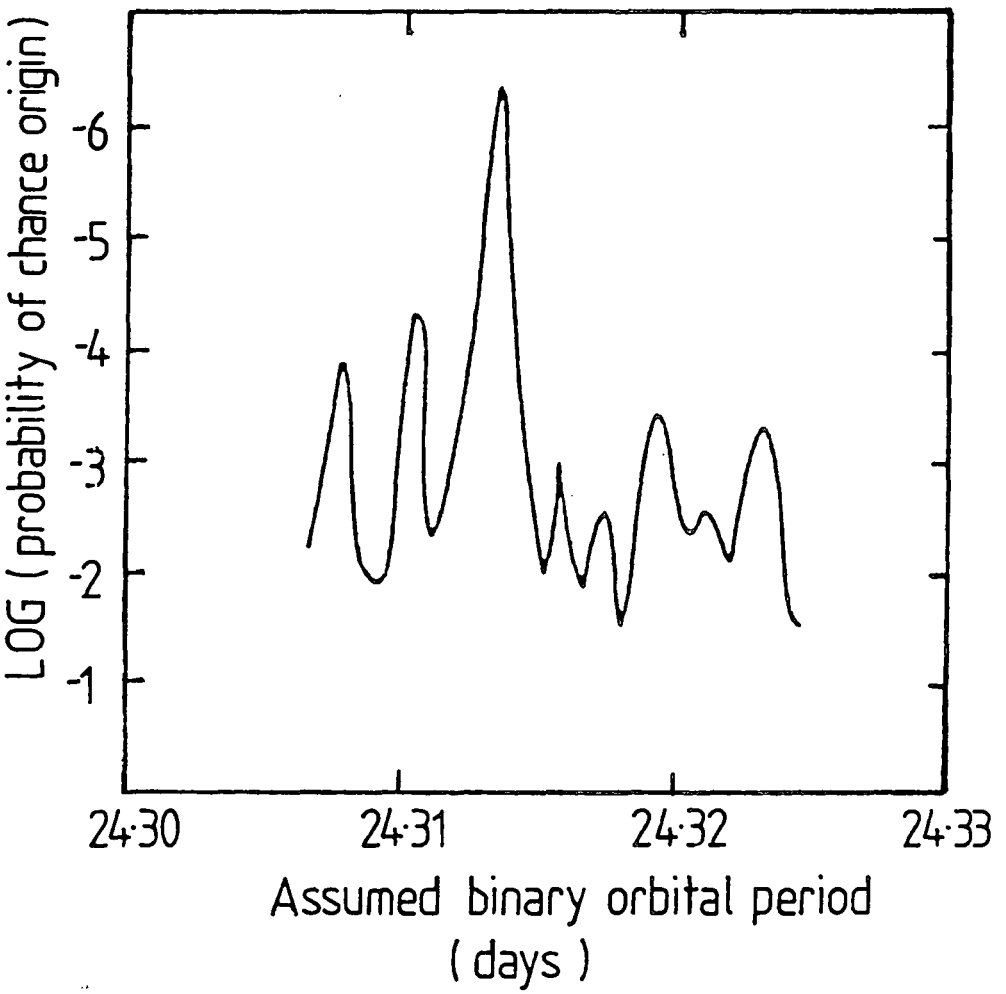

Figure 6.29: The variation of chance probability of periodicity with orbital period.

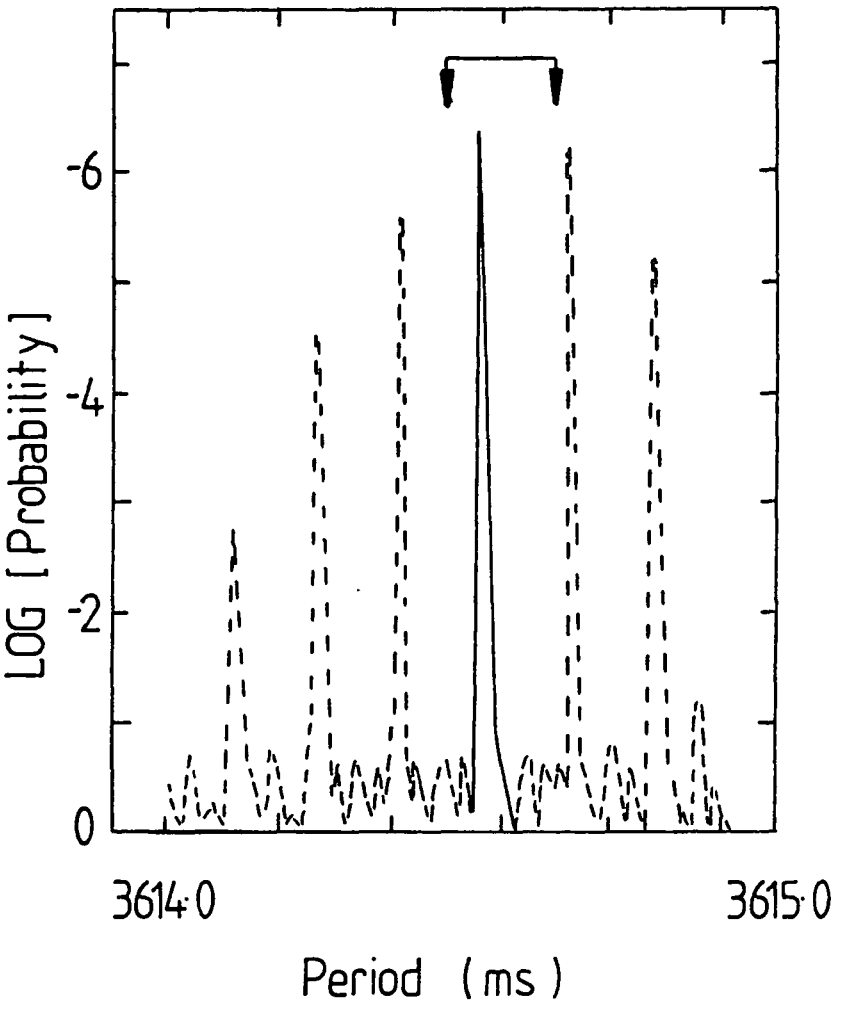

Figure 6.30: The chance probability of periodicity for data focussed using an orbital period = 24.135 days.

considerably in the X-ray observations (see fig.1.3). The search was confined to 10 independant periods about the ephemeris value with the Rayleigh test applied to the whole dataset. Data from the 9 nights of observation were combined in phase and the test applied.

The analysis of single telescope responses for all detectors, gives a best probability of no periodicity = $1.0 \cdot 10^{-2}$ at a period 3.61457 +/- 0.00001 s.

As the orbital parameters are uncertain, the variation of this pulsar period with orbital period may be investigated. If the mean values of all other parameters are chosen then the probability of the chance origin of the pulsar periodicity (3.61457 s) varies with orbital period as shown in fig. 6.29. It is clear that if the orbital period is relaxed to the next sampling peak (24.135 days) in the variation then the significance of the V.H.E. gamma-ray periodicity is increased to $\sim 5.0 \cdot 10^{-7}$.

Some account of the 'degrees of freedom' expended in this analysis must now be made.

i. The 10 independent periods tested reduce the significance to $5.0 \cdot 10^{-6}$

ii. Relaxing the orbit to the adjacent sampling peak is justified if 2 more degrees of freedom are introduced. So the overall significance of this result is = $1.0 \cdot 10^{-5}$

A plot of the probablity of no periodicity against period tested with the data focussed using an orbital period of 24.135 days is given as fig.6.30. The 'sidebands' are due to combination of the two periods in the data ($\sim$ 24 hours and $\sim$ 3.614 s).

The relaxation of the orbital period to a value removed five formal standard deviations from the X-ray ephemeris value is allowed as the uncertain orbit is multi-dimensional. The validity of this analysis has been checked by simulations of the focussing routine (M^{c}Comb, private communication).

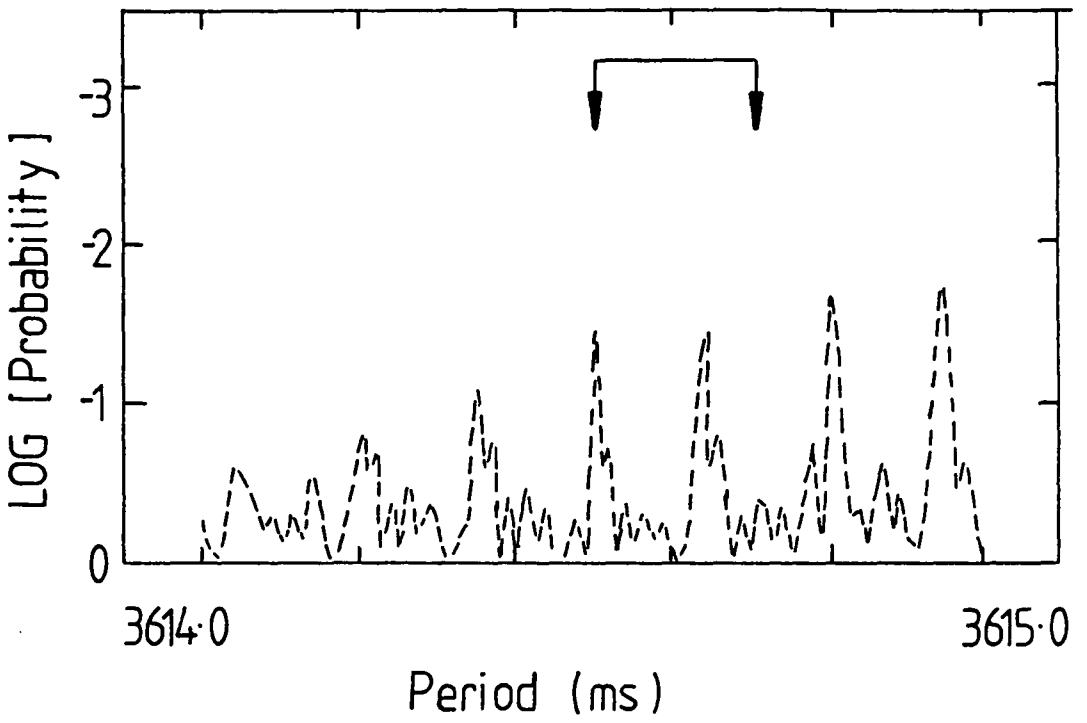

Figure 6.31: The chance probability of periodicity in data taken from PSR2223 analysed at 3.61 s.

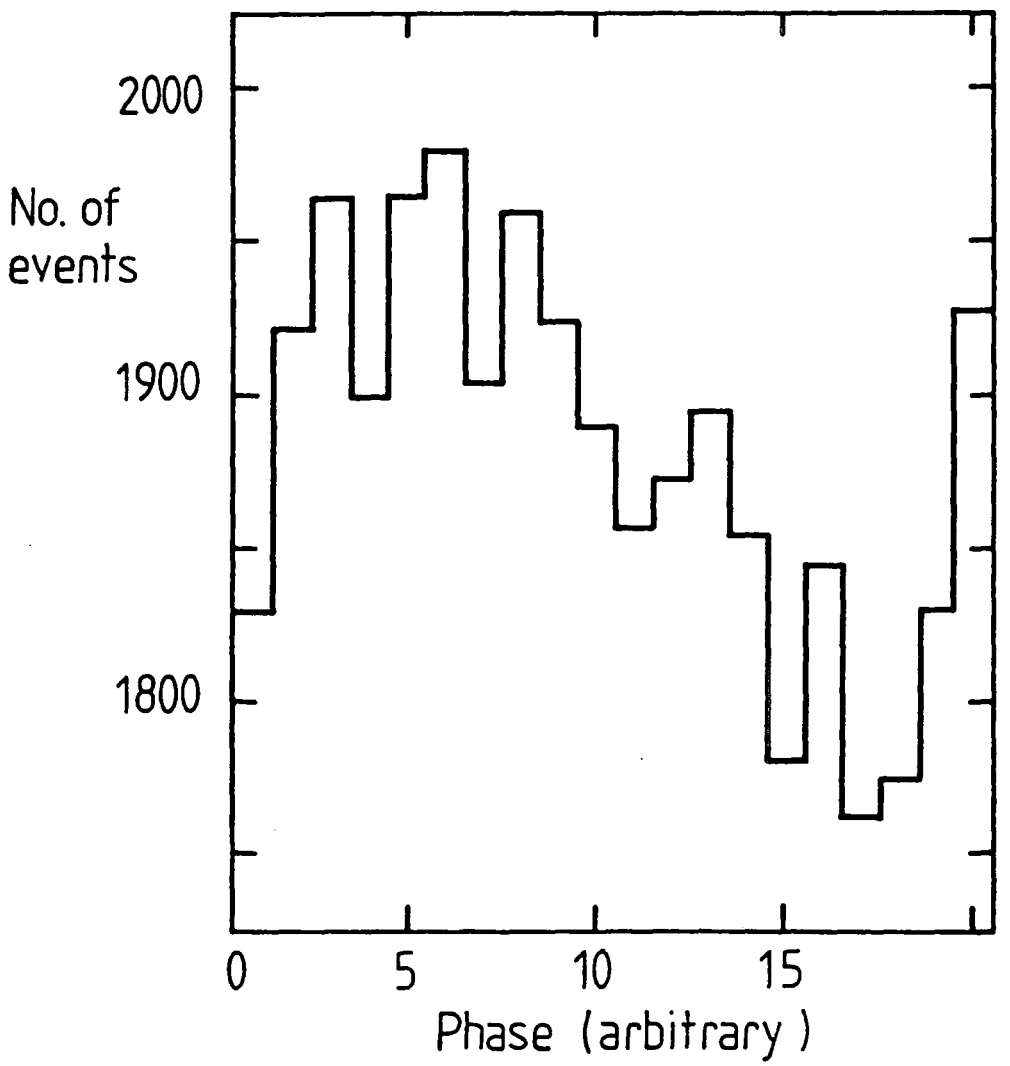

Figure 6.32: The V.H.E. gamma-ray 'light curve' for 4U0115 + 63.

As a check for any instrumental origin to the above periodicity, the data taken with the telescopes pointing at PSR2223 were analysed using the same procedure as that outlined above. The results are presented as fig.6.31 and show no significant detection of periodicity.

The 'light curve' of the V.H.E. gamma-ray pulse is given in fig.6.32. It shows that the detected emission has a broad light curve. It is therefore similar, in this respect to the pulsed emission from Cygnus X-3 and Hercules X-1, and unlike the narrow light curve detected from the Crab Pulsar (see section 6.6). The similarity in the pulsar emission from the binary X-ray sources may point to a common production mechanism (see section 7.6).

The data were analysed for evidence of variability over the nine days of the observation. The results indicate that there was no significant variabilty in the gamma-ray flux. As there were no sections of the data especially rich in gamma-ray candidate events (in contrast to the events detected over the 0.63 phase region of the Cygnus X-3 orbit), no analysis of the pulse amplitude values for the supposed gamma-ray events has been made. Any future investigation of the pulse amplitude values may proceed in a similar way to the analysis performed for the Crab pulsar (section 6.6.4). The pulsed events, say phases 0 - 0.3 in the 'light curve' may be compared with an assumed background, the events corresponding to phases 0.5 - 1.0.

6.5.3:The V.H.E. gamma-ray flux from 4U0115+63

The detection of pulsed V.H.E. emission from 4U0115 + 63 is highly significant and corresponds to an excess of (2.0 +/- 0.4) % of the proton background. The V.H.E. gamma-ray flux may then be calculated as,

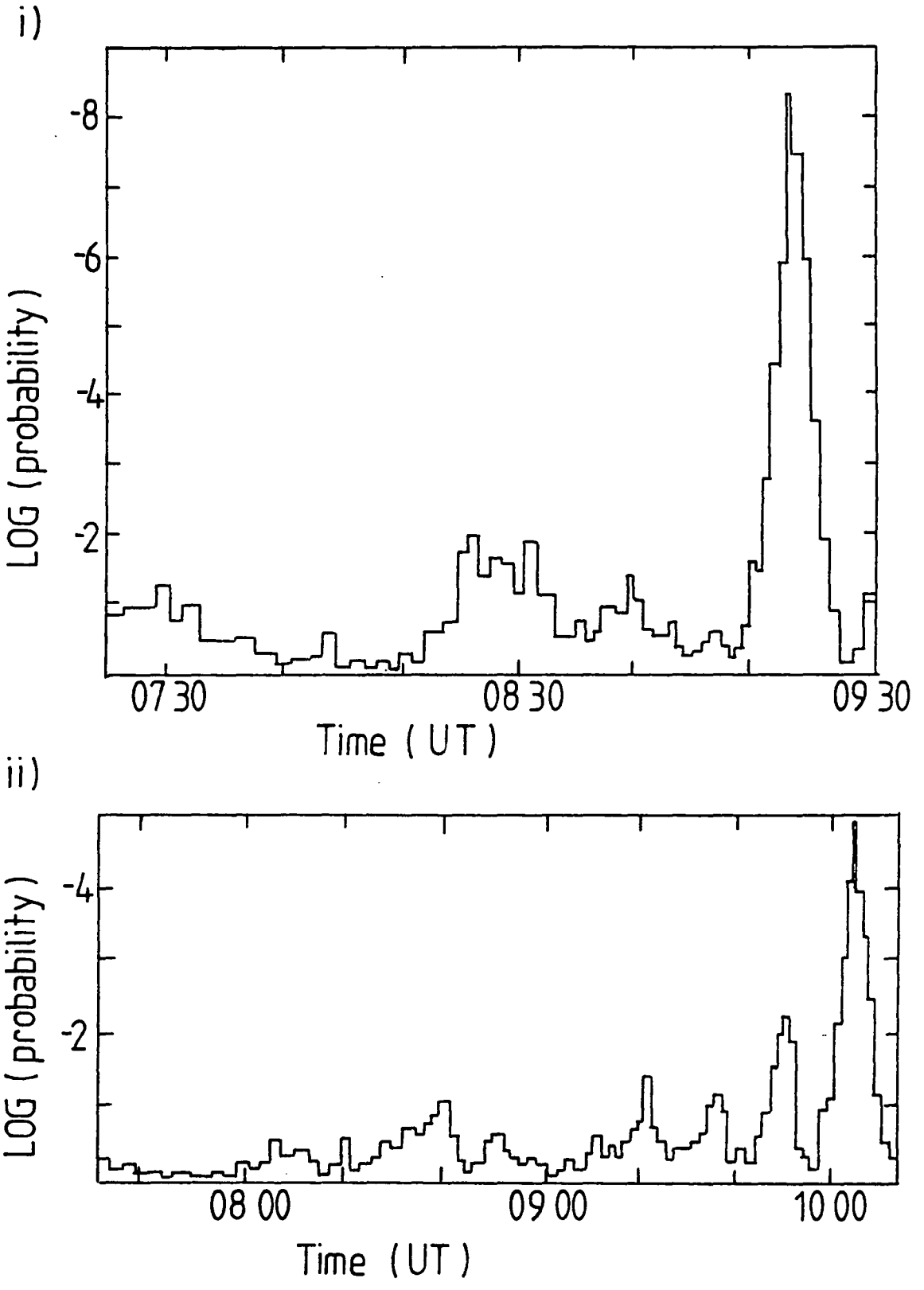

Figure 6.33: The transient periodicity detected from the Crab pulsar in 1981. i - 23/10/81, ii - 31/10/81.

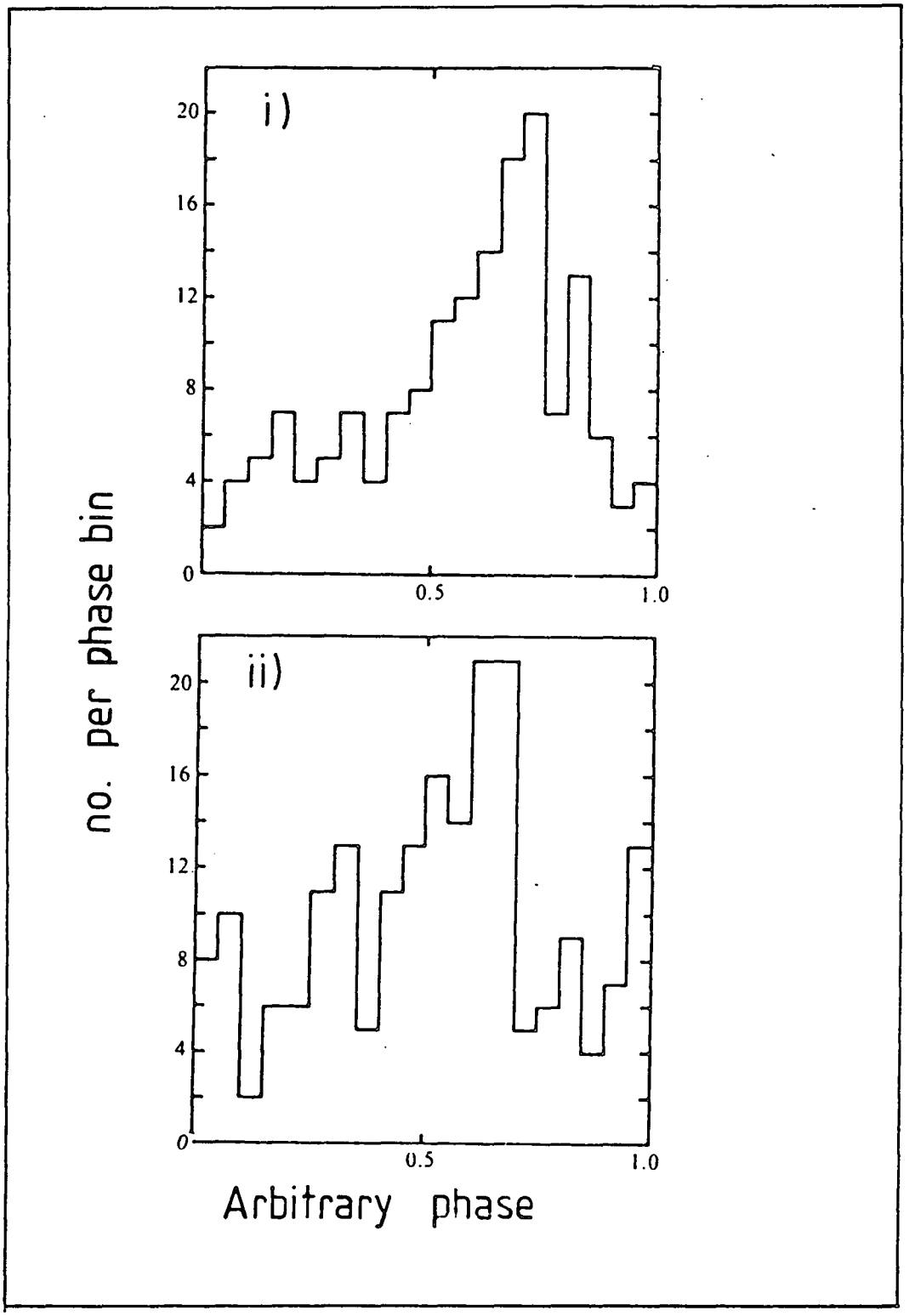

Figure 6.34: The 'light curves' of the 1981 transient bursts from the Crab pulsar. i - 23/10/81, ii - 31/10/81.

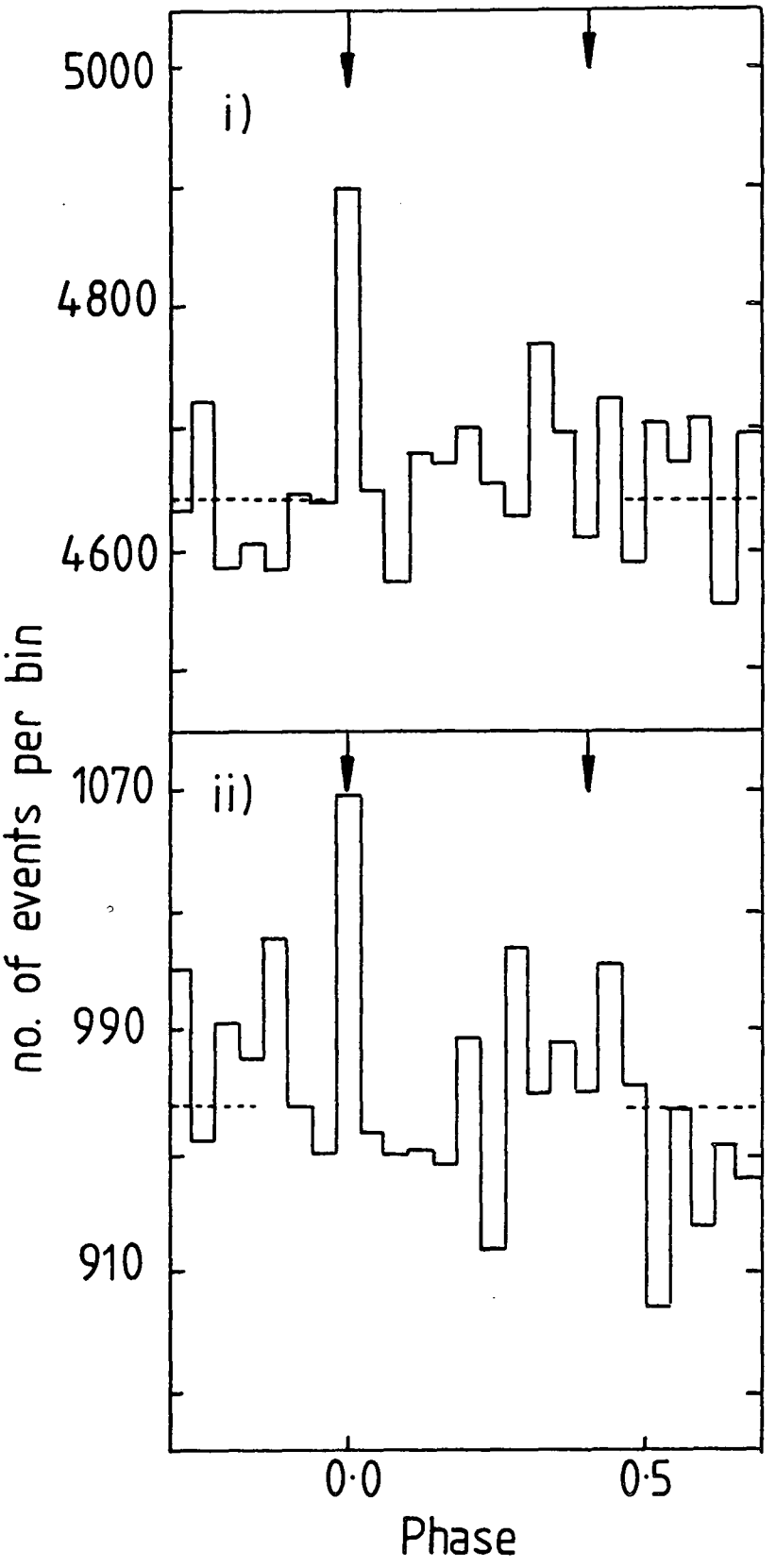

Figure 6.35: The 'light curves' for the continuous emission from the Crab pulsar detected in 1982 (i - I-fold, ii - II-fold datasets).

$(7 +/- 1.4)\ 10^{-11}\ cm^{-2}\ s^{-1}$.

A full discussion of these results is given in the next chapter.

6.6: The Crab Pulsar.

6.6.1:A summary of previous analyses.

The results of observations of this object made in 1981 and 1982 have been reported in detail elsewhere (Kirkman, 1985), and a brief summary is given below.

Strong transient effects were found in the 1981 data (Gibson et al, 1982a), strongly pulsed at the radio period of ~ 33 ms. Two such bursts were detected, on the 23rd and 31st of October; a plot of the profile of these bursts with time is given as fig.6.33. The 'light curves' for these two bursts are shown in fig.6.34, and indicate that the pulsed events were confined to a single peak of F.W.H.M. ~ 6 ms. Unfortunately, the radio ephemeris that was available did not allow a more accurate determination of the phase of the pulsed events to be found.

In 1982 an accurate, contemporary ephemeris was made available from radio measurements of the pulsations made at Jodrell Bank (Lyne, private communication) - see Table 5.1. In addition, the large amount of data collected in November 1982 were taken with very accurate relative timing due to careful monitoring of the crystal clock time. The clock was not reset for the duration of the observation, allowing a timing resolution of ~ 1 μs to be achieved (see section 3.5.1). When the November 1982 data were analysed strong evidence for a persistent but low level periodicity was found (see fig.6.35). An 'Epoch folding' technique was used. There is strong evidence for gamma-ray emission with a narrow V.H.E. mainpulse, coincident with the radio mainpulse (Dowthwaite et al, 1984b). In addition, there is an

interpulse in the phase region 0.33 to 0.47 in the ~ 33ms 'light curve', and some indication of a bridging region of pulsed emission between the main and inter-pulses.

The accurate timing allows the events comprising the mainpulse to be resolved further. This analysis indicates that the mainpulse emission is limited to a duration of ~ 0.4 ms, between phases 0.98 and 0.992 in the 'light curve'. The V.H.E. pulsations are therefore narrower than those at other frequencies, and this result will be discussed in relation to possible models for the emission in section 7.3.2.

An increase in the sensitivity of the array was noted for events detected by two telescopes. This II-fold detection of periodicity, independent of the I-fold detector responses discussed above, leads to an overall probability that the pulsations arise by chance of ~ 10^{-5}. In addition, fast inter-detector timing indicated that the pulsed events came from near the centre of the field of view adding further evidence (at a chance probability of ~ 3.5 10^{-3}) of pulsar periodicity.

In conclusion, the Dugway experiment has detected strong transient emission and weak continuous pulsed emission from the Crab Pulsar.

6.6.2: The 1983 observations of the Crab Pulsar.

Observations of the Crab Pulsar were conducted in the latter part of 1983 (section 4.4.2), with an improved Mark II version of detector 4. An accurate radio ephemeris was available in 1983, but unfortunately the relative timing accuracy of the system did not match that achieved in November 1982.

The 'Epoch folding' technique was used to analyse the data in the same way as for the 1982 observations. The results are presented as fig.6.36i and fig.6.36ii for the independent single and two-fold

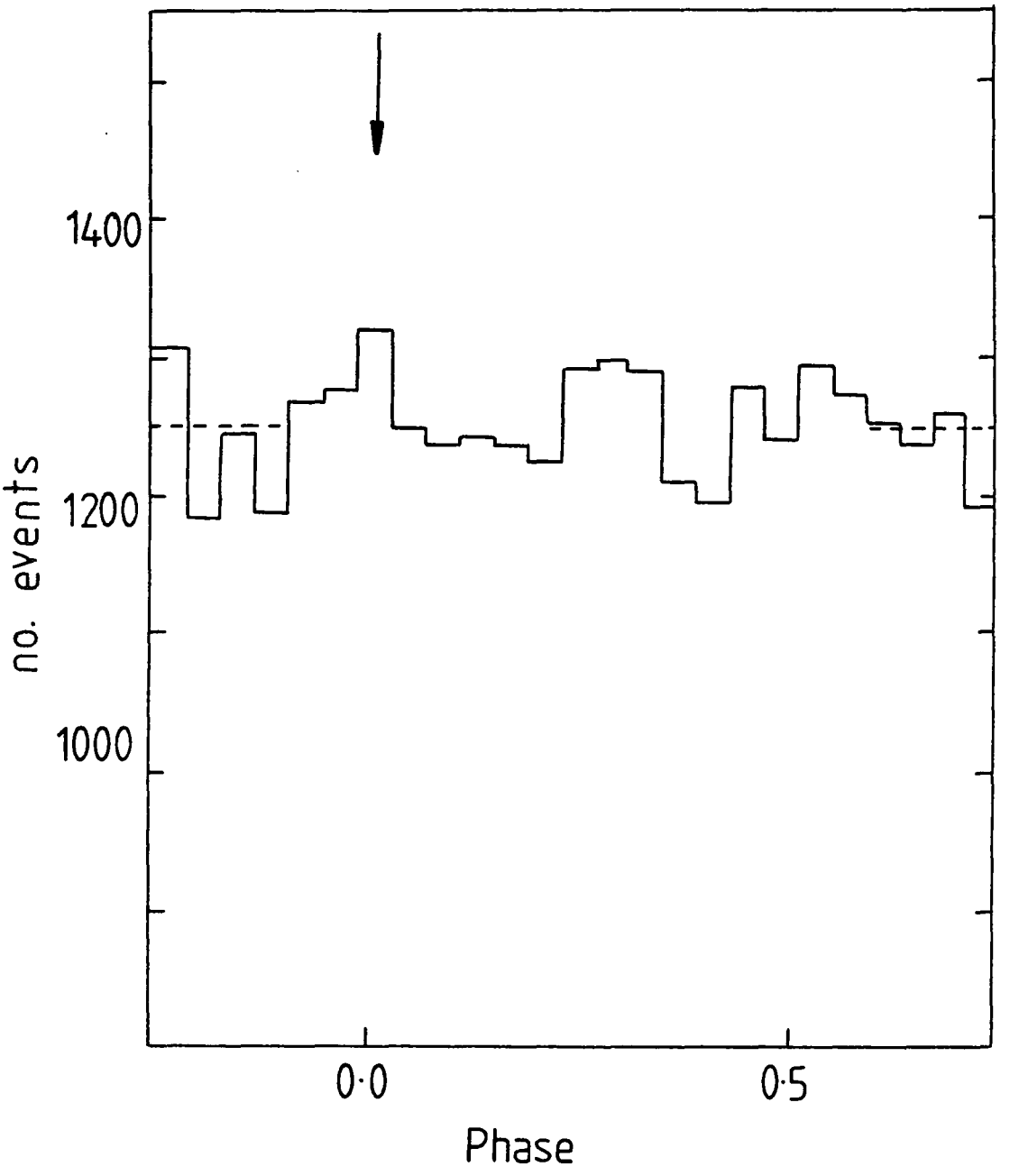

Figure 6.36: i, The 'light curve' for the continuous emission from the Crab pulsar detected in 1983 I-fold dataset.

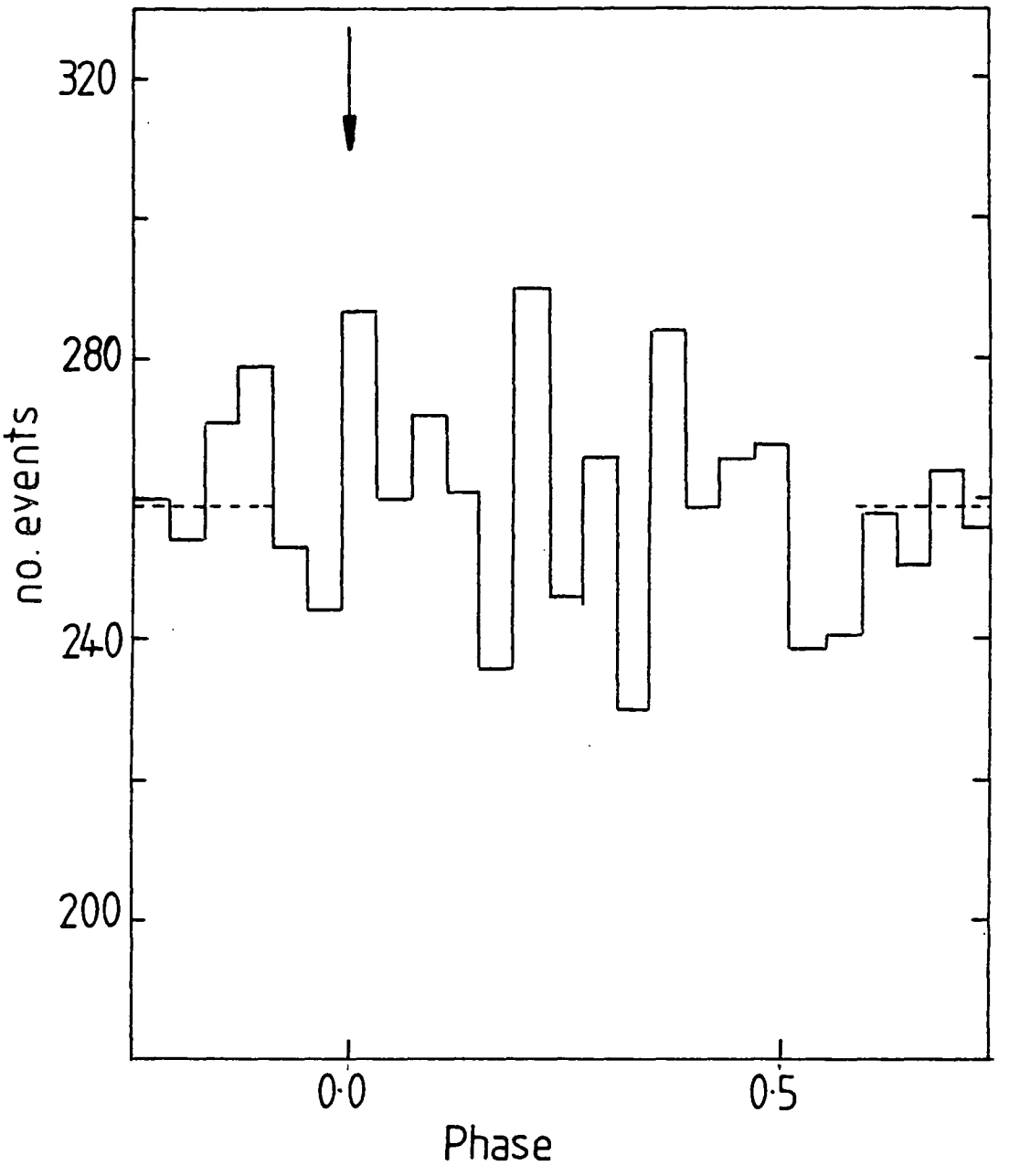

Figure 6.36: ii, The 'light curve' for the continuous emission from the Crab pulsar detected in 1983 II-fold dataset.

datasets respectively. There is clear confirmation of emission at the radio mainpulse in the data from single telescope responses, but there is no indication of the interpulse or bridging region apparent in the November 1982 results. The single fold results correspond to a detection of periodicity at a chance probability of $\sim 1.5 \cdot 10^{-3}$.

There is no evidence of pulsed emission from the II-fold dataset, although with few events to analyse this is not surprising.

The timing of the system was not as accurate in 1983 as in November 1982 and so, the mainpulse events cannot be resolved beyond the $\sim$ 1.3 ms bin width given in fig.6.36i . However the single bin mainpulse does indicate that the V.H.E. gamma-ray pulsations have a narrow 'light curve'.

In summary, the limited observations conducted in 1983 confirm the 1982 results.

6.6.3: Transient pulsed emission from the Crab Pulsar.

The data collected in 1982 and 1983 have been searched for further evidence of bursts of V.H.E. gamma-rays - similar to the large effects discovered in the October 1981 data. The data were searched in two ways;

i: Sections of data (200 events per section), were analysed for periodicity using the Rayleigh test. The results are presented elsewhere (Kirkman, 1985).

ii: The data were separated into 5, 10 and 15 minute independent sections, and then analysed for periodic content. Sections of the order of 10 minutes were chosen to match the length of the bursts seen in 1981.

Two tests for periodicity were made. The V-test (see section 5.4.1) was used to search for pulsed emission with a broad, light curve (similar to the bursts detected in 1981). In addition, the data were

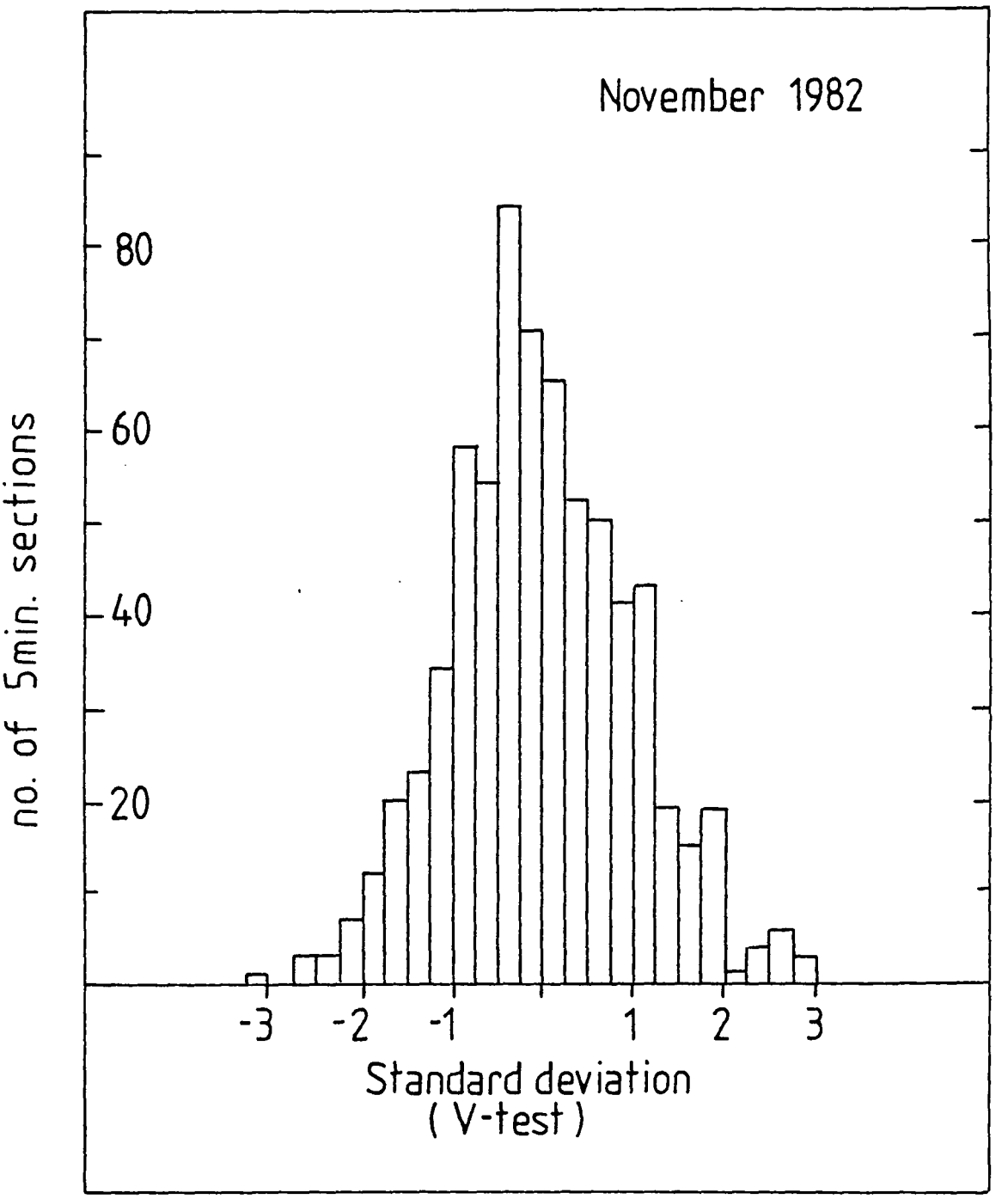

Figure 6.37: The distribution of the V-test statistic for the November 1982 data analysed in a search for 5 minute transient emission.

Dataset	Bin size /min	x^2 probability
I-fold	5	0·97
	10	0·75
	15	0·92
II-fold	5	0·58
	10	0·73
	15	0·32

Table 6.7: The results of the V-test search for transient emission from the Crab pulsar.

Dataset	Bin size (minutes)	Binomial probability			
		>0·1	>0·01	>0·001	>0·0001
I-fold (1982+83)	5	1106	87	7	-
	10	545	50	4	-
	15	373	49	1	-
II-fold (1983)	5	140	18	2	-
	10	151	13	1	1
	15	97	11	-	-

Table 6.8: The results of the Binomial test for transient emission from the Crab pulsar.

tested for periodic bursts with narrow peaked light curves by comparing events coincident with the radio mainpulse to those at other phases using a binomial test. For this analysis the mainpulse was chosen as the 0.0 to 0.04 phase region of the light curve.

This analysis showed that there were no further bursts of periodic events of the same strength as those detected in October 1981. This is in agreement with the results of search i, above.

It is also possible to investigate the number of smaller bursts detected, above expectation.

A plot of the distribution of the probabilities resulting from a V-test on 5 minute sections of the I-fold data is given as fig. 6.37. The deviation of these distributions from the normal curve is an indication of the degree to which the periodic effect is due to small bursts rather than a continuous low level emission. A suitable measure of the deviation is given by a Chi-squared statistic. The results are presented in table 6.7, for each of the 5, 10 and 15 minute sections.

These results show that there is no evidence to indicate that the V.H.E. pulsations from the Crab pulsar observed in 1982 and 1983 are due to transient effects of low strength.

The distributions of the probabilities resulting from binomial tests are also close to expectation for the 5, 10 and 15 minute sections (see table 6.8). It is therefore possible to rule out single bin (narrow peaked) bursts from the pulsar.

The emission in 1982 and 1983 has been shown to be consistent with a continuous low strength flux rather than a series of periodic bursts.

Detector	Probability (Median test)
1	0·25
2	0·28
3	0·48
4	0·25

Overall probability = 0·3

Table 6.9: The results of the pulse amplitude analysis of the mainpulse events.

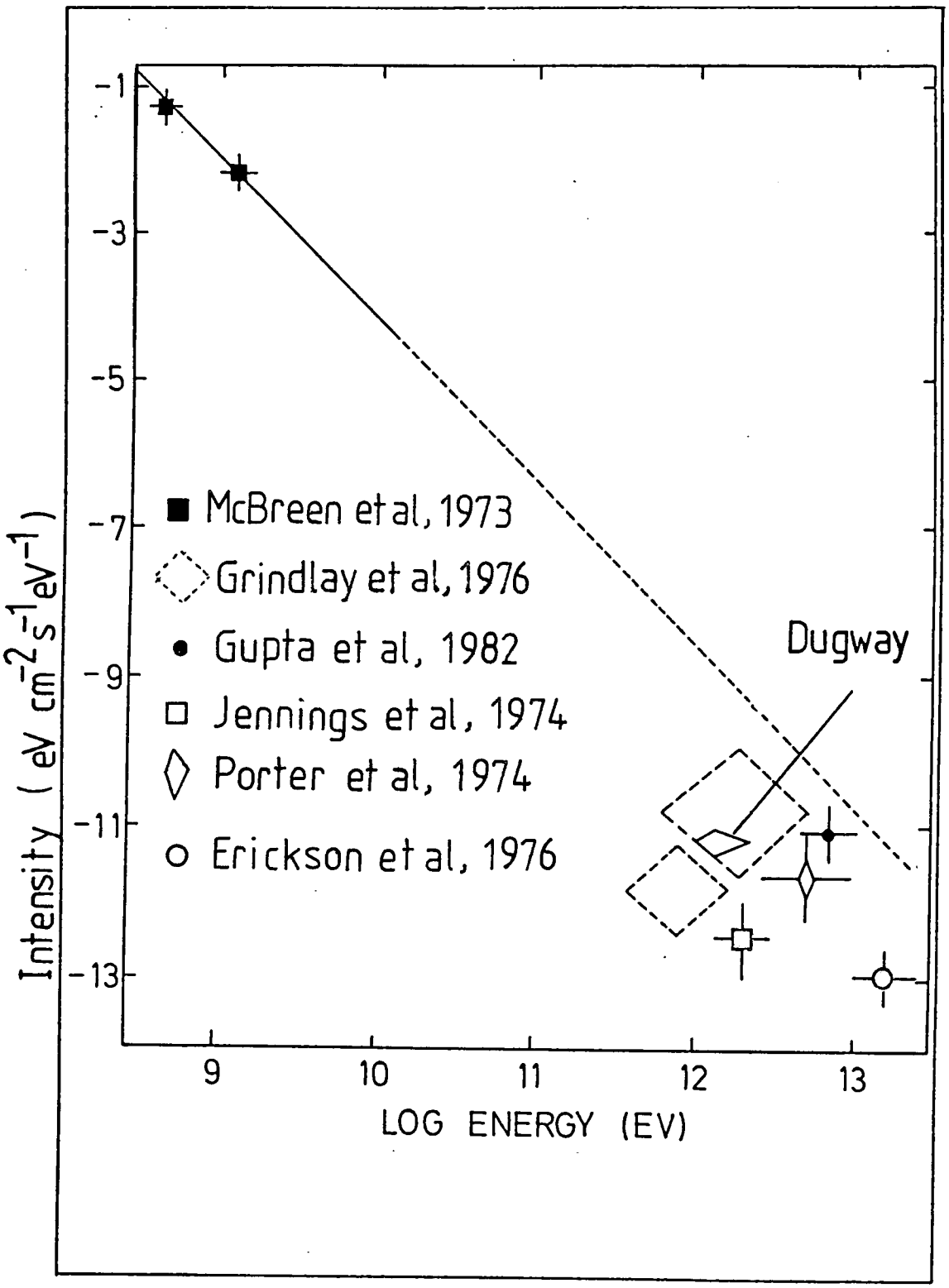

Figure 6.38: The V.H.E. gamma-ray spectrum from the Crab pulsar.

6.6.4: The analysis of the Pulse amplitude values.

The well defined excess of events detected at the radio mainpulse, means that an investigation of the pulse amplitude distribution of these events can be made. The events occurring in the mainpulse phase region (0.98 - 0.992) have been compared with the events at other phases (the assumed background for the 1982 data). The mainpulse events were dichotomized about the median pulse amplitude value calculated from the background as described in section 5.5.2.

Table 6.9 gives the results of this analysis. There is a small imbalance of the mainpulse events in favour of the larger pulse amplitudes and the significance of this effect has been evaluated using the Median test (see section 5.5.3).

There is an indication that the mainpulse events have larger pulse amplitudes than expected from the distribution of those corresponding to 'background' phases. The significance of the imbalance is given in table 6.9, and corresponds to an overall (all detectors) difference of $\sim$ 0.3 (the combined probability calculated using equation 6.5).

Although this result is of marginal significance, it is consistent with the strong two fold effect noted in these data. This would infer a relatively shallow spectral slope.

6.6.5: The V.H.E. gamma-ray spectrum.

A plot of the spectrum from this object in the 1 - 10^4 GeV region is given as fig.6.38. The points relating to the Dugway measurements are listed below.

The excess at the mainpulse in the November 1982 data corresponds to 0.233 +/- 0.054 % of the cosmic ray background and indicates a detection of a flux of V.H.E. gamma-rays = (7.9 +/- 1.8) 10^{-12} cm^{-2}

Table 6.10: The upper limits to 'broad' pulse emission from the radio pulsars observed by the Dugway array.

Pulsar	Period (ms)	Period derivative (10^{-15}ss^{-1})	Phase	Epoch	Flux limit (10^{-11}cm^{-2}s^{-1})
PSR0950	253·06503679	0·2321	0·132652	1501·00	4·1
PSR1929	226·51704512	1·1580	0·986992	1704·00	6·76
PSR1133	1187·91119970	3·7322	0·087832	1665·00	4·63
PSR2223	682·5333	9·5	-	3889·33	3·10
PSR0355	156·38021	4·39	-	1593·85	3·63
PSR1508	739·67789849	5·0389	-	0625·96	3·83
PSR1930	144·4278896	577·8	0·53914	2676·00	8·46

s^{-1} at Energies > 1000 GeV.

The flux for transient emission observed on the 23rd of October 1981 peaks at a value = (2.0 +/- 0.3). 10^{-10} cm^{-2} s^{-1} at energies > 3000 GeV.

The flux value for the continuous emission is in broad agreement with results from other groups working at these energies. The results have important implications for the high energy emission from pulsars and these will be discussed in section 7.3.

6.7:Other Radio Pulsars.

Seven suitable radio pulsars were observed by the Dugway experiment, the details of these observations are described in Table 4.2.

The data were barycentred and then tested for evidence of periodicity using the Rayleigh test. As in other analyses, the Rayleigh test was chosen as it is powerful in tests for periods of unknown 'duty cycle'. Two subsets of the data were investigated, the low energy, single telescope responses, and the higher energy, but possibly more sensitive (e.g. the Crab Pulsar results) two-fold responses.

The results of this analysis are given in table 6.10. No significant detection of periodicity is found from these objects, and upper limits to the V.H.E. gamma-ray flux for broad pulse emission have been calculated (- see section 5.7).

These upper limits are in good agreement with previously reported results at V.H.E. (Porter and Weekes, 1978), and will be discussed in the next chapter.

Object	Hrs. of data	Flux limit (10^{-12} cm^{-2}s^{-1})
Cyg X-1	4	500
3C273	13	500
NGC4151	3	300
SS433	3	300
CAS-A	3	600
PER X-1	2	300
2CG135	11	50

Table 6.11: Upper limits for gamma-ray emission.

6.8: Miscellaneous observations

The Dugway array of telescopes made limited drift scan observations of the following objects;

Cygnus X-1

Perseus X-1

3C273

NGC4151

SS433

Cassiopeia A

2CG135

A summary of the observations was given in table 4.2.

The 'drift scan' analysis procedure was applied to the data for each of these objects (section 5.2). There is no significant indication of V.H.E. gamma-ray emission, and 3 standard deviation upper limits to the V.H.E. gamma-ray flux have been derived (section 5.7). These are listed in table 6.11.

The calculated upper limits are in good agreement with values quoted by other experiments (Porter and Weekes, 1978).

Chapter 7: A discussion of the results.

7.1: Introduction

The detailed results of the programme of observations are reviewed and interpreted in this chapter with a discussion of the implications for the models proposed. A review of the proposed source mechanisms is given and a mention is made of the relationship between the production of V.H.E. gamma-rays and the other possible high energy emissions from these systems.

The most likely source of the high energy particles responsible for the V.H.E. gamma-ray emission is a system including a collapsed star, and the results place important constraints on the form of physical process working in these objects. A particular aim of the Dugway experiment was to determine the luminosity at these energies and so to establish whether a class of astronomical objects exists radiating predominantly in the V.H.E. region.

7.2: The production of V.H.E. and U.H.E. gamma-rays.

The prerequisites for V.H.E. gamma-ray production are higher energy particles interacting with electromagnetic fields and/or matter by the methods discussed in chapter 1. Astronomical V.H.E. gamma-ray production sites must provide these conditions.

The two most promising suggestions are radio and X-ray binary pulsars. In the former case models have been proposed in which particles are accelerated by the very large potential differences produced near a rapidly spinning magnetised neutron star, for instance, (Ruderman, 1981), (Arons, 1983).

For binary X-ray pulsars the process of accretion may play a part.

Acceleration mechanism	Maximum particle energy (eV)
Pulsar acceleration	$\sim 5.10^{16}$
Accretion disc	$\sim 10^{16}$
Shock acceleration	$10^{16} - 10^{17}$
Turbulent Magnetosphere	Depends on the r.m.s. turbulent velocity but could explain observations
Free pulsar (Crab)	$> 10^{15}$ possible

Table 7.1: The maximum particle energy produced by the various acceleration mechanisms proposed to power V.H.E. and U.H.E. gamma-ray sources.

Various methods have been suggested for transforming the gravitational potential energy of accretion into particles of high enough energies. These include the dynamo action of an associated magnetised neutron star (Chanmugam and Brecher, 1985), the Fermi acceleration in shocks developed in the accretion flow onto the neutron star (Kazanas and Ellison, 1986), and the acceleration of particles due to the distorted magnetic field produced during turbulent flow in the accretion process (Wang, 1986).

The nature of the accelerated particles is also uncertain. It is unlikely that electrons could be accelerated to ultra high energies in the intense magnetic and radiation fields surrounding pulsars, though they may be significant at lower gamma-ray energies (Protheroe, 1986). The energy loss mechanisms, i.e. synchrotron and inverse Compton losses are not so effective in the case of nucleons, so these particles will probably be involved in the production of U.H.E. gamma-rays. The particles must then interact to produce the gamma-ray spectrum.

In free pulsar systems such as the Crab pulsar the gamma-rays may be produced by curvature or synchrotron radiation. In binary systems the V.H.E. and U.H.E. particles may interact with target material to produce neutral mesons which then decay to give the gamma-rays.

In all of these cases the maximum possible energy of the particles has been calculated by Protheroe (1986), and these figures are reproduced in table 7.1, along with estimates of the highest energy particles that may be produced by free pulsars e.g. the Crab pulsar.

Details of all the main models are discussed in relation to the individual objects observed by the Dugway array. The discussion will emphasise the interpretation of the Dugway results presented in chapter 6.

7.3: V.H.E. gamma rays from radio pulsars

There have been few reports of gamma ray emission from the large number of radio pulsars so far discovered. In spite of this these stars are capable of producing very large amounts of energy as can be seen from their rotational energy loss;

$$W = I. P. P' \qquad - 7.1$$

for a typical moment of inertia, $I = 10^{45}$ gcm^2, and for a one second period pulsar which is slowing down in 10^6 years then the energy output is

$$\sim 10^{33} \text{ erg s}^{-1}$$

This large amount of energy shows that these stars are among the most energetic objects in the Galaxy. With relevance to this work, many of the models so far proposed indicate that a significant fraction of this luminosity may appear as gamma-rays.

The conventional view of a pulsar is of a rotating magnetised neutron star. Charged particles are 'lifted' from the surface of the star by strong electrostatic forces to create a 'magnetosphere', a corotating region of plasma. The tangential velocity of the particles increases with distance from the surface, until at the 'light cylinder' the corotation is at the speed of light.

Goldreich and Julien (1969) showed that the rotating magnet would act as a 'homopolar generator' with large potential drops ($\sim 10^{16}$ eV) being developed. Positive and negative charge would then be released from the stars crust and would travel out from the polar surface via open field lines - see fig 7.1. These charges may reach energies in excess of 10^{12} eV, and could account in principle for the radiation at various frequencies.

It is also possible to estimate the energy loss from a non-aligned rotating magnetic dipole (this calculation is performed for the

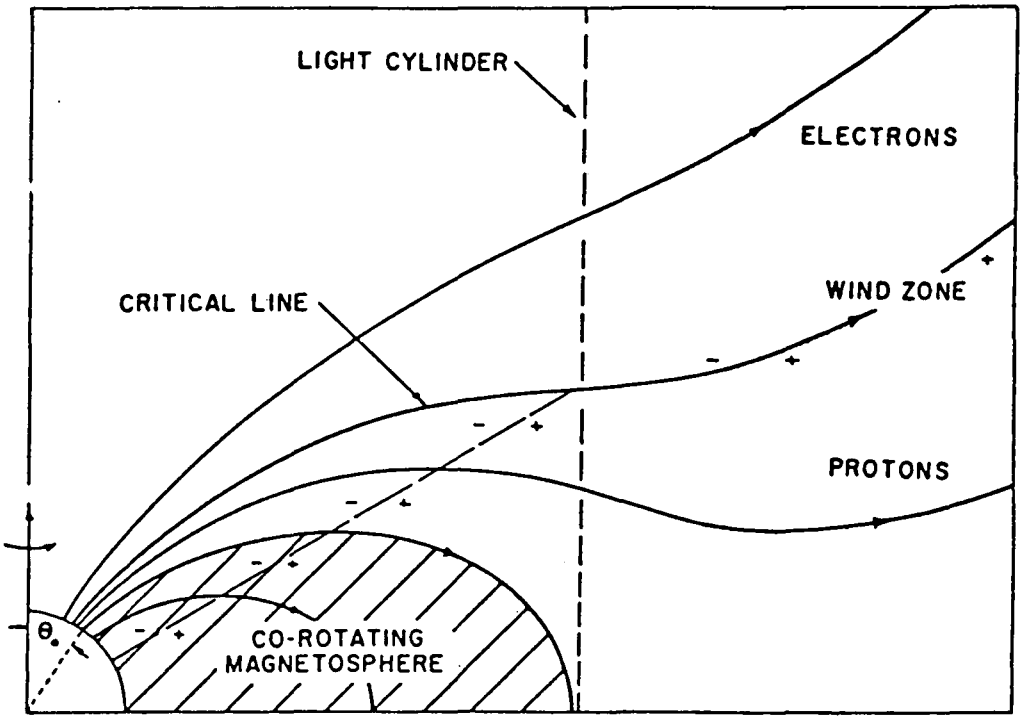

Figure 7.1: The 'Goldreich and Julien' model of a pulsar.

unrealistic case where the dipole is surrounded by a vacuum). If Φ is the angle between the magnetic moment vector M, and the rotation axis, z then,

$$\frac{d^2M}{dt^2} = \frac{B \cdot a^3}{2} \cdot \sin \Phi \cdot w^2 \qquad - 7.2$$

where, w is the angular frequency of the rotation and B is the magnetic field strength at the pole, a, is the radius system. In this case, the energy radiated by a time-varying dipole is given by,

$$\frac{dE}{dt} = \frac{B^2 \cdot a^6}{6c^3} \cdot \sin^2 \Phi \cdot w^4 \qquad - 7.3$$

If reasonable values are chosen for $B = 10^{12}$ G, $\Phi = \pi/4$ and a = 10km, then the following energy losses are possible,

Pulsar (Period = 1s) $\sim 10^{32}$ ergs^{-1}

The Crab pulsar $\sim 10^{38}$ ergs^{-1}

Pulsar (Period = 10ms) $\sim 10^{38}$ ergs^{-1}

A different scheme for the particle accelerator was described by Gunn and Ostriker (1969). Here the energy loss from a rotating dipole was considered. The charges are accelerated to V.H.E. energies by the outgoing low frequency radiation if they are released at the 'wave zone'.

There is as yet no fully satisfactory model to explain the pulsed emission from these objects, but the two most promising models are discussed in relation to the Durham V.H.E. results in the next section.

7.3.1: The V.H.E. emission from the Crab pulsar

The Durham experiment observed a burst of V.H.E. emission from the Crab Pulsar in 1981 (Gibson et al, 1982a). The burst had a broad light curve and corresponded to a peak luminosity of $(1.6 +/- 0.4) \cdot 10^{36}$ ergs^{-1} at energies > 2400 GeV , assuming a integral gamma ray spectral

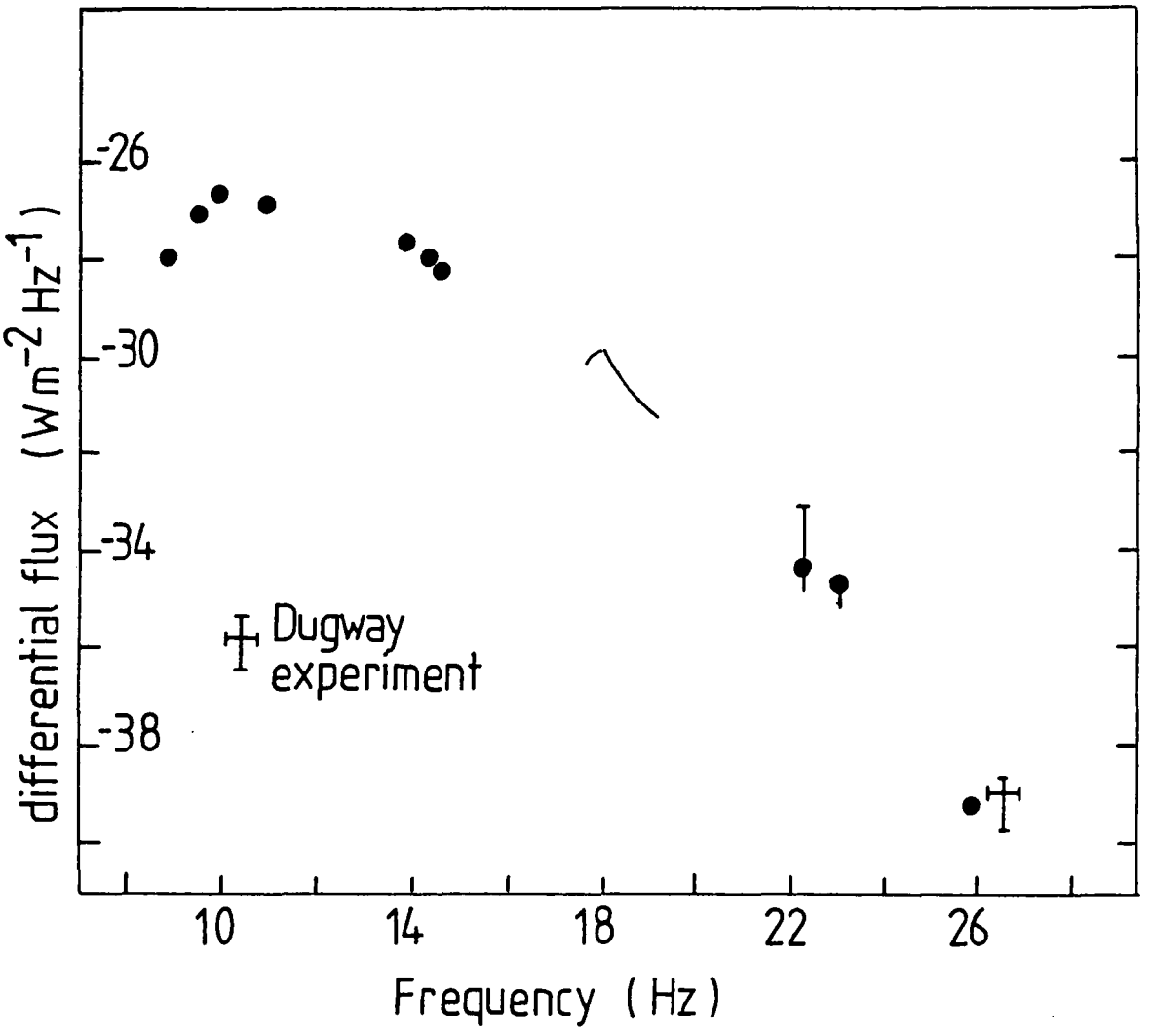

Figure 7.2: The spectrum of the Crab pulsar and it's nebula from radio to gamma-ray energies.

index of -1.4 and a distance to the pulsar of 2 kpc. Only two such bursts have been seen in three observing periods, both in 1981.

There is also strong evidence for a lower level continuous emission characterised by a narrow peaked light curve (~ 0.4 ms). The emission is coincident with the main pulse detected at other wavelengths (fig 1.4 shows a plot of the 'light curve' for this object from radio to V.H.E.). In addition there is an indication of an interpulse emission - see section 6.6.1. The time averaged luminosity of the V.H.E. gamma-rays is calculated as,

$$\sim 2.0\ 10^{34}\ \text{ergs}^{-1} \text{ at energies } > 1000 \text{ GeV.}$$

The spectrum of the Crab pulsar shows signs of flattening in the V.H.E. energy region. The evidence from the pulse amplitude measures, though of very low significance also points to a flattening.

The Durham results are in general agreement with other groups working at these energies (e.g. Porter and Weekes, 1978 , Grindlay et al, 1976) but indicate that the mainpulse emission is considerably narrower than that at lower energies (Dowthwaite et al, 1984b). This observation confirms an earlier prediction for the width of the mainpulse (McBreen et al, 1973).

7.3.2: Implications for the models proposed for the Crab pulsar

The two radio pulsars detected at V.H.E. energies (i.e. the Crab and Vela pulsars) are relatively fast, young objects emitting most of their power in the X-ray or low energy gamma-ray region see fig 7.2. In the case of the Crab the luminosity at keV - MeV energies is $\sim 10^2$ times the V.H.E. value which is in turn $\sim 10^4$ times the radio luminosity. This fact has been noted (Grindlay, 1982) as implying that the attenuation of V.H.E. gamma-rays is > 99% near the pulsar. The mechanism responsible for the absorption is pair production in the magnetic field. This assumes that the 10^{12} eV or higher spectrum is

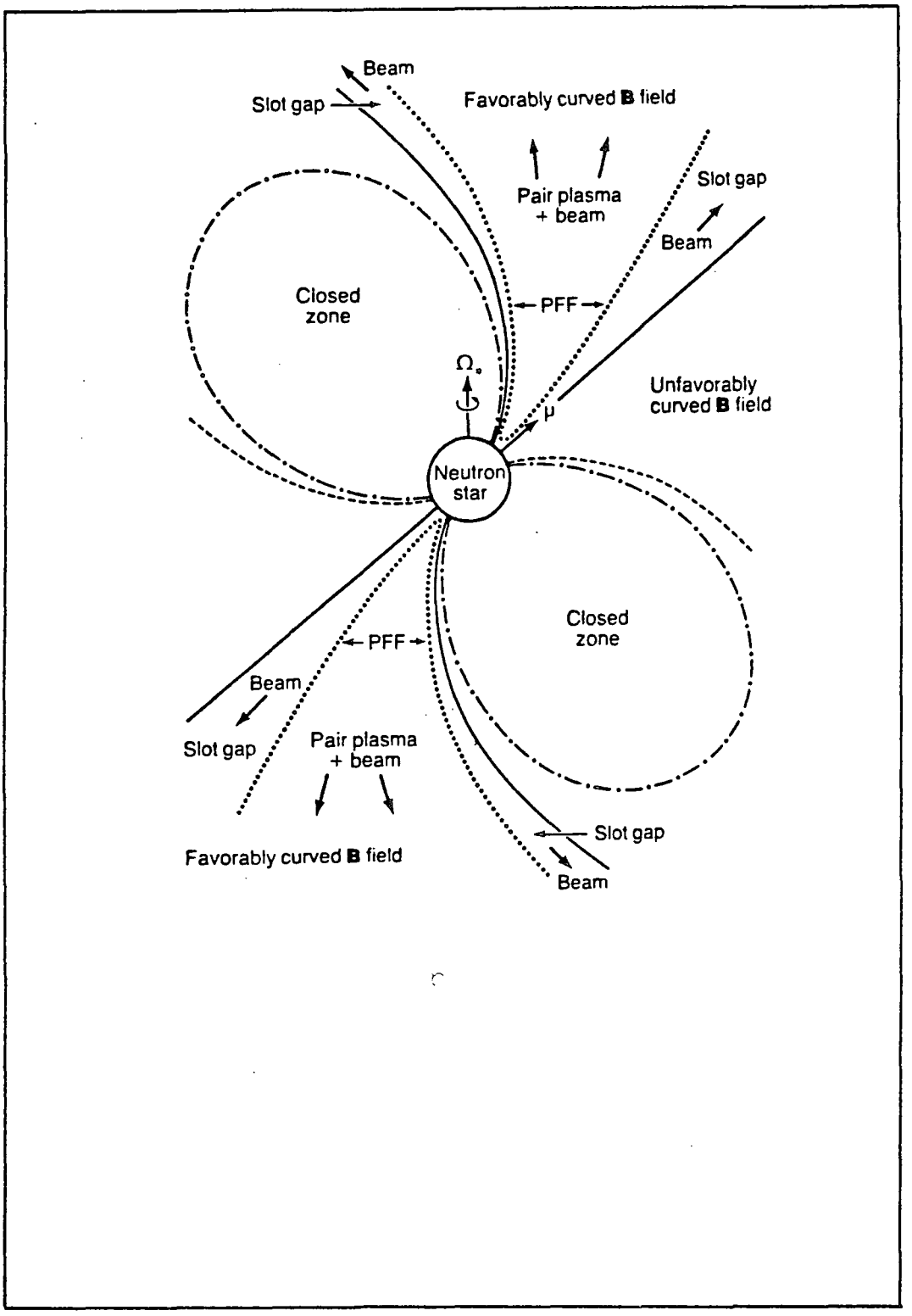

Figure 7.3: The 'Slot Gap' model for gamma-ray production by a pulsar.

the primary spectrum of the object.

Alternatively the gamma-ray spectrum may well be secondary to the primary particle beam and caused, along with the lower energy flux by interactions near the radius of light cylinder of the object.

Two models have been proposed to explain the V.H.E. and lower energy fluxes and they are now reviewed.

The 'Slot gap' model.

These ideas were first discussed in detail by Arons (Arons, 1983) - fig 7.3 represents the model.

The high energy particles are accelerated in a sheath of open magnetic field lines. The electric potential built up in this sheath ('slot gap') increases as the square root of the distance from the pulsar surface. The potential values close to the light cylinder of the pulsar are sufficient to be able to accelerate particles to energies $> 10^{13}$ eV for moderate pulsar rotation rates. Gamma-rays are then readily produced by curvature radiation as the particles travel along the field lines which are curved back in the region of the light cylinder, or by synchrotron radiation from particles moving across the field lines. There should be both electron and ion producing polar caps - indicating two different populations of pulsar. The pulsars emission beam should also exhibit polarisation elongation in the longitudinal direction. Unfortunately there is little evidence for two populations and what elongation there is to the emission beam seems to be in the latitudinal direction (Taylor and Stinebring, 1986).

The 'Outer gap' model.

This model is discussed in detail in two papers by Cheng, Ho and Ruderman (1986a and 1986b) and is an extention to earlier models

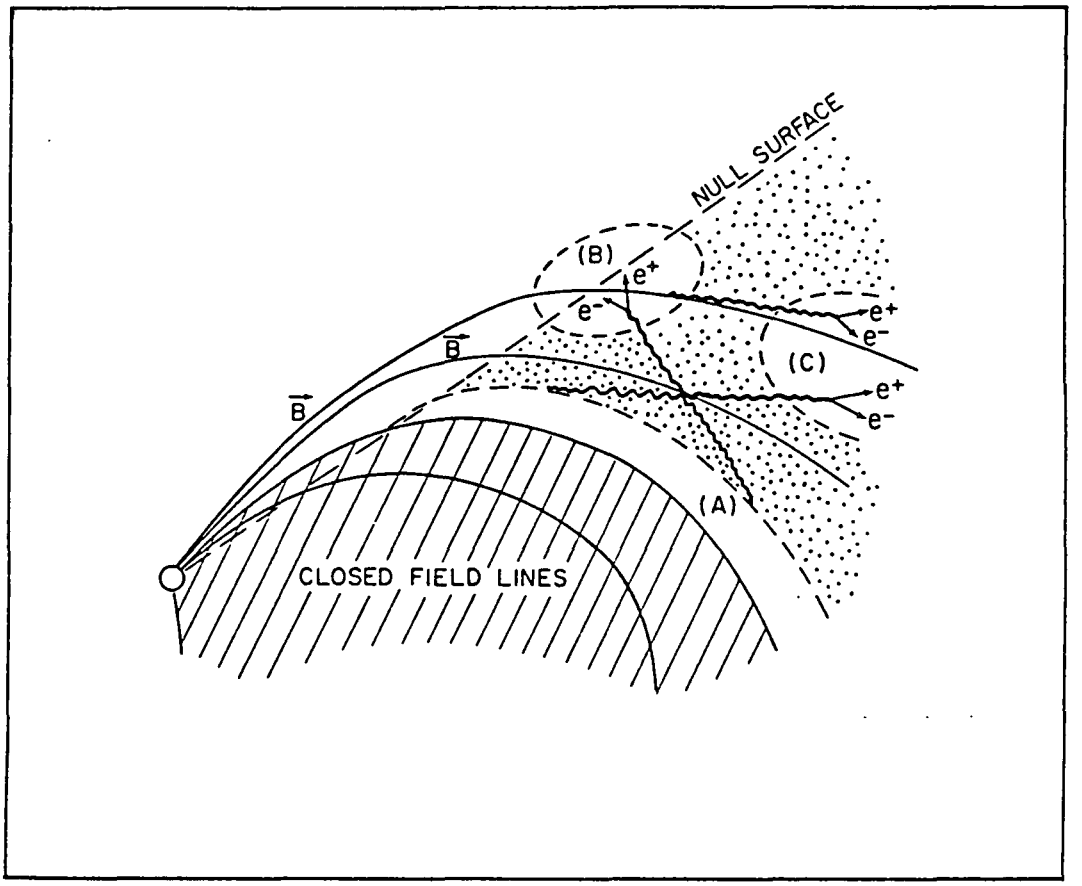

Figure 7.4: The 'Outer Gap' model for gamma-ray production by a pulsar (Cheng, Ho and Ruderman).

(Ruderman and Sutherland, 1975 and Sturrick, 1971). It differs from the 'slot gap' model in that the particle acceleration occurs much further from the star.

The flow of current in the magnetosphere of a pulsar can result in a 'slot-like gap' being developed and maintained in the outer parts of the magnetosphere. This 'gap' is a region of charge depletion and deep within it the potential drops can be very large ($\sim 10^{15}$ V). The potential drop produced by a spinning, magnetised neutron star across the 'open' magnetic field lines is given by,

$$V \sim \frac{w^2 . B_s . a^3}{c^2} \qquad - 7.4$$

where,

w = rotation frequency

B_s = surface magnetic field

a = neutron star radius

It is this potential drop which drives the current flow in the outer magnetosphere and leads to the formation of the 'gap'.

Pair production occurs in the 'gap' leading to the acceleration of the electrons and positrons. These particles produce high energy gamma-rays which pair produce again and so on leading to a cascade. The process is summarised in fig. 7.4. The exact mechanisms responsible for the cascade development differ for the Crab and Vela pulsars. The primary beam radiates due to curvature radiation in the Crab pulsar, but loses energy through inverse-Compton scattering on infra-red photons in the Vela pulsar.

The optical to GeV gamma-ray flux from the Crab pulsar can then be explained by Inverse-Compton and synchrotron radiation mechanisms. V.H.E. gamma-rays are also produced, though not in the same process as above. The model suggests that they may be due to synchrotron emission from secondary e^+ e^- pairs produced as higher energy gamma-rays

interact with the IR-optical photons. If there are fluctuations in the production of optical photons then V.H.E. gamma-rays may escape the Magnetosphere.

It follows from the serious attenuation of V.H.E. gamma-rays by pair production in the magnetic field that the observed flux should originate from beyond or close to the light cylinder. Certain constraints can be placed on the relation between the V.H.E. flux and the flux of optical photons (since the optical photon field is of sufficient energy to induce strong photon-photon absorption). Grindlay has noted (Grindlay, 1982) that this predicts that the angular separation of the optical and V.H.E. gamma-ray mainpulses should be a minimum i.e. the V.H.E. gamma-ray mainpulse should be considerably narrower than the mainpulse at optical wavelengths. Figure 1.4 shows the width of the 'light curve' from the Crab pulsar from radio to gamma-ray energies. The narrow V.H.E. mainpulse (width ~ 0.4 ms) is in agreement with Grindlay above and therefore supports the basic model proposed by Ruderman and Sutherland. The result indicates that the emission region should be no larger than a few hundred km in diameter.

Further work is needed both to confirm the narrow emission at V.H.E. and to test for fluxes at higher energies. The full understanding of the physics of pulsars and in particular their emission mechanisms has not been achieved. However, the presence of a V.H.E. gamma-ray flux indicates that the emission is likely to occur near or outside the light cylinder.

7.3.3: Other radio pulsars.

The results of the Durham observations of a selection of radio pulsars are given in section 6.7. No positive excesses are found and only upper limits are derived. These limits are in general agreement with other results from V.H.E. experiments (Porter and Weekes, 1978).

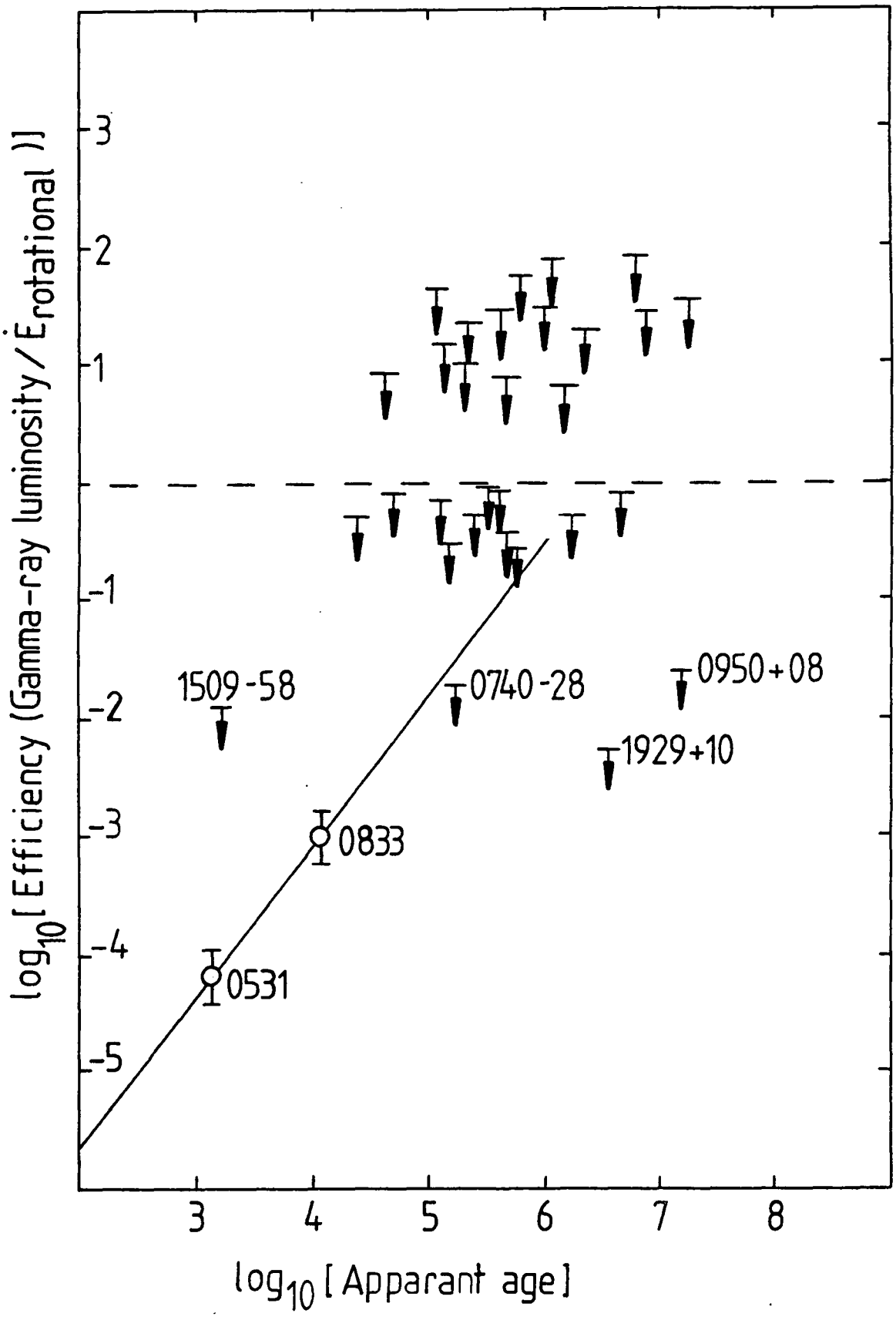

Figure 7.5: A plot of the relationship between efficiency of gamma-ray emission and pulsar age.

With the discovery of the Crab and Vela pulsars at gamma-ray wavelengths several authors have looked at the predictions of models for gamma-ray emission from other pulsars. The model proposed by Ruderman and Sutherland (1975) predicts that the total power in the high energy positrons emitted by the pulsar depends on the pulsar parameters as,

$$W \sim B^{6/7} \cdot P^{-15/7} \cdot \rho^{4/7} \qquad - 7.5$$

where B is the magnetic field strength at the stellar surface, P is the rotational period, and ρ is the radius of curvature of the field lines (the gamma-ray emission is assumed to be due to curvature radiation).

If the efficiency for gamma-ray production is defined to be n where,

$$n = \frac{L_\gamma}{E'} \qquad - 7.6$$

$$= \frac{L_\gamma \cdot P^3}{(4\pi \cdot I \cdot P')}$$

then the efficiency can be seen to depend on the apparent age of the pulsar P/P',

$$n \sim (P/P')^x \qquad - 7.7$$

where X depends on the value of p chosen, but is restricted $1 < X < 2$.

A plot of this relationship is given as fig.7.5. The Vela and Crab pulsars - known gamma-ray emitters are used as normalising points, with other pulsars shown for comparison. It is evident that this model predicts that pulsars become more efficient at producing gamma-rays as they age. So, gamma-ray experiments should investigate 'ordinary' radio pulsars despite the negative results so far achieved. In particular the recently discovered 1.56 ms pulsar (Backer et al, 1982) is regarded as a very old pulsar and may be able to produce gamma-rays very efficiently (Usov, 1983).

7.4: Cygnus X-3

7.4.1: Summary of the models proposed for this system.

The Cygnus X-3 system is thought to be a special case of a low mass X-ray binary, with many unusual features including an ability to accelerate particles to U.H.E. energies producing the recently detected flux of 10^{15} eV gamma-rays (Samorski and Stamm, 1983). The system has also produced huge radio outbursts such as those seen in 1972 (Gregory , 1972) and 1982.

Among the many ideas used to explain the complex and extended (radio to gamma-ray) emission are;

(a) An X-ray binary in which the collapsed star (neutron star) emits radiation which is detected as X-rays by reflection from the non-degenerate star. (Basko et al, 1974)

(b) An X-ray binary, with a strong stellar wind emanating from the non-degenerate star. (Davison and Ostriker, 1974)

(c) Further to the model suggested by Basko et al, the idea was extended to include a fast pulsar, rotating with a speed at least that of the Crab pulsar. (Bignami et al, 1977)

(d) 'A cocooned X-ray binary pulsar' (Milgrom and Pines, 1978).n.b. The V.H.E. and U.H.E. emission from the pulsar should not be attenuated by the shell of gas.

(e) An 'Accretion Disc Corona' (A.D.C.), was found to give a good explanation of the spectoral and temporal flux at lower X-ray energies (White and Holt, 1982)

(f) Comparisons have been made between the Cygnus X-3 and the SS433 systems (Grindlay, 1982). The proposed model involves a non-aligned rotator, the particle acceleration achieved in a jet emanating from an accretion disc — this model does not require the presence of a fast pulsar.

With the discovery of V.H.E. and U.H.E. gamma-rays and the possible detection of energetic muons (Marshak et al, 1985) these models have been severely tested. At present there are only two possible types of model proposed that can account for such huge releases of energy;

i. Fast pulsar acceleration and ii. Accretion driven processes, with the possibility that some combination of the two may be needed to explain all the observed properties.

7.4.2: Accretion powered mechanisms

A discussion of the turbulent magnetospheres produced in systems containing a neutron star and undergoing accretion has been given by Wang (1986). The gamma-ray emission occurs during 'non-steady accretion' when large scale vortexes are formed in the pulsar magnetosphere itself, or where it interferes with any accretion disc. As the distorted magnetic field reconnects, 'neutral sheets' are formed along which large potential differences are produced. Consequently, particle acceleration takes place leading to the high energy radiation as the accelerated ions collide with the diamagnetic plasma in the accretion flow, producing pions which decay to give the U.H.E. gamma-rays.

There are likely to be many of these transient vortexes and they could supply the observed gamma-ray spectrum with the maximum particle energy, E determined by the r.m.s. turbulent velocity V,

$$E \sim \frac{n.e.V.B.d}{c} \qquad - 7.8$$

where B is the magnetic field intensity, and d is the scale size of the reconnecting loop structures, and n is an efficiency parameter.

Chanmugam and Brecher (1985) have described a model in which ions are accelerated in an accretion disc around the neutron star. The mechanism of acceleration involves a unipolar inductor such as that

suggested for binary radio sources (Lovelace, 1976) in which the magnetised neutron star acts as a dynamo. Particles with energies $\sim 10^{17}$ eV may be produced. The potential difference set up in the disc is given by;

$$V = - \frac{(GM)^{1/2}}{c} B_z(r_1) . r_1^{1/2} . \ln(r_2/r_1) \qquad - 7.9$$

where,

r_1, is the inner radius of the disc

r_2, is the outer radius of the disc

B_z, the axial component of the poloidal magnetic field

M, is the mass of the degenerate star

and V, is measured in statvolts (=300V)

The basic energy source is disc accretion.

This model has several advantages; it is very efficient, and since it relies on a general system of accretion onto a neutron star it may explain the fact that 3 such sources have been observed at V.H.E. energies, 4U0115 + 63, Hercules X-1 in addition to Cygnus X-3. This mechanism requires a relatively low magnetic field, as the disc must come close to the collapsed object and a high magnetic field pushes the 'Alfen radius' out to relatively large distances.

Collisionless shocks are expected in the accretion flow onto collapsed objects (Hawley et al, 1984). This phenomenon has been used by Kazanas and Ellison (1986) to develop a model for 'diffusive shock acceleration' of ions. Proton-proton collisions along with photo-dissociation of helium ions would then produce U.H.E. neutrons which then escape from the region of high magnetic field to impinge on the atmosphere of the companion. Hadronic interactions in the stellar atmosphere then produce the pions which decay to give the observed V.H.E. and U.H.E. gamma-ray flux.

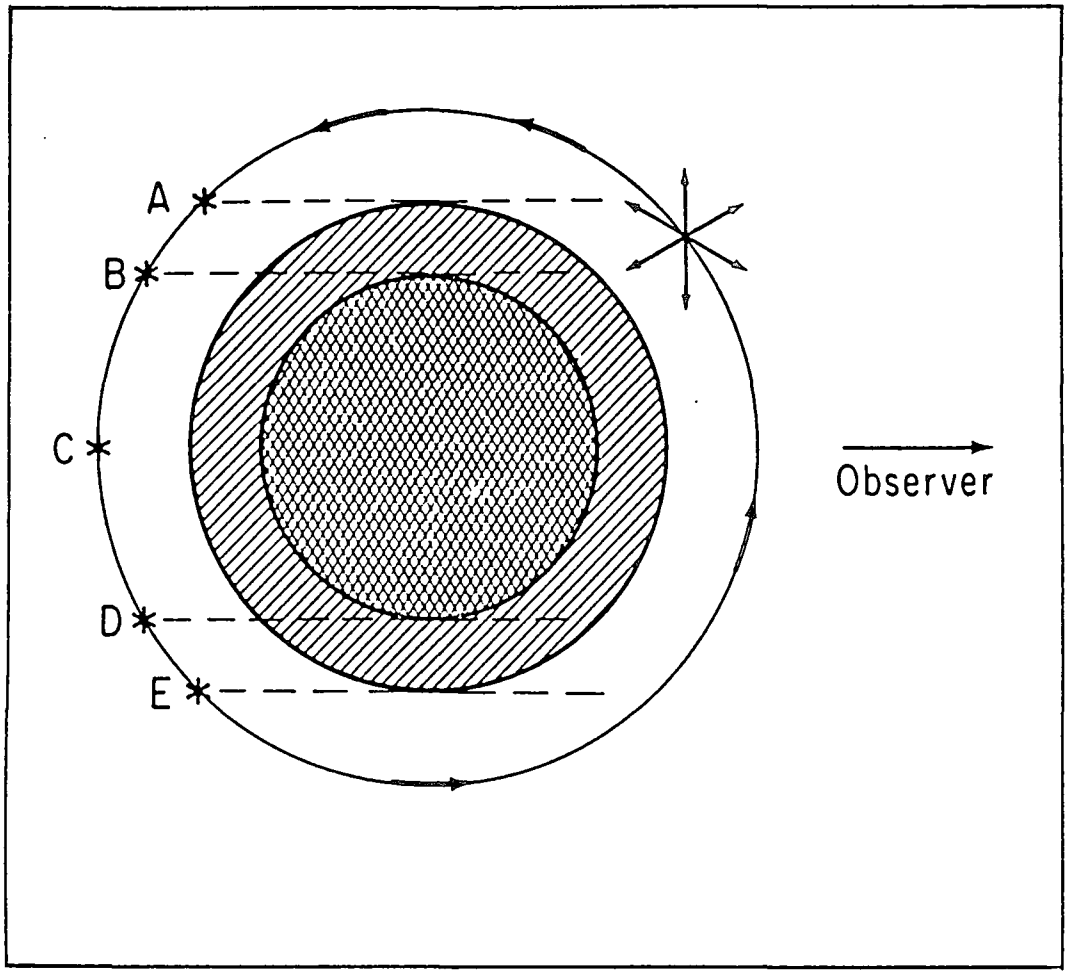

Figure 7.6: A model proposed by Vestrand and Eichler for the Cygnus X-3 system.

The maximum proton energy produced is given by,

$$E < 0.06 \, (r / R_L) . (r_L / \lambda) \, B_{12}^{1/2} \qquad - 7.10$$

where,

r is the distance from the centre of the neutron star

r_L, is the gyroradius of the particles

R_n, is the radius of the neutron star

B_{12}, the surface magnetic field in units of 10^{12} G

λ, is the mean free path of the particles

This final model predicts that a large number of UHE neutrons should escape the system and may be detectable above the cosmic ray background.

Although these ideas may play a part in systems like Cygnus X-3 it seems likely, in the light of the discovery of the 12.6ms period (section 6.2.9) that the gamma-rays are produced by a mechanism that retains the pulsar periodicity i.e. the particles are accelerated by the pulsar.

7.4.3: Pulsar acceleration model.

A schematic description of a possible system is given in fig 7.6, with the V.H.E. emission resulting from particle interactions in the atmosphere of the companion star, the particles are themselves accelerated by the high magnetic field around the collapsed object (Vestrand and Eichler, 1982). The basic model predicts emission at two phases in the orbit, at A and B as the high energy particles (assumed to be emitted in all directions) interact by either thin bremsstrahlung or nuclear interaction to produce neutral pions in the stellar atmosphere.

The model for gamma-ray emission from the Crab and Vela pulsars

suggested by Cheng, Ho and Ruderman (section 7.3.2) indicates that U.H.E. particles may well be produced in such objects. Charged particles may be accelerated through the full potential drop set up in the 'gap' to be ejected at the light cylinder boundary.

As the potential drop and particle flow through the 'gap' are roughly proportional to w^2 . B (where w = the rotational frequency and B = the surface value of the magnetic dipole field) high energy particles can be produced in rapidly rotating pulsars.

The power carried in the emergent beam is,

$$E \sim 10^{36} \text{ ergs}^{-1}$$

- for a pulsar such as the Crab.

The detection of a fast pulsar period in the V.H.E. gamma-ray emission lends support to a system such as that in fig. 7.6. In addition, the geometry of the model can explain the two peaks observed in the data. In the Vestrand and Eichler model the primary particles are electrons, but in more recent interpretations protons have been suggested (Hillas, 1984). Here the U.H.E. and V.H.E. gamma-rays are secondaries of the cascade that develops from a monoenergetic beam of particles interacting by synchrotron or bremsstrahlung in the target gas.

7.4.4: The implications of the Durham results.

The 4.8 hour orbital modulation

The evidence for V.H.E. emission modulated with the orbital period is now very strong with significant excesses observed by four groups (Neshpor et al, 1979), (Danaher et al, 1981), (Lamb et al, 1982) and (Dowthwaite et al, 1983). The V.H.E. emission is of relatively short duration, certainly less than 1/8 th of a period - see section 6.2. In addition there is some evidence to suggest that there are times of

emission as short as 2-3 minute duration - see fig 6.21 i.e. ~ 0.01 of a period. The phase of the V.H.E. gamma-ray effect is confined to the 0.63 region in the 1981-1982 Durham data in agreement with measurements made elsewhere (Danaher et al, 1981). The object has also been detected at phases closer to 0.2 in the extensive monitoring of this object throughout the 1970's by the Crimean group (Neshpor et al, 1979). There is some indication in the Durham data of emission at phase 0.13

Therefore there is some evidence for two peaks in the 4.8 hour gamma-ray light curve, the peaks separated by ~ 1/2 an orbital period. Although the two peaks are in agreement with the general prediction of the Vestrand and Eichler model, the phase of the main peak (0.63) occurs when the pulsar is expected to be in front of the companion star, according to the conventional interpretation of the X-ray data (Hillas, 1984). As noted by Hillas, an X-ray spike is also observed at this phase and it may be that there is a gas target in this direction.

Minute timescale periodicity

Recent X-ray results (Van der Klis and Jansen, 1985) have shown that there are 5-20 % modulations in the 1-10 keV flux from Cygnus X-3. These modulations exhibit a quasi-periodicity in the range 50 - 1500 s. This effect occurs at phases 0 - 0.75.

The Durham data at phase 0.63 have been analysed for periodicity in this range - see section 6.2.9. There is no evidence for any periodic V.H.E. emission at this phase and in this period range.

Van der Klis and Jansen explain these oscillations as the result of quasi-periodic phenomena in the accretion disc occulting the source. There is no confirmation of similar behaviour in the gamma-ray flux.

Long term periodicity

Previous discussions of the long term variation in the strength of the 0.63 phase emission in the Durham data have considered only the confirmation of the 34.1 day modulation of the X-ray flux (Molteni et al, 1980). The systematic search for a favoured periodicity shows that the 0.63 excesses are more strongly modulated with a ~ 19 day period (see section 6.2.5). This is in good agreement with the variation of the time of occurence of the X-ray maximum (Bonnet-Bidaud and Van der Klis, 1981). There has been recent confirmation of this ~ 19 day modulation to the V.H.E. gamma-ray emission from the Russian experiment (Neshpor and Zyskin, 1986).

The X-ray modulation has been interpreted as apsidal motion in the Cygnus X-3 system due to the pertubations of the orbit as the collapsed object distorts the companion star. A detailed investigation of the apsidal motion infers an eccentricity of ~ 0.03 i.e. the orbit is almost circular (Bonnet-Bidaud and Van der Klis, 1981). The predictions of the cocoon and stellar wind models (b and d above), suggest the need for a large orbital eccentricity, and so the V.H.E. results are to this extent at odds with these models.

Pulsar periodicity

The searches for fast pulsar periodicity in the strong excesses at phase 0.63 have revealed a period of ~ 12.6 ms. This periodicity does not appear in all the 1983 and 1982 data - see sections 6.2.7 - 6.2.9.

The strongest evidence for periodicity came from two nights data in 1983 with the section length equal to 7-10 minutes. Such effects should show evidence for the orbital modulation of the period, and so the data have been analysed for periodicity with a range of period

derivatives. The results lead to a best choice of a small negative derivative ~ 1.0 . 10^{-7} , indicating that the V.H.E. emission occurs at the rear of the orbit, and that the orbital velocity is ~ 80 kms^{-1}(Chadwick et al, 1985b). Although the significance of these results is low they are once again at odds with the accepted X-ray interpretation of the orbit with the pulsar placed in front of the companion at this phase. This result and an additional analysis of the 1982 data in a search for a period derivative are discussed in detail elsewhere (Chadwick, Phd thesis in preparation).

The Durham results therefore provide the first strong evidence for the existence of a pulsar in the Cygnus X-3 system. In addition the strength of the periodicity would seem to be modulated with the 4.8 hour and perhaps the 19 day variations adding further evidence to the validity of these modulations to the gamma-ray flux.

7.4.5: The gamma-ray spectrum and luminosity of Cygnus X-3

The fluxes detected from the object are summarised in section 6.2.10, and indicate that the spectral slope may be steeper than the cosmic ray background in the V.H.E. region.

The differential spectral slope in this region is usually taken to be -2.2. The distance to Cygnus X-3 is uncertain but almost certainly > 10kpc. If the source emits isotropically then a luminosity in excess of 10^{36} $ergs^{-1}$ is inferred for V.H.E. emission.

n.b. In a recent paper (Apparao, 1984) it has been suggested that the V.H.E. gamma radiation will be attentuated at the object by a photon-photon absorption process with the infrared photon field. Though the exact reduction to the flux is not fully described in the absence of an infrared spectrum, it is likely that the luminosity at energies > 1000 GeV may be considerably higher than the value

indicated above.

The U.H.E. gamma radiation is not expected to suffer a similar attenuation at the source and the luminosity inferred by the observations at Haverah Park (Lloyd Evans et al, 1983) is $\sim 3\ 10^{36}$ ergs^{-1}. However, there should be attenuation of the U.H.E. flux at energies greater than $\sim 10^{15}$ eV as the gamma-rays interact with the 2.7 K microwave remnant.

The results of the pulse amplitude analysis are quite difficult to explain, especially as there is strong evidence for a U.H.E. flux from the object. This would infer that the spectrum is a single power law in the V.H.E. to U.H.E. region, and would not agree with the prediction for a spectrum steepening in the V.H.E. region (section 6.2.6). In addition, recent pulse amplitude analysis of the data from the Mount Hopkins experiment (Cawley et al, 1985b) shows an imbalance in favour of the larger light flashes. The situation is therefore confusing, and in light of the relatively low significance of these results no firm conclusions can be drawn.

7.4.6: Summary.

The detection for the first time of a 12.6 ms pulsar in the Cygnus X-3 system (Chadwick et al, 1985b) points to a model similar to that proposed by Vestrand and Eichler (Vestrand and Eichler, 1982). The V.H.E. results seem to indicate that the pulsar is situated behind the companion at the time of emission. Alternatively, the emission may occur in front of the companion with an intervening gas target.

Despite the discovery of the fast pulsar several problems remain.

i: The relatively sharp feature (phase = 0.63) seen in the emission at E > 1000 GeV is not expected as the cosmic rays will not be confined to a thin beam due to Alfen scattering processes within the system (Grindlay,1982).

ii: It is interesting to note that the light curve for the pulsar

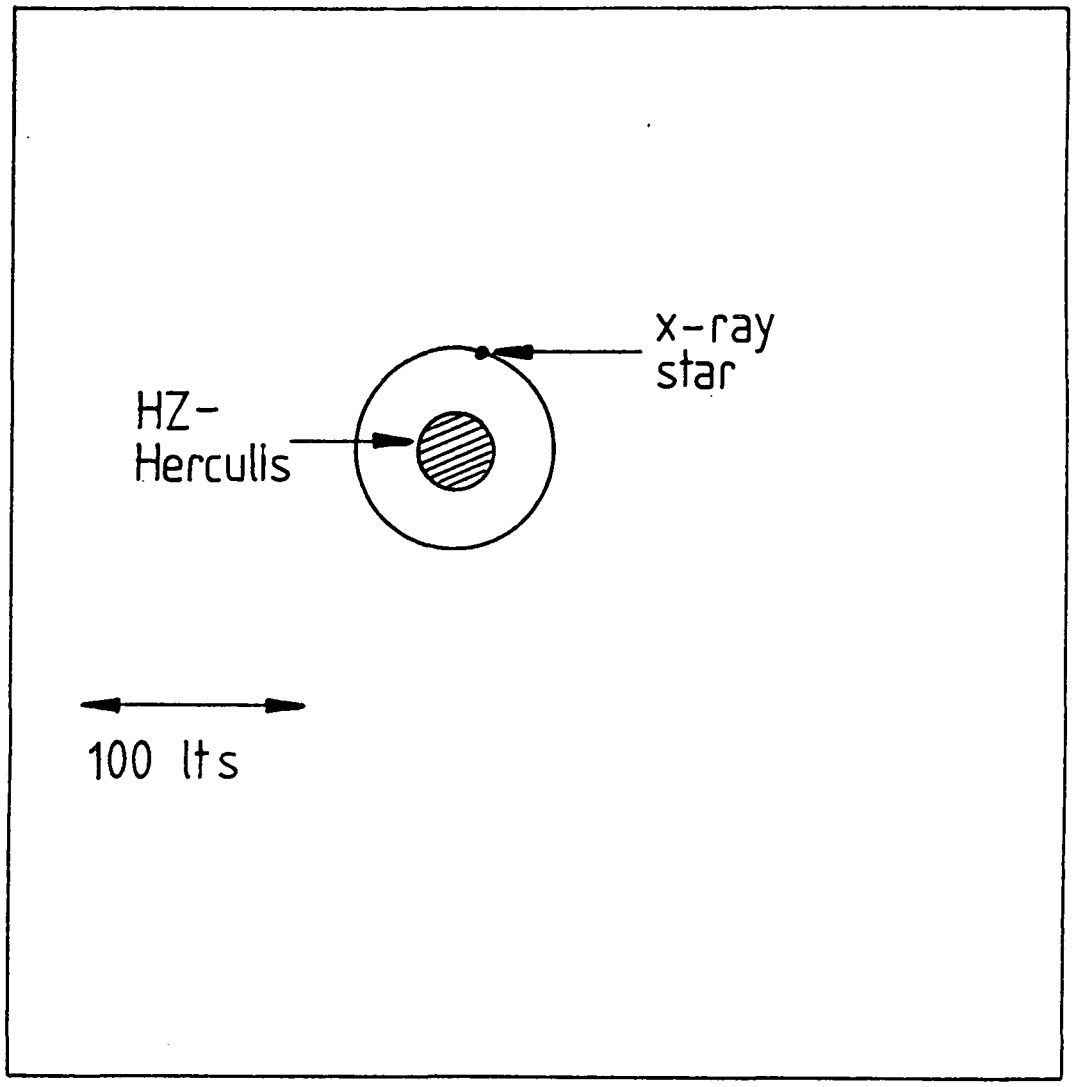

Figure 7.7: A schematic description of the Hercules X-1 system.

periodicity has a broad 'duty cycle' - see fig.6.22. The form of the light curve is similar to that discovered by the Durham group from Hercules X-1 and 4U0115 + 63, where both of these objects are thought to be powered by an accretion mechanism. The Cygnus X-3 light curve is unlike the sharp peak detected from the Crab pulsar.

These considerations indicate that despite the prescence of a fast pulsar, accretion may also play an important role in the emission process. The Cygnus X-3 system may well be quite unusual in the Galaxy providing a large percentage of the cosmic ray flux. Although the detail of the system is still undetermined, the V.H.E. ms periodicity, if confirmed, will provide an important key to its understanding.

7.5: Hercules X-1.

Hercules X-1 is considered to be the prototype low mass binary X-ray pulsar. The system contains a neutron star of estimated mass $0.4 < M_n/Mo < 2.2$ with a companion of spectral type A or F of mass $1.4 < M/Mo < 2.8$ (Mo = solar mass). The collapsed object is highly magnetised with fields as great as $5.\ 10^{12}$ G inferred from the observation of the X-ray cyclotron lines at 58 keV (Trumper et al, 1978). The schematic of the system is given in fig.7.7. The 35 day X-ray modulation (-see section 1.5.2) is thought to be produced as the pulsar is alternately revealed and obscured behind the accretion disc (Petterson, 1975).

7.5.1: A review of the V.H.E. emission.

The Hercules X-1 system gave an intense burst of V.H.E. gamma-rays on the 17th of April 1983. The burst lasted for three minutes and was strongly periodic at the pulsar period of 1.24 s. The flux of V.H.E. gamma-rays corresponding to this burst is $1.2\ .\ 10^{-9}\ cm^{-2}\ s^{-1}$ at

energies > 1000 GeV. If the distance to the object is assumed to be 5 kpc and the differential spectral index is taken to be -3, then the burst luminosity is $\sim$ 5. 10^{36} ergs^{-1}.

Subsequent monitoring of this source in July 1983 indicated, albeit at a low significance level, that the time-averaged flux from the object is $\sim$ 3 . 10^{-11} cm^{-2} s^{-1}. This implies a source luminosity of $\sim$ 2 10^{35} erg s^{-1}. Further details of the burst are given in section 6.4.

Later in 1983 the 'Fly's eye' U.H.E. detector observed another burst, lasting 40 minutes at energies > 10^{14} eV (Balustraitis et al, 1985).

7.5.2: Models of the V.H.E. emission

The models for this system have been discussed by Eichler and Vestrand (1985). In their discussion they reject particle acceleration by rotation of the accretion disc (as suggested for Cygnus X-3 by Chanmugham and Brecher). This is because the inner radius of the disc is thought to be $\sim$ 300 stellar radii from the collapsed object, and it would be difficult for a large enough fraction of the total rotational energy to be passed to the disc.

The 'Beam-dump' model.

This model is similar to that developed by Vestrand and Eichler (1982) to explain the V.H.E. emission from Cygnus X-3. Particles are accelerated in a region corotating with the pulsar and flow outwards to interact with the surrounding accretion disc. The method of acceleration is not certain, but the high efficiency of 'shock acceleration' in the region of the neutron star makes it a suitable method, as the efficiency of U.H.E. particle acceleration must be high in the Hercules X-1 system. Using this method particles of energy as high as 9.10^{6} mc^{2}. $R_6^{-1/6}$ can escape the shock region (R = R_6 x 10^{6} cm

= the radius of the shock). This is enough to account for the observed U.H.E. and V.H.E. flux of gamma-rays.

One prediction from this acceleration method is that particles are not likely to be accelerated to energies $> 10^{17}$ eV, and therefore U.H.E. gamma-rays at energies $> 10^{16}$ eV should not be observed. Recent observations (Protheroe and Clay, 1985), (Samorski and Stamm, 1985) yield detections of gamma-rays near to these energies.

The above explanation, which places the source of particle acceleration close to the pulsar readily explains the detection of the pulsar periodicity in the V.H.E. and U.H.E. emission.

The observed high energy gamma-rays are produced when the beam interacts with a column thickness roughly equal to the radiation length of the particles. The interactions may be described as follows;

p + N -> pi mesons + hadrons
-> V.H.E. gamma-rays + muons + neutrinos

where p represents a proton and N a nuclide.

If the disc were thicker then the gamma-rays produced would be absorbed, any thinner and there would be a rapid fall in the number of gamma-rays produced. The correct conditions are thought to occur at the onset and offset of the X-ray high state, just as the accretion disc grazes our line of sight. The Durham V.H.E. burst came at the expected onset of the X-ray high state. The U.H.E burst came at a different phase in the 35 day cycle and would require thickening of the disc in the line of sight. There is some independent evidence from X-ray observations (Parmar et al, 1985) that such a thickening may have occurred.

Confirmation of the V.H.E. burst has come from observations made in the spring of 1984 by the Whipple observatory 10 m^2 reflector (Cawley et al, 1985c). The emission shows similar characteristics to the 3 minute burst described above, but in a later observation the emission occurred at a phase thought to coincide with the X-ray eclipse (Gorham

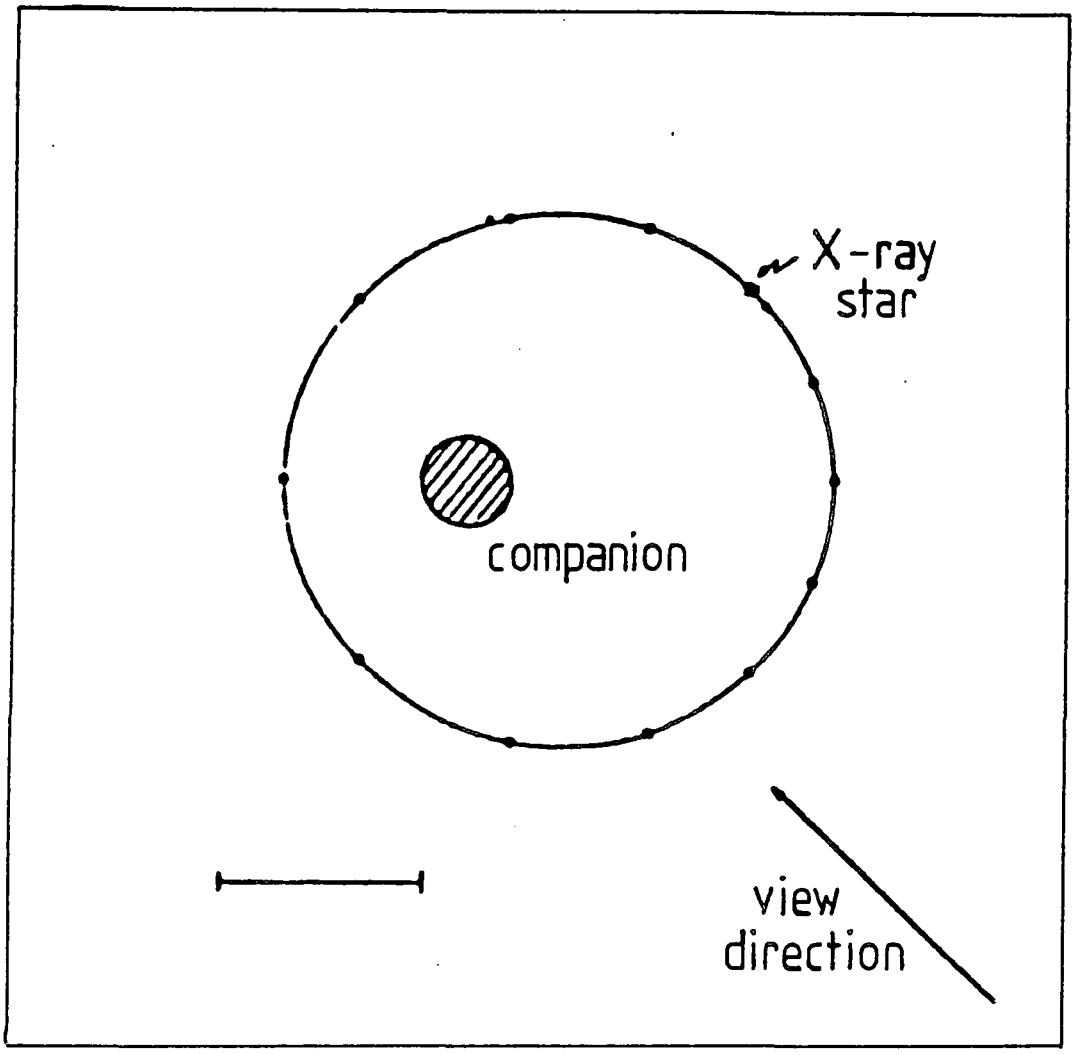

Figure 7.8: A schematic description of the 4U0115 + 63 system.

et al, 1986). It is difficult to imagine how the gamma-rays could be produced in the accretion disc. Despite this, with modest assumptions of the parameters of the Hz-Herculis magnetic field it is possible that the particle beam may be steered to interact with the stellar limb (Gorham and Learned, 1986).

It therefore seems likely that the Hercules X-1 system is an emitter of V.H.E. and U.H.E. gamma-rays at certain points in the 35 day cycle. The model described above indicates that this system may have similarities with Cygnus X-3.

7.6: 4U0115+63.

The properties of the binary X-ray pulsar 4U0115+63 are reviewed in section 1.5.3. The pulsar has a period of 3.6 s and the system is known to undergo periods of enhanced hard X-ray emission. The components are widely separated in contrast to Cygnus X-3 and Hercules X-1 and the system is thought to be of larger total mass than the other two. The transient nature of the X-ray emission is thought to be due to a combination of the large separation and the small radius of the companion (V635 Cassiopeiae). The schematic description of the system is given in fig.7.8.

This X-ray binary pulsar was targeted for observation because it has values of period, P, luminosity, L, and period derivative, P', very close to that of the established V.H.E. emitter Hercules X-1 - see fig.4.3.

The period has been measured over 14 years with very little change, even though the period derivatives vary widely - a summary of the erratic behaviour of the period derivative is given as fig.1.3. This strange behaviour suggests that X-ray emission occurs at times of substantial and rapid accretion onto the collapsed object resulting in

large measured values of the spin up, these periods are then interspersed by longer periods of spin down.

The Durham observations indicate a detection of an excess of V.H.E. gamma-rays at 2 +/- 0.4 % of the cosmic ray background rate pulsed with the 3.6 s X-ray period, with a flux of (7 +/- 1.4) 10^{-11} cm^{-2} s^{-1} . With a reasonable assumption of the differential spectral index at E > 1000 GeV, i.e. - 3.0 and a distance to the object of ~ 5 kpc, the inferred luminosity is 6 . 10^{35} erg s^{-1} for isotropic emission. This value is in close agreement with that found at these energies from the similar object Hercules X-1 - see section 7.5. The gamma-ray 'light curve' is broad, see fig.6.32, and once again similar to the 'light curves' from Hercules X-1 and Cygnus X-3 at these energies. The broad light curve may then confirm that the V.H.E. emission may occur at times of accretion.

Further observations of this object are required to establish the full features of the high energy emission particularly to observe the behaviour over the full orbit and to establish the nature of the accretion process.

There have been suggestions (Lamb and Weekes, 1986) that the detection of 4U0115+63 is the identification of Cas γ-1, an object detected at V.H.E. in the 1970's by the group working at the Crimean Astrophysical Observatory (Stepanian et al, 1972). However, recent radio observations (Gregory et al, 1986) have identified an alternative for Cas γ-1, within the gamma-ray error box.

7.7: The drift scan objects.

The six objects subjected to a limited 'drift scan' observing programme do not show any evidence of V.H.E. emission - see section 6.8.

The upper limits derived for all of these objects are in good

agreement with the previously quoted values, and more extensive observations are required to comment on any implications of the results for the proposed models of these systems. Such observations could be made with the new generation of Cerenkov telescopes - such as the Mark III telescope described in section 3.8. where data rates may well be such that useful upper limits could be derived.

7.8: Evidence for a class of V.H.E. object.

There is a growing number of objects found to be emitting V.H.E. gamma-rays including two radio pulsars (the Vela and Crab), a millisecond pulsar (PSR1953+29), an active Galaxy, (Centaurus A), binary X-ray pulsars (Hercules X-1, 4U0115+63) and normal Galaxies (The Milky Way, M31). In addition the unusual object Cygnus X-3 produces a large proportion of its luminosity in the V.H.E. and U.H.E. region.

Despite the highly significant detection of both of the radio pulsars at these energies the calculated luminosity shows that such objects radiate primarily at other wavelengths.

However there is now evidence that some binary X-ray pulsars do emit a considerable amount of their energy in the high energy region (V.H.E. and U.H.E.) of the electromagnetic spectrum. - the V.H.E. and U.H.E. gamma-ray spectrum representing the primary emission from these objects. In a recent paper (Hillas, 1984), Hillas has proposed that the unusual system Cygnus X-3 may be capable of accelerating particles in a monoenergetic beam to energies of 10^{17} eV providing all the high energy cosmic rays necessary to give the observed flux - making up for the leakage from the Galaxy; Cygnus X-3 may well be a unique object in our Galaxy.

In a later paper (Hillas, 1985) it has been suggested that the lower energy (10^{12} eV) part of the cosmic spectrum may be produced by a number of objects similar to Hercules X-1 and particularly

4U0115+63 (seen at V.H.E. but not at U.H.E.). In this case there is a definite prediction for more V.H.E. gamma-ray sources of this type in the Galaxy.

THE DURHAM NORTHERN HEMISPHERE VEGA CATALOGUE.

SOURCE	HRS	FLUX (10^{-12} cm^{-2} s^{-1}) MEAN	FLUX (10^{-12} cm^{-2} s^{-1}) PEAK	D (KPS)	S (DIF)	LUMIN (ERGS s^{-1}) MEAN	LUMIN (ERGS s^{-1}) PEAK	SIG.	COMMENTS
PSR0531	137	7.9±1.8	200±30	2	2.4	$2.1\ 10^{34}$	$1.4\ 10^{36}$	10^{-5} 2.10^{-4}	CONT.PULSED SIG.IN VERY NARROW (0.4ms) MAIN PULSE. ALSO 15 MIN. OUTBURST WITH BROAD LIGHT CURVE
CYGX-3	307	5.0±1.2	300±70	11	2.2	$9.0\ 10^{35}$	$5.4\ 10^{37}$	10^{-5}	4.8 HR.MOD.SIG.IN PHASE WITH X-RAY. SIG.SEEMS TO LAST ONLY A FEW MINS. POSS.19 AND/OR 34 DAY CYCLES
HERX-1	32	30±15	1200±300	5	3.0	$2.0\ 10^{35}$	$1.2\ 10^{37}$	$2\ 10^{-2}$ $7\ 10^{-5}$	SHORT (3 MIN) OUTBURST AT EXPECTED 'TURN-ON' TIME - BROAD LIGHT CURVE. EVIDENCE FOR CONT.WEAKER EMISSION
4U0115	25	70±14	-	5	3.0	$6\ 10^{35}$.	-	10^{-5}	HERX-1 LIKE OBJECT DAY-TO-DAY VARIATION STRONGEST TIME-AVER SIG.AT 1000 GEV
GAL.PL.	4	$3\ 10^{5}$ s^{-1}	-	1-2	-	10^{39} -10^{40}.	-	$5\ 10^{-4}$	CONFIRMATION OF EARLIER RESULTS WITH EVIDENCE TO REJECT ORIGIN IN BRIGHTNESS OF GAL. PLANE
M31	5	220±70	-	470	3.0	$4\ 10^{40}$.	-	10^{-2}	VHE LUMINOSITY CONSISTENT WITH CYGNUS REGION OF GALACTIC PLANE
2CG195	63	-	-	-	-	-	-	-	ANALYSIS IN PROGRESS
2CG065	64	30±7	-	3.5	3.0	$3\ 10^{36}$	-	$3\ 10^{-8}$	ASSOCIATION OF FAST BINARY PULSAR PSR1953+29 WITH COS-B SOURCE 2CG065
4C21	132	-	-	-	-	-	-	-	ANALYSIS IN PROGRESS

FLUX LIMITS ON OTHER OBJECTS: (OBJECT, HRS, 3SD LIMIT) ; (CYGX-1, 4, 500) (SS433, 3, 300) (PERX-1, 2, 300) (2CG135, 11, 50) (3C273, 13, 500) (NGC4151, 3, 300) (CAS-A, 3, 400) (PSR0355+54, 36, 36) (PSR0655+64, 10, anal.in prog.) (PSR0950+08, 47, 41) (PSR1133+16, 27, 46) (PSR1508+55, 33, 36) (PSR1913+16, 15, anal.in prog.) (PSR1929+10, 11, 68) (PSR1930+22, 4, 85) (PSR2223+65, 49, 31) (PERIODIC LIMITS FOR PULSARS - CONTINUOUS LIMITS FOR OTHERS)

Figure 8.1: A catalogue of the results obtained by the Durham University V.H.E. gamma-ray experiment at Dugway, Utah.

Chapter 8: Conclusions and Future Work.

Ultra and Very high energy gamma-ray emission from binary X-ray pulsars and certain radio pulsars is now well established, with the results of the Dugway experiment making an important contribution. A catalogue of these results is given in fig. 8.1. The list of V.H.E. gamma-ray emitters will almost certainly grow as improvements are made in the observation techniques.

The new generation of Cerenkov light detectors (including the Halakeala facility, the Whipple telescope and the Durham University Southern Hemisphere telescope) has been designed to take advantage of major improvements in performance over previous arrays. They have relatively low energy thresholds and have optical and electronic systems specially designed for Cerenkov work. Specifically they incorporate near optimum fields of view with the accurate timing facilities needed for the detection of rapidly periodic objects.

There have been major efforts to provide both effective analysis techniques to recover the weak V.H.E. gamma-ray signals and to be able to reject a significant fraction of the cosmic ray background by software cuts in the data.

The pulse amplitude measures have been shown to be of limited use for the Mark I Dugway array. However, there is now some evidence for a small difference in the characteristics of gamma-ray and cosmic ray initiated Cerenkov flashes. Further study of the flash intensity, along with the use of the 'inter-detector fast timing' technique may enable a significant increase in the signal/noise ratio to be made. The analysis of the data from periodic sources is made much more effective when an accurate ephemeris is available from measurements at

other wavelengths. With such an ephemeris the relatively weak emission from the Crab pulsar was detected using the Dugway array. Collaboration between groups working at several wavelengths will increase with simultaneous observations of an object over a wide energy range being one possibility.

With the ability to manufacture low-cost mirrors, very large reflectors may be made, and it may be possible to build large instruments to conduct extensive surveys, for instance measurements of the Galactic centre. In the meantime most of the observing programs will concentrate on the 'favoured' objects for V.H.E. gamma-ray emission i.e. fast radio pulsars, binary X-ray pulsars and the recently discovered millisecond pulsars.

The Durham group has reported V.H.E. gamma-ray emission from a millisecond pulsar in a binary system - PSR1953+29, the COS-B source 2CG065+00 (Chadwick et al, 1985a). This discovery lends some support to recent theories linking millisecond pulsars with low-mass binary X-ray pulsars (e.g. Shaham, 1987). In this theory the millisecond pulsars result from the spin-up of the degenerate component of the X-ray source as it slowly accretes matter from the low-mass companion. In the light of this model there is a prediction that fast pulsars should be found in low-mass X-ray binary stars. The 12 millisecond periodicity in the V.H.E. gamma-ray flux from Cygnus X-3 would lend support to the evolutionary connection between these two classes of object. More supporting evidence has come with the detection of 'quasi-periodic' oscillations in the X-ray flux (Van der Klis and Jansen, 1985). These oscillations may results from the 'beating' of the rotational period of the collapsed object with the orbital motion of the accreting matter. A similar 'quasi-periodic' component is found in the X-rays from another low-mass X-ray binary, GX5-1 (Van der Klis et al, 1985). In this case, the inferred rotational period and

magnetic field are remarkably close to those proposed for PSR1953+29.

Any direct confirmation of the 12 millisecond period from Cygnus X-3 is likely to come from experiments investigating the V.H.E. region, as only at these high energies will the pulsed radiation penetrate the dense cocoon or stellar wind in the vicinity of the system.

Cygnus X-3 is particularly interesting in the light of recent measurements made by experiments designed to search for proton decays. There is some evidence for a flux of muons associated with the radiation from this object (Marshak et al, 1985), (Battistoni et al, 1985), though other experiments do not provide confirmation (e.g.Oyama et al, 1986). Such a detection of muons is not consistent with the observed V.H.E. and U.H.E. photon flux and implies that there may be an alternative neutral flux from this object; an unknown low-mass particle, nicknamed a 'cygnet'. These particles interact with the terrestial nuclei to produce another new particle, more massive than the first which then produces the muons. Neither of these particles need have been detected in accelerator experiments (Ruddick, 1986). Though evidence for the new particle is limited, and the flux of muons detected by Marshak et al may be more readily explained by modifying our knowledge of high energy particle interactions in the atmosphere, the result indicates that a study of cosmic high energy particle accelerators, such as Cygnus X-3 may complement the work done using terrestial beam colliders.

The new V.H.E. gamma-ray experiments should provide confirmation of the presence of a 12 millisecond pulsar in the Cygnus X-3 system, in addition to providing new measurements of the other gamma-ray emitting objects. The new Durham University facility is expected to confirm earlier reports of discrete sources in the Southern Hemisphere, and in view of the success of the Dugway experiment new sources may be discovered. In conclusion, the V.H.E. gamma-ray observations have already provided important clues to the physical processes dominating

fast radio and binary X-ray pulsars and the new, sensitive telescopes should develop this subject into a major branch of observational astronomy.

References.

Albats, P., Frye, Jr., G.M., Zych, A.D., Mace, O.B., Hopper, V.D., Thomas, J.A., 1972, Nature, Vol.240, p.221.

Apparao, K.M.V., 1984, Astrophys. J., Vol.287, p.384.

Arons, J., 1983, Astrophys. J., Vol.266, p.215.

Ash, M.E., Shapiro, I.I. and Smith, W.B., 1967, Astrophys. J., Vol.72, p.338.

Backer, D.C., Kulkarni, S.R., Heiles, C., Davis, M.M., Goss, W.M., 1982, Nature, Vol.300, p.615.

Baltrusaitis, R.M., Cassiday, G.L., Cooper, R., Elbert, J.W., Gerhardy, P.R., Loh, E.C., Mizumoto, Y., Sokolsky, P., Sommers, P., Steck, D., 1985, Astrophys. J., Vol.293, L69.

Basko, M.M., Sunyaev, R.A. and Titarchuk, L.G., 1974, Astron. Astrophys., Vol.16, p.241.

Batschelet, E., 1981, 'Circular Statistics in Biology', Acad. Press.

Battistoni, G., Bellotti, E., Bloise, C., Bologna, G., Campana, P., Castagnoli, C., Castellina, A., Chiarella, V., Ciocio, A., Cundy, D., D'Ettorre-Piazzoli, B., Fiorini, E., Galeotti, P., Iarocci, E., Luguori, C., Mannocchi, G., Murtas, G., Negri, P., Nicoletti, G.,

Picchi, P., Price, M., Pullia, A., Ragazzi, S., Rollier, M., Saavedra, O., Satta, L., Serri, P., Vernetto, S., and Zanotti, L., 1985, Phys. Rev. Lett., Vol.155B, p.465.

Bhat, P.N., Gupta, S.K., Ramana Murthy, P.V., Sreekantan, B.V., Tonwar, S.C., Viswanath, P.R., 1980, Astron. Astrophys., Vol.81, L3.

Bignami, G., Maraschi, L. and Treves, A., 1977, Astron. Astrophys., Vol. 16, p.241.

Blackett, P.M.S., 1948, 'Emission spectra of the night sky and aurora', Rep. Gassiot Comm. of the Roy. Soc., p.34.

Blandford, R. and Teukolsky, S.A., 1976, Astrophys. J., Vol.205, p.580.

Bonnet-Bidaud, J.M. and Van der Klis, M., 1981, Astron. Astrophys., Vol.101, p.299.

Boriakoff, V., Buccheri, R., and Fauci, F., 1983, Nature, Vol.304, p.417.

Browning, R. and Turver, K.E., 1977, Nuovo Cimento, Vol.38A, p.223.

Buccheri, R., S'Amico, N., Massaro, E., Scarsi, L., 1978, Nature, Vol.274, p.572.

Buccheri, R. and Sacco, B., 1984, Invited paper, Int. Workshop on Data Analysis in Astronomy.

Cawley, M.F., Fegan, D.J., Gibbs, K., Gorham, P.W., Kenny, S., Lamb, R. C., Liebing, D.F., Porter, N.A., Stenger, V.J., and Weekes T.C., 1985a, 19th Int. Conf. on Cosmic Rays, La Jolla, (conf. proceedings, Vol.3, p.453.)

Cawley, M.F., Fegan, D.J., Gibbs, K., Gorham, P.W., Lamb, R.C., Liebing, D.F., Porter, N.A., Stenger, V.J., Turver K.E., and Weekes T.C. 1985b, Astrophys. J., Vol.296, p.185.

Cawley, M.F., Fegan, D.J., Gibbs, K., Gorham, P.W., Hillas, A.M., Lamb, R.C., Liebing, D.F., MacKeown, P., Porter, N.A., Stenger, V.J., and Weekes, T.C., 1985c, 19th Int. Conf. on Cosmic Rays, La Jolla, (preprint no.2173, Center for Astrophysics).

Cerenkov, P.A., 1934, Dokl. Akad. Nauk. SSSR., Vol.2, p.451.

Chadwick, P.M., Dowthwaite, J.C., Harrison, A.B., Kirkman, I.W., McComb, T.J.L., Orford, K.J., and Turver, K.E., 1985a, Nature, Vol.317, p.236.

Chadwick, P.M., Dipper, N.A., Dowthwaite, J.C., Gibson, A.I., Harrison, A.B., Kirkman, I.W., Lotts, A.P., Macrae, J.H., McComb, T.J.L., Orford, K.J., Turver, K.E., and Walmsley, M., 1985b, Nature, Vol.318, p.462.

Chadwick, P.M., Dowthwaite, J.C., Harrison, A.B., Kirkman, I.W., McComb, T.J.L., Orford, K.J., and Turver, K.E., 1985c, Astron. Astrophys., Vol.151, L1.

Chanmugam, G., and Brecher, K., 1985, Nature, Vol.313, p.767.

Cheng, K.S., Ho, C., and Ruderman, M.A., 1986a, Astrophys.J., Vol.300, p.500.

Cheng, K.S., Ho, C., and Ruderman, M.A., 1986b, Astrophys.J., Vol.300, p.522.

Cherry, M.L., Chupp, E.L., Dunphy, P.D., Forrest, D.J., and Ryan, J.M., 1980, Astrophys. J., Vol.242, p.1257.

Clark, G.W., Garmire, G.P., Kraushaar, W.L., 1968, Astrophys. J. Lett., Vol.153, L203.

Cocke, W.J., Disney, M.J., and Taylor, D.J., 1969, Nature, Vol.221, p.525.

Coe, M.J., Quenby, J.J., Engel, A.R., 1978, Nature, Vol.274, p.343.

Craig, M.A.B., 1984, PhD thesis, University of Durham.

Danaher, S., Fegan, D.J., Porter, N.A., Weekes, T.C., 1981, Nature, Vol.289, p.568.

Davidsen, A., and Ostriker, J., 1974, Astrophys. J., Vol.189, p.331.

Dowthwaite, J.C., Gibson, A.I., Harrison, A.B., Kirkman, I.W., Lotts, A.P., Macrae, J.H., Orford, K.J., Turver, K.E., and Walmsley, M., 1983, Astron. Astrophys., Vol.126, p.1.

Dowthwaite, J.C., Harrison, A.B., Kirkman, I.W., Macrae, J.H., Orford, K.J., Turver, K.E., and Walmsley, M., 1984a, Nature, Vol.309, p.691.

Dowthwaite, J.C., Harrison, A.B., Kirkman, I.W., Macrae, J.H., McComb, T.J.L., Orford, K.J., Turver, K.E., and Walmsley, M., 1984b, Astrophys. J., Vol.286, L35.

Dowthwaite, J.C., Harrison, A.B., Kirkman, I.W., Macrae, J.H., Orford, K.J., Turver, K.E., and Walmsley, M., 1984c, Astron. Astrophys., Vol.136., L14.

Dowthwaite, J.C., Harrison, A.B., Kirkman, I.W., Macrae, J.H., Orford, K.J., Turver, K.E., and Walmsley, M., 1985, Astron. Astrophys., Vol.142., p.55.

Eadie, W.T., Drijard, D., James, F.E., Roos, M., Sadoulet, B., 1971, 'Statistical Methods in Experimental Physics', North-Holland, p.283.

Eichler, D. and Vestrand, W.T., 1985, Nature, Vol.318, p.345.

Fegan, D.J., McBreen, B., O'Mongain, E., Porter, N.A., Slevin, P.J., 1968, Canad. J. Phys., Vol.46, S433.

Fomin, V.P., Vladimirsky, B.M., and Stepanian, A.A., 1977, Proc. 15th Int. Conf. Cosmic Rays, Plovdiv, Vol.1, p.12.

Forman, W. Jones, C., Liller, W., 1972, Astrophys. J. (Lett.), Vol.177, L103.

Forman, W. Jones, C., Tananbaum, H., 1976, Astrophys. J. (Lett.), Vol.206, L29.

Frank, I.M., and Tamm, Ig., 1937, Dokl. Acad. Nauk., Vol.14, p.109.

Fritz, G., Henry, R.C., Meekins, J.F., Chubb, T.A., Friedman, H., 1969, Publ. Astron. Soc. Pacific, Vol.81, p.539.

Galbraith, W. and Jelley, J.V., 1953, Nature, Vol.171, p.349.

Galbraith, W. and Jelley, J.V., 1955, J. Atmos. and Terrestial Phys., Vol.6, p.250.

Gal'per, A.M., Kirillov-Ugiriumov, V.G., Kurochkin, A.V., Leikov, P.G., Luchkov, B.I., Yurkin, Yu.T., 1976, Pisma v Astron. Zh., Vol.2, p.254.

Giacconi, R., Gorenstein, P., Gursky, H., and Waters, J.R., 1967, Astrophys. J. Lett., Vol.148, L119.

Gibson, A.I., Harrison, A.B., Kirkman, I.W., Lotts, A.P., Macrae, J.H., Orford, K.J., Turver, K.E., and Walmsley, M., 1982a, Nature, Vol.296, p.833.

Gibson, A.I., Harrison, A.B., Kirkman, I.W., Lotts, A.P., Macrae, J.H., Orford, K.J., Turver, K.E., and Walmsley, M., 1982b, Proc. Int. Workshop on Very High Energy Gamma Ray Astronomy (Ooctacamund), eds. P.V. Ramana Murthy and T.C. Weekes, (Bombay: Tata Institute), p.97.

Ginzburg, V.L., 1940, Zh. Fiz. SSSR., Vol.2, p.441.

Goldreich, P. and Julian, W.H., 1969, Astrophys. J., Vol.157, p.869.

Gorham, P.W. and Learned, J.G., Nature, 1986, Vol.323, p.422.

Gorham, P.W., Cawley, M.F., Fegan, D.J., Gibbs, K.G., Lamb, R.C., Liebing, D.F., Porter, N.A., Stenger, V.J. and Weekes, T.C., 1986, Astrophys. J., Vol.308, L11, p.113.

Gould, R.J. and Schreder, G., 1966, Phys. Rev. Lett., Vol.16, p.252.

Gregory, P.C., 1972, Nature, Vol.239, p.439.

Gregory, P.C., Duric, N., Reid, A., Picha, J., Stevenson, T. and Taylor, A.R., 1986, Vol.323, p.602.

Grindlay, J.E., 1975, Phys. Rev. D., Vol.11, p.517.

Grindlay, J.E., Helmken, H.F., and Weekes, T.C., 1976, Astrophys. J., Vol.209, p.592.

Grindlay, J.E., 1982, Proc. Int. Workshop on Very High Energy Gamma Ray Astronomy (Ooctacamund), eds. P.V. Ramana Murthy and T.C. Weekes, (Bombay: Tata Institute), p.178.

Gunn, J.E. and Ostriker, J.P., 1969, Nature, Vol.221, p.454.

Gupta , S.K., Ramana Murthy, P.V., Sreekantan, B.V., Tonwar, S.C., 1978, Astrophys. J., Vol.221, p.268.

Hartman, D.H., Fan, C.Y., Gough, M.P., Turver, K.E. and Weekes, T.C., 1979, Nuovo Cimento, Vol.51A, p.131.

Hawley, J.F., Smarr, L.L. and Wilson, J.R., 1984, Astrophys. J. Suppl., Vol.55, p.211.

Hearn, D., 1969, Nucl. Instrum. Methods, Vol.70, p.200.

Heitler, W., 1954, 'The Quantum theory of radiation', London, The Oxford University Press.

Hermsen, W., 1980, PhD thesis, University of Leiden.

Hermsen, W., 1983, Space Sci. Rev., Vol.36, p.61.

Hillas, A.M. 1975, Proc. 14th Int. Cosmic Ray Conf., Munich, Vol.9, p.3439.

Hillas, A.M. 1984, Nature, Vol.312, p.50.

Hillas, A.M. 1985, Proc. 19th Int. Cosmic Ray Conf., La Jolla, Vol.5, p.296.

Holt, S., Boldt, E., Serlemitsos, P. and Kaluzienski, L., 1976, Nature, Vol.260, p.592.

Jelley, J.V., 1968, Prog. in Cosmic Ray Phys., Vol.9, p.41.

Jelley, J.V. and Porter, N.A., 1963, Quart. J. Roy. Astr. Soc., Vol.4, p.275.

Kazanas, D. and Ellison, D.C., 1986, Nature, Vol.319, p.380.

Kifune, T., Nishijima, K., Hara, T., Hatano, Y., Hayashida, N., Honda, M., Kamata, K., Mori, M., Nagano, M., Tanahashi, G., Teshima, M., 1986, Astrophys. J., Vol.301, p.230.

Kirkman, I.W., 1985, PhD thesis, University of Durham.

Kuiper, N.H., 1960, Ned. Ak. Wet. Proc., A63, p.38.

Lamb, R.C., 1978, Nature, Vol.272, p.429.

Lamb, R.C., Fichtel, C.E., Hartman, R.C., Kniffen, D.A., Thompson, D.J., 1977, Astrophys. J., Vol.212, L63.

Lamb, R.C., Godfrey, C.P., Wheaton, W.A., Tumer, T., 1982, Nature, Vol.296, p.543.

Lamb, R.C. and Weekes, T.C., 1986, Astrophys. Lett. Vol.25, p.73.

Leahy, D.A., Elsner, R.F. and Weiskopf, M.C., 1983, Vol.272, p.256.

Lloyd-Evans, J., Coy, R.N., Lambert, A., Lapikens, J., Patel, M., Reid, R.J.O. and Watson, A.A., 1983, Nature, Vol.305, p.784.

Li, T.P. and Ma, Y.Q., 1983, Astrophys. J., Vol.272, p.317.

Lovelace, R.V.E., 1976, Nature, Vol.262, p.649.

Macrae, J.H., PhD thesis, University of Durham.

Mallett, L., 1926, C.R. Acad. Sci., Paris, Vol.183., p.274.

Manchester, R.N. and Taylor, J.H., 'Pulsars', (San Fransisco: W. H. Freeman, 1977).

Marshak, M.L., Bartlet, J., Courant, H., Heller, K., Joyce, T., Peterson, E.A., Ruddick, K., Schupe, M., Ayres, D.S., Dawson, J., Fields, T., May, E.N., Price, L.E., Sivaprasad, K., 1985, Phys. Rev. Lett. Vol.54, p.2079.

Mardia, K.V., 1972, 'Statistics of Directional Data' (New York, Academic Press).

Mayer-Hasselwander, H. A., Bennett, K., Bignami, G.F., Buccheri, R., D'Amico, N., Hermsen, W., Kanbach, G., Lebrun, F., Lichti, G.G., Masnou, J.L., Paul, J.A., Pinkau, K., Scarsi, L., Swanenburg, B.N. and Wills, R.D., 1980, Proc. Texas Symp. 9th Relativ. Astrophys., N.Y. Acad. Sci., Vol.336, p.211.

McBreen, B., Ball, S.E., Campbell, M., Greisen, K. and Koch, D., 1973, Astrophys. J., Vol.184, p.571.

McKechnie, S.P., Mount, K.E. and Ramsden, D., 1976, Astrophys. J. Lett., Vol.207, L151.

Milgrom, M. and Pines, D., 1978, Astrophys. J., Vol.220, p.272.

Molteni, D., Rapisarda, M., Robba, R. and Scarsi, L., 1980, Astron. Astrophys., Vol.87, p.88.

Mood, A.M., 1950, 'Introduction to the theory of Statistics', New York, McGraw-Hill.

Morrison, P., 1958, Nuovo Cimento, Vol.7, p.858.

Mukanov, D.B., Nestrova, N.M., Stepanian, A.A., Fomin, V.P., 1980, Izvestiya Krymskoi Astrofiz. Obs., Vol.62, p.98.

Nagase, F., Sato, N., Makishima, K., Kawai, N. and Mitani, K., ISAS, Res. Note 234 (Institute of Space and Astronautical Science, Tokyo, 1983), 1983, Summer Workshop in Astronomy and Astrophys., Santa Cruz.

Neshpor, Yu.I., Stepanian, A.A., Fomin, V.P., Gerasimov, S.A., Vladimirsky, B.M. and Zyskin, Yu. L., 1979, Astrophys. Space Sci., Vol.61, p.349.

Neshpor, Yu. I. and Zyskin, Yu. L., 1986, Pis'ma v Astron. Zh. (USSR), Vol.12, p.456.

Ogelman, H., Fichtel, C.E., Kniffen, D.A. and Thompson, D.J., 1976, Astrophys. J., Vol.209, p.584.

O'Mongain, E., 1973, Nature, Vol.241, p.376.

Oyama, Y., Arisaka, K., Kajita, T., Koshiba, M., Nakahata, M., Suzuki, A., Takita, M., Totsuka, Y., Kifune, T., Suda, T., Sato, N., Takahashi, K. and Miyano, K., 1986, Phys Rev. Lett., Vol.56, p.991.

Parmar, A.N., Pietsch, W., McKechnie, S., White, N.E., Trumper, J., Voges, W. and Barr, P., 1985, Nature, Vol.313, p.119.

Perotti, F., Della-Ventura, A., Sechi, G., Villa, G., Di Cocco, G., Baker, R.E., Butler, R.C., Dean, A.J., Martin, S.J. and Ramsden, D., 1979, Nature, Vol.282, p.484.

Petterson, J.A., 1975, Astrophys. J. Lett., Vol.201, L61.

Porter, N.A. and Weekes, T.C., 1978, Smithsonian Astrophys. Obs. Special Report, No. 381.

Protheroe, R.J., 1984, Astronom. Exp., Vol.1, p.33.

Protheroe, R.J., 1985, Astronom. Exp., Vol.1, p.137.

Protheroe, R.J., 1986, Proc. Astron. Soc. Australia (Invited Paper).

Protheroe, R.J. and Clay, R.W., 1985, Nature, Vol.315, p.205.

Ramana Murthy, P.V., 1983, 18th Int. Cosmic Ray Conf., Bombay, India: Tata Inst. Fundamental Res. (Aug. 1983), Conference Papers (preprint).

Rappaport, S. and Joss, P.C., 1977, Nature, Vol.266, p.683.

Rappaport, S., Clark, G.W., Cominsky, L., Joss, P.C. and Li, F., 1978, Astrophys. J. Lett., Vol.244, p.1.

Resvanis, L., Tzamarias, S., Voulgaris, G., Learned, J., Stenger, V., Weeks, D., Gaidos, J., Loeffler, F., Olson, J., Palfrey, T., Sembroski, G., Wilson, C., Camerini, U., Finley, J., Frankowski, M., Fry, W., Jennings, J., Jaworski, M., Kenter, A., Koepsel, R., Lomperski, M., Loveless, R., March, R., Mathews, J., Morse, R., Reeder, D., Sandler, P., Slane, P. and Szentgyorgyi, A., 1986, Proceedings of the N.A.T.O. Advanced Research Workshop on V.H.E. Gamma ray Astronomy, (Durham), p.225.

Ricketts, M.J., Paul, R., Page, C.G. and Pounds, K.A., 1981, Space Sci. Rev., Vol.30, p.399.

Ruddick, K., 1986, Phys. Rev. Lett., Vol.57, p.531.

Ruderman, M.A. and Sutherland, P.G., 1975, Astrophys. J., Vol.196, p.57.

Ruderman, M.A., 1981, 'IAU Symposium 95, Pulsars', (Dordrecht: Reidel), p.156.

Salvati, M. and Massaro, E., 1978, Astron. Astrophys., Vol.67, p.55.

Samorski, M.A., and Stamm, W., 1983, Astrophys. J. Lett., Vol.283, L17.

Samorski, M.A., and Stamm, W., 1985, Astrophys. J., Vol.286, L17.

Shaham, J., 1987, Sci. American, Vol.256, no.2, p.34.

Siegel, S., 1956, 'Non-parametric Statistics for the Behavioural Sciences', New York, McGraw-Hill.

Staelin, C.H. and Reifenstein, E.C., 1968, Science, Vol.162, p.1481.

Stepanian, A.A., Vladimirsky, B.M. and Fomin, V.P., 1972, Nature, Vol.239, p.40.

Stepanian, A.A., Fomin, V.P. and Valdimirsky, B.M., 1983, Izv. Krym. Astrofiz. Obs. (USSR), Vol.66, p.234.

Strong, A.W., 1982, Proc. Int. Workshop on Very High Energy Gamma Ray Astronomy (Ooctacamund), eds. P.V. Ramana Murthy and T.C. Weekes, (Bombay: Tata Institute), p.141.

Sturrock, P., 1971, Astrophys. J., Vol.164, p.529.

Tananbaum, H., Gursky, H., Kellog, E.M., Levinson, R., Schreier, E. and Giacconi, R., 1972, Astrophys. J. Lett., Vol.174, L143.

Taylor, J.H., Fowler, L.A. and McCulloch, P.M., 1979, Nature, Vol.277, p.437.

Taylor, J.H. and Stinebring, R.D., 1986, Ann. Rev. Astron. Astrophys., Vol.24, p.285.

Tornabene, H.S., 1977, Proc 15th Int. Cosmic Ray Conf., Plovdiv, Vol.9,. p.156.

Tornabene, H.S. and Cusimano, F.J., 1968, Canad. J. Phys., Vol.46, p.5581.

Trumper, J., Pietsch, W., Reppin, C., Voges, W., Staubert, R. and Kendziorra, E., 1978, Astrophys. J. Lett., Vol.219, L105.

Turver, K.E. and Weekes, T.C., Phil. Trans. Roy. Soc. Lond., 1981, A301, p.615.

Usov, V.V., 1983, Nature, Vol.305, p.409.

Van der Klis, M. and Bonnet-Bidaud, J.M., 1981, Astron. Astrophys., Vol.95, L5.

Van der Klis, M. and Jansen, F.A., 1985, Nature, Vol.313, p.768.

Van der Klis, M., Jansen, F.A., van Paradijs, J., Lewin, W.H.G., Van den Heuvel, E.P.J., Trumper, J.E. and Sztajno, M., 1985, Nature, Vol.316, p.225.

Vestrand, W.T. and Eichler, D., 1982, Astrophys. J., Vol.251, p.112.

Wang, Y.M., 1986, Astrophys. Space Sci., Vol.121, p.193.

Watson, G.S., 1961, Biometrika, Vol.48, p.109.

Weekes, T.C., Danaher, S., Fegan, D.J. and Porter, N.A., 1981, Astron. Astrophys., Vol.104, L4.

Weekes, T.C., Helmken, H.F. and Grindlay, J.E., 1979, Proc. Int. Cosmic Ray Conf., Kyoto, Vol.1, p.133.

Wheaton, W.A., Doty, J.P., Primini, F.A., Cooke, B.A., Dobson, C.A., Goldman, A., Hecht, M., Hoffman, J.A., Howe, S.K., Scheepmaker, A., Tsiang, E.Y., Lewin, W.H.G., Matteson, J.L., Gruber, D.E., Baity, W.A., Rothschild, R., Knight, F.K., Nolan, P. and Peterson, L.E., 1979, Nature, Vol.282, p.587.

White, N.E. and Holt, S.S., 1982, Astrophys. J., Vol.268, L17.

Wills, R.D., Bennett, K., Bignami, G.F., Buccheri, R., Caraveo, P.A., Hermsen, W., Kanbach, G., Masnou, J.L., Mayer-Hasselwander, H.A., Paul, J.A. and Sacco, B., 1982, Nature, Vol.296, p.723.

Zatsepin, V.T. and Chudakov A.E., 1962, Sov. Phys. J.E.T.P., Vol.15, p.1126.

Addenda and Errata

The following are additional references cited in the text;

Erickson, R.A., Fickle, R.K. and Lamb, R.C., 1976, Astrophys. J., Vol.210, p.539.

Grindlay, J.E., 1971, Smithsonian Astrophys. Obs. Special Report, no. 334.

Grindlay, J.E., Helmken, H.F., Hanbury Brown, R., Davis, J., Allen, L.R., 1975, Astrophys. J. (Lett.), Vol.197, L9.

Gupta, S.K., Ramana Murthy, P.V., Sreekantan, B.V., Tonwar, S.C. and Viswanath, P.R., 1982, Proc. Int. Workshop on Very High Energy Gamma Ray Astronomy (Ooctacamund), eds. P.V. Ramana Murthy and T.C. Weekes, (Bombay: Tata Institute), p.279.

Kelley, R.L., Rappaport, S., Brodheim, M.J., Cominsky, L., Stothers, R., 1981, Astrophys. J., Vol.251, p.630.

Jennings, D.M., White, G., Porter, N.A., O'Mongain, E., Fegan, D. and White, J., 1974, Nuovo Cimento, Vol.20, p.295.

Meegan, C.A., Fishman, G.J., Haymes, R.C., 1979, Astrophys. J.(Lett.) Vol.234, L123.

Porter, N.A., Delaney, D. and Weekes, T.C., 1974, Proc. 9th ESLAB symposium, (Frascati: ESRO), p.295

Reppin C., Pietsch, W., Trumper, J., Voges, W., Staubert, R., 1979, Astrophys. J. Vol.234, p.329.

Weekes, T.C., Helmken, H.F., 1977, 'Recent advances in Gamma Ray Astro.' ESASP-124, p.39.